NMR Spectroscopic Investigations On Small Organic Molecules: Catalyst Stabilities, Low-Abundance Conformers, Intermediates And Reaction Mechanisms

Dissertation

Zur Erlangung des Doktorgrades
der Naturwissenschaften (Dr. rer. nat.)
der Fakultät für Chemie und Pharmazie
der Universität Regensburg

vorgelegt von

Michael Haindl
aus Mühldorf am Inn

Februar 2016

Die vorliegende Dissertation beruht auf Arbeiten, die zwischen Oktober 2011 und Februar 2016 im Arbeitskreis von Frau Professor Dr. Ruth M. Gschwind am Institut für organische Chemie der Universität Regensburg durchgeführt wurden.

Promotionsgesuch eingereicht am:	18. Februar 2016
Die Arbeit wurde angeleitet von:	Prof. Dr. Ruth M. Gschwind
Prüfungsausschuss:	
Vorsitzender:	Prof. Dr. Olga Garcia Mancheño
1. Gutachter:	Prof. Dr. Ruth M. Gschwind
2. Gutachter:	Prof. Dr. Werner Kremer
3. Prüfer:	PD Dr. Sabine Amslinger

Danksagung

Zuerst gebührt mein Dank all denjenigen, die zum Erfolg dieser Dissertation beigetragen haben. Meiner Doktormutter Prof. Dr. Ruth M. Gschwind möchte ich für die Überlassung des spannenden Themas und die hohe mir übertragene Eigenverantwortung danken, die mich stets motiviert hat. Allen beteiligten Kollegen und Kooperationspartnern danke ich für die vielen fruchtbaren Anregungen und Diskussionsrunden. Bei meinem Vorgänger Dr. Markus Schmid bedanke ich mich für die ausgezeichneten Vorarbeiten und „Steilvorlagen“, die ihren Teil zum Gelingen dieser Arbeit beigetragen haben.

Meinen lieben Kollegen und Freunden an der Universität Regensburg danke ich für die lockere und angenehme Arbeitsatmosphäre, die Kochabende (meistens Dienstags), die tiefgreifenden Gespräche und die vielen lustigen Momente und Geschichten, die das gemeinsame Leben an der Universität Regensburg geschrieben hat. Sie werden mir immer in Erinnerung bleiben.

Bei meinen Eltern Inge und Holger Haindl möchte ich mich besonders bedanken. Ihr habt mir das Leben geschenkt und seid seitdem immer da, wenn ich euch brauche. Danke!

Auch meinen Schwiegereltern Eva und Martin Wengbauer gebührt großer Dank. Eure offene und herzliche Art hat mir immer imponiert.

Der größte Dank aber gilt meiner lieben Ehefrau Judith Haindl und meinem einjährigen Sohn Simon Haindl. Durch eure Zuneigung, euer Lachen, euer Weinen, euer Verständnis, eure offenen Ohren und eure ständige, nicht nachlassende Unterstützung habt ihr mir gezeigt, was das Wichtigste ist im Leben – die eigene Familie.

NMR Spectroscopic Investigations On Small Organic Molecules: Catalyst Stabilities, Low-Abundance Conformers, Intermediates And Reaction Mechanisms

Table of Contents

1 Introduction and Outline

For decades, the field of NMR spectroscopy is divided into two parts, *i.e.* the investigation of large molecules, mostly biological macromolecules like proteins or nucleic acids and the investigation of small molecules, which includes all compounds below a molecular weight of about 1500 Da. In the year 1999 the "large molecules" field was so dominant, that the "small molecules" scientific NMR community, together with sponsors of the industry, decided to name their, until today, largest US/European conference on that topic SMASH ("**S**mall **M**olecules **A**re **S**till **H**ot"). About at the same time the "gold rush" (*Angew. Chem. Int. Ed.* **2008**, *47*, 6138.; *Chem. Soc. Rev.* **2009**, *38*, 2178.) in organocatalysis had its starting point and until today, this research field was so successful, that it even developed to an independent area in asymmetric catalysis. While, from day one, synthetic explorations pushed organocatalysis forward, investigations on the underlying reaction mechanisms were rare at the beginning. It was small molecules NMR which enabled the *in situ* detection and characterization of the elusive proline, prolinol and prolinol ether enamines, central intermediate species in organocatalysis and showed the power and elegance of that methodology in organic chemistry (Schmid M. B, Ph.D. Thesis, University of Regensburg, **2011**).

Based on that pioneering work, this thesis uses the generated momentum of NMR in organocatalysis and more general in the field of small molecules in order to shed more light into reaction mechanisms and involved intermediates in proline catalysis and a new type of nitro chemistry, to identify reaction conditions that ensure catalyst stabilities and to detect and characterize low abundant dipeptide conformers.

In chapter 2 the reaction mechanism of the enamine formation pathway in the proline catalyzed self-aldolization/self-condensation reaction of aldehydes is revisited. It was unclear, whether the enamine is formed from the iminium ion or from the oxazolidinone species. The methodic innovation in this work is the combination of 1D selective EXSY spectroscopy together with the initial rate approximation (IRA) approach. It enables, for the first time, the determination of rate constants in between interconnected intermediate species during the ongoing reaction (*in situ*). Together with top-notch theoretical calculations, including one of the most accurate solvent models available today (DCOSMO-RS), the results of this study show that the active reaction mechanism can strongly depend on the applied reaction conditions. While the direct precursor in this reaction and under these conditions was identified to be the iminium ion and not the oxazolidinone as earlier studies suggested, the exact pathway is variable. Depending on the catalyst amount, water concentration

and additive addition three different pathways can be active including *e.g.* internal or external deprotonation steps or the assistance of water in the mechanism.

In chapter 3 the reaction conditions for the cleavage of the TMS protecting group from the very popular organocatalyst diphenylprolinol trimethylsilyl ether (Jørgensen-Hayashi catalyst) is investigated. In this study a very systematic approach is adopted. The influence on the TMS cleavage rates is determined of eight solvents with different combinations of dielectric constants (ε_r) and hydrogen bond acceptor properties (β) as well as seven acidic and basic additives. It can be shown that unless in DMSO and DMF, very polar (high ε_r values) and at the same time strong hydrogen bond accepting (high β values) solvents, the catalyst is very robust. However, a combination of those solvents with weak acids like benzoic acid dramatically accelerates the TMS cleavage and the catalyst completely degrades within only a few hours.

The relevance of *cis*-conformers of a pseudo-dipeptide (double-protected glycin) is eludicated in chapter 4. In computational publications it was often decided to ignore the possible existence of *cis*-conformers in short peptides and proteins that are not stemming from proline amino acids. The herein presented evidence for the population of low-abundant *cis*-conformers in a pseudo-dipeptide makes this decision very questionable. In combination with detailed theoretical calculations, a full characterization by NMR in terms of thermodynamic and kinetic constants shows that this *cis*-peptides are in deed very low abundant but in the samt time are formed with high rates. Peptide bond isomerization rate constants are again determined by the combination of 1D selective EXSY spectra with the IRA approach. The deduced rates show that a number of molecules exceeding the whole population of the main *trans*-conformer in one minute reaction time isomerizes once to those *cis*-isomers which makes them very relevant in terms of their kinetic accessibility.

Finally, in chapter 5, a refinement is presented of a preliminary study on a new secondary amine catalyzed nitroalkene dimerization reaction followed by a fragmentation towards conjugated enynes. A two-pathway crossroad reactivity is discovered enabling, not only the generation of conjugated enynes but also that of 5-membered cyclic nitronates at the same time. Both, enynes and cyclic nitronates, are very valuable structural motifs which can be found in a variety of commercial drugs and drug candidates. The reaction is splitted into two parts by identification of conditions that allow for the isolation of the organocatalytic nitroalkene dimerization product. The underlying reaction mechanisms are investigated in detail by *in situ* NMR. ^{1}H reaction monitoring together with ^{13}C^{15}N-coupling constant analysis and standard 2D NMR experiments lead to the detection and identification of a completely new biciclic intermediate species which sits at the crossroad for the two discovered reactions.

Concomitantly, the synthesis of isotopic ^{13}C and ^{15}N labeled starting materials is described and its application reveals the formation of carbon dioxide, bimolecular nitrogen and water as side products which are key to the comprehension of the underlying mechanisms. The study is meant to lie the foundation for following synthetic investigations which may explore the scope and possible stereoselectivity of this reactions.

2 The Proline Enamine Formation Pathway Revisited in Dimethyl Sulfoxide: Rate Constants Determined *via* NMR

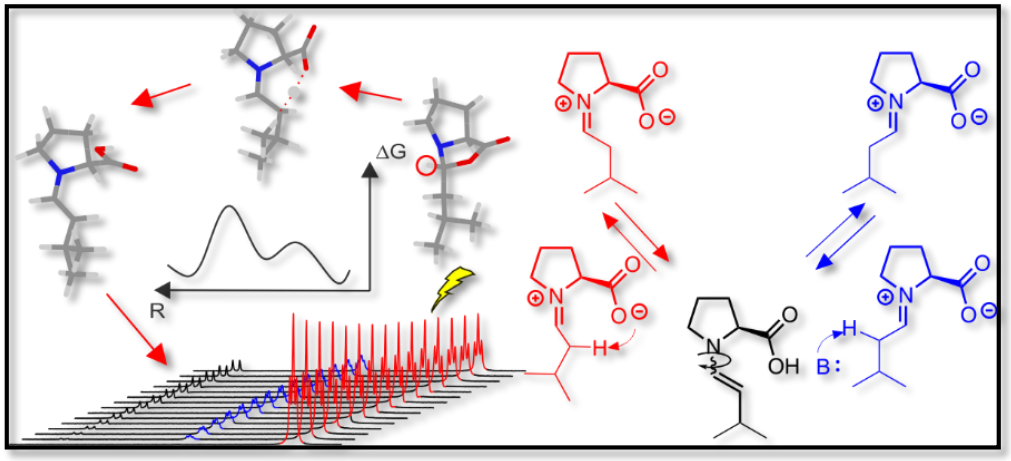

All calculations were performed by J. Hioe.

M. H. Haindl, J. Hioe, R. M. Gschwind,
J. Am. Chem. Soc. **2015**, 137, 12835.

http://dx.doi.org/10.1021/jacs.5b03420

2.1 Abstract

Enamine catalysis is a fundamental activation mode in organocatalysis and can be successfully combined with other catalytic methods, *e.g.*, photocatalysis. Recently, the elusive enamine intermediates were detected, and their stabilization modes were revealed. However, the formation pathway of this central organocatalytic intermediate is still a matter of dispute, and several mechanisms involving iminium and/or oxazolidinone are proposed. Here, the first experimentally determined rate constants and rates of enamine formation are presented using 1D selective exchange spectroscopy (EXSY) buildup curves and initial rate approximation. The trends of the enamine formation rates from *exo*-oxazolidinones and *endo*-oxazolidinones upon variation of the proline and water concentrations as well as the nucleophilic/basic properties of additives are investigated together with isomerization rates of the oxazolidinones. These first kinetic data of enamine formations in combination with theoretical calculations reveal the deprotonation of iminium intermediates as the dominant pathway in dimethyl sulfoxide (DMSO). The dominant enamine formation pathway varies according to the experimental conditions, *e.g.*, the presence and strength of basic additives. The enamine formation is zero-order in proline and oxazolidinones, which excludes the direct deprotonation of oxazolidinones via E2 mechanism. The nucleophilicity of the additives influences only the isomerization rates of the oxazolidinones and not the enamine formation rates, which excludes a nucleophile-assisted anti elimination of oxazolidinones as a major enamine formation pathway.

2.2 Manuscript

Introduction

Enamine catalysis is one of the central activation modes in organocatalysis and has proven to be a very powerful method for the enantioselective α-functionalization of carbonyl compounds (*e.g.*, in aldol or Mannich reactions, Michael additions, α-halogenations, α-oxygenations, α-aminations, or domino reactions).[1,2] The primary synthesis applications using proline enamine catalysis were followed by versatile and powerful further developments, *e.g.*, prolinol[3–5] and prolinolether catalysts[6–9] di-/trienamine[10–12] catalysis, and combinations with photocatalysis.[13–15] Proline oxazolidinones[16] and stabilized enamines[17] were characterized by X-ray crystallography. However, for decades, exclusively oxazolidinones were detected as intermediates by *in situ* NMR.[18–22] Recently, we observed the elusive proline enamines by *in situ* NMR[23] and elucidated the stabilization modes of enamines versus oxazolidinones.[23,24] Furthermore, the mechanism of aldol addition versus aldol condensation was investigated,[25] and the formation pathways, conformational preferences, and stereoinduction modes of prolinol and prolinol ether enamines were revealed.[26,27] The formation of imines or iminium ions are generally accepted to proceed via carbinolamines.[28–30] NMR studies on two combinations of aldehydes/ketones with prolinol/prolinolether as catalysts corroborated this intermediate.[31,32] However, the formation pathway of the central proline enamine intermediate is still discussed controversially. In the most generally accepted mechanism first proposed by Houk and List,[33,34] the enamine is formed directly from the *E*/*Z* zwitterionic iminium via intramolecular deprotonation of one of its α-protons by the carboxylate moiety (Fig. 1, pathway I). For this process, Sunoj *et al.* calculated the lowest energy barrier for *Z*-iminium.[35] In a second pathway, they proposed a water-assisted proton transfer with an amphoteric water molecule protonating the carboxylate and deprotonating the α-proton (Fig. 1, II). In this water-assisted pathway, the calculated barriers of *Z*- and *E*-iminium are similar, but both are considerably higher than that in the water-free deprotonation from *Z*-iminium.[35] In a third pathway, they calculated the participation of an external base in the deprotonation step (Fig. 1, III). However, with external base the resulting energy barriers are again significantly higher.[35] In the following, all enamine formation pathways via deprotonation from iminium carboxylates herein are referred to as “iminium pathways”.

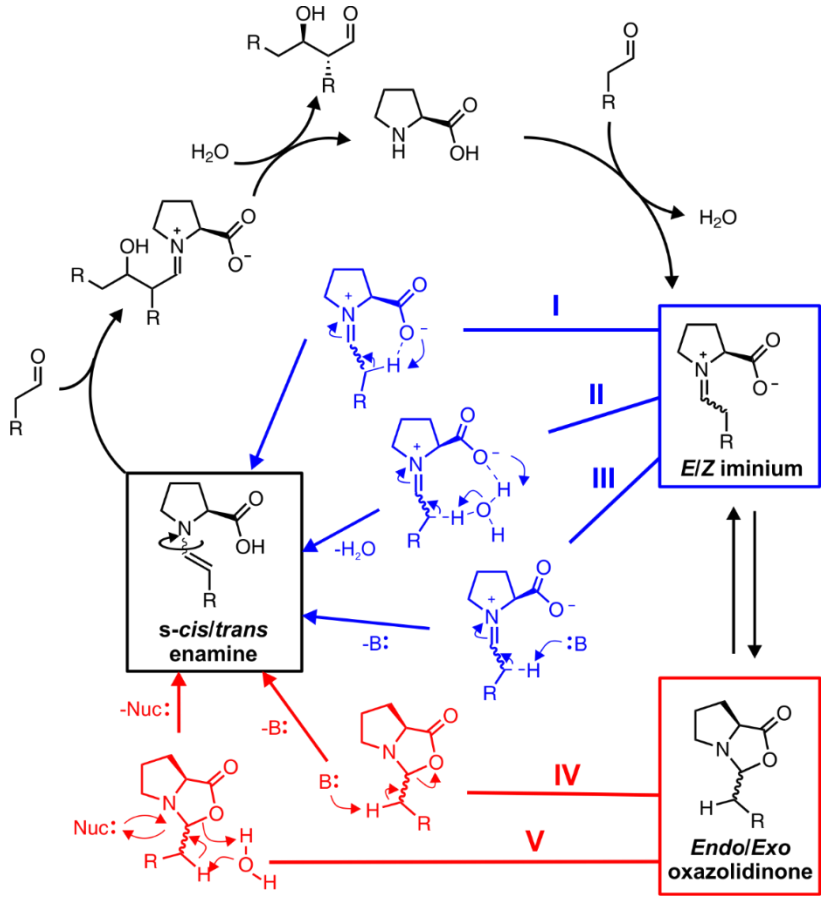

Fig. 1: Catalytic cycle of L-proline-catalyzed aldol reactions and proposed enamine formation pathways. Enamine formations *via* deprotonation of iminium carboxylates are shown in blue (I, intramolecular; II, water-assisted; III, external-base-induced). Deprotonations of oxazolidinones are shown in red (IV, with external base; V, nucleophile-assisted). For the sake of clarity, the *E*-/*Z*-iminium isomers, the diastereomeric *endo*-/*exo*-oxazolidinones, and the *s-cis*-/*s-trans* enamine conformers are presented in condensed forms using waved bonds.

In contrast, in the model of Seebach and Eschenmoser the enamine intermediate is formed directly from the oxazolidinone species. [20] An external base such as an additional proline, oxazolidinone, or product molecule is proposed to deprotonate the oxazolidinone α-proton and to induce an *anti* E2 elimination (Fig. 1, IV)). Our own NMR investigations of proline enamine intermediates seemed to corroborate a direct formation of enamines from oxazolidinones providing only exchange spectroscopy (EXSY) cross peaks from oxazolidinones to enamines and none from the aldehydes.[23] In addition, initial studies hinted at a nucleophile-assisted enamine formation from oxazolidinones (Fig. 1, V).[31] A nucleophilic ring opening would allow for a water-assisted anti elimination from oxazolidinones and avoid the missing microreversibility of the Seebach–Eschenmoser pathway. Despite the fact that oxazolidinones are also generated *via* iminium ions, all enamine formation pathways via direct deprotonation from oxazolidinones are referred to herein as “oxazolidinone pathways”.

To differentiate between the discussed enamine formation pathways in this work, rates and rate constants of enamine formation were determined experimentally using 1D selective EXSY buildup curves and the initial rate approximation. The presented large number of enamine formation rate constants starting from both *endo*-/*exo*-oxazolidinones, the influence of various additives (L-proline, water, bases, and nucleophiles) on these rate constants, the resulting trends, and the comparison with oxazolidinone isomerization rate constants allow for the first time a detailed experimental insight into the so-far hidden mechanistic relation between enamines and oxazolidinones. These extensive experimental data in combination with theoretical calculations indicate that the enamine is formed via neither E2 elimination nor a nucleophile-assisted pathway from the oxazolidinone but rather via deprotonation of iminium ions.

Results and Discussion

Model System and Methods. As a model system for this mechanistic study of the enamine formation pathway, the L-proline-catalyzed intermolecular aldol reaction of 3-methylbutanal in dimethyl sulfoxide (DMSO)-d_6 with 100% L-proline was chosen (Fig. 2A).

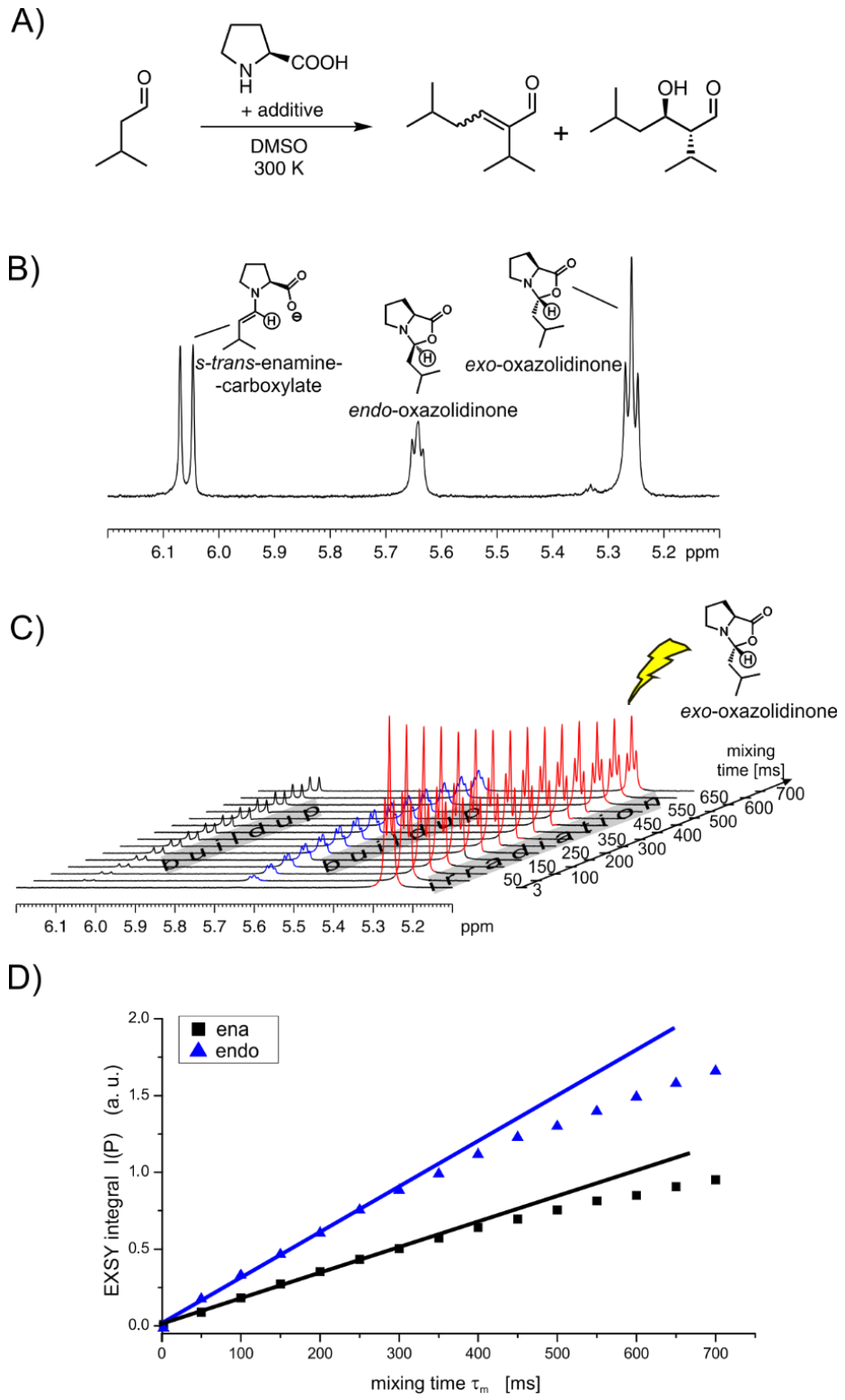

Fig. 2: (A) L-Proline-catalyzed self-aldolization of 3-methylbutanal. (B) Section of the ^{1}H spectrum showing well-separated H1 signals (circles) of the enamine and the two oxazolidinones (sample: L-proline (saturated), 3-methylbutanal (50 mM), DABCO (50 mM) in DMSO-d_6 at 300 K). (C) Stack plot of 1D selective EXSY spectra of this sample (irradiation on H1 of *exo*-oxazolidinone, mixing times 3–700 ms). (D) 1D selective EXSY build-up curves (sample without additives); blue (P = *endo*-oxazolidinone) and black (P = enamine) lines represent the initial slopes ($I_{rm}(P)/\tau_m$) used for the initial rate approximation.

In previous studies, we observed for this system the highest enamine concentration in combination with a slow subsequent aldolization rate. At 300 K, the resulting ^{1}H-spectra show well-separated signals of the H1 protons of the enamine as well as of the *exo*- and *endo*-oxazolidinone (Fig. 2B). In addition, the quite similar signal intensities of all three intermediates are ideal for the investigation of chemical exchange between these three species.[a]

In principle, for such a slow exchange on the NMR time scale, magnetization transfer,[37–44] usually called EXSY (exchange spectroscopy), can be used to determine individual rate constants. In 2D EXSY experiments as previously applied in our enamine studies,[23] the complete exchange matrix can be observed qualitatively within one spectrum. However, the quantitative interpretation of EXSY cross peak ratios used in these studies to differentiate between the reaction pathways requires an iminium isomerization being fast compared to all other processes, which is not the case. In addition, multistep transfers similar to spin diffusion in NOESY spectra hampered a reliable quantitative interpretation (for details, see chapter 2.4.2). Both problems are circumvented in the present study. The determination of direct reaction rate constants in combination with theoretical calculations avoids the mechanistic prerequisites for the application of the EXSY cross peak ratios. The problem of mixed rates due to multistep transfers can be solved by using the initial rate approximation, similar to the nuclear Overhauser effect (NOE).

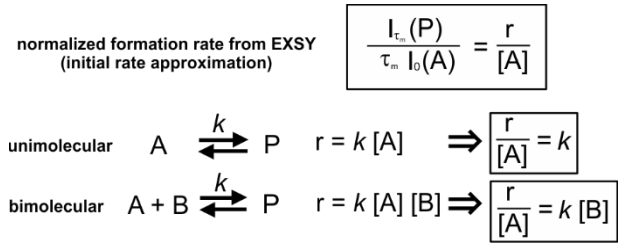

Fig. 3: Normalized formation rate from EXSY spectra using the initial rate approximation corresponds to rate constants for unimolecular reactions and rate constants times the concentration of the reaction partner B in the case of bimolecular reactions. r, rate; k, rate constant; τ_m, mixing time; $I_{\tau m}(P)$, EXSY integral of the product signal (*e.g.*, enamine) at τ_m; A, starting material (irradiated species); P, product (buildup species);$I_0(A)$, EXSY integral of the starting material signal (*endo*- or *exo*-oxazolidinone) at τ_m = 0 s; [A] and [B], equilibrium concentrations of A and B.

Within the initial linear buildup of the exchange signal, the slope of this buildup ($I_{\tau m}(P)/\tau_m$, see Fig. 2D) normalized by the integral of the starting material ($I_0(A)$) is directly correlated to the formation rate of the product (r) divided by the equilibrium concentration of the starting material ([A], see Fig. 3).[44,45] In case the rate-determining step is an unimolecular reaction, the normalized formation rate is equivalent to the rate constant (k). For bimolecular reactions, the normalized formation rate is the

[a] So far no iminium can be detected in our system. Therefore, only oxazolidinones and enamine can be directly investigated.

rate constant multiplied by the equilibrium concentration of the second reaction partner (k[B], Fig. 3). In the following, for the sake of readability, all "normalized rates" are denoted as "rates".

2D EXSY buildup curves are extremely time-consuming and not applicable to one sample in reacting systems. Therefore, in this mechanistic study 1D selective EXSY build-up curves were measured, irradiating selectively the well-separated H1 protons of *endo*-/*exo*-oxazolidinone or enamine. Using very short mixing times, exclusively the irradiated signal is observed (Fig. 2C). After a considerable mixing time, the signals of exchanging molecules appear. With the enamine model system described above, considerable amounts of both intermediates, oxazolidinones and enamines, can be detected. To the best of our knowledge, this allows us for the first time to measure EXSY build-up curves between reaction intermediates. Thus, as an unique feature, this study provides rate constants and reaction orders of the rate-limiting steps between intermediate species and not for the whole reaction pathway. In case several reaction steps are involved between the observed intermediates, the rate-limiting step has to be at least 1 order of magnitude slower than all other steps; otherwise, mixed rates are observed.

Previous studies showed that the presence or addition of extra water does not affect the relative ratios of enamine to oxazolidinones but rather reduces their absolute amounts considerably.[23,46,47] Therefore, dry solvents and starting materials were used for all experiments to obtain optimal signal intensities. Nevertheless, a potential participation of water in the formation pathway of enamines cannot be neglected because in all samples at least 1 equiv of water is present, originating from the condensation reaction of aldehyde and proline to oxazolidinones and enamines. In the following, the reaction rate constants from *exo*-oxazolidinone and *endo*-oxazolidinone to the enamine are discussed. (For data regarding the back reaction from enamine to oxazolidinones, see chapter 2.4.8.) First, we investigated the influence of the amount of L-proline and water on the enamine formation rates. In addition, the effect of various additives with varying basic and nucleophilic properties was tested (1,4-diazabicyclo[2.2.2]octane (DABCO), trimethylamine (TEA), sodium carbonate, and sodium benzenesulfinate). Acidic additives cannot be applied in this experimental setup because proline enamines are not detectable together with hydrogen bond donors (*e.g.*, in MeOH, no enamine ^{1}H-signal can be detected).[23,24]

Participation of Proline, Oxazolidinones, and Water

First, the dependence of the enamine formation rate on the amount of L-proline and water was studied because both are intrinsic components of the reaction. Because the oxazolidinone pathway according to Seebach's proposal (Fig. 1, IV) includes the

participation of a second proline, oxazolidinone, or product as base (E2 elimination), for this pathway it is expected that the enamine formation rate increases with the proline concentration (Fig. 3). In Fig. 4A, the experimentally determined rates of enamine formation from both *endo*-oxazolidinone and *exo*-oxazolidinone are presented. At any L-proline or water concentration investigated in the additive-free case, the rate starting from *endo*-oxazolidinone is smaller than that from *exo*-oxazolidinone.

Upon increasing L-proline concentration, the enamine formation is not accelerated but rather remains constant within the experimental error range with a slightly decreasing trend. Similar results were obtained in acetonitrile (see chapter 2.4.3). This indicates that the rate-determining step of the enamine formation is zero-order in L-proline (unimolecular; r/[A] =k). Our current and previous[23] NMR studies also showed that at higher L-proline concentrations the amount of the two oxazolidinones increases directly proportionally (see chapter 2.4.10). Therefore, the rather constant enamine formation rates also exclude the involvement of a second oxazolidinone in the enamine formation pathway (zero-order in oxazolidinone). Thus, Seebach's E2 elimination pathway from oxazolidinone (Figure 1, IV) with either proline or oxazolidinone as external base is not supported by our data. Another possibility would be an aldol product or oxazolidinone product as external base in pathway IV. In this case, an induction period of enamine and product formation would be expected from an autocatalytic process. However, in none of our enamine aldol studies[23,25] was such an induction period observed. An adduct of L-proline and oxazolidinone or of two oxazolidinones as reaction intermediates and a subsequent E1 elimination cannot be excluded by these experimental data because the rate-limiting step would be again zero-order in proline. However, theoretical calculations of potential adduct complexes and subsequent E1 eliminations suggest that such processes are extremely unfavorable under synthesis conditions (see chapter 2.4.17). Thus, the experiments exclude all enamine formation pathways that are first-order in proline or oxazolidinones under synthesis conditions in DMSO and acetonitrile. Theoretical calculations suggest that pathways starting from proline/oxazolidinone adducts which would be zero-order in proline or oxazolidinone are highly unlikely.

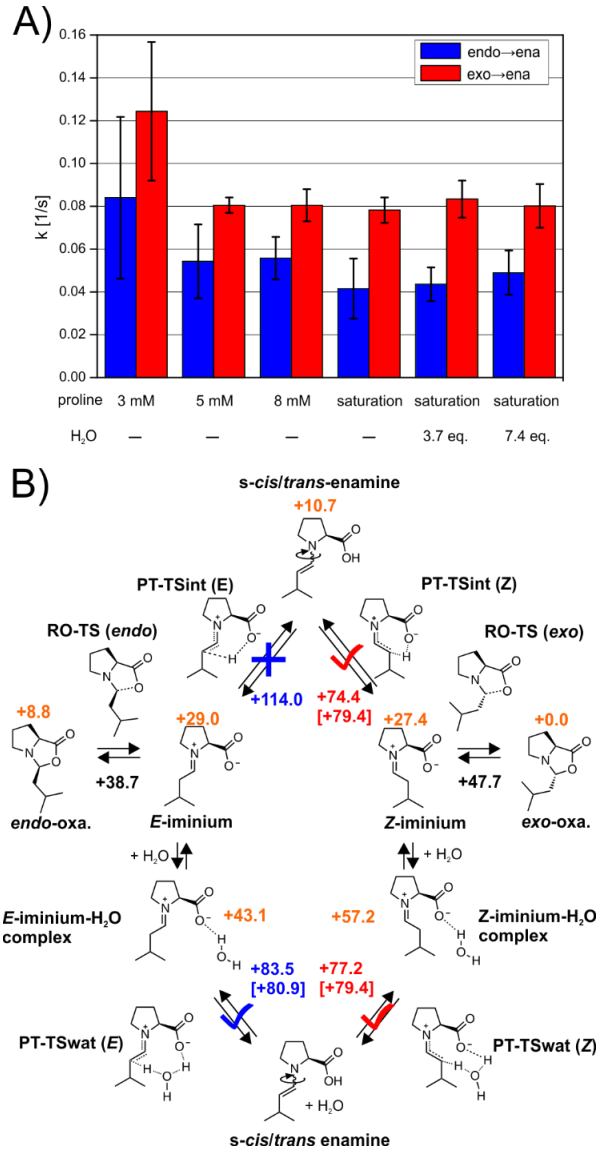

Fig. 4: (A) Enamine formation rate constants from *endo*-/*exo* oxazolidinone dependent on L-proline and external water amount (sample: 50 mM 3-methylbutanal in DMSO-d_6 at 300 K). (B) Summary of calculated free energy barriers $\Delta G^{\ddagger}_{298}$ (kJ mol^{-1}) (ring opening and proton transfer) and thermodynamics stability (orange; referenced to *exo*-oxazolidinone) using a cluster continuum model at CCSD(T)/CBS level of theory in DMSO. For the CBS extrapolation procedure, please refer to chapter 2.4.18. The experimental values are shown in brackets.

Next, the influence of increasing amounts of water was investigated. The addition of external water does not significantly affect the rates of enamine formation from *exo*/*endo*-oxazolidinone (Fig. 4A), indicating again zero-order in water for this step.

In addition, we determined the enamine formation and the oxazolidinone isomerization rate constants for the linear aldehyde 3-phenylpropanal in the additive-free case in DMSO (approximately 0.5 equiv of water). The results are very similar; therefore, the influence of the aldehyde structure is assumed to be minor. (For more details also concerning additional results in acetonitrile, please refer to chapter 2.4.12 and chapter 2.4.3.)

Theoretical Calculation of the Enamine Formation

To translate these experimental data into mechanistic enamine formation pathways, various theoretical calculations of potential enamine formation pathways were carried out and compared to the experimentally determined rate constants. The low stability of iminium and enamine has been reported by Houk and Blackmond as the major problem in predicting the experimental reactant/product distribution (oxazolidinone/enamine).[48] In this case, the inclusion of an explicit solvent molecule in the model is becoming compulsory to cover the missing interaction between solvent and solute. This is also confirmed by our present study. At least one solvent molecule is needed to predict the enamine/oxazolidinone ratio and, as shown later, the barrier heights correctly. (For the data regarding the discussion of solvent molecule and the simulation without explicit solvent, refer chapter 2.4.17.) Therefore, calculations with a cluster continuum model[49–51] were carried out.

The contribution of additional L-proline or oxazolidinone in bimolecular mechanisms was excluded experimentally and therefore omitted in the theoretical calculations. Our previous EXSY studies suggested a nucleophile-assisted enamine formation from oxazolidinone (Fig. 1, V).[31] Therefore, we tried to simulate the ring opening of oxazolidinone by DABCO as nucleophile/base together with a simultaneous α-proton transfer to the carboxylate group and a subsequent dissociation of the nucleophile. Furthermore, we also tried to abstract the α-proton by DABCO and to locate an E2 elimination transition state as proposed by Seebach (Fig. 1, IV). However, all attempts to locate any transition state lead to either iminium–nucleophile adducts or oxazolidinones. The only transition state found stems from the addition of a nucleophile to the iminium ion after the ring opening of the oxazolidinone facilitating the *E*-/*Z*-iminium isomerization. As shown later, this is corroborated by the experimental data, which show that nucleophiles accelerate the *exo*-/*endo*-oxazolidinone exchange rate but not the enamine formation rates (see below and chapter 2.4.5.). Therefore, the Houk–List pathway was recalculated on a refined level of theory (Fig. 4B) and compared to the experimental rate constants (Fig. 4A).

Our calculations showed that in the Houk–List pathway the *endo*-oxazolidinone is exclusively connected with the *E*-iminium and the *exo*-oxazolidinone with the *Z*-iminium (Fig. 4B) which is consistent with previous calculations of Sharma and Sunoj.[35] Without water, the activation barrier of the subsequent internal deprotonation step from *Z*-iminium to enamine is calculated to be +74.4 kJ mol^{-1} compared to +114 kJ mol^{-1} when starting from *E*-iminium. Rather, this higher activation barrier (by approximately 40 kJ mol^{-1}) from *E*-iminium is due to the unfavorable geometry of the transition state. In case of a water-assisted deprotonation step, the situation changes. Now the activation barrier starting from an *E*-iminium water complex is

considerably lower (+83.5 kJ mol^{-1}) than in the water-free pathway. In the case of deprotonation from *Z*-iminium *via* water, the barrier is only marginally higher (+77.2 kJ mol^{-1}) than that in the internal deprotonation. Qualitatively, these two preferred pathways are in agreement with the previous calculations of Sunoj and Sharma using a smaller model in the gas phase and a lower level of theory (ΔG_{298} B3LYP/6-31G**).[35] As expected, the change of phase (gas phase to condensed phase) and theoretical model in our present work led to three significant differences. First, the ring-opening barriers in the study of Sunoj and Sharma are rather high (+53.6 kJ mol^{-1} (*endo*) and +73.6 kJ mol^{-1} (*exo*)) compared to ours (+38.7 kJ mol^{-1} (*endo*) and + 47.4 kJ mol^{-1} (*exo*)) most probably because of the fact that they did not include solvent effects in their calculation. (See chapter 2.4.17 for further discussion.) Second, the energy barrier for the water-assisted deprotonation from *E*- and *Z*-iminium are very similar in the gas phase at the DFT level of theory (differing by 2.5 kJ mol^{-1}) and quite low (+53.6 kJ mol^{-1} for *E*-iminium and +51.1 kJ mol^{-1} for *Z*-iminium). In our calculation, the difference amounts to 6.3 kJ mol^{-1}, and the barriers are significantly higher (Fig. 4B). Again, this is an artifact from the gas-phase calculation. As stated in their supporting information, the solvent correction in acetonitrile leads to an increase of barrier height by ~40 kJ mol^{-1} for both *E*–/*Z*–iminium–enamine transition states, which would approach our predicted values. Third, although it does not have a significant impact, we also notice here that the energy barrier difference between *Z*-iminium and *E*-iminium for the water-free pathway is slightly higher (+54.0 kJ mol^{-1}) in their calculation than in our present data (+39.6 kJ mol^{-1}).

Next, the experimentally determined rate constants were converted into activation barriers and compared to our theoretical calculation. (For details, see chapter 2.4.19.) The activation barriers for the ring-opening processes are at least 20 kJ mol^{-1} lower than those of the deprotonation processes from iminium ions to enamines. This translates to several orders of magnitude difference in rate constants. Hence, the experimental rate constants correspond exclusively to the barrier of the deprotonation process. The experimental conditions being closest to those of our theoretical calculations (one L-proline, one aldehyde, and one water molecule) are those at saturation with L-proline and without additional water. For this sample, an activation barrier of +79.4 kJ mol^{-1} is experimentally determined starting from *Z*-iminium and of +80.9 kJ mol^{-1} starting from *E*-iminium. This is qualitatively and quantitatively in good agreement with our theoretical data for the internal deprotonation from *Z*-iminium as well as with that of the water-assisted deprotonation from both *E*-and *Z*-iminium (numbers in Fig. 4B). Considering the absence and the presence of water in the three pathways of the lowest transition states, at first glance one would

expect that increasing amounts of water would affect these pathways differently. However, the experimental data show that the rate-determining steps of all pathways are zero-order in water. (See Fig. 4A and discussion above.) That is directly obvious for the water free pathway starting from *Z*-iminium. For the water-assisted pathways starting from *E*-and *Z*-iminium, the theoretical data suggest the formation of an intermediate consisting of iminium and water, followed by a deprotonation step that is zero-order in water because the reference iminium intermediate already includes water. Thus, from the experimental data the assistance of water cannot be directly deduced, but the measured rate constants are in agreement with the most preferred pathways from theoretical calculations.

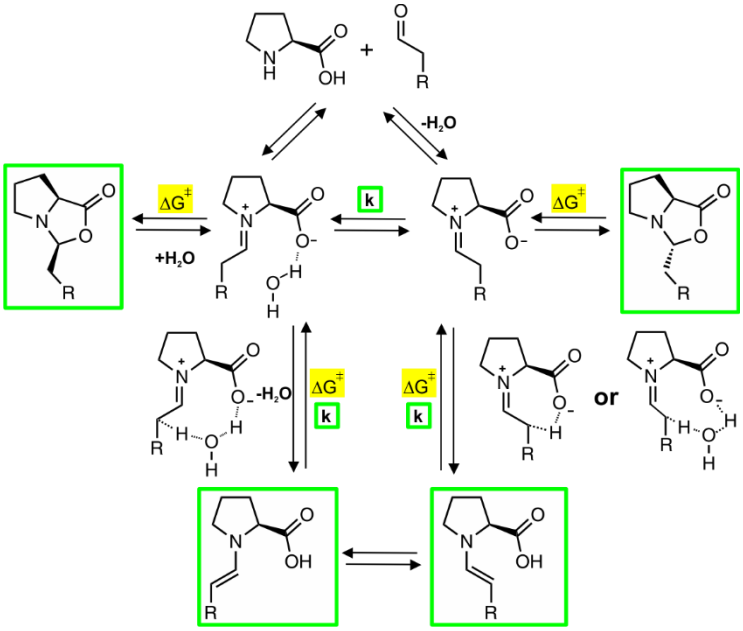

Fig. 5: Summary of enamine formation without additives for R=C_3H_7 and phenyl in DMSO. The experimentally measured intermediates and rate constants are highlighted in green, and the calculated activation barriers are highlighted in yellow.

A summary of the active enamine formation pathways without additives is shown in Fig. 5. Without additives, the dominant process is the proton transfer from *Z*-iminium, which is connected with the *exo*-oxazolidinone. The water-assisted deprotonation of *E*-iminium is also observed but at a slower rate.

Influence of Basic Additives

Next, the influence of basic additives (DABCO, TEA, sodium carbonate and sodium benzenesulfinate) was measured to elucidate a potential correlation between enamine formation rates and basicity. However, not all pK_{aH} values of the additives are known in DMSO. Therefore, an internal basicity scale was created. Our previous enamine study with basic additives showed that the amount of enamine increases at the expense of oxazolidinone with increasing basicity of the additive.[24] Therefore,

the ratio of enamine to total intermediate concentration was used as a measure for the internal basicity in DMSO. The results showed an increasing basicity from sodium benzenesulfinate over TEA and DABCO to sodium carbonate. (For data and details, see chapter 2.4.4.)

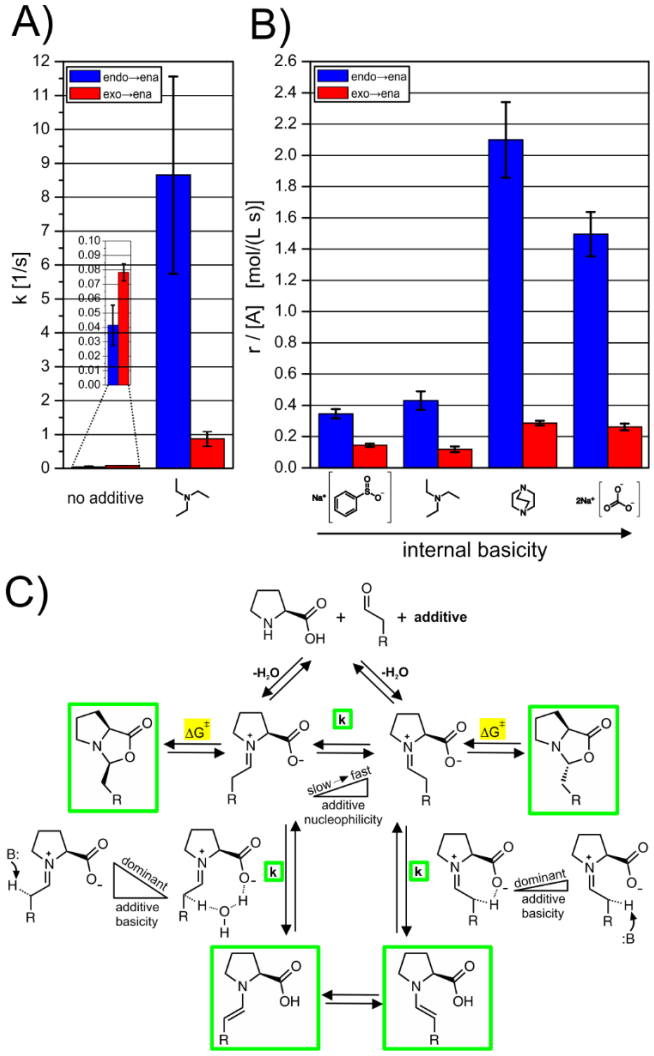

Fig. 6: (A) The enamine formation rate constants drastically increase with the addition of the basic additive TEA, whereas the relative rate constants from *endo*- and *exo*-oxazolidinone invert. (B) The enamine formation rates increase with the basicity of the additives. Additives invert the relative rates from *endo*- and *exo*-oxazolidinones and accelerate especially those from *endo*-oxazolidinone (sample: L-proline (saturated), 3-methylbutanal (50 mM), additive (50 mM, for sodium carbonate: saturated solution) in DMSO-d_6 at 300 K). (C) Summary of enamine formation pathways in the presence of additives. Basic additives accelerate strongly the deprotonation from *E*-iminium but only slightly that from *Z*-iminium. Nucleophiles accelerate the *E*-/*Z*-iminium isomerization.

In contrast to the measurements with varying water and proline concentrations, the rate of enamine formation is dependent on the concentration of the additives. This indicates that the rate-limiting deprotonation step is bimolecular (participation of starting molecule and base). (See Fig. 3 bimolecular and chapter 2.4.15 for details.) In Fig. 6A, the rate constants for the additive-free sample and those with TEA are

given. Upon addition of TEA, the rate constant of enamine formation increases drastically, and the relative order of enamine formation rate constants starting from *endo*- and *exo*-oxazolidinones are inverted. In Fig. 6B, the normalized rates for all additives (50 mM) as well as their correlation with the internal basicity scale are presented. All additives show high enamine formation rates starting from *endo*-oxazolidinone. In contrast, the rates starting from *exo*-oxazolidinone are much lower. Overall, both trends follow the relative internal basicity of the additives but with different slopes. One exception is sodium carbonate, which shows a considerably lower enamine formation rate from *endo*-oxazolidinone than from DABCO.[b] Another striking change is the general switch of the relative rate constants and rates starting from *endo*-oxazolidinones and *exo*-oxazolidinones, respectively. Without basic/nucleophilic additives, the rate constants from *endo*-oxazolidinone are smaller than those from *exo*-oxazolidinone (Fig. 4A and Fig. 6A, first entry). With basic/nucleophilic additives, the situation is inverted; in all cases, the rate constants (Fig. 6A, second entry) and rates (Fig. 6B) from *endo*-oxazolidinone are significantly larger than those from *exo*-oxazolidinone. These experimental data fit to the theoretical calculations shown in Fig. 4B with additional pathways of *E*- and *Z*-iminium deprotonation by external bases (Fig. 6C). The rapid increase of the rate constant and rates from *endo*-oxazolidinone indicates that external bases can easily deprotonate the *E*-iminium. For *exo*-oxazolidinone, the slope with increasing basicity is significantly lower, which can be explained by steric hindrance and electrostatic repulsion between the base and the carboxylate moiety in the case of the *Z*-iminium.

External bases potentially could also deprotonate the oxazolidinones directly as previously proposed by Seebach *et al.*[20] *Endo*-oxazolidinones are well-known to be sterically more congested than the corresponding *exo*-oxazolidinones. However, for the proposed E2 *anti* elimination not the internal steric hindrance but rather the steric hindrance of one of the two α-protons in *anti*-conformation to the oxazolidinone CO bond has to be considered. Nevertheless, the structures of *endo*-and *exo*-oxazolidinones do not exhibit significant differences in the steric hindrance of these α-protons (chapter 2.4.11). Thus, steric arguments of the oxazolidinones cannot explain the very different behavior of enamine formation rates from *endo*- and *exo*-oxazolidinones with increasing basicity. This excludes the direct deprotonation of oxazolidinones (Fig. 1, IV) as a major pathway in the presence of bases.

[b] Most probably this is due to the bad solubility of sodium carbonate in DMSO. The amount of sodium carbonate dissolved is much lower than that in the other additive samples. Therefore, the enamine formation rates are not as high as expected from its internal basicity.

Influence of Nucleophilic Additives

Next, a correlation of the enamine formation rates toward Mayr's nucleophilicity scale[53] was considered. Benzenesulfinate shows hardly any basicity, but it is a very strong S nucleophile (N-value of 19.6 in DMSO). For the tertiary amine bases DABCO and TEA, only N-values in acetonitrile are available, which are considerably lower (18.8 and 17.1, respectively). The experimental enamine formation rates from both oxazolidinones are significantly lower for benzenesulfinate than for DABCO (Fig. 6B), which supports the discussion above, *i.e.*, that not the nucleophilicity but rather the basicity of the additive is crucial for the enamine formation rate constants. These results exclude pathway V (see Fig. 1), *i.e.*, a nucleophile-assisted anti elimination of oxazolidinones leading to enamines as a major formation pathway in DMSO.

However, another effect of additional nucleophiles was observed experimentally: the accelerated exchange between *exo*-oxazolidinones and *endo*-oxazolidinones. (For details, see chapter 2.4.5.)

Conclusion

Detailed experimental enamine formation rate constants and rates from both *endo*-oxazolidinone and *exo*-oxazolidinone are presented. Their dependence on the addition of L-proline, water, and additives with various basic and nucleophilic properties was investigated. The mechanistic interpretation of these data is confirmed by higher level theoretical calculations of the enamine formation pathway. First, the enamine formation is zero-order in proline and oxazolidinones, which excludes the Seebach pathway V proposing an E2 deprotonation of oxazolidinones. Prereacting oxazolidinone–proline complexes undergoing E1 elimination cannot be excluded experimentally but are highly unlikely according to theoretical calculations. Without additives, the fastest process is the proton transfer from *Z*-iminium (pathways I + II from *exo*-oxazolidinone*),* whereas the deprotonation of E-iminium follows the water-assisted pathway II (from *endo*-oxazolidinone) at a slower rate. Basic additives change the situation considerably. Now, the deprotonation *via* an external base is preferred (pathway III). The acceleration of the enamine formation is significantly more pronounced for *E*-iminium (from *endo*-oxazolidinone) than for *Z*-iminium (from *exo*-oxazolidinone) and correlates to the basicity of the additive. These trends are in agreement with the steric and electronic properties of the iminium intermediates (pathways I, II, and III) but not with those of the oxazolidinones (exclusion of pathway IV with basic additives). The nucleophilicity of the additives influences only the isomerization rates of the two oxazolidinones but not the enamine formation rates. This excludes a nucleophile-assisted anti elimination of oxazolidinones as a major enamine formation pathway (pathway V). Thus, the first kinetic data of

enamine formation together with theoretical calculations reveal that enamines are most likely formed *via* deprotonation of iminium intermediates (Houk–List pathway) in DMSO. The dominant pathway varies according to the experimental conditions, *e.g.*, the presence and strength of a basic additive.

Computational Details

The geometry of all systems was optimized in the gas phase at TPSS-D3/aug-SVP level of theory (Ahlrichs SVP[54,55] augmented with diffuse function from aug-cc-VDZ[56,57]) corrected with empirical dispersion from Grimme.[58,59] Harmonic vibrational frequency and thermochemical correction were carried out at the geometry optimization level. Single point calculations were done at domain-based local pair natural orbital (DLPNO)–coupled cluster singles doubles with triples from perturbation theory (CCSD(T))/complete basis set (CBS)[60,61] using density fitting (Split-RI-J) and semi-numerical approximation for the exchange term (RIJCOSX) for the reference wave function[62–64] and DLPNO approximation for the post-HF part. Two-point extrapolation technique to approach CBS was used using def2-QZVPP and def2-TZVPP basis sets as implemented in ORCA.[65,66] The solvent correction ΔG_{solv} was calculated at TPSS-D3/aug-TZVP (Ahlrichs TZVP[54,55] augmented with diffuse function from aug-cc-VDZ[56,57]) using COSMO model in DMSO and subsequently added to the single-point energy.[67,68] The software used was ORCA-3.0.3. The extrapolation procedure, energies, and structures are provided in chapter 2.4.20.

Acknowledgments

We gratefully acknowledge financial support from the DFG, grant GS 13/4-1. We thank Dr. Markus Schmid for the initial NMR investigations leading to the proposal of the nucleophile assisted deprotonation pathway from oxazolidinones. We also thank the Leibniz Rechenzentrum for providing computational facility.

2.3 Additions

The first EXSY-buildup studies between enamines and oxazolidinones were performed by Markus Schmid (Schmid, M. B. Ph. D. Thesis, University of Regensburg, Regensburg-Germany, January 2011). Using the identical model system, similar additives and excitation on enamines instead of oxazolidinones but not the initial rate approximation this EXSY study led to the proposal of the nucleophile assisted deprotonation pathway from oxazolidinones cited in the manuscript and mentioned in the acknowledgement.

During our NMR study we were made aware of a kinetic isotope effect (KIE) study by Vetticatt *et al.* (M. A. Ashley, J. S. Hirschi, J. A. Izzo, and M. J. Vetticatt, JACS **2016**; DOI: 10.1021/jacs.5b10876) probing the enamine formation in L-proline catalyzed α-amination (using DEAD) of 3-phenylpropanal in acetonitrile. Combining ^{13}C-, ^{2}H-KIEs and theoretical calculations they propose a direct enamine formation from oxazolidinones catalyzed by a bifunctional base. This is in direct conflict with our results in DMSO. Therefore, we determined the enamine formation and the oxazolidinone isomerization rate constants for the linear aldehyde 3-phenylpropanal in the additive free case in DMSO (approx. 0.5 equiv water). The results are very similar and therefore the influence of the aldehyde structure is assumed to be minor (for more details also concerning additional results in acetonitrile please refer to chapter 2.4.12 and chapter 2.4.3). Additional NMR experiments in acetonitrile (the lower enamine amount allows only a limited access to kinetic data, see chapter 2.4.3) showed for the *exo*-oxazolidinone similar trends as in DMSO. The apparent discrepancy between our NMR study and the KIE study by Vetticatt *et al.* may be attributed to the different solvents (supporting deviating proline interactions) and the presence or absence of a strong electrophile. Also the application of basic additives in our system (see chapter 2.2) shows that the enamine pathway can be modulated by variations of the experimental conditions. Overall the results of the two studies both based on experimental as well as theoretical data give a very valuable insight into the variability of reactions mechanisms depending on the reaction conditions.

2.4 Supporting Information

2.4.1 Experimental Details

Organocatalytic reactions were conducted inside a standard 5 mm NMR tube prepared inside a glove box by adding 30 mmol aldehyde (distilled and stored over 3 Å molecular sieve) to a suspension of 30 mmol (100 mol%) L-proline and 30 mmol additive in 0.6 mL DMSO-d_6. The NMR tube was transferred to the spectrometer immediately after starting the reaction.

NMR spectra were recorded at 300 K on a Bruker Avance DRX 600 (600.13 MHz) and on a Bruker Avance III 600 (600.25 MHz) spectrometer, the latter equipped with a TCI cryoprobe with z-gradient. For the EXSY spectra mixing times from 2.4 ms to 700 ms were used. NMR data was processed and evaluated with Bruker´s TOPSPIN 3.2 pl 1.

2.4.2 Tripping Hazards Interpreting 2D EXSY Crosspeak Ratios

In the senior authors work in 2010[23] ratios of 2D EXSY crosspeaks have been used to support a direct conversion of the oxazolidinone into the enamine and to exclude an iminium based mechanism. The basic idea was to use ratios of crosspeaks to gain insight into the reaction mechanism without having direct spectroscopic access to a potential intermediate. This method is valid and sound in case of one central non detectable intermediate. In case of two connected intermediates such as the *E*- and *Z*-iminium intermediates, this idea is also applicable but only under the special requirement that the two not detectable iminium intermediates are exchanging fast with each other and slow with all other products, intermediates or molecules. In the previous publication that was assumed to be the case. However, the actual calculations showed that in the enamine mechanism the inverse situation is active. The ring-opening of the oxazolidinones is fast compared to the isomerization of the iminium intermediates. As a result the fast exchange between the two oxazolidinones (including the iminium intermediates) and the slow exchange to the other products/intermediates should always gain similar values and no differentiation between the oxazolidinone and the iminium pathway should be possible.

In order to find the source of error producing deviating values, we reproduced all of our former values and checked every exchange ratio. We noticed one exception from the assumption that all oxazolidinone or iminium isomerization rates are at least one order of magnitude higher than the enamine or aldehyde formation rates: the *exo*-oxazolidinone – enamine rate was only 5 times smaller than the oxazolidinone isomerization rate. This caused mixed rates and produced the published deviations of the EXSY cross peak ratios, which were misinterpreted as oxazolidinone pathway. However, even without these mixed rates from reaction kinetics, the EXSY mixing

times have to be within the linear buildup. Otherwise again mixed rates (now due to spin diffusion) may be generated. In the previous work using another model system with small intermediate intensities, a mixing time of 700 ms had to be applied. Our current data shows that this was definitely outside of the linear EXSY buildup and indeed cross peaks including indirect transfers were measured. A combination of both problems led to the deviating EXSY cross peak ratios hinting at an oxazolidinone pathway.

Now we are fully aware of the two problems and with the new model system and the adapted EXSY methods both problems can be avoided. However, in the case of sulfinate (fast oxazolidinone exchange, slow enamine formation) and within the linear build-up of the EXSY curves no aldehyde signals were detected. Therefore, the previous model cannot be cross checked with our refined kinetic data.

2.4.3 Solvent Effects in Acetonitrile

In order to test the influence of solvent effects the sample 3-phenylpropanal (50 mM), L-proline was investigated additionally in acetonitrile. In acetonitrile the amount of enamine is very low. Therefore, 1D selective EXSY build-up curves from oxazolidinones to enamines are extremely challenging. Due to the very low signal intensities, EXSY build-up curves for the lower populated *endo*-oxazolidinone isomer are not accessible. For the higher populated *exo*-oxazolidinone we determined rate constants at three different L-proline amounts in solution. Since low solubility of L-proline hampers the reliability of a stock solution approach, L-proline amounts are referenced relatively to each other by the sum of ^{1}H-integrals of free proline, *endo*-/*exo*-oxazolidinone and enamine.

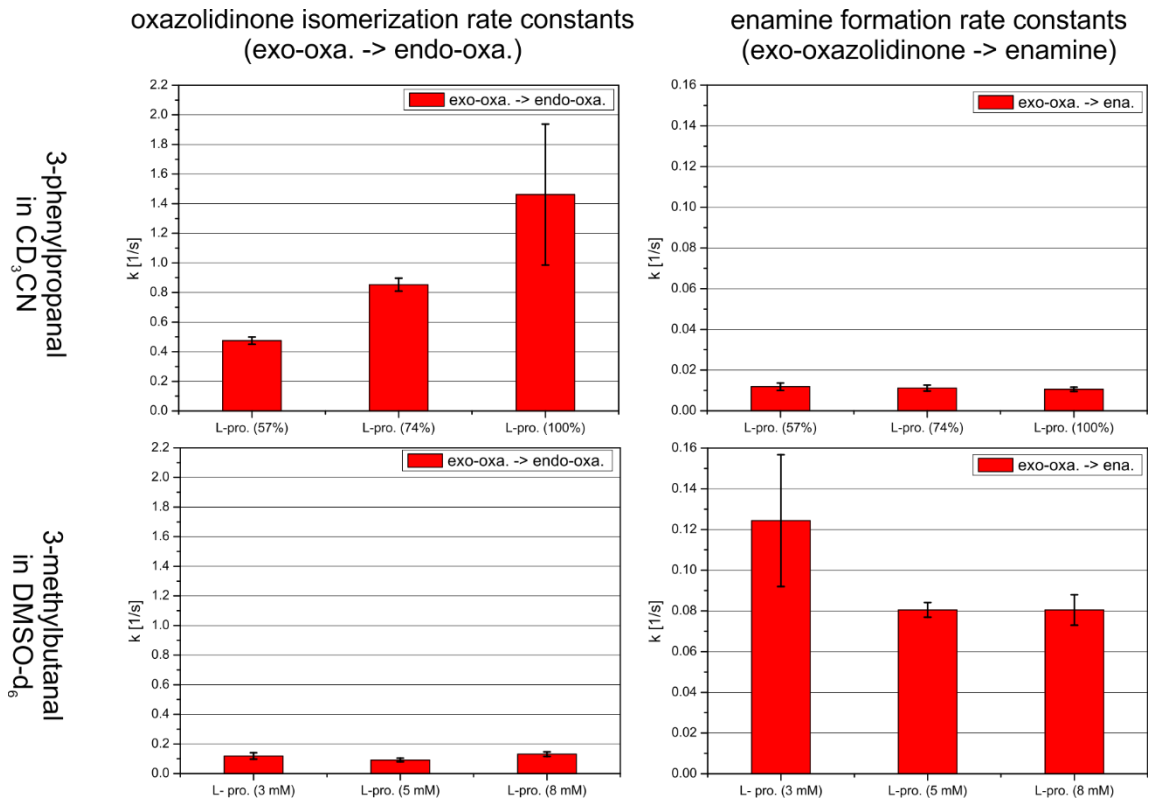

Fig. 7: Rate constants of enamine formation (right row) oxazolidinone isomerization (left row) starting from exo-oxazolidinone. Sample top: L-proline (relative amount as shown), 3-phenylpropanal (50 mM) in acetonitrile-d_3. Sample bottom: L-proline (concentration as shown), 3-methylbutanal (50 mM) in DMSO-d_6.

In contrast to the situation in DMSO, where additional L-proline does not further act as a base accelerating the enamine formation (Fig. 7, bottom right-hand side) or as a nucleophile accelerating the oxazolidinone isomerization (Fig. 7, bottom left-hand side), the situation in acetonitrile is changing.

The oxazolidinone isomerization rate increases from 57% L-proline to 100% L-proline up to a value of 1.46 s^{-1} (Fig. 7, top left). In contrast to the situation in DMSO, this indicates that in acetonitrile L-proline is acting as a strong nucleophile (O or N nucleophilicity of around 18 for proline carboxylate and pyrrolidine on the Mayr nucleophilicity scale) during the oxazolidinone isomerization process. In addition, the downfield shift of the ^{1}H signal of the α-proton of L-proline (4.16 ppm, exclusively L-proline in acetonitrile: 3.87 ppm) indicates a partial protonation of the L-proline nitrogen in acetonitrile. (A full protonation of the L-proline nitrogen by the addition of 100 mol% phosphoric acid in DMSO leads to a downfield shift of the α-proton from 3.61 ppm to 4.30 ppm)

The enamine formation rate in acetonitrile is considerably lower than in DMSO but also shows no increase upon higher L-proline concentrations (Fig. 7, top right-hand side). This indicates that also in acetonitrile the rate determining step of the enamine formation from *exo*-oxazolidinone is zero order in L-proline.

Both effects differing from the situation in DMSO, *i.e.* the accelerated oxazolidinone isomerization as well as the higher enamine formation rate without additives in acetonitrile might be connected to the fact that L-proline is dissolved as a neutral Dimer in DMSO.[31] Since, rate constants from *endo*-oxazolidinone are so far not accessible in acetonitrile, we cannot exclude the involvement of additional L-proline in the rate determining step of enamine formation starting from *endo*-oxazolidinone.

2.4.4 Internal Basicity Scale

The increasing enamine ratio of the additive series sodium benzenesulfinate, TEA, DABCO and sodium carbonate correlates with the pk_{aH} values except for the inversion of DABCO and TEA which we ascribe to the difference of the solvent (to our knowledge no literature pk_{aH} values exist for DABCO and sodium carbonate in DMSO). In the previous work we have shown that the basicity of additives and the amount of enamine is correlating.[24] Therefore we suggest the application of the amount of the generated enamine as a qualitative, internal measure for the basicity of the used additives in DMSO (see Fig. 8, right-hand side).

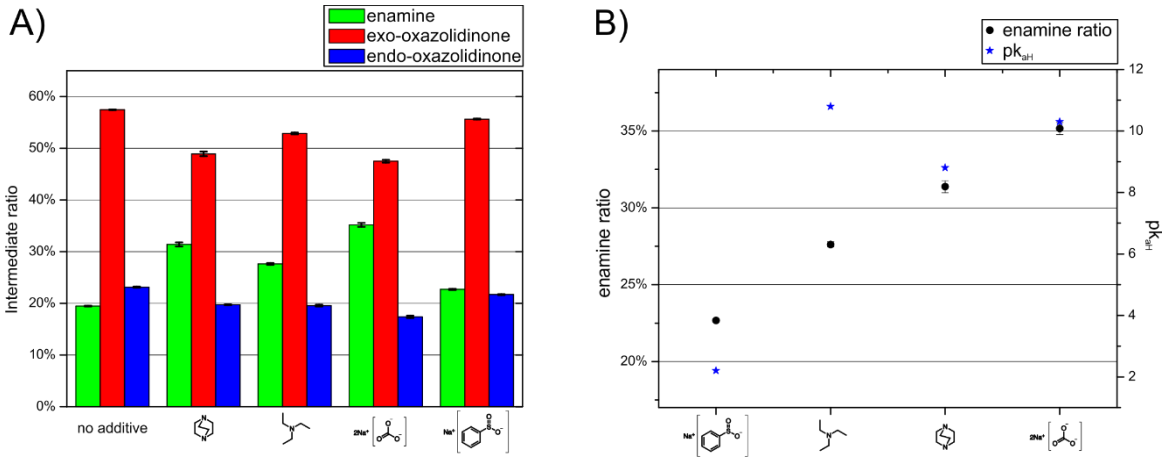

Fig. 8: Decent differences in the intermediate distribution are shown in A) where quasi thermodynamic equilibrium intermediate ratios in dependency of used additives are depicted. The *exo*-oxazolidinone to *endo*-oxazolidinone ratio is roughly constant at about 2.5 to 1.0. Sample: L-proline (saturated), 3-methylbutanal (50 mM), additive (50 mM, for sodium carbonate: saturated solution) in DMSO-d_6 at 300 K. B) Literature pk_{aH} values[69–72] in water and the enamine ratios in DMSO-d_6 during the self-condensation reaction.

2.4.5 Influence of Additive Nucleophilicity

Since nucleophilicity parameters (Mayr's nucleophilicity scale[53]) are not available for all tested additives in DMSO, we propose the normalized oxazolidinone isomerization rates as an internal nucleophilicity scale. We assume that the oxazolidinone isomerization process consists of C-O bond cleavage to the iminium followed by the rate determining nucleophile catalyzed rotation around the iminium double bond and subsequent ring closure to the second oxazolidinone isomer. This would mean that the normalized oxazolidinone isomerization rates can be used as a relative internal nucleophilicity scale for the studied additives.

In Fig. 9 the effect of nucleophilic additives on the normalized isomerization rates of the oxazolidinones (A) and on the enamine formation rates (B) is presented, again obtained applying the initial rate approximation to experimental 1D EXSY build-up curves. The normalized isomerization rates starting from both oxazolidinones increase in the row TEA, DABCO, sodium carbonate and sodium benzenesulfinate, following (insofar as data exists) Mayr's nucleophilicity scale. The enamine formation rates clearly do not show a correlation with the nucleophilicity of the additive.

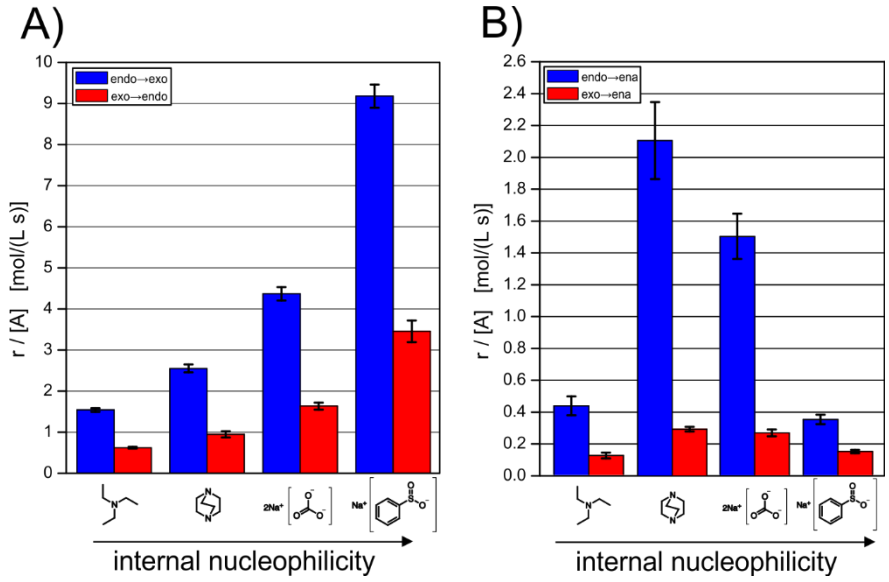

Fig. 9: Normalized rates of the A) oxazolidinone isomerization process B) enamine formation in dependence of applied additives, ordered by increasing nucleophilicity. (Sample: L-proline (saturated), 3-methylbutanal (50 mM), additive (50 mM, for sodium carbonate: saturated solution) in DMSO-d_6 at 300 K).

These additional experimental data corroborate our relative activation barriers calculated for the iminium and the enamine formation. Under any experimental conditions the normalized oxazolidinone isomerization rates are significantly larger than the normalized enamine formation rates. This is in agreement with our theoretical calculations that not the iminium formation but the enamine formation is the rate

determining step in DMSO. The isomerization equilibrium between the oxazolidinones can be used to validate our initial rate approximation approach (see chapter 2.4.8). In this equilibrium, the normalized rates multiplied with the concentration of the irradiated oxazolidinone should be equal in both directions, which was found to be valid for all data sets within the experimental error.

Theoretical data for the influence of nucleophiles. As expected from chemical considerations, also theoretical calculations revealed a significant reduction of the isomerization barrier between *E*- and *Z*-iminium intermediates using OH^- as nucleophile and transforming the iminium double bond into a hydroxylamine single bond. A calculation of rotational transition state of the addition product hydroxylamine carboxylate has been performed at SCS-MP2/CBS level of theory in DMSO continuum (see Fig. 10). The results clearly showed that the rotational barrier is tremendously reduced (typical rotational barrier of N(sp^2)-center is about 60 to 80 kJ/mol)

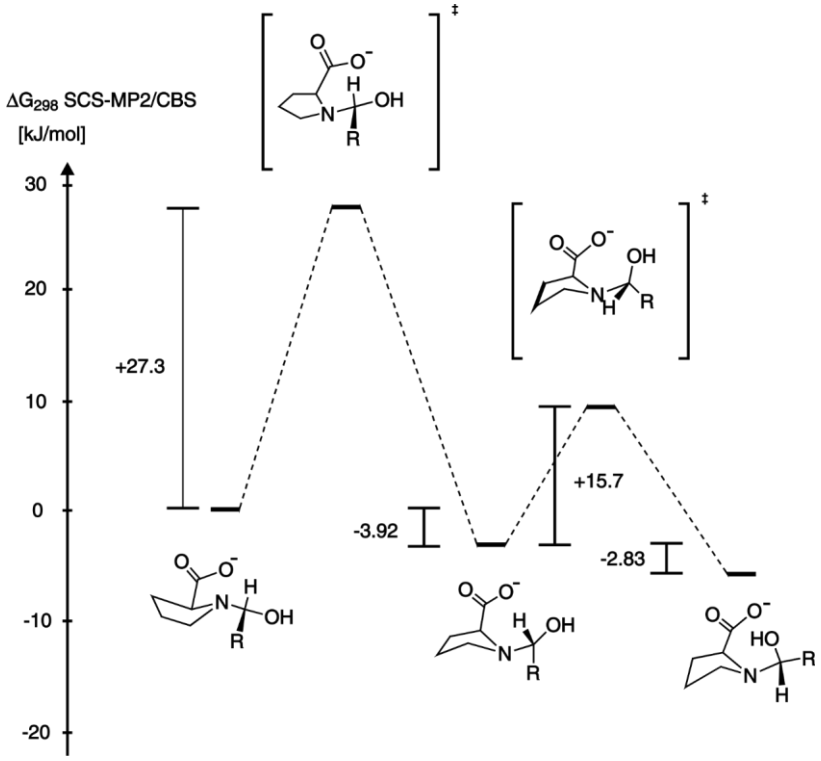

Fig. 10: Rotational barrier (second barrier) of S,R-hydroxylamine carboxylate at SCS-MP2/CBS level of theory. R=C_3H_7

2.4.6 EXSY Buildup Curves

A requirement for the calculation of exact rate constants and normalized rates from EXSY integrals according to the initial rate approximation is the linearity of the build-up at the used mixing time. Therefore buildup curves have been generated for mixing times from 2.4 ms to 700 ms by subsequent acquisition of 1D EXSY experi-

ments for each mixing time and integration of the *endo*-oxazolidinone, *exo*-oxazolidinone and enamine resonances. A linear fit function was applied for the first data points in the linear area. For some samples and some resonances (no additive *endo*-oxa., TEA *endo*-oxa., 3 mM L-proline *exo*-oxa., L-proline *endo*-oxa., 8 mM L-proline *endo*-oxa., 3.7 equiv water *endo*-oxa., 3-phenylpropanal in DMSO-d_6 *exo*-oxa.) the very first data point was not used because it was clearly outside of the linear area. The EXSY integrals for the mixing times 50 ms and 0 ms were calculated from the fit functions and used for calculation of rate constants and normalized rates. All generated EXSY build-up curves are shown below.

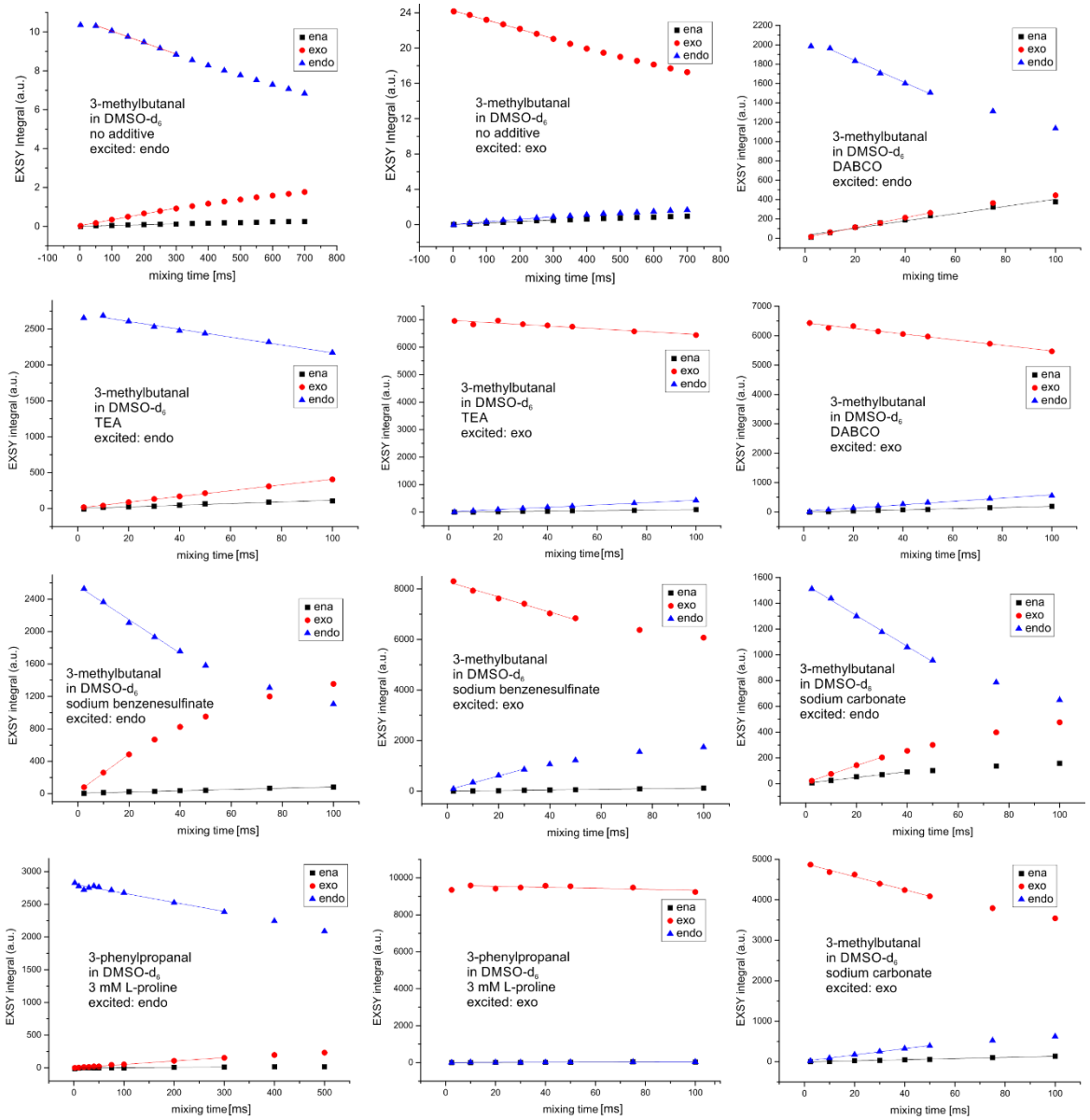

Fig. 11: Selective 1D EXSY build-up curves 1/3.

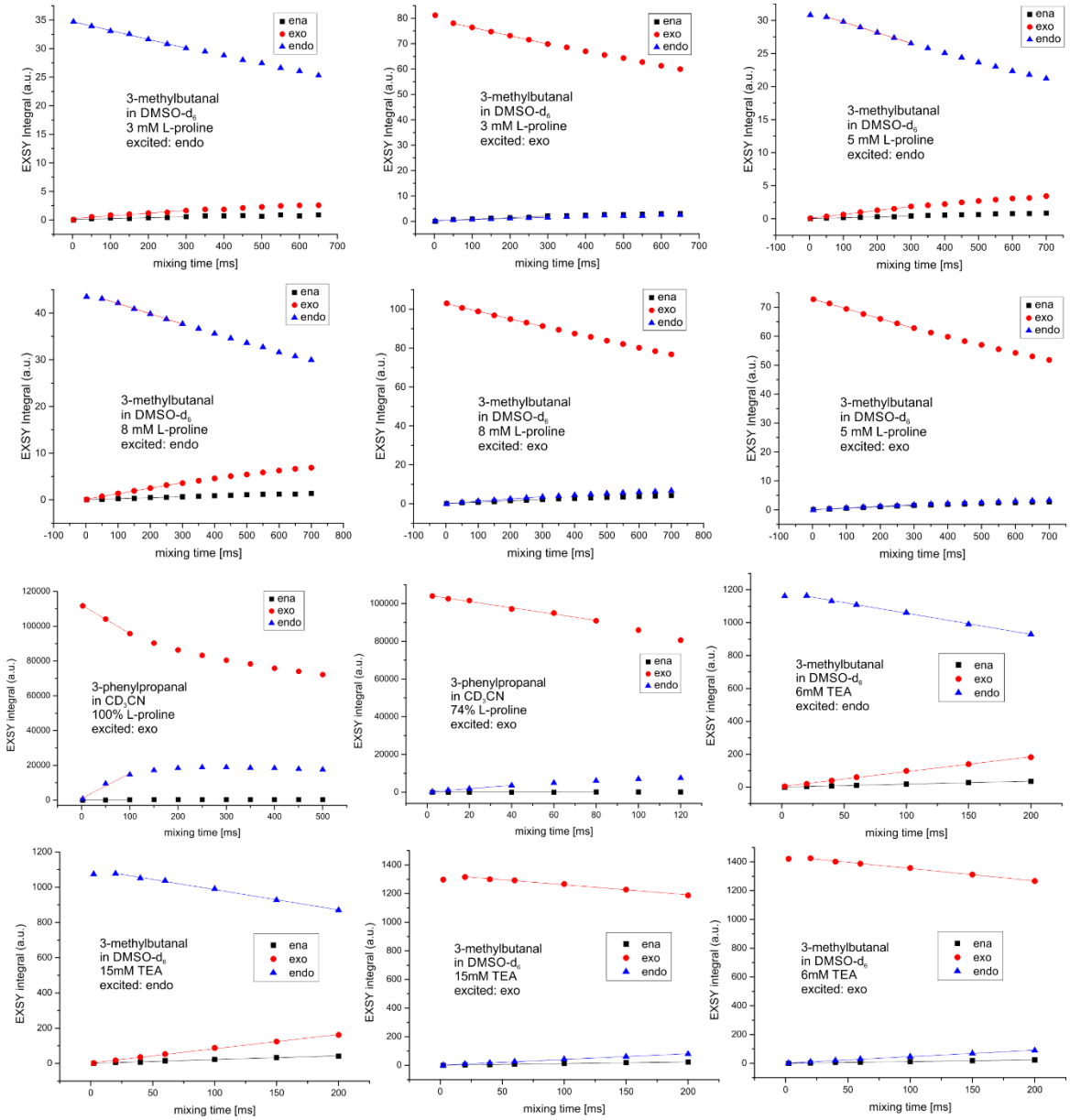

Fig. 12: Selective 1D EXSY build-up curves 2/3.

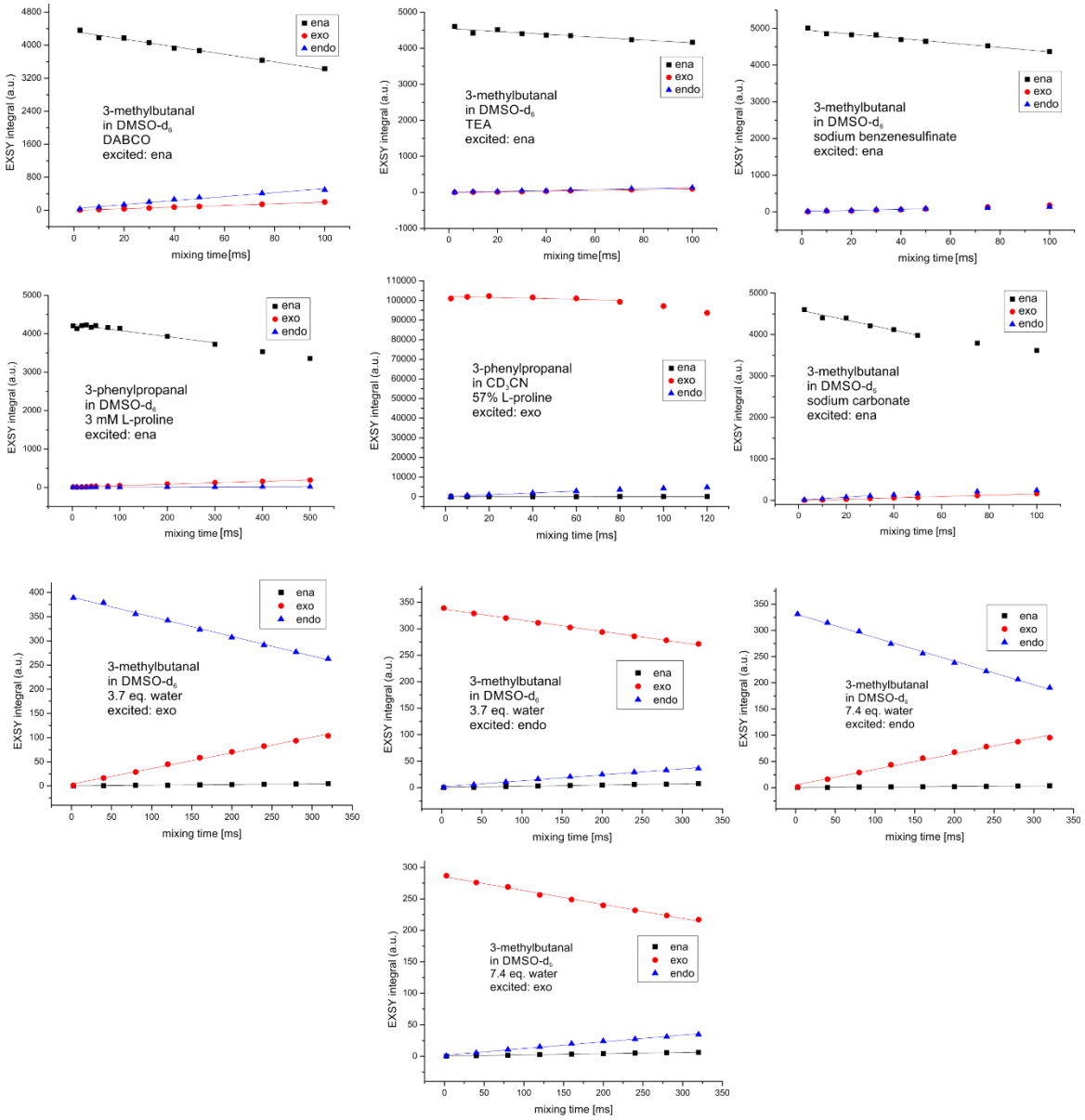

Fig. 13: Selective 1D EXSY build-up curves 3/3.

2.4.7 Rate Constants (k) and Rates (r)

All rate constants and rates calculated according to the equations in Fig. 3 in chapter 2.2 and Equation 1 below are listed.

Table 1: Calculated rate constants of enamine formation/back reaction are presented from *endo*-/*exo*-oxazolidinone ($k_{exo\text{-}ena}$, $k_{endo\text{-}ena}$ and $k^{-1}_{exo\text{-}ena}$, $k^{-1}_{endo\text{-}ena}$) and oxazolidinone isomerization ($k_{exo\text{-}endo}$, $k^{-1}_{exo\text{-}endo}$). n.d.: not determined; Sample: L-proline (saturated), aldehyde: 3-methylbutanal (or as stated) (50 mM), additive (50 mM, for sodium carbonate: saturated solution) in DMSO-d_6 at 300 K.

sample	$k_{exo\text{-}endo}$ [s^{-1}]	$k^{-1}_{exo\text{-}endo}$ [s^{-1}]	$k_{exo\text{-}ena}$ [s^{-1}]	$k_{endo\text{-}ena}$ [s^{-1}]	$k^{-1}_{endo\text{-}ena}$ [s^{-1}]	$k^{-1}_{exo\text{-}ena}$ [s^{-1}]
no additive (saturation L-proline)	0.132±0.015	0.338±0.032	0.078±0.006	0.042±0.014	n. d.	n. d.
3.7 equiv water	0.431±0.046	1.023±0.106	0.083±0.009	0.044±0.008	n. d.	n. d.
7.4 equiv water	0.485±0.061	1.218±0.165	0.080±0.010	0.049±0.010	n. d.	n. d.
3 mM L-proline	0.119±0.021	0.273±0.063	0.124±0.032	0.084±0.038	n. d.	n. d.
5 mM L-proline	0.092±0.012	0.227±0.015	0.080±0.004	0.054±0.017	n. d.	n. d.
8 mM L-proline	0.131±0.015	0.326±0.030	0.080±0.008	0.068±0.011	n. d.	n. d.
3-phenylpropanal (DMSO)	0.057±0.014	0.194±0.013	0.047±0.010	0.010±0.009	0.009± ±0.004	0.116± ±0.01
3-phenylpropanal 100% L-pro. (acetonitrile)	1.461±0.476	n. d.	0.011±0.001	n. d.	n. d.	n. d.
3-phenylpropanal 74% L-pro. (acetonitrile)	0.853±0.044	n. d.	0.011±0.001	n. d.	n. d.	n. d.
3-phenylpropanal 57% L-pro. (acetonitrile)	0.474±0.024	n. d.	0.012±0.002	n. d.	n. d.	n. d.
TEA	n. d.	n. d.	0.868±0.218	8.650±2.910	n. d.	n. d.

Table 2: Calculated rates of enamine formation/back reaction are presented from *endo*-/*exo*-oxazolidinone ($r_{exo\text{-}ena}$, $r_{endo\text{-}ena}$ and $r^{-1}_{exo\text{-}ena}$, $r^{-1}_{endo\text{-}ena}$) and oxazolidinone isomerization ($r_{exo\text{-}endo}$, $r^{-1}_{exo\text{-}endo}$). Sample: L-proline (saturated), 3-methylbutanal (50 mM), additive (50 mM, for sodium carbonate: saturated solution) in DMSO-d_6 at 300 K.

sample	$r_{exo\text{-}endo}$ [mol L^{-1} s^{-1}]	$r^{-1}_{exo\text{-}endo}$ [mol L^{-1} s^{-1}]	$r_{exo\text{-}ena}$ [mol L^{-1} s^{-1}]	$r_{endo\text{-}ena}$ [mol L^{-1} s^{-1}]	$r^{-1}_{endo\text{-}ena}$ [mol L^{-1} s^{-1}]	$r^{-1}_{exo\text{-}ena}$ [mol L^{-1} s^{-1}]
sod. benzene-sulfinate	3.457±0.262	9.181±0.283	0.145±0.010	0.346±0.030	0.332±0.042	0.303±0.036
TEA	0.622±0.021	1.542±0.046	0.119±0.019	0.430±0.059	0.293±0.021	0.196±0.016
DABCO	0.949±0.077	2.552±0.095	0.286±0.014	2.098±0.242	1.301±0.133	0.437±0.024
sod. carbonate	1.635±0.085	4.368±0.165	0.262±0.021	1.495±0.142	0.795±0.066	0.329±0.026

2.4.8 Method Validation

Since the oxazolidinone isomers and enamine are in a quasi-thermodynamic equilibrium during the EXSY measurements, the back and forth reaction of the enamine formations (*exo*↔ena and *endo*↔ena) as well as the back and forth reaction of the oxazolidinone isomerization (*exo*↔*endo*) have to show the same rates. In other words, the normalized rates multiplied with the intermediate ratio of the starting molecule must be equal for all three forth and back reactions. For all samples the *endo*/*exo* isomerization rates were calculated and are equal as expected (Fig. 14 A). Rates for the enamine back reaction (ena→endo and ena→exo) were determined for all additive samples as well as for an additive free sample (Fig. 14B/C). Again, all these rates show the expected equality within the error range.

Determined value

$$\frac{I_{\tau_m}(P)}{\tau_m\, I_0(A)} = \frac{r}{[A]} \qquad \textbf{Equation 1}$$

([A] is the equilibrium intermediate concentration of the starting (irradiated) molecule)

equals

k for unimolecular reactions (no additive, water or proline as additive).
k[B] for bimolecular reactions (basic/nucleophilic additives).

Equilibrium conditions ($r_{a\to b} = r_{b\to a}$) for

A) oxazolidinone isomerization rates:

$$\frac{I_{\tau_m}(endo)}{\tau_m\, I_0(exo)}[\mathrm{exo}] = \frac{I_{\tau_m}(exo)}{\tau_m\, I_0(endo)}[endo] \qquad \textbf{Equation 2}$$

B) enamine formation rates from endo-oxazolidinone:

$$\frac{I_{\tau_m}(ena)}{\tau_m\, I_0(endo)}[endo] = \frac{I_{\tau_m}(endo)}{\tau_m\, I_0(ena)}[ena] \qquad \textbf{Equation 3}$$

C) enamine formation rates from exo-oxazolidinone:

$$\frac{I_{\tau_m}(ena)}{\tau_m\, I_0(exo)}[exo] = \frac{I_{\tau_m}(exo)}{\tau_m\, I_0(ena)}[ena] \qquad \textbf{Equation 4}$$

In the following data points the equilibrium intermediate concentration [A] was substituted by the intermediate ratio of A (wich equals [A] x [sum of all intermediates]$^{-1}$) Since, [sum of all intermediates] is constant for each sample, the equilibrium conditions stay the same.

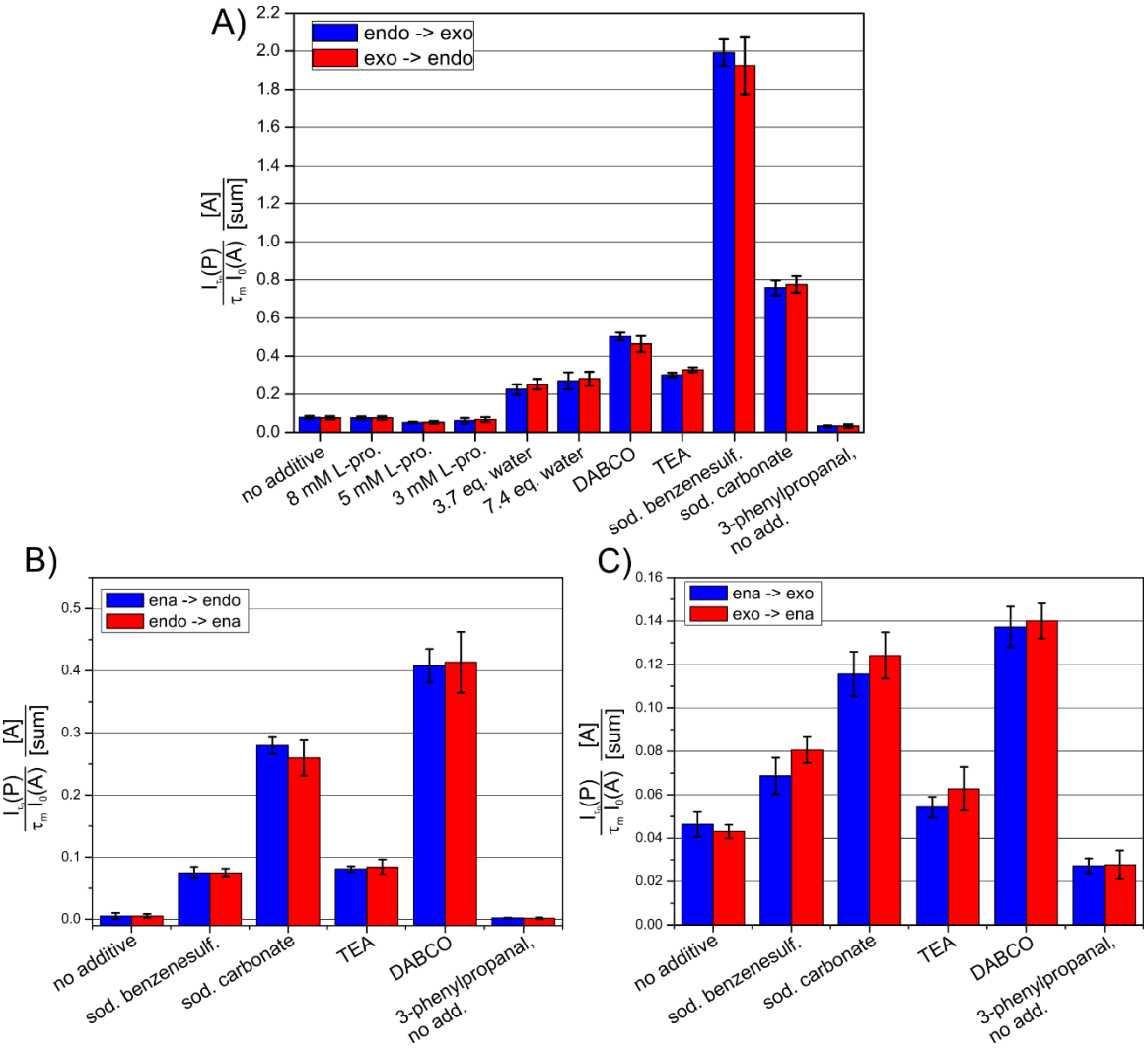

Fig. 14: Rates normalized by the sum of all intermediate concentrations ([sum]=[ena]+[endo-oxa.]+[exo-oxa.]) are presented. In A) oxazolidinone isomerization rates, in B) enamine formation rates from endo-oxazolidinone (forth and back reaction), and in C) enamine formation rates from exo-oxazolidinone (forth and back reaction) are shown. The unit of the normalized rates for samples no additive, 8 mM L-pro., 5 mM L-pro, 3 mM L-pro., 3.7 equiv water, 7.4 equiv water and 3-phenylpropanal no add. is (s^{-1}). The unit of the rates for samples DABCO, TEA, sodium benzenesulfinate and sodium carbonate is (mol L^{-1} s^{-1}).

2.4.9 Reaction Kinetics

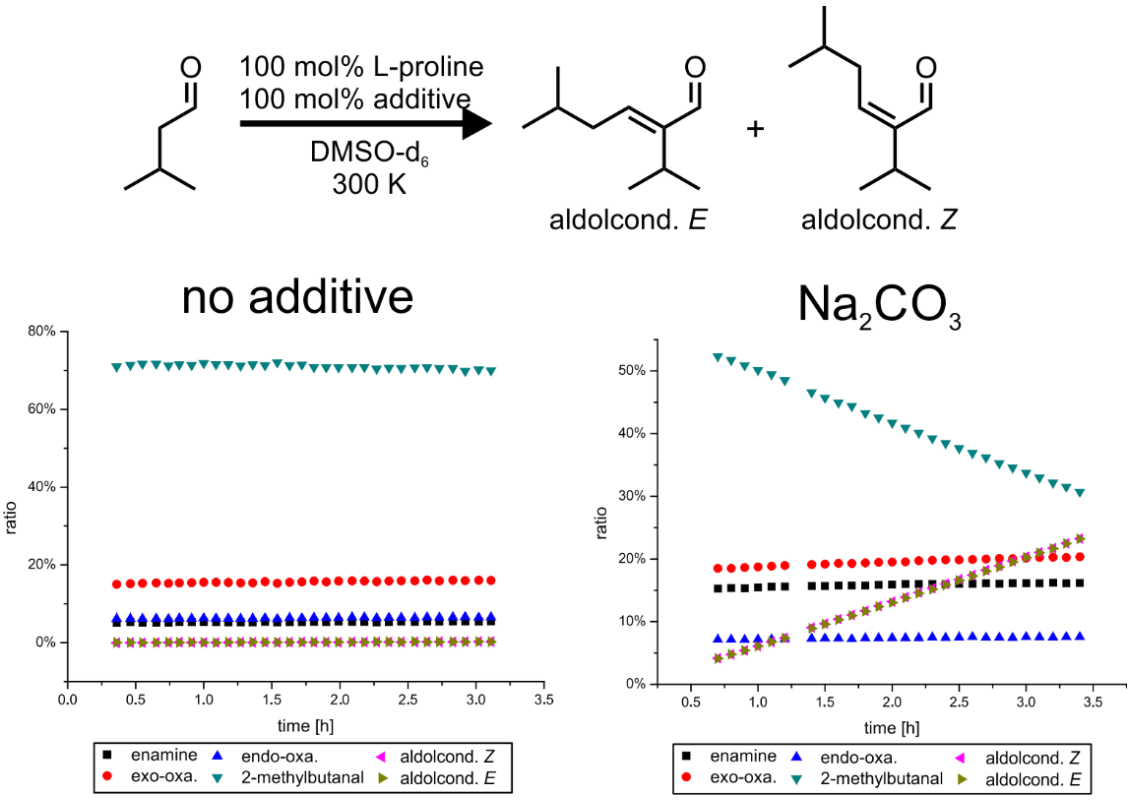

Fig. 15: Two plots showing exemplarily the reaction kinetics of the elapsing self-condensation reaction.

As can be seen in Fig. 15, basic additives accelerate the reaction towards the products. Nevertheless, relative intermediate ratios stay rather constant.

2.4.10 Influence of L-Proline Concentration on the Intermediate Concentrations

Upon addition of L-proline the intermediate ratio is staying constant. In contrast, the absolute concentrations of oxazolidinones and enamine are increasing directly proportional to the L-proline concentration (see Table 3).

Table 3: Intermediate concentrations (normalized integrals) in dependency of L-proline concentration. Sample: 3-8 mM L-proline, 50 mM 3-methylbutanal in DMSO-d_6.

L-Pro Conc.	Intermediate Conc. (a. u.)			Sum of Intermediate Conc. (a. u.) (1st set to 8)
	Ena.	Exo-Oxa.	Endo-Oxa.	
8 mM	1.53	4.61	1.86	8.0
5 mM	1.05	3.12	1.23	5.4
3 mM	0.55	1.62	0.66	2.8

2.4.11 Steric of α-Protons of *Endo*/*Exo*-Oxazolidinone

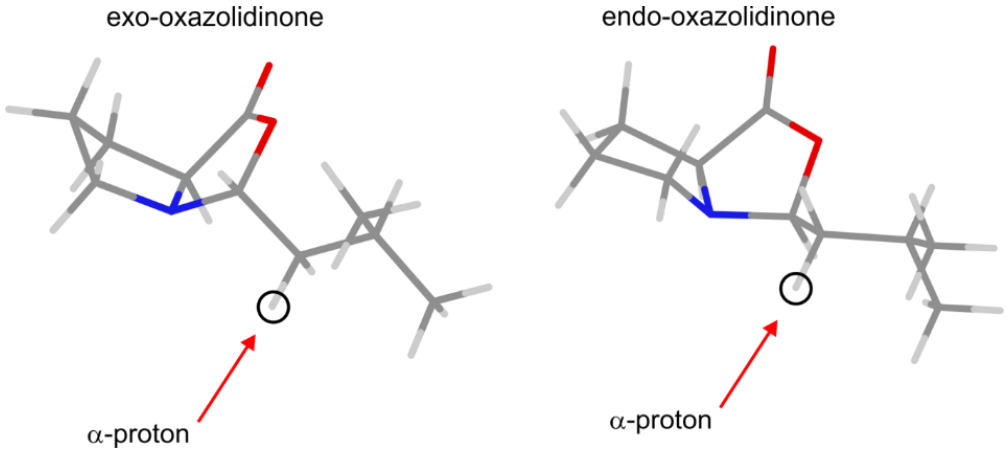

Fig. 16: Calculated geometry of the *exo*- and *endo*-oxazolidinone α-protons (circles) in anti-position to the cyclic C-O bond.

Although it is well known that the *endo*-oxazolidinone is sterically more congested than the *exo*-oxazolidinone, the depicted molecule structures (see Fig. 16) show that the steric accessibility of these α-protons for a theoretical deprotonation is very similar.

2.4.12 Influence of the Aldehyde

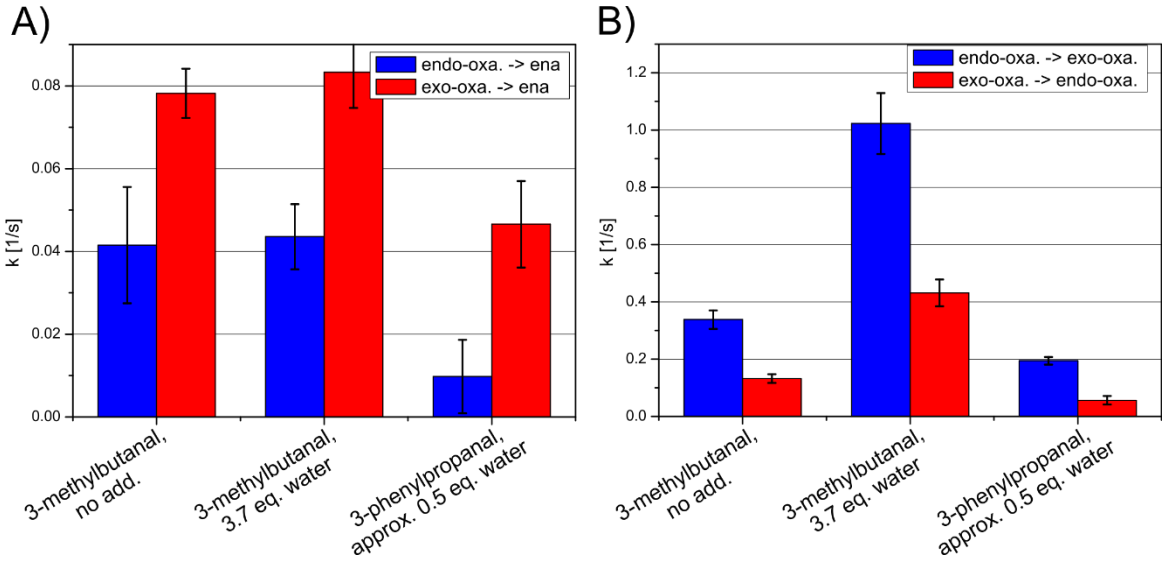

Fig. 17: A) Enamine formation rate constants. B) Oxazolidinone isomerization rates. Sample: aldehyde (50 mM), L-proline (saturated), different water amounts in DMSO-d_6.

The situation is not changing upon aldehyde variation from 3-methylbutanal to 3-phenylpropanal. Without basic or nucleophilic additives the *exo*-oxazolidinone → enamine formation is still considerably faster than the *endo* → enamine formation (see Fig. 17A). In addition, the oxazolidinone isomerization rates are in the same order of magnitude (see Fig. 17B).

2.4.13 Product formation in Dependency of L-Proline Concentration

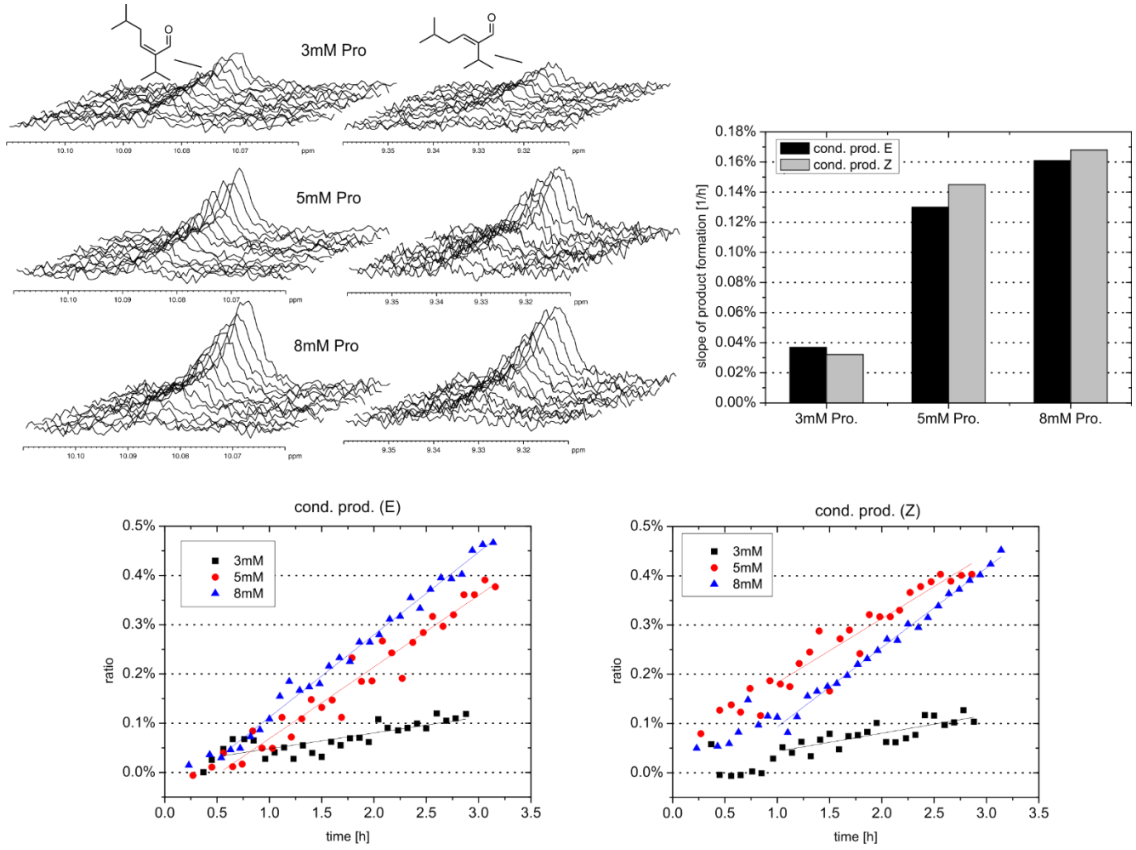

Fig. 18: ^{1}H NMR monitored product ratios (bottom), stacked plots of the raw ^{1}H spectra (top left, every second spectrum was included) and slope of product formation (top right) are shown for the condensation products (*E* and *Z*) of the aldol-condensation depending on the L-proline concentration. Samples: L-proline (3 mM/5 mM/8 mM), 3-methylbutanal (50 mM) in DMSO-d_6 @ 300 K.

The presented data in Fig. 18 shows that, as expected (aldol-condensation is at least first order in L-proline), the slope of product formation is increasing with increasing amount of L-proline. Only traces of aldol-addition products were detected.

2.4.14 Comparison of Consecutively Measured ^{1}H Spectrum and 1D ^{1}H Selective EXSY Spectrum

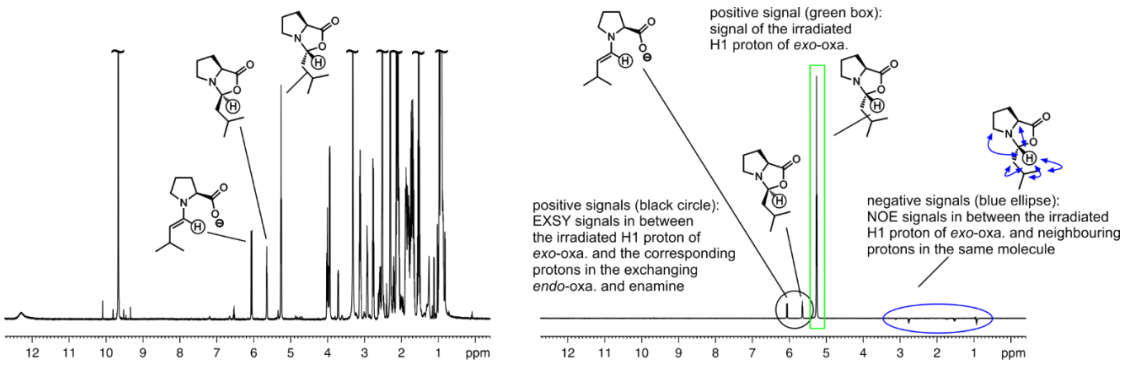

Fig. 19: A comparison is presented of a 1D ^{1}H Spectrum (left-hand side) with a 1D ^{1}H selective EXSY spectrum (right-hand side, *exo*-oxazolidinone irradiated) measured one directly after the other. Sample: L-proline (saturation), 3-methylbutanal (50 mM) in DMSO-d_6 @ 300 K; EXSY mixing time: 700 ms

The direct comparison of consecutively measured ^{1}H Spectrum and 1D ^{1}H selective EXSY spectrum in Fig. 19 shows that the EXSY spectrum is considerably less crowded than the ^{1}H spectrum. The interpretation is much easier as no signal overlap occurs because only the irradiated *exo*-oxazolidinone (irradiated proton and NOE signals of neighboring protons in the same molecule) as well as the corresponding signals of exchanging species (*endo*-oxazolidinone, enamine) are showing up. No other signals are observed. Therefore *e.g.* the occurrence of EXSY signals between oxazolidinones or enamine and potential product-oxazolidinones or the condensation product can be definitely excluded.

2.4.15 Rate Constant Determination on the Additive Sample Triethylamine (Bimolecular)

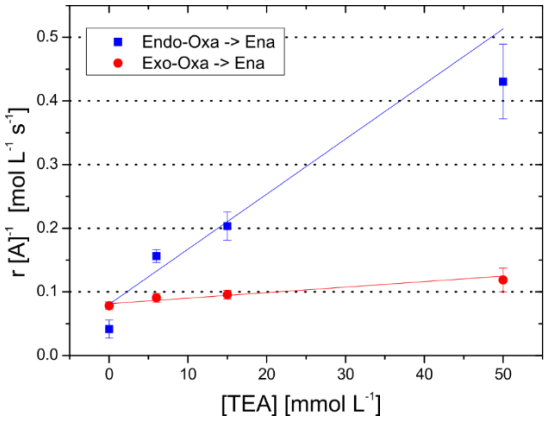

$$\frac{r}{[A]} = k\,[TEA] + r_0$$

$$r_0 = k_0 \times 1\ \text{molL}^{-1}$$

k is slope of line

$k_{\text{endo-ena}} = 8.650 \pm 2.910\ \text{s}^{-1}$
$k_{\text{exo-ena}} = 0.868 \pm 0.218\ \text{s}^{-1}$

Fig. 20: Plot of normalized rates r[A]$^{-1}$ against the concentration of triethylamine [TEA]. The slopes of the drawn line equals the enamine formation rate constants $k_{\text{endo-ena}}$ and $k_{\text{exo-ena}}$. The underlying equation and the value of these rates are depicted on the right-hand side of the figure where k_0 is the corresponding rate constant without basic additives (unimolecular reaction mechanism). R^2 values for the shown fits are 0.83 for red line and 0.72 for blue line.

As shown in chapter 2.2, in samples containing basic/nucleophilic additives, the determined normalized rates equal k times the concentration of the applied base (bimolecular reaction mechanism). Since, enamine is also formed without addition of base, the intercept of the lines drawn in Fig. 20 must physically represent the rates without additives (r_0). In order to achieve unit consistency, r_0 must be adjusted to k_0 times 1 mol L^{-1}. The enamine formation rate constants from *endo*/*exo*-oxazolidinone $k_{endo\text{-ena}}$ and $k_{exo\text{-ena}}$ with the additive TEA therefore equals the slopes of the lines drawn in Fig. 20.

2.4.16 Stacked Plots of the Enamine Build-Up Section of Raw EXSY Spectra for the Samples of Different L-Proline Concentrations and Water Amounts

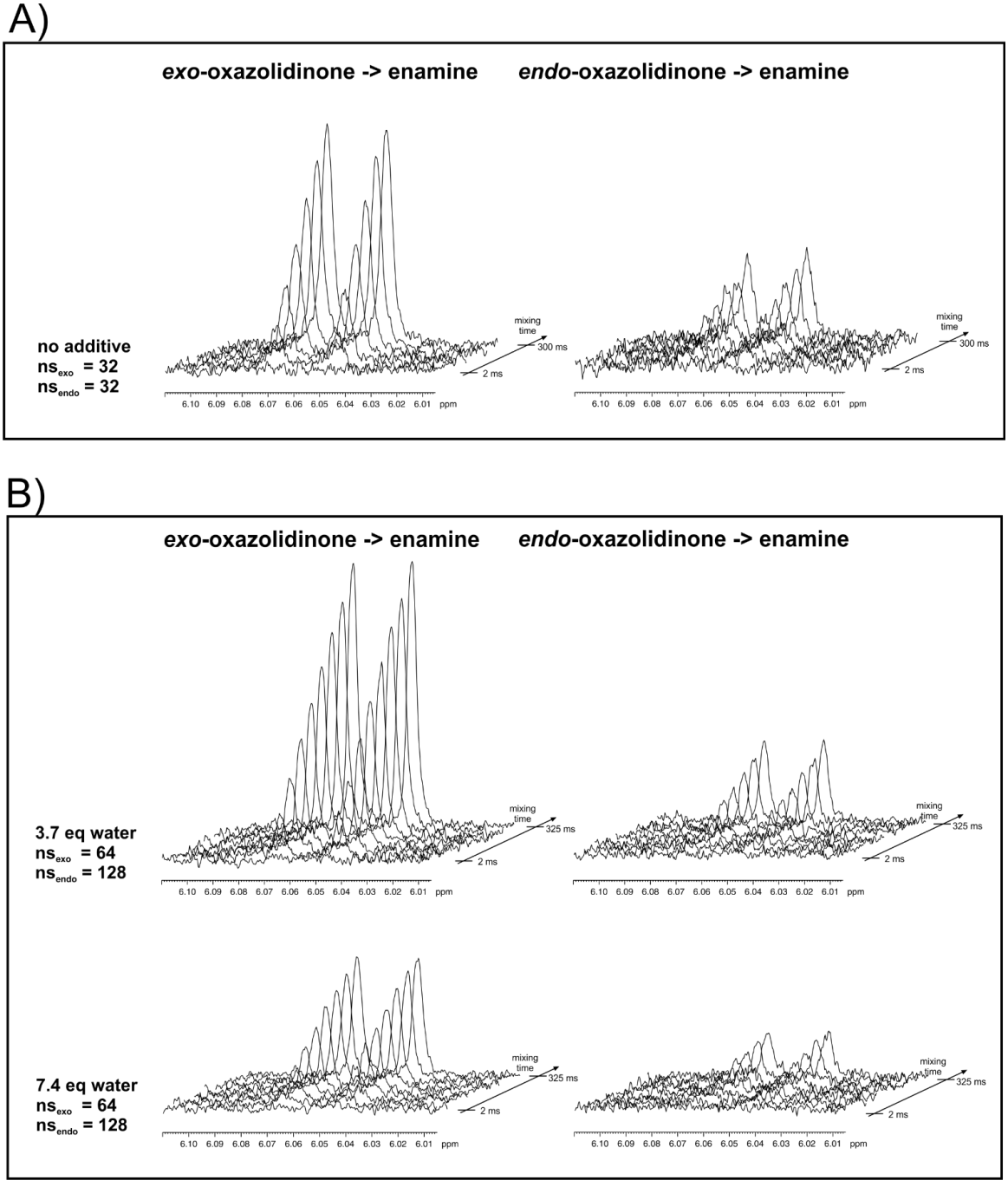

Fig. 21: Stacked plots are presented of the enamine build-up region in the raw EXSY spectra used for the calculation of enamine formation rate constants for the samples A) no additive B) 3.7 equiv water / 7.4 equiv water. ns: number of scans.

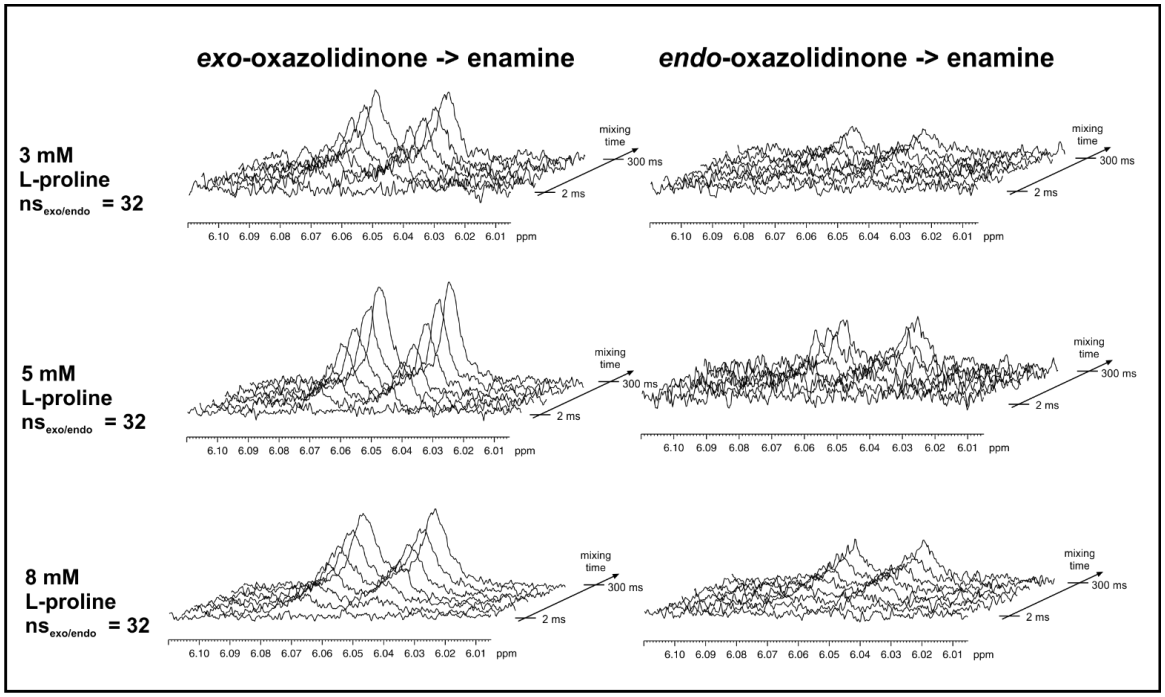

Fig. 22: Stacked plots are presented of the enamine build-up region in the raw EXSY spectra used for the calculation of enamine formation rate constants for the samples 3 mM/5 mM/8 mM L-proline. ns: number of scans.

In Fig. 21 and Fig. 22 stacked plots are shown of raw EXSY build-ups of the enamine region for the samples with varying water and L-proline amounts. These are the examples where EXSY signal intensities are lowest and therefore integration bares the highest errors. However, all of these build-ups are clearly above the noise level.

2.4.17 Energy Profiles

Gas Phase Fig. 23 shows that simulation in the gas-phase without solvent correction yields too low proton transfer barrier from Z-iminium (+40.5 kJ mol^{-1} when compared to the experimental measured activation barrier (+79.4 kJ mol^{-1}). Most probably this is due to the low stability of zwitterionic intermediates in the gas-phase. Notice also that the experimental thermodynamic stability of enamine/oxazolidinone (~4-5 kJ mol^{-1}) cannot be reproduced in the gas-phase, and, also as shown later, in the solution phase without explicit DMSO.

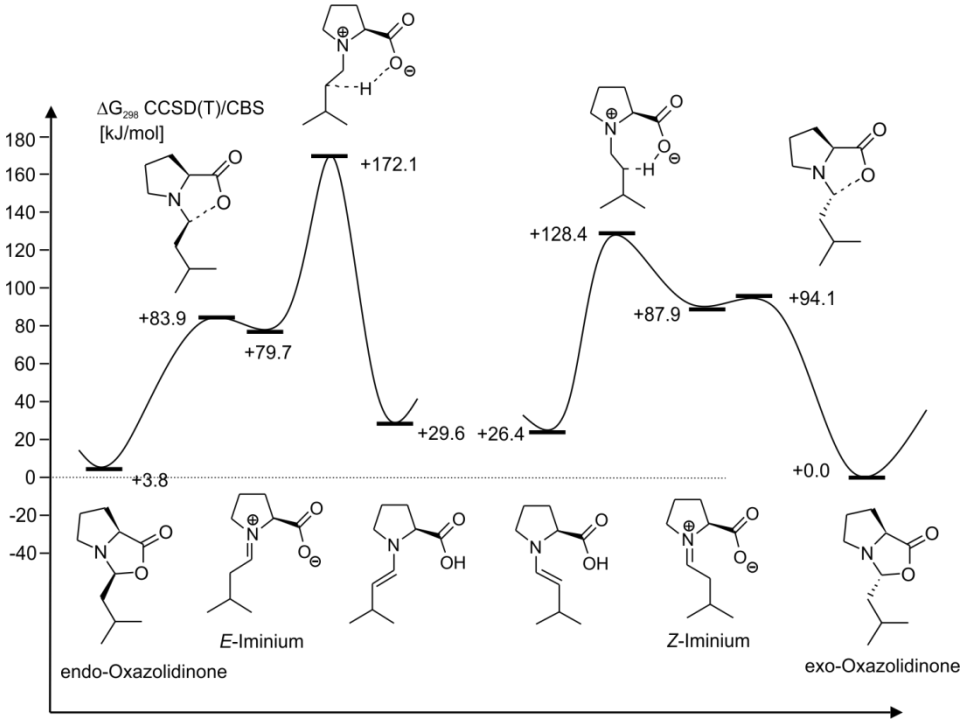

Fig. 23: Free energy profile at DG298 CCSD(T)/CBS level of theory in the gas-phase. All energies are relative to the *exo*-oxazolidinone.

Condensed Phase At this point we are aware that the question regarding the number of solvent molecules included in the simulation is very important. As the experimental data showed, the ratio between oxazolidinone and enamine in DMSO at room temperature corresponds to an energy difference of 4-5 kJ mol^{-1} in favor of oxazolidinone. Without explicit solvent molecule the enamine is by 20-26 kJ mol^{-1} less stable than the oxazolidinone (Fig. 23). An inclusion of one solvent molecule seems to improve the quality of prediction as the energy difference is reduced to 10.7 kJ mol^{-1}. Note: increasing the number of solvent molecules may of course increase the accuracy, but this may introduce more problems regarding the conformational space. Considering the cost/gain ratio we concluded that the number of explicit solvent molecules included in the simulation is justified as the deviation to the experimental data is acceptable.

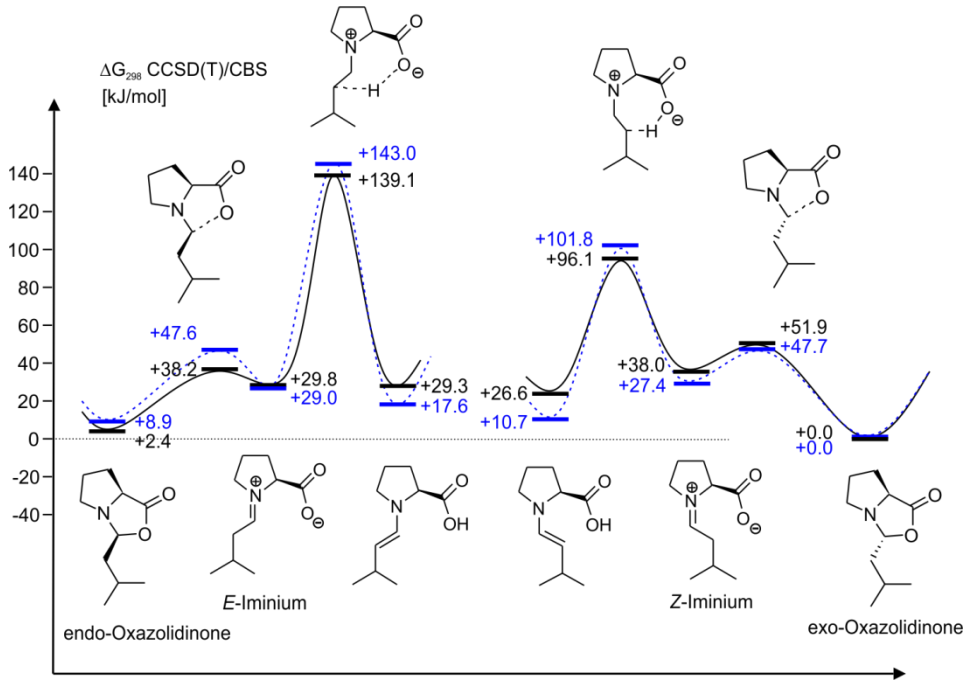

Fig. 24: Free energy profile at DG298 CCSD(T)/CBS (+ DMSO continuum (COSMO)) level of theory with explicit DMSO (blue) and no explicit DMSO (black). All energies are relative to the *exo*-oxazolidinone.

Both results (with explicit DMSO and without DMSO; Fig. 24) showed that the energy barrier of the internal proton transfer from *Z*-iminium is significantly lower from the *E*-iminium. Noteworthy to be mentioned here is that the relative energetic of *s-cis/s-trans* enamine relative to *exo/endo*-oxazolidinone. Without explicit DMSO the enamine is thermodynamically by approx. ~20-30 kJ mol^{-1} less stable than the respective *exo-/endo*-oxazolidinone. This is rather due to the missing hydrogen bridge interaction of the carboxylate proton and the solvent molecule, which cannot be represented by applying only continuum model. Also very important here is the stabilization of iminium intermediates and the destabilization of the transition state towards the enamine formation. The energy barrier regarding the proton transfer from *Z*-iminium without any explicit DMSO (+58.1 kJ mol^{-1}) is significantly lower than the measured barrier (+79.4 kJ mol^{-1}), which is rather a huge deviation considering the theory level used in this study. The calculation with explicit DMSO together with continuum model (+74.4 kJ mol^{-1}) showed however better agreement with the experimental data. For the proton transfer from *E*-iminium, neither the simulation with (+114 kJ mol^{-1}) nor without explicit DMSO (+109.3 kJ mol^{-1}) can reproduce the measured energy barrier (+80.9 kJ mol^{-1}). We therefore concluded that the enamine formation from *E*-iminium must follow another pathway. As the experimental data and the calculations show, water is a possible candidate which may assist the enamine formation in the case of *E*-iminium (see chapter 2.2).

Remarkably, the experimental relative energy between *exo*- and *endo*-oxazolidinones (~2-3 kJ mol^{-1} in favor of *exo*-oxazolidinone) is reproduced by the calculations without explicit DMSO (+2.4 kJ mol^{-1} in favor of *exo*-oxazolidinone). The results with explicit DMSO show a somewhat larger preference for *exo*-oxazolidinone (+8.9 kJ mol^{-1}). This may indicate that oxazolidinone is not interacting strongly with the solvent molecule. The ring opening barrier of a smaller model in the gas-phase at ΔG_{298} B3LYP/6-31+G** as reported in the literature are very high (+53.6 kJ mol^{-1} for *endo* and +73.6 kJ mol^{-1} for *exo*.[35] This is rather due to the missing solvent effects which stabilizes the transition state as the bond breaks generating a charge separation. Now since the reaction is endergonic, according to the Hammond postulate the transition state must be located near to the zwitterionic intermediate rather than the reactants. Therefore charge separation causes significant destabilization of the transition state. We performed recalculations using the transition state and oxazolidinone geometry of Sunoj and Sharma at our level of theories and included solvent correction (IEFPCM; MeCN as solvent).

Table 4: Ring opening barrier (in kJ mol^{-1}) of *exo*/*endo*-oxazolidinone to *Z*/*E*-iminium intermediates using model from the previous work by Sunoj and Sharma at two different level of theories (with and without solvent correction).

	ΔG_{298} B3LYP/6-31+G**	$\Delta G_{298,solv}$ (in MeCN) B3LYP/6-31+G**	ΔG_{298} CCSD(T)/CBS	$\Delta G_{298,solv}$ (in MeCN) CCSD(T)/CBS
TS *exo*-oxa -> *Z*-iminium	+73.7	+41.3	+97.5	+65.1
TS *endo*-oxa -> *E*-iminium	+53.5	+12.4	+83.6	+42.4

The corrected barrier height for B3LYP/6-31+G** in continuum are +41.3 kJ mol^{-1} (+10.0 kcal mol^{-1}) for the ring opening of *exo*-oxazolidinone to *Z*-iminium, and +12.4 kJ mol^{-1} for *endo*-oxazolidinone to *E*-iminium. Note that the CCSD(T)/CBS//B3LYP/6-31+G** calculated barriers are significantly higher than the DFT results (see Table 4). Notice that the solvent correction to the barrier is very large and amounts to 32-41 kJ mol^{-1}. In addition to the calculation in DMSO, a comparable simulation with our model system and COSMO in acetonitrile showed only marginal changes in reaction energies and ring opening barriers. The ring opening barrier from *endo*-oxazolidinone to *E*-iminium is estimated to be +36.4 kJ mol^{-1} in acetonitrile and +35.8 kJ mol^{-1} in DMSO.

Comparison of Direct COSMO-RS Solvent Model vs. Standard COSMO Model with Gas-Phase Geometry. Our results without explicit solvent molecule showed that standard COSMO model could not predict the barrier height for the proton transfer from *Z*-iminium correctly. More devastatingly, the thermodynamic stability gap between oxazolidinone and enamine is very large, which is most probably due to the missing description of hydrogen bond between solvent and substrate. As shown previously, this is partially corrected in the cluster continuum model (CCM). Due to sampling problems, the latter approach may introduce another significant error. Therefore we have decided to use only one explicit solvent molecule to avoid the problem regarding conformational space. Here we investigated a more sophisticated continuum approach, the direct COSMO-RS (DCOSMO-RS)[78], in combination with the gas-phase structure without explicit solvent molecule. The program used for the DCOSMO-RS was TURBOMOLE6.6.[73]

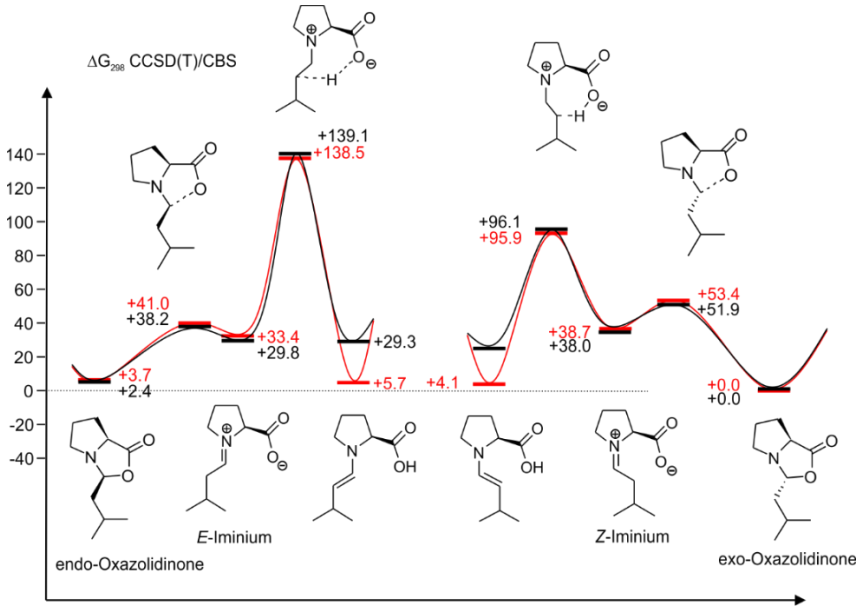

Fig. 25: A comparison is presented of potential energy surfaces using standard COSMO model (solid black line) and DCOSMO-RS model (solid red line) using on gas-phase structures. All energies are relative to *exo*-oxazolidinone.

Fig. 25 shows that DCOSMO-RS is superior in predicting the thermodynamic stability of neutral non-charged separated molecule (between *exo*- and *endo*-oxazolidinone or between oxazolidinones and enamines) when compared to standard COSMO model. It is very surprising that the use of explicit solvent molecule is even becoming unnecessary. Nevertheless the barrier heights for the internal proton transfer from *Z*-iminium to enamine are definitely still too low. One possible error source is the relaxation of the zwitterionic intermediates (iminium) in solution phase, which cannot be taken into account during the optimization in the gas-phase. The relaxation in solution phase seems to be corrected when explicit solvent molecule is introduced in

the simulation (Fig. 24). In this case the *Z*-iminium gains 10 kJ mol^{-1} stabilization when compared to the result in the gas-phase. Notice also that the proton transfer transition state from *Z*-iminium is also destabilized in CCM, though the magnitude of the destabilization is less. Finally the net destabilization of the transition state and stabilization of the iminium lead to more accurate barriers.

Comparison of Direct COSMO-RS Model vs. Standard COSMO Model with Solution Phase Geometry. Since we are dealing with charged separated species that may relax considerably in the condensed phase, we optimized all intermediates and transition state without explicit solvent molecule using SMD model[74] in DMSO at TPSS-D3/aug-SVP level of theory as implemented in Gaussian09 revision D.01.[75] Subsequent single points calculation was performed at CCSD(T)/CBS level of theory. The energy profile at CCSD(T)/CBS is corrected by adding ΔG_{solv} from two solvation models: standard COSMO, and direct COSMO-RS (DCOSMO-RS) at TPSS-D3/aug-TZVP.

We are very aware that the frequency calculation using continuum model is highly intriguing.[76] Yet in some cases, when the structure in the solution phase is deviating significantly from the gas-phase structure, the optimization in the solution phase is necessary. A previous study conducted by Truhlar concluded that the error originating from the used gas-phase partition function in the calculation of second derivatives is negligible.[77]

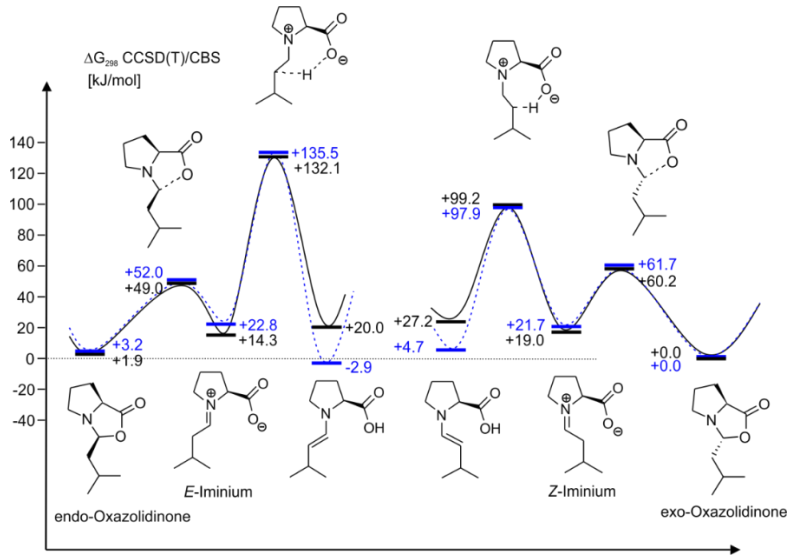

Fig. 26: Comparison of potential energy surface of solution-phase-optimized structure corrected with standard COSMO model (solid black line) and DCOSMO-RS model (dashed blue line). All energies are relative to *exo*-oxazolidinone.

Both solvation models successfully predicted the internal proton transfer barrier height from *Z*-iminium correctly (Fig. 26). Similar to the calculation using the gas-phase structure (solvent corrected and not corrected), the energy difference between oxazolidinones and enamines is too large when using standard COSMO approach. In

contrast, DCOSMO-RS outperformed again the other solvation model and predict the thermodynamic stability between oxazolidinone and enamines much better, despite the fact that now the enamines are overstabilized and becoming marginally more stable than the oxazolidinones by 2.6 kJ mol^{-1}.

At this point, we have demonstrated that DCOSMO-RS is one of the most accurate state-of-the-art solvation techniques that should be considered in the future. Furthermore the relaxation in the solution phase is a remedy when explicit solvent molecule is not present.

Test of Density Functional. To test how significant the reaction profile and electronic structure may be altered with the variation of density functional, we recalculated the enamine formation from *exo*-oxazolidinone at using B3LYP-D3/aug-SVP and M06-2X-D3/aug-SVP geometry in the gas phase, followed by thermochemical correction at the same level and single point calculation at CCSD(T)/CBS level of theory. The results showed that the geometries of all intermediates and transition states are similar for all DFT functional put under consideration (B3LYP-D3, TPSS-D3 and M06-2X-D3). The reaction profile is robust as long as the high level theory such as SCSMP2 and CCSD(T), of course in combination with appropriate basis set, is used (see Fig. 27, left-hand side). Care must be taken in the evaluation of reaction energies and barrier at DFT level, because it is known that DFT may show erratic behavior (see Fig. 27, right-hand side).

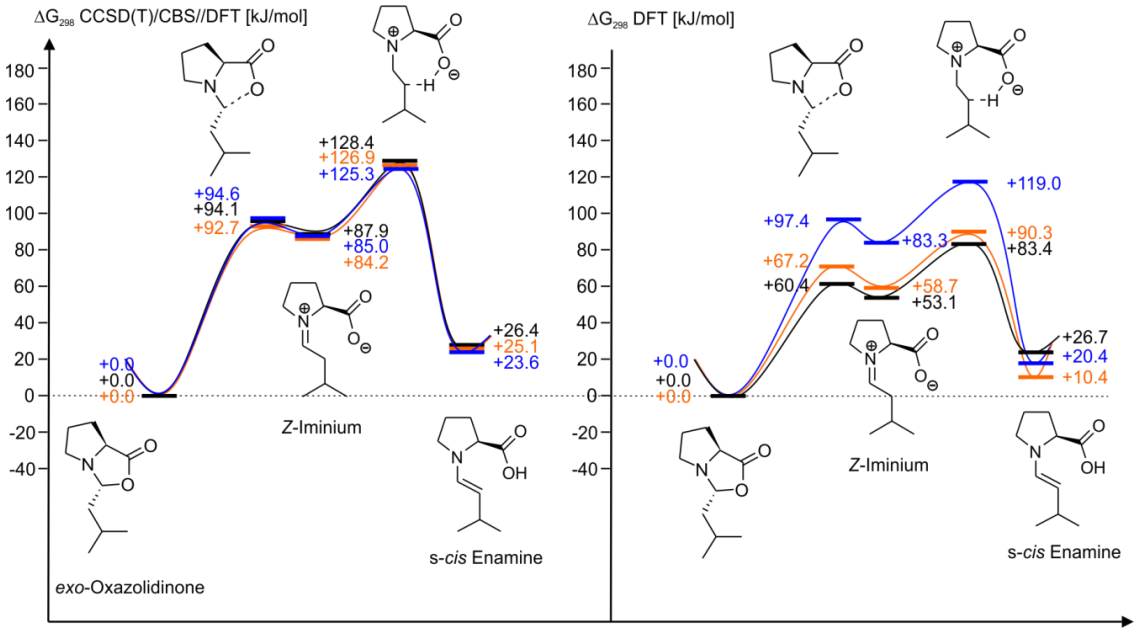

Fig. 27: Left-hand side: Potential energy surface using different DFT geometry (TPSS-D3: black line; B3LYP-D3: orange line; M06-2X-D3: blue line) at ΔG_{298} CCSD(T)/CBS level of theory. Right-hand side: Potential energy surface using at TPSS-D3/aug-SVP, B3LYP-D3/aug-SVP and M06-2X-D3/aug-SVP.

Proline as Bifunctional Acid-Base Catalyst. As proline may act as a bifunctional acid-base catalyst, which deprotonates oxazolidinone and subsequently generates enamine (as discussed and postulated by one of the referees). The precomplex consisting of protonated oxazolidinone (with isopentanal and 3-phenylpropanal as the aldehyde) and proline as well as the corresponding transition state leading to enamine were optimized at B3LYP/6-31+G(d,p), followed by thermochemical correction at the same level and single point calculation at SCS-MP2/def2-TZVPP level of theory (see chapter 2.4.18 below). The potential energy surface of the gas phase is solvent corrected using CPCM in acetonitrile.

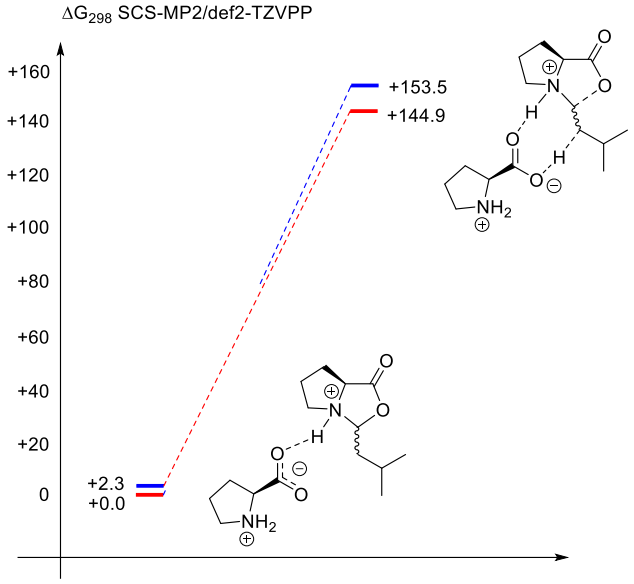

Fig. 28: Energy barriers are presented of deprotonation from *endo* (red)/*exo* (blue)-oxazolidinone leading to enamine.

Note that the reaction energy obtained at SCS-MP2/def2-TZVPP is almost quantitative and very similar with the predicted value at CCSD(T)/CBS level of theory. We were able to locate analogue TS for our systems (both *exo*- and *endo*-oxazolidinone) proposed by the referee (see Fig. 28). Nevertheless the reaction barrier is much higher compared to other possible pathways. This is also true for the system used by the referee (3-phenylpropanal) which showed a very similar barrier height (+150.6 kJ mol^{-1}; not shown in Fig. 28). This, in contrast to the other pathways, is not consistent with the measured rate constants.

2.4.18 Theoretical Section

Two points extrapolation formula to approach SCS-MP2/CBS total energy is defined in Equation 5, Equation 6 and Equation 7.

$$E_{\mathrm{SCF}}^{X} = E_{\mathrm{SCF}}^{\infty} + Ae^{-\alpha\sqrt{X}} \qquad \textbf{Equation 5}$$

$$E_{\mathrm{corr,MP2}}^{\infty} = \frac{X^{\beta} E_{\mathrm{corr,MP2}}^{X} - (X-1)^{\beta} E_{\mathrm{corr,MP2}}^{X-1}}{X^{\beta} - (X-1)^{\beta}}$$ **Equation 6**

$$E_{\mathrm{MP2}}^{\infty} = E_{\mathrm{corr,MP2}}^{\infty} + E_{\mathrm{SCF}}^{\infty}$$ **Equation 7**

For the basis set def2-TZVPP (X=3) and def2-QZVPP (X=4), the used α equals 7.88 and β equals 2.97. Finally DLPNOCCSD(T) at CBS level is approximated using Equation 8.

$$E_{\mathrm{CCSD(T)}}^{\infty} = E_{\mathrm{CCSD(T)}}^{\mathrm{def2\text{-}TZVPP}} + E_{\mathrm{MP2}}^{\infty} - E_{\mathrm{MP2}}^{\mathrm{def2\text{-}TZVPP}}$$ **Equation 8**

2.4.19 Conversion of Measured Rate Constants to Energy Barriers

The experimental rate constant was converted into energy barrier using Eyring equation (Equation 9).

$$-\Delta G^{\ddagger \mathrm{o}} = -RT\ln(\frac{k}{k^{\ddagger}})$$ **Equation 9**

With

$$k^{\ddagger} = \frac{k_B T}{h}$$ **Equation 10**

R = gas constant (8.314 J $K^{-1}mol^{-1}$)

T = temperature (298.15 K)

k_B = Boltzmann's constant (1.380658 x 10^{-23} J K^{-1})

h = Planck's constant (6.6260755 x 10^{-34} J s)

2.4.20 Optimized Geometries of the Most Stable Conformations

Structures Optimized in Gas Phase

Exo-Oxazolidinones (TPSS)

C	1.578165	0.415533	0.816901
C	1.838804	-1.802003	-0.070631
C	3.059918	-0.954714	-0.470605
H	1.359636	0.833479	1.811501
H	2.125027	-2.570293	0.665648
H	1.361076	-2.307272	-0.921971
C	-0.308431	-0.519574	-0.194524
N	0.876693	-0.862735	0.567021
O	-0.018602	0.761653	-0.876583
C	1.028282	1.367220	-0.256498
O	1.439243	2.465830	-0.554498
C	3.075044	0.131395	0.618186
H	3.508307	-0.255247	1.552346
H	3.610655	1.044413	0.328133
C	-1.540209	-0.329774	0.683496
H	-1.740941	-1.300148	1.167184
H	-1.278047	0.380302	1.484786
C	-2.799286	0.161370	-0.053756
H	-2.546960	1.113020	-0.549446
H	-0.478526	-1.254303	-0.991117
H	2.903205	-0.493140	-1.458441
H	3.988005	-1.540697	-0.508047
C	-3.921037	0.427410	0.962262
H	-4.199869	-0.502515	1.485481
H	-3.605028	1.163372	1.717561
H	-4.819679	0.814507	0.459033
C	-3.263884	-0.834764	-1.128561
H	-4.188021	-0.478590	-1.607016
H	-2.510189	-0.968909	-1.918889
H	-3.472582	-1.819861	-0.679106

Exo-Oxazolidinones (B3LYP)

C	-1.569176	0.392268	-0.685641
C	-1.858678	-1.617627	0.521845
C	-3.208642	-1.311748	-0.122411
H	-1.315316	0.701265	-1.709819
H	-1.607763	-2.685440	0.527021
H	-1.846521	-1.255340	1.567542
H	-3.340129	-1.930095	-1.019558
H	-4.049096	-1.507857	0.553023
C	0.331435	-0.492445	0.316313
N	-0.909780	-0.872273	-0.320981
O	0.103871	0.838426	0.880102
C	-0.957236	1.414218	0.276240
O	-1.322902	2.535417	0.498997
C	-3.087307	0.176408	-0.506816
H	-3.640838	0.422199	-1.418412
H	-3.463683	0.829445	0.289483
C	1.505321	-0.435717	-0.648784
H	1.665958	-1.460245	-1.016376
H	1.204774	0.165826	-1.518392
C	2.809112	0.122853	-0.062074
H	2.606140	1.150545	0.271629
H	0.542654	-1.153268	1.163377
C	3.887724	0.178206	-1.147720
H	4.128582	-0.832169	-1.509796
H	3.556807	0.774330	-2.008575
H	4.812896	0.625772	-0.761612
C	3.289833	-0.682257	1.150366
H	4.255720	-0.303560	1.508667
H	2.585447	-0.622267	1.989113
H	3.422678	-1.742347	0.887519

Exo-Oxazolidinones (M06-2X)

C	1.557183	0.382854	0.780998
C	1.819702	-1.832405	-0.056208
C	3.019766	-0.987716	-0.498425
H	1.344331	0.833568	1.759060
H	2.131033	-2.577416	0.687982
H	1.340823	-2.369684	-0.882259
C	-0.328262	-0.569866	-0.174774
N	0.866503	-0.895068	0.570884
O	-0.047332	0.658410	-0.889838
C	0.989477	1.287521	-0.315862
O	1.388989	2.361599	-0.652867
C	3.046231	0.114396	0.563924
H	3.496351	-0.252281	1.493903
H	3.566687	1.024595	0.251173
C	-1.537461	-0.350981	0.719033
H	-1.772950	-1.319796	1.183375
H	-1.240808	0.327674	1.531830
C	-2.772530	0.203042	0.004392
H	-2.523213	1.210254	-0.356087
H	-0.528781	-1.336329	-0.930034
H	2.834272	-0.547362	-1.487108
H	3.949379	-1.562871	-0.548270
C	-3.932682	0.315155	0.991140
H	-4.225719	-0.680836	1.350880
H	-3.656790	0.922357	1.861784
H	-4.808114	0.774696	0.517389
C	-3.161894	-0.650790	-1.202416
H	-4.106655	-0.300529	-1.634057
H	-2.403238	-0.607664	-1.992203
H	-3.296873	-1.700410	-0.904173

***Z*-Iminium (TPSS)**

C	-1.366290	0.159940	-0.785089
C	-1.773082	-1.738466	0.658227
C	-3.067502	-0.933760	0.475725
H	-0.876789	0.345885	-1.748280
H	-1.839067	-2.729590	0.186326
H	-1.443827	-1.854073	1.698715
C	0.527958	-1.146410	0.047960
N	-0.751065	-0.951595	-0.094598
O	-0.113669	1.500456	0.850032
C	-1.110524	1.556372	0.110284
O	-1.959813	2.413391	-0.168086
C	-2.845363	-0.207113	-0.865361
H	-3.051175	-0.876766	-1.716099
H	-3.443093	0.705691	-0.961879
C	1.598785	-0.459534	-0.731633
H	1.710567	-0.999331	-1.693934
H	1.293829	0.570217	-0.959685
C	2.955785	-0.457512	0.008954
H	3.209553	-1.509241	0.238813
H	0.813632	-1.937850	0.748570
H	-3.172233	-0.194431	1.281483
H	-3.949683	-1.586740	0.478614
C	2.865753	0.324958	1.328724
H	2.583644	1.370292	1.141432
H	2.097528	-0.093359	1.996516
H	3.833586	0.301646	1.851580
C	4.055466	0.102027	-0.904772
H	5.026020	0.100871	-0.386925
H	4.156813	-0.493117	-1.825400
H	3.828119	1.141014	-1.189779

***Z*-Iminium (B3LYP)**

C	1.404862	0.292138	0.722321
C	1.755078	-1.836768	-0.371027
C	3.037810	-1.004258	-0.431445
H	0.990283	0.616263	1.680658
H	1.873443	-2.714249	0.278180
H	1.375367	-2.159732	-1.345812
C	-0.505727	-1.130327	0.19271 7
N	0.764499	-0.930623	0.266210
O	0.068032	1.281113	-1.049500
C	1.065072	1.492081	-0.344009
O	1.855297	2.430226	-0.239026
C	2.890178	-0.046460	0.759643
H	3.168210	-0.542978	1.700917
H	3.474785	0.870615	0.652439
C	-1.565917	-0.305648	0.819910
H	-2.003420	-0.903676	1.640994
H	-1.142610	0.603074	1.251086
C	-2.699925	0.076887	-0.161724
H	-2.212468	0.572991	-1.008987
H	-0.807136	-2.036585	-0.336545
H	3.072732	-0.430552	-1.365314
H	3.931623	-1.635039	-0.378518
C	-3.629595	1.083363	0.518591
H	-4.097903	0.647403	1.413920
H	-3.080308	1.983934	0.820213
H	-4.431458	1.391292	-0.164535
C	-3.476496	-1.144830	-0.660854
H	-4.283366	-0.832422	-1.335727
H	-2.844803	-1.845808	-1.222287
H	-3.934806	-1.691908	0.176713

***Z*-Iminium (M06-2X)**

C	1.386097	0.256475	0.786748
C	1.762374	-1.790173	-0.442833
C	3.012775	-0.913846	-0.480316
H	0.969504	0.499282	1.767780
H	1.920945	-2.684538	0.171788
H	1.375078	-2.082167	-1.422791
C	-0.500705	-1.161094	0.175743
N	0.758230	-0.943104	0.244933
O	0.013961	1.347986	-0.873977
C	1.038023	1.507312	-0.200577
O	1.847193	2.420566	-0.087875
C	2.871926	-0.067986	0.789047
H	3.162011	-0.644050	1.678189
H	3.441074	0.863367	0.751956
C	-1.567547	-0.353023	0.814522
H	-2.010222	-0.955919	1.626167
H	-1.148845	0.560474	1.238590
C	-2.676847	0.006800	-0.197019
H	-2.170939	0.372999	-1.097961
H	-0.793771	-2.047234	-0.394126
H	2.989358	-0.259789	-1.359262
H	3.925520	-1.515301	-0.510694
C	-3.513931	1.148363	0.371576
H	-3.965395	0.858393	1.331005
H	-2.892731	2.037021	0.528424
H	-4.323456	1.413484	-0.318134
C	-3.548664	-1.200531	-0.536690
H	-4.299853	-0.928387	-1.286782
H	-2.971296	-2.039404	-0.945989
H	-4.078535	-1.556459	0.357760

TS _Exo_-Oxazolidinone → _Z_-Iminium (TPSS)

C	1.430465	0.373537	0.744608
C	1.894621	-1.795769	-0.241033
C	3.130109	-0.890756	-0.365459
H	1.020660	0.744831	1.690784
H	2.073188	-2.636993	0.446268
H	1.525526	-2.186766	-1.197798
C	-0.410899	-0.984590	0.043986
N	0.860049	-0.918110	0.367602
O	0.014543	0.988867	-1.140748
C	0.968564	1.404109	-0.420797
O	1.613417	2.462823	-0.427425
C	2.939654	0.140624	0.764324
H	3.267987	-0.264044	1.734660
H	3.463291	1.085096	0.577433
C	-1.518125	-0.284273	0.760355
H	-1.860950	-0.979398	1.555922
H	-1.145744	0.620285	1.255442
C	-2.729185	0.073802	-0.132971
H	-2.337555	0.688274	-0.956037
H	-0.681574	-1.810112	-0.622029
H	3.126077	-0.379193	-1.337632
H	4.060312	-1.466156	-0.276133
C	-3.726069	0.912143	0.681364
H	-4.105354	0.343847	1.547153
H	-3.255988	1.833590	1.055323
H	-4.587982	1.198073	0.060890
C	-3.416430	-1.172719	-0.714506
H	-4.269239	-0.879091	-1.344002
H	-2.738403	-1.771110	-1.341879
H	-3.798006	-1.819953	0.092940

TS _Exo_-Oxazolidinone → _Z_-Iminium (B3LYP)

C	1.429153	0.390959	0.719483
C	1.868551	-1.824892	-0.148460
C	3.093913	-0.931334	-0.368489
H	1.056310	0.808352	1.659348
H	2.073832	-2.613061	0.588916
H	1.483901	-2.290339	-1.062673
C	-0.412655	-0.980205	0.098058
N	0.848944	-0.915497	0.418341
O	0.018385	0.882672	-1.183248
C	0.941720	1.356240	-0.472334
O	1.536328	2.432082	-0.521365
C	2.935916	0.159551	0.703042

H	3.293647	-0.192295	1.680961
H	3.450208	1.091220	0.452536
C	-1.514304	-0.253851	0.786287
H	-1.870780	-0.944543	1.575550
H	-1.135022	0.638535	1.291212
C	-2.712398	0.124841	-0.104381
H	-2.325389	0.820027	-0.858035
H	-0.695359	-1.829291	-0.527396
H	3.053946	-0.478239	-1.366508
H	4.029850	-1.493644	-0.281919
C	-3.761847	0.847114	0.743926
H	-4.164029	0.184457	1.524992
H	-3.336395	1.732285	1.234517
H	-4.601907	1.179783	0.121112
C	-3.319005	-1.086140	-0.819641
H	-4.216015	-0.788801	-1.377228
H	-2.625465	-1.530023	-1.544737
H	-3.617075	-1.865099	-0.101261

TS *Exo*-Oxazolidinone → *Z*-Iminium (M06-2X)

C	1.417901	0.411554	0.676434
C	1.826172	-1.862173	-0.021797
C	3.019343	-0.979599	-0.391896
H	1.080946	0.915037	1.586155
H	2.086465	-2.567970	0.776732
H	1.397408	-2.414749	-0.863499
C	-0.435053	-0.990689	0.228910
N	0.828473	-0.912863	0.508881
O	-0.038090	0.702762	-1.223873
C	0.897029	1.247452	-0.593444
O	1.492192	2.302684	-0.770072
C	2.919570	0.175918	0.611658
H	3.319635	-0.116502	1.591143
H	3.417788	1.087696	0.273721
C	-1.511625	-0.192948	0.876827
H	-1.912310	-0.859043	1.664012
H	-1.098082	0.688511	1.375054
C	-2.673999	0.221544	-0.039932
H	-2.302331	1.047442	-0.654815
H	-0.744884	-1.885659	-0.315965
H	2.896301	-0.591863	-1.409641
H	3.964314	-1.527145	-0.335738
C	-3.838146	0.709382	0.818571
H	-4.255094	-0.115578	1.413276
H	-3.521041	1.501302	1.508026
H	-4.639834	1.110667	0.188381
C	-3.106979	-0.906200	-0.973464
H	-4.017427	-0.622523	-1.512992
H	-2.334356	-1.120376	-1.720637
H	-3.327327	-1.825204	-0.409410

TS *Z*-iminium → s-*Cis*-Enamine (TPSS)

C	1.422719	0.113339	0.745182
C	1.390332	-1.910689	-0.644667
C	2.819974	-1.365841	-0.527387
H	0.992273	0.291627	1.743291
H	1.278128	-2.860405	-0.098071
H	1.042485	-2.052354	-1.677463
C	-0.744250	-0.775800	-0.096454
N	0.569839	-0.870713	0.020621
O	0.333915	1.954903	-0.433693
C	1.475236	1.496450	-0.016359
O	2.567444	2.043229	-0.146055
C	2.783937	-0.585771	0.799907
H	2.830222	-1.275222	1.657052
H	3.580375	0.162865	0.878892
C	-1.499076	0.292037	0.464598
H	-1.206514	0.543668	1.496820
H	-0.744243	1.222609	-0.068033
C	-3.011195	0.347990	0.223784
H	-3.351168	1.300297	0.662804
H	-1.193631	-1.491176	-0.794413
H	3.031907	-0.673246	-1.353625
H	3.564373	-2.172928	-0.539767
C	-3.760550	-0.790216	0.945685
H	-3.453351	-1.769550	0.542499
H	-3.543842	-0.784710	2.024994
H	-4.849896	-0.696147	0.810742
C	-3.359981	0.384067	-1.274251
H	-4.443170	0.518186	-1.414079
H	-2.835821	1.206437	-1.780998
H	-3.080296	-0.557601	-1.775702

TS *Z*-Iminium → s-*Cis*-Enamine (B3LYP)

C	1.399634	0.332182	0.685452
C	1.763210	-1.887343	-0.278413
C	3.064160	-1.080893	-0.304521
H	0.943639	0.621067	1.642031
H	1.826894	-2.724420	0.431064
H	1.459779	-2.278931	-1.256551
C	-0.534717	-1.104236	0.129532
N	0.759769	-0.918146	0.205056
O	-0.036875	1.639914	-0.765174
C	1.167319	1.515279	-0.329880
O	2.122253	2.221620	-0.606779
C	2.867825	-0.061087	0.825993
H	3.050202	-0.526458	1.804631
H	3.503472	0.821104	0.718213
C	-1.495860	-0.128176	0.500756
H	-1.264791	0.378985	1.447803
H	-0.960293	0.799795	-0.225993
C	-2.979950	-0.423905	0.295978
H	-3.261984	-1.315884	0.881881
H	-0.838393	-2.024987	-0.377373
H	3.166368	-0.552664	-1.260384
H	3.943609	-1.718908	-0.166365
C	-3.299906	-0.705459	-1.178092
H	-3.043249	0.165223	-1.796663
H	-2.741445	-1.567707	-1.567113
H	-4.368258	-0.920882	-1.310478
C	-3.812224	0.753694	0.813329
H	-4.885528	0.564660	0.682408
H	-3.626829	0.934086	1.880713
H	-3.556913	1.672177	0.267009

TS *Z*-Iminium → s-*Cis*-Enamine (M06-2X)

C	1.395227	0.334990	0.684852
C	1.756163	-1.881090	-0.268185
C	3.047303	-1.064580	-0.307363
H	0.924979	0.644850	1.626420
H	1.829512	-2.703270	0.454957
H	1.445728	-2.282307	-1.238175
C	-0.532963	-1.092782	0.136868
N	0.752325	-0.911906	0.210682
O	-0.005098	1.604903	-0.808633
C	1.188029	1.488464	-0.370207
O	2.159713	2.158572	-0.658240
C	2.855252	-0.067378	0.839474
H	3.023694	-0.553866	1.808953
H	3.494711	0.812758	0.748196
C	-1.496679	-0.108838	0.503047
H	-1.263256	0.390749	1.452990
H	-0.967131	0.790553	-0.235937
C	-2.972950	-0.426985	0.298508
H	-3.242088	-1.330171	0.870202
H	-0.840863	-2.023533	-0.351430
H	3.122183	-0.515247	-1.252786
H	3.932868	-1.696005	-0.194164
C	3.282302	-0.682671	-1.178022
H	-3.037327	0.208646	-1.769907
H	-2.706149	-1.523541	-1.584709
H	-4.345048	-0.913129	-1.318090
C	-3.817428	0.732145	0.824806
H	-4.886128	0.535233	0.681024
H	-3.640254	0.899771	1.894037
H	-3.561105	1.655367	0.288905

***s-Cis*-Enamine (TPSS)**

C	1.374628	0.192888	0.699867
C	1.885977	-1.625989	-0.807233
C	3.095078	-1.461266	0.120966
H	0.969426	0.175320	1.724355
H	1.589599	-2.674321	-0.956206
H	2.083567	-1.173693	-1.799304
H	3.038775	-2.194683	0.939122
H	4.052548	-1.588573	-0.401890
C	-0.506862	-1.052184	-0.337441
N	0.843290	-0.910142	-0.079434
O	1.141809	1.608179	-1.219246
C	1.030238	1.576250	0.136145
O	0.737534	2.551131	0.799405
C	2.919153	-0.028440	0.669301
H	3.360245	0.111678	1.663313
H	3.386945	0.692632	-0.015877
C	-1.509700	-0.279333	0.143564
C	-2.969365	-0.529064	-0.153222
H	-3.034551	-1.420392	-0.801284
H	-0.737694	-1.901012	-0.988863
C	-3.588791	0.661590	-0.915201
H	-3.512131	1.581767	-0.313546
H	-3.061687	0.830927	-1.865281
H	-4.654050	0.484849	-1.133632
C	-3.760938	-0.821399	1.138788
H	-4.824828	-1.009383	0.922726
H	-3.347974	-1.699428	1.656177
H	-3.699596	0.038503	1.825799
H	-1.288554	0.571983	0.797238
H	0.918408	2.514569	-1.504252

***s-Cis*-Enamine (B3LYP)**

C	1.310271	0.152592	0.705406
C	1.761003	-1.853262	-0.581144
C	3.086095	-1.126765	-0.315370
H	0.785854	0.299742	1.660686
H	1.730112	-2.834458	-0.075271
H	1.592579	-2.022933	-1.654110
C	-0.588013	-1.075319	-0.269343
N	0.758248	-0.950049	-0.031989
O	1.380277	1.575730	-1.269817
C	1.241708	1.465969	-0.078852
O	1.063592	2.525613	0.739982
C	2.784259	-0.261415	0.917941
H	2.851158	-0.854335	1.838938
H	3.455745	0.598277	1.019802
C	-1.564728	-0.241053	0.138260
C	-3.024761	-0.452268	-0.162996
H	-3.116194	-1.381980	-0.747103
H	-0.849867	-1.960488	-0.853429
C	-3.587911	0.697127	-1.015062
H	-3.498540	1.652331	-0.477255
H	-3.036693	0.790369	-1.958926
H	-4.650908	0.538213	-1.244506
C	-3.844450	-0.623280	1.126522
H	-4.908627	-0.782994	0.903262
H	-3.479856	-1.476492	1.712241
H	-3.763460	0.275920	1.754576
H	-1.319904	0.655413	0.713660
H	3.334889	-0.485386	-1.168753
H	3.919028	-1.819200	-0.148915
H	1.077893	3.328668	0.197436

***s-Cis*-Enamine (M06-2X)**

C	1.292563	0.107088	0.768215
C	1.766911	-1.831330	-0.592537
C	3.072043	-1.064858	-0.336884
H	0.795421	0.284398	1.731129
H	1.807547	-2.852234	-0.183191
H	1.544280	-1.899493	-1.665450
C	-0.585181	-1.129054	-0.194931
N	0.754728	-1.041713	0.100073
O	1.264359	1.406982	-1.276893
C	1.164584	1.371003	-0.082594
O	0.989288	2.469918	0.670365
C	2.780456	-0.250313	0.930237
H	2.892177	-0.867897	1.828633
H	3.418956	0.632675	1.035700
C	-1.545843	-0.268107	0.181208
C	-3.000338	-0.442170	-0.161423
H	-3.098064	-1.364832	-0.753024
H	-0.852000	-2.008242	-0.785654
C	-3.503500	0.728714	-1.012329
H	-3.398669	1.670215	-0.455648
H	-2.922883	0.816073	-1.937290
H	-4.562876	0.604014	-1.269804
C	-3.852584	-0.591414	1.103316
H	-4.913677	-0.715398	0.852732
H	-3.527784	-1.455220	1.694065
H	-3.755114	0.305230	1.730664
H	-1.293259	0.620667	0.766955
H	3.268468	-0.386763	-1.173604
H	3.932561	-1.729949	-0.217867
H	0.966230	3.236296	0.081701

***Endo*-Oxazolidinone**

C	1.902253	0.378214	0.700485
C	1.244390	-1.605173	-0.370456
C	2.756834	-1.728370	-0.166976
H	2.021905	0.823443	1.701713
H	0.705803	-2.556170	-0.266275
H	1.030252	-1.183320	-1.372666
H	2.958427	-2.397579	0.681811
H	3.266631	-2.124857	-1.055134
C	-0.367792	0.074724	0.528469
H	-0.644628	0.532158	1.490486
N	0.857016	-0.670307	0.713716
O	-0.016078	1.223231	-0.357150
C	1.319028	1.454844	-0.233037
O	1.900133	2.354813	-0.795983

C	-1.525156	-0.687231	-0.084200
H	-1.225696	-1.028430	-1.085837
C	-2.829131	0.127126	-0.193288
H	-2.596645	1.058337	-0.736184
H	-1.696100	-1.583327	0.536331
C	3.194293	-0.282288	0.173968
H	3.996139	-0.259314	0.922682
H	3.545183	0.263098	-0.713466
C	-3.859326	-0.664867	-1.012586
H	-3.472214	-0.898816	-2.015967
H	-4.105697	-1.615485	-0.511100
H	-4.791148	-0.091463	-1.127387
C	-3.401528	0.495930	1.185509
H	-2.709671	1.125679	1.764537
H	-4.343684	1.052633	1.071214
H	-3.610814	-0.415008	1.770815

E-Iminium

C	-1.808680	-0.026187	-0.781309
C	-0.628081	-1.779757	0.417396
C	-2.007220	-1.540139	1.047997
H	-1.997579	0.177389	-1.843055
H	-0.573532	-2.754146	-0.091543
H	0.204781	-1.692547	1.123341
C	0.566660	-0.232206	-1.122079
H	0.437553	0.578763	-1.838132
N	-0.533162	-0.715271	-0.618070
O	-0.524178	1.939758	-0.157992
C	-1.676441	1.453677	-0.079207
O	-2.753071	1.866263	0.375131
C	1.939764	-0.703978	-0.800883
H	1.923811	-1.633165	-0.213225
C	2.761104	0.378077	-0.034656
H	2.712144	1.307677	-0.625179
H	2.453539	-0.917319	-1.753199
C	-2.830209	-0.932697	-0.103653
H	-3.195486	-1.717795	-0.785854
H	-3.672287	-0.327665	0.249649
C	2.154620	0.655812	1.348806
H	1.128023	1.036730	1.250957
H	2.156471	-0.264051	1.958384
H	2.753903	1.411100	1.878074
C	4.225872	-0.073030	0.058867
H	4.660491	-0.242462	-0.938255
H	4.827683	0.689757	0.573803
H	4.303580	-1.010573	0.632960
H	-2.432655	-2.468434	1.449329
H	-1.922230	-0.806472	1.862335

TS *Endo*-Oxazolidinone → *E*-Iminium

C	1.838722	0.208139	0.754714
C	1.118329	-1.527543	-0.765040
C	2.610060	-1.754540	-0.493817
H	1.892748	0.275405	1.850264
H	0.508011	-2.439167	-0.760221
H	0.948639	-0.983903	-1.708952
C	-0.495951	-0.306246	0.663187
H	-0.611210	0.352034	1.522476
N	0.726923	-0.652003	0.358983
O	0.262918	1.923068	0.070205
C	1.493109	1.710181	0.252857
O	2.495150	2.432704	0.151886
C	-1.707276	-0.887370	0.007777
H	-1.560665	-0.912559	-1.085944
C	-3.003818	-0.123968	0.352162
H	-3.048792	-0.037095	1.453061
H	-1.801005	-1.941900	0.332482
C	3.089685	-0.409317	0.102393
H	3.904203	-0.550895	0.823192
H	3.451655	0.276632	-0.674944
C	-2.987867	1.291268	-0.248229
H	-2.084000	1.846888	0.038162
H	-3.006539	1.231653	-1.348821
H	-3.874284	1.854185	0.079439
C	-4.232527	-0.919911	-0.112678
H	-4.272557	-1.916651	0.352711
H	-5.158054	-0.386515	0.148332
H	-4.217182	-1.052430	-1.206774
H	2.727332	-2.567698	0.238326
H	3.151688	-2.033034	-1.407036

TS *E*-Iminium → s-*Trans*-Enamine

C	-1.814798	0.106137	-0.775588
C	-1.034453	-1.435714	0.862151
C	-2.554988	-1.674116	0.749337
H	-1.797469	0.330824	-1.851585
H	-0.442685	-2.352414	0.980820
H	-0.797823	-0.738259	1.681766
C	0.538408	-0.439256	-0.762579
H	0.622843	0.036706	-1.745764
N	-0.694279	-0.802276	-0.428071
O	-0.393266	1.688118	0.460963
C	-1.592487	1.468900	0.012536
O	-2.573237	2.201840	0.110206
C	1.576592	-0.200275	0.175710
H	0.770868	0.835038	0.377220
C	2.985356	0.133403	-0.294156
H	2.896831	0.651126	-1.265709
H	1.517896	-0.737266	1.130248
C	-3.064516	-0.664381	-0.323012
H	-3.521208	-1.194377	-1.169811
H	-3.797262	0.048312	0.073568
C	3.670184	1.090051	0.696620
H	3.100409	2.023986	0.800427
H	3.749293	0.623741	1.691666
H	4.686578	1.338147	0.357505
C	3.815098	-1.146983	-0.508777
H	3.329979	-1.813933	-1.237882
H	4.823804	-0.904735	-0.875901
H	3.922778	-1.697553	0.439570
H	-3.044769	-1.522161	1.719368
H	-2.756312	-2.707203	0.435469

s-T*rans*-Enamine

C	1.722192	0.036111	-0.776716
C	0.660248	1.668600	0.665172
C	2.191242	1.836298	0.757457
H	1.678775	-0.258950	-1.835905
H	0.147673	2.594356	0.347259
H	0.227041	1.352093	1.630061
C	-0.738094	-0.003004	-0.535857
N	0.474593	0.629296	-0.346050
O	1.821927	-1.392170	1.213387
C	2.114395	-1.191999	0.052116
O	2.881268	-2.052478	-0.676818
C	2.729488	1.182229	-0.532405
H	2.666597	1.876898	-1.382492
H	3.765245	0.830317	-0.438812
C	-1.912369	0.318217	0.053350
C	-3.206593	-0.396487	-0.243668
H	-2.998505	-1.172592	-1.001556
H	-0.701334	-0.824243	-1.260495
C	-4.257002	0.571586	-0.825112
H	-4.473863	1.376553	-0.103481
H	-3.890764	1.033903	-1.753382
H	-5.200019	0.045234	-1.041892
C	-3.756527	-1.095409	1.017227
H	-4.699676	-1.619775	0.795163
H	-3.029424	-1.821588	1.409266
H	-3.956254	-0.351405	1.805988
H	-1.956943	1.132789	0.786112
H	2.570792	1.296797	1.635605
H	2.491265	2.888736	0.843427
H	3.128161	-2.786379	-0.080671

Exo-Oxazolidinone + DMSO

C	1.399489	2.094437	0.465345
C	0.181344	2.073754	-1.557143
C	0.424745	3.548581	-1.232348
H	2.441035	2.107534	0.824931
H	0.238803	1.837146	-2.627880
H	-0.809848	1.752426	-1.181540
C	1.025855	0.006429	-0.505823
N	1.283495	1.395596	-0.832387
O	0.351441	0.027494	0.823136
C	0.579276	1.221486	1.426922
O	0.164285	1.492827	2.532717
C	0.834402	3.520383	0.259193
H	1.579382	4.287614	0.503999
H	-0.030144	3.672225	0.920506
C	2.286830	-0.840278	-0.388860
H	2.750327	-0.863241	-1.389114
H	2.996092	-0.328402	0.282133
C	2.042691	-2.278560	0.108873
H	1.554283	-2.206405	1.095282
H	0.287738	-0.426219	-1.189831
C	3.384872	-3.003503	0.294415
H	3.913643	-3.092161	-0.668740
H	4.038846	-2.458740	0.992704
H	3.230923	-4.018848	0.690259
C	1.113656	-3.063311	-0.833335
H	0.977478	-4.092406	-0.466858
H	0.120452	-2.599687	-0.919544
H	1.552376	-3.122379	-1.843354
S	-2.590549	-0.478377	-0.066057
O	-1.899044	-1.124237	-1.283608
C	-4.388553	-0.788301	-0.304139
H	-4.931956	-0.463274	0.594251
H	-4.693273	-0.193703	-1.173569
H	-4.533212	-1.859317	-0.498825
C	-2.359331	-1.640442	1.337004
H	-1.293557	-1.602040	1.584528
H	-2.961328	-1.294456	2.188325
H	-2.661017	-2.642600	1.004380
H	1.249768	3.934604	-1.848472
H	-0.463148	4.169296	-1.413938

Z-Iminium + DMSO

C	0.559830	-2.567894	0.708334
C	0.638265	-1.680001	-1.553186
C	1.912867	-2.477099	-1.253122
H	-0.174092	-3.105933	1.322294
H	0.014928	-2.187811	-2.303900
H	0.771807	-0.629444	-1.842570
C	-1.109776	-0.917015	-0.024568
N	-0.112534	-1.712499	-0.262170
O	1.027287	-0.451820	1.839699
C	1.414346	-1.642478	1.754540
O	2.309152	-2.280894	2.324530
C	1.470339	-3.451615	-0.143898
H	0.920386	-4.307830	-0.567387
H	2.302026	-3.818196	0.467764
H	2.292856	-2.982084	-2.150635
H	2.700227	-1.813444	-0.867654
S	0.972645	2.429704	-0.760871
C	2.485285	1.480327	-0.332727
H	2.195535	0.644843	0.321798
H	2.917990	1.145330	-1.283429
H	3.179392	2.159792	0.180582
C	0.335106	2.560519	0.954007
H	-0.658184	3.017706	0.879962
H	0.307416	1.551179	1.389061
H	1.014524	3.214306	1.518272
O	0.034067	1.446137	-1.505320
H	-1.332714	-0.203314	-0.819555
C	-1.932810	-0.942109	1.219323
H	-2.020002	-1.983009	1.574044
H	-1.368660	-0.405308	2.000144
C	-3.336677	-0.322374	1.027783
H	-3.863544	-0.471048	1.984927
C	-3.262440	1.190791	0.764143
H	-2.760209	1.706187	1.595850
H	-2.706165	1.415138	-0.159526
H	-4.272449	1.613437	0.658624
C	-4.132328	-1.052396	-0.067344
H	-4.188660	-2.133030	0.135314
H	-5.158662	-0.661867	-0.129331
H	-3.665363	-0.914043	-1.056336

TS *Exo*-Oxazolidinone → *Z*-Iminium + DMSO

C	0.898623	-2.776343	0.759718
C	0.570515	-1.990670	-1.521112
C	2.065236	-2.229821	-1.261013
H	0.476181	-3.564668	1.395440
H	0.168624	-2.720155	-2.240949
H	0.310325	-0.976732	-1.853866
C	-1.031464	-1.472524	0.264502
N	-0.073129	-2.247796	-0.204979
O	0.492466	-0.529932	1.585213
C	1.280975	-1.532316	1.689153
O	2.290941	-1.671468	2.390142
C	2.076868	-3.242573	-0.097248
H	1.914316	-4.268311	-0.463205
H	2.999748	-3.213744	0.493628
H	2.581654	-2.597823	-2.157132
H	2.550638	-1.296222	-0.942326
S	-0.069204	2.266572	-0.944408
C	1.627852	1.646210	-0.613720
H	1.547431	0.805576	0.089547
H	2.042110	1.342302	-1.582587
H	2.219316	2.467844	-0.187381
C	-0.539213	2.472583	0.819497
H	-1.603957	2.733023	0.830853
H	-0.336692	1.528757	1.343358
H	0.058783	3.296208	1.233202
O	-0.875461	1.060721	-1.485121
H	-1.383217	-0.698753	-0.426271
C	-1.880606	-1.817634	1.446022
H	-2.685981	-2.473510	1.054918
H	-1.314840	-2.405462	2.179877
C	-2.537175	-0.600853	2.132877
H	-1.717256	0.061157	2.446537
C	-3.468393	0.167115	1.180303
H	-2.938847	0.548556	0.295532

H	-4.290317	-0.481579	0.835066
H	-3.917537	1.027378	1.699456
C	-3.292010	-1.063755	3.387877
H	-2.616818	-1.574027	4.090891
H	-3.741712	-0.205328	3.908553
H	-4.103295	-1.761320	3.122055

TS *Z*-Iminium → s-*Cis*-Enamine + DMSO

C	0.533561	-2.141636	0.492581
C	1.270452	-1.500746	-1.764293
C	2.470006	-1.956241	-0.922217
H	-0.260410	-2.821286	0.839701
H	1.066803	-2.202091	-2.589214
H	1.360408	-0.478690	-2.153856
C	-1.026156	-0.946915	-1.022716
N	0.138302	-1.542764	-0.809629
O	-0.326596	-0.248302	1.767310
C	0.723440	-0.994436	1.543570
O	1.818218	-0.831572	2.080657
C	1.841765	-2.860696	0.155694
H	1.626564	-3.861286	-0.249962
H	2.472011	-2.953271	1.047185
C	-2.079091	-0.918843	-0.078447
H	-2.224086	-1.860450	0.474440
H	-1.279447	-0.428653	0.925584
C	-3.366700	-0.166338	-0.425611
H	-3.738361	-0.511511	-1.409292
H	-1.070618	-0.351716	-1.939362
H	2.943914	-1.091708	-0.438542
H	3.223339	-2.474685	-1.529656
C	-3.115134	1.350192	-0.524813
H	-2.836896	1.747681	0.463618
H	-2.295189	1.581141	-1.220465
H	-4.021088	1.873985	-0.867011
C	-4.454464	-0.471481	0.615981
H	-5.384647	0.067165	0.380774
H	-4.681290	-1.548474	0.650272
H	-4.121848	-0.160551	1.619207
S	1.217356	2.686094	-0.565002
O	0.583453	1.546792	-1.394732
C	0.150646	2.909272	0.911325
H	0.656042	3.602128	1.598347
H	-0.788096	3.346538	0.551632
H	-0.014697	1.924680	1.372668
C	2.653723	1.959215	0.320777
H	3.363914	1.647605	-0.455138
H	3.100375	2.745796	0.944997
H	2.326346	1.107360	0.932954

s-Cis-Enamine + DMSO

C	-1.315800	-1.525099	0.808315
C	-2.575712	-2.215276	-1.161248
C	-1.733750	-3.400435	-0.658875
H	-1.626194	-1.067728	1.761212
H	-3.659422	-2.421467	-1.076274
H	-2.355428	-1.968141	-2.211928
C	-2.406490	0.210522	-0.570939
N	-2.185146	-1.115326	-0.275584
O	0.650346	-1.159628	-0.574908
C	0.148039	-1.134761	0.546066
O	0.791381	-0.803195	1.657710
C	-1.477483	-3.063915	0.822278
H	-2.349368	-3.321644	1.441401
H	-0.597999	-3.574187	1.236752
C	-1.934357	1.287345	0.106152
C	-2.260553	2.711684	-0.273267
H	-2.907629	2.682875	-1.167837
H	-3.044551	0.364213	-1.447221
C	-0.986850	3.504149	-0.637337
H	-0.303841	3.544662	0.226713
H	-0.456069	3.024817	-1.472805
H	-1.230696	4.539587	-0.924143
C	-3.035796	3.431278	0.851146
H	-3.275445	4.468881	0.568020
H	-3.973478	2.902966	1.075998
H	-2.432470	3.460550	1.773096
H	-1.294122	1.151376	0.985083
H	-0.779769	-3.432461	-1.202273
H	-2.246181	-4.363534	-0.789216
S	3.727077	0.689600	0.066817
C	3.734657	-0.567932	-1.265418
H	3.972959	-0.061727	-2.211613
H	4.522370	-1.284941	-1.005201
H	2.740893	-1.035717	-1.281806
C	2.306454	1.675105	-0.541441
H	2.081000	2.406029	0.243297
H	2.620420	2.188652	-1.460633
H	1.458137	1.003157	-0.723010
O	3.236800	-0.047022	1.347917
H	1.770216	-0.548617	1.469270

Endo-Oxazolidinone + DMSO

C	0.839121	-2.343813	0.663367
C	0.134048	-2.095622	-1.598580
C	1.356405	-3.017272	-1.614327
H	0.670491	-3.056416	1.489285
H	-0.648228	-2.411237	-2.302056
H	0.417246	-1.056580	-1.842444
C	-1.139262	-1.166670	0.357993
H	-1.741789	-1.552472	1.197358
N	-0.353657	-2.240683	-0.203491
O	-0.152489	-0.249193	1.020726
C	0.983491	-0.943210	1.271333
O	1.931068	-0.471949	1.865341
C	-1.990372	-0.390022	-0.632176
H	-1.330696	0.241512	-1.248022
C	-3.107096	0.469558	-0.006017
H	-3.694472	-0.179568	0.669502
H	-2.453102	-1.138701	-1.294801
C	2.020153	-2.761988	-0.243620
H	2.540932	-3.644704	0.147791
H	2.746914	-1.939951	-0.300704
C	-2.559386	1.651736	0.811884
H	-1.948447	1.313176	1.658840
H	-1.931112	2.291130	0.171999
H	-3.386618	2.262835	1.203593
C	-4.045162	0.971728	-1.116454
H	-4.483734	0.132286	-1.677891
H	-4.867097	1.569864	-0.695010
H	-3.491472	1.605229	-1.827563
S	1.754607	1.263872	-1.147409
C	1.530914	2.460285	0.224229
H	1.362007	3.453911	-0.211394
H	0.656098	2.114188	0.783743
H	2.421510	2.432013	0.865456
C	3.155589	2.130821	-1.965635
H	3.399757	1.550685	-2.863410
H	2.824478	3.142010	-2.237362
H	4.011648	2.156590	-1.277094
O	0.545911	1.436505	-2.087715
H	2.028829	-2.798212	-2.454891
H	1.032800	-4.065643	-1.692961

E-Iminium + DMSO

C	0.831850	-2.305259	0.974895
C	0.282497	-2.017054	-1.386816
C	1.794136	-2.222920	-1.219659
H	0.435356	-2.945732	1.773255
H	-0.203374	-2.853736	-1.912508
H	0.021497	-1.063684	-1.863144
C	-1.403065	-1.577006	0.362665
H	-1.612526	-1.615889	1.432450
N	-0.230092	-2.003300	0.008073
O	0.239996	-0.275353	2.114230
C	1.233080	-0.901544	1.672209
O	2.450591	-0.636445	1.673113
C	-2.423998	-1.061728	-0.594558
H	-1.937329	-0.339387	-1.272280
C	-3.615482	-0.391725	0.119092
H	-4.009733	-1.106931	0.863903
H	-2.778004	-1.903499	-1.220047
C	1.936810	-2.940347	0.136141
H	1.780481	-4.026077	0.031612
H	2.908543	-2.750742	0.605870
C	-3.154033	0.877165	0.854917
H	-2.338077	0.663347	1.560628
H	-2.779725	1.611999	0.126403
H	-3.988483	1.329646	1.410893
C	-4.733732	-0.083163	-0.886440
H	-5.088708	-0.998381	-1.385417
H	-5.591615	0.385700	-0.382198
H	-4.373626	0.612307	-1.661178
H	2.218827	-2.791834	-2.056716
H	2.293778	-1.247165	-1.169219
S	0.688784	2.297589	-0.955977
C	2.402612	1.726198	-0.632746
H	2.403748	0.947457	0.145252
H	2.780467	1.347817	-1.590871
H	2.990793	2.599556	-0.317365
C	0.235150	2.624819	0.789255
H	-0.775836	3.049071	0.777366
H	0.269546	1.673601	1.346196
H	0.948602	3.357564	1.191119
O	-0.119659	1.051873	-1.398185

TS *Endo*-Oxazolidinone → *E*-Iminium

C	0.657581	-2.402469	0.754857
C	0.294734	-1.864976	-1.594702
C	1.792269	-2.099734	-1.330901
H	0.236270	-3.114801	1.479953
H	-0.136016	-2.622497	-2.268102
H	0.102592	-0.859423	-1.984783
C	-1.341418	-1.302792	0.198018
H	-1.745445	-1.603280	1.164679
N	-0.335753	-2.027174	-0.259191
O	-0.014314	-0.222029	1.519409
C	0.961240	-1.047693	1.531301
O	2.081471	-0.921078	2.049654
C	-2.130641	-0.381865	-0.673133
H	-1.452997	0.429867	-0.997042
C	-3.398481	0.181722	-0.003354
H	-3.973923	-0.672518	0.398035
H	-2.406122	-0.932262	-1.590598
C	1.843436	-2.941362	-0.038918
H	1.717524	-4.014052	-0.251928
H	2.769191	-2.791520	0.529415
C	-3.052373	1.122283	1.162278
H	-2.390064	0.642041	1.895273
H	-2.532539	2.014902	0.782300
H	-3.967647	1.451993	1.676130
C	-4.272318	0.892483	-1.048187
H	-4.570727	0.205555	-1.855267
H	-5.185566	1.294714	-0.585228
H	-3.721947	1.732011	-1.502268
H	2.283454	-2.589670	-2.181548
H	2.278376	-1.130029	-1.162137
S	1.404373	2.407580	-0.927387
C	2.845606	1.597350	-0.126890
H	2.506547	0.826600	0.579808
H	3.443572	1.166845	-0.939680
H	3.422828	2.377004	0.389717
C	0.515939	2.825913	0.622551
H	-0.406003	3.339253	0.323594
H	0.305102	1.886233	1.153978
H	1.152007	3.499631	1.213162
O	0.582308	1.292047	-1.614291

TS *E*-Iminium → s-Trans-Enamine

C	-1.493768	-1.554169	0.891466
C	-2.480525	-1.802807	-1.307838
C	-2.132912	-3.211307	-0.774365
H	-1.760654	-1.123319	1.866443
H	-3.525027	-1.713058	-1.650677
H	-1.825492	-1.519232	-2.152364
C	-2.216035	0.467676	-0.350195
N	-2.269699	-0.903319	-0.172888
O	0.579386	-1.787950	-0.348246
C	-0.002586	-1.315783	0.629089
O	0.546048	-0.477030	1.499160
C	-1.904416	-3.027609	0.744021
H	-2.837534	-3.183183	1.303939
H	-1.143021	-3.711739	1.141045
C	-2.510350	1.146297	-1.485805
C	-2.512538	2.653495	-1.574323
H	-2.125133	3.048948	-0.618593
H	-1.924992	1.015687	0.551728
C	-3.941554	3.205125	-1.769381
H	-4.378695	2.814614	-2.702671
H	-4.591528	2.901381	-0.936293
H	-3.936894	4.305358	-1.829214
C	-1.587749	3.147400	-2.706428
H	-1.580678	4.247366	-2.761737
H	-0.556469	2.798615	-2.550489
H	-1.932347	2.760233	-3.679034
H	-2.802129	0.602377	-2.390674
S	3.292293	0.665174	-0.582666
C	3.527165	-0.973702	-1.366552
H	3.679377	-0.819226	-2.444199
H	4.425444	-1.406145	-0.910099
H	2.630220	-1.570900	-1.152590
C	1.744879	1.129124	-1.451200
H	1.375134	2.034254	-0.955934
H	1.996204	1.343035	-2.499062
H	1.023859	0.306635	-1.370804
O	2.900239	0.377808	0.896599
H	1.503413	-0.216320	1.224259
H	-1.212673	-3.570177	-1.250122
H	-2.93371	3-3.935186	-0.977910

Z-Iminium + H_2O

C	-1.310168	0.094132	-0.100076
C	-1.595755	-2.292106	0.379100
C	-2.904597	-1.549752	0.672538
H	-0.900924	0.572774	-0.996936
H	-1.671733	-2.896620	-0.538282
H	-1.226900	-2.915446	1.202515
C	0.656597	-1.314905	0.234965
N	-0.628096	-1.191442	0.115769
O	-0.964805	2.271900	0.843395
C	-1.031200	1.056652	1.165414
O	-0.933480	0.484885	2.264696
C	-2.795032	-0.290995	-0.209622
H	-3.443223	0.523095	0.135704
C	1.602862	-0.182723	0.077080
H	1.259871	0.498839	-0.720435
C	3.071338	-0.601777	-0.150529
H	3.095303	-1.310589	-0.998055
H	1.025811	-2.314236	0.484952
C	3.666933	-1.295720	1.084789
H	3.649056	-0.613888	1.949734
H	3.112175	-2.206059	1.361787
H	4.710532	-1.588558	0.899493
C	3.890014	0.638333	-0.543227
H	4.941338	0.372321	-0.727025
H	3.483239	1.102645	-1.452503
H	3.860651	1.389760	0.262337
O	0.292426	2.376982	-1.514132
H	-0.198282	2.487823	-0.644822
H	0.297401	3.251453	-1.928663
H	1.526069	0.417799	1.007036
H	-3.776696	-2.172639	0.434764
H	-2.933369	-1.262135	1.730926
H	-3.058775	-0.515339	-1.255686

TS *Z*-Iminium → s-*Cis*-Enamin + H_2O

C	-1.469004	0.113211	-0.545233
C	-1.580614	-1.777232	0.910748
C	-2.795842	-1.873957	-0.047060
H	-0.843792	0.615207	-1.294099
H	-1.070347	-2.732795	1.082815
H	-1.866830	-1.343102	1.879608
C	0.662025	-0.969036	0.229093
N	-0.657057	-0.847975	0.222660
O	-1.266744	2.038949	0.963150
C	-2.085174	1.177454	0.452195
O	-3.289714	1.105134	0.690340
C	-2.554907	-0.794507	-1.138229
H	-2.184369	-1.251105	-2.067138
H	-3.461765	-0.219389	-1.352485
C	1.598901	-0.144568	-0.442538
H	1.217105	0.304291	-1.372464
C	3.066036	-0.596999	-0.546937
H	3.128457	-1.442082	-1.258187
H	1.019338	-1.752105	0.906325
C	3.637034	-1.074908	0.800360
H	3.530650	-0.290674	1.567674
H	3.139340	-1.985133	1.167454
H	4.706590	-1.310164	0.696884
C	3.916954	0.552365	-1.114885
H	4.956993	0.229240	-1.271468
H	3.517848	0.895618	-2.080957
H	3.919456	1.411915	-0.426172
O	1.136574	2.194513	0.647093
H	-0.065947	2.083762	0.767017
H	1.506790	2.356923	1.529928
H	1.493890	1.001192	0.229724
H	-2.862669	-2.876014	-0.489119
H	-3.721473	-1.667521	0.499043

E-Iminium + H_2O

C	-1.736048	-1.347073	0.974229
C	-0.336773	-1.814790	0.548365
N	0.022374	-0.868177	-0.538938
C	-1.119991	-0.037572	-0.934767
C	-2.329152	-0.735317	-0.310611
C	1.232766	-0.570292	-0.904193
C	2.464557	-1.200894	-0.346242
C	3.756149	-0.561812	-0.896298
C	-0.893782	1.472809	-0.390519
O	-1.934471	2.137152	-0.348688
O	0.310689	1.769306	-0.131191
H	-1.157244	0.049397	-2.028787
H	-3.116061	0.001727	-0.115261
H	-2.722985	-1.522615	-0.973597
H	-1.635413	-0.573487	1.748264
H	-2.335390	-2.174443	1.375985
H	0.409554	-1.745921	1.347986
H	-0.346764	-2.830463	0.123427
H	2.433213	-1.097309	0.753578
H	0.913261	1.043115	1.309569
O	1.194799	0.465135	2.070643
H	3.714534	-0.612647	-1.999970
H	1.316723	0.181252	-1.689932
H	1.282685	1.062409	2.826912
H	2.442618	-2.285284	-0.563778
C	3.856963	0.915002	-0.475539
H	3.961442	0.990026	0.617882
H	4.732639	1.386320	-0.944955
H	2.962404	1.490080	-0.757449
C	4.985045	-1.354948	-0.427767
H	5.904198	-0.925674	-0.851647
H	5.069108	-1.320007	0.670653
H	4.929777	-2.411055	-0.733855

TS *E*-Iminium → s-*Trans*-Enamin + H_2O

C	-1.904135	-1.684796	0.470340
C	-0.366484	-1.790398	0.375755
N	0.030904	-0.603840	-0.409686
C	-1.109025	0.309010	-0.593860
C	-2.293982	-0.664575	-0.620569
C	1.276631	-0.338118	-0.770762
C	2.427733	-0.969250	-0.246658
C	3.808143	-0.812073	-0.890603
C	-1.261331	1.359043	0.572500
O	-2.315233	1.994886	0.562665
O	-0.304337	1.470375	1.432116
H	-0.979109	0.869317	-1.529465
H	-3.231106	-0.140910	-0.404164
H	-2.365097	-1.148089	-1.606552
H	-2.193431	-1.298937	1.456884
H	-2.387569	-2.660415	0.332473
H	0.122422	-1.766131	1.360871
H	-0.023014	-2.688766	-0.159137
H	2.320684	-0.117203	0.852269
H	0.909397	1.035303	1.549623
O	1.999265	0.745251	1.749530
H	3.884219	-1.528578	-1.729960
H	1.385068	0.565700	-1.377809
H	2.076761	0.421593	2.661200
H	2.258085	-1.948237	0.220470
C	4.049704	0.599099	-1.452723
H	3.894097	1.361303	-0.673081
H	5.083140	0.686292	-1.817670
H	3.383176	0.824814	-2.298862
C	4.897437	-1.184160	0.132230
H	5.892975	-1.167730	-0.335125
H	4.901541	-0.473555	0.974122
H	4.730601	-2.194061	0.536779

Structures Optimized in Solution Phase (using SMD in DMSO)

Exo-Oxazolidinone

C	1.558105	0.422834	0.705093
C	1.892911	-1.582473	-0.510633
C	3.216454	-1.287310	0.194029
H	1.269732	0.745967	1.717468
H	1.636117	-2.649755	-0.551713
H	1.911323	-1.182240	-1.543871
H	3.302131	-1.905268	1.100579
H	4.086157	-1.486066	-0.446740
C	-0.325851	-0.493030	-0.319503
N	0.912662	-0.858624	0.336223
O	-0.074610	0.848531	-0.928544
C	0.966611	1.425205	-0.290215
O	1.326806	2.565522	-0.518937
C	3.086090	0.204874	0.570761
H	3.609719	0.454941	1.501743
H	3.487112	0.846918	-0.226416
C	-1.499388	-0.374788	0.645716
H	-1.644197	-1.374108	1.089512
H	-1.205474	0.304447	1.462687
C	-2.821718	0.108249	0.019776
H	-2.633499	1.084758	-0.457565
H	-0.538506	-1.167228	-1.156649
C	-3.870079	0.314532	1.122934
H	-4.082699	-0.635782	1.641276
H	-3.518196	1.039489	1.874185
H	-4.816023	0.690541	0.701887
C	-3.341012	-0.860857	-1.053912
H	-4.300448	-0.507084	-1.462981
H	-2.638742	-0.960731	-1.895793
H	-3.503448	-1.864273	-0.625603

Z-Iminium

C	-1.406329	0.353036	-0.557042
C	-1.817632	-1.755397	0.601664
C	-3.036903	-1.456339	-0.269142
H	-1.048227	0.453998	-1.589119
H	-1.460485	-2.790283	0.590102
H	-1.977867	-1.425310	1.639275
H	-2.957064	-1.998201	-1.223520
H	-3.972028	-1.747087	0.226456
C	0.472453	-1.139808	-0.022457
N	-0.788135	-0.867785	0.009253
O	-0.545031	1.503581	1.396685
C	-1.026066	1.657483	0.247485
O	-1.305191	2.714770	-0.374125
C	-2.927218	0.064645	-0.491123
H	-3.433148	0.399177	-1.404575
H	-3.367952	0.601120	0.362338
C	1.497135	-0.284936	-0.678163
H	1.447720	-0.511677	-1.761119
H	1.236828	0.778880	-0.570513
C	2.924342	-0.555879	-0.159309
H	3.113765	-1.638200	-0.266374
H	0.773293	-2.088724	0.432021
C	3.051121	-0.186370	1.325883
H	2.881958	0.892584	1.473289
H	2.317139	-0.730793	1.942154
H	4.056192	-0.430998	1.702404
C	3.948435	0.199994	-1.015067
H	4.972124	-0.000317	-0.662777
H	3.884407	-0.102654	-2.072117
H	3.776035	1.287585	-0.959551

TS Exo-Oxazolidinone → *Z*-Iminium

C	1.437723	0.416918	0.756492
C	1.933333	-1.796239	-0.130365
C	3.134387	-0.868766	-0.355212
H	1.067236	0.809101	1.712168
H	2.160210	-2.570286	0.618063
H	1.558139	-2.281615	-1.040471
C	-0.363050	-0.899384	-0.015178
N	0.884954	-0.908084	0.433940
O	0.027646	0.836168	-1.165482
C	0.920137	1.353429	-0.406673
O	1.411956	2.496311	-0.486611
C	2.955793	0.209341	0.730421
H	3.303797	-0.157062	1.708085
H	3.472639	1.149131	0.500636
C	-1.494271	-0.275103	0.740473
H	-1.796845	-1.044983	1.478878
H	-1.146126	0.594524	1.314098
C	-2.731139	0.104900	-0.099444
H	-2.403423	0.857434	-0.832519
H	-0.613871	-1.701351	-0.715658
H	3.076703	-0.410449	-1.354254
H	4.088072	-1.406147	-0.273245
C	-3.786254	0.742213	0.816208
H	-4.135594	0.020082	1.573454
H	-3.378369	1.618746	1.344233
H	-4.660769	1.071150	0.233186
C	-3.318410	-1.095068	-0.858056
H	-4.232600	-0.797047	-1.394884
H	-2.617142	-1.499883	-1.603625
H	-3.583044	-1.908032	-0.160976

TS Z-Iminium → s-*Cis* Enamine

C	1.414309	0.221166	0.559952
C	1.802554	-1.723001	-0.859425
C	2.907094	-1.683145	0.199082
H	0.934048	0.201605	1.553308
H	1.369224	-2.713916	-1.036089
H	2.156329	-1.301569	-1.815407
C	-0.523478	-0.948194	-0.458927
N	0.784940	-0.830572	-0.276114
O	0.107960	1.903100	-0.651541
C	1.218492	1.656208	-0.005532
O	2.093956	2.501994	0.196778
C	2.897449	-0.209240	0.645563
H	3.297899	-0.066989	1.656574
H	3.490366	0.406812	-0.044117
C	-1.474397	-0.057940	0.083509
H	-1.257500	0.308694	1.100520
H	-0.794232	1.027449	-0.457006
C	-2.954862	-0.284274	-0.202340
H	-3.041292	-0.669388	-1.233434
H	-0.820293	-1.705956	-1.191627
C	-3.731960	1.040658	-0.124876
H	-3.640502	1.484586	0.880764
H	-3.346893	1.770766	-0.853859
H	-4.802779	0.881955	-0.328968
C	-3.561306	-1.332068	0.749864
H	-4.625661	-1.508723	0.523263
H	-3.027632	-2.292283	0.667511
H	-3.487638	-0.989940	1.795996
H	3.880142	-1.993302	-0.203670
H	2.643127	-2.347565	1.035940

s-*Cis* Enamine

C	-1.309765	0.140408	-0.701295
C	-1.728850	-1.925914	0.517857
C	-3.069437	-1.219908	0.292250
H	-0.772729	0.207121	-1.662888
H	-1.634141	-2.817010	-0.131600
H	-1.574132	-2.240052	1.560654
C	0.603329	-1.046447	0.316251
N	-0.752842	-0.895132	0.146337
O	-1.339842	1.560891	1.248935
C	-1.247715	1.545834	-0.098933
O	-1.184224	2.566622	-0.764944
C	-2.783813	-0.309086	-0.914452
H	-2.835529	-0.882665	-1.850890
H	-3.475126	0.540350	-0.993609
C	1.579794	-0.216731	-0.139203
C	3.050019	-0.436882	0.132117
H	3.153765	-1.384021	0.690483
H	0.874657	-1.931494	0.901318
C	3.633571	0.694019	1.004721
H	3.526104	1.668072	0.498282
H	3.108494	0.754472	1.970849
H	4.705859	0.529830	1 .202479
C	3.850461	-0.566129	-1.179800
H	4.921138	-0.732671	-0.976354
H	3.479798	-1.407130	-1.786472
H	3.757884	0.354173	-1.780737
H	1.321955	0.677821	-0.718706
H	-1.340663	2.498647	1.534725
H	-3.333548	-0.618289	1.174367
H	-3.886935	-1.926313	0.094737

Endo-Oxazolidinone

C	1.913049	0.372669	0.687144
C	1.236549	-1.623992	-0.365282
C	2.744910	-1.756894	-0.147016
H	2.044209	0.817393	1.687392
H	0.685121	-2.565481	-0.246479
H	1.035663	-1.219439	-1.376436
H	2.939169	-2.404573	0.721025
H	3.254920	-2.184744	-1.020661
C	-0.368068	0.082156	0.521699
H	-0.642174	0.549413	1.478323
N	0.853685	-0.662869	0.700301
O	0.004481	1.250009	-0.360934
C	1.329397	1.460667	-0.225636
O	1.910627	2.385271	-0.765529
C	-1.525068	-0.668848	-0.103889
H	-1.229152	-0.993187	-1.112952
C	-2.840941	0.131359	-0.188120
H	-2.630205	1.075821	-0.717989
H	-1.687354	-1.577922	0.499470
C	3.193778	-0.307343	0.152970
H	4.007470	-0.263694	0.887576
H	3.533202	0.202395	-0.759835
C	-3.866860	-0.655774	-1.016724
H	-3.486452	-0.858751	-2.030471
H	-4.094213	-1.623384	-0.538449
H	-4.809338	-0.093684	-1.110649
C	-3.406748	0.470792	1.199241
H	-2.719172	1.099421	1.785692
H	-4.356823	1.019593	1.103492
H	-3.601524	-0.450095	1.774221

E-Iminium

C	1.831769	-0.014328	-0.514917
C	0.471497	1.838519	0.346260
C	1.939436	2.265522	0.323364
H	2.160576	-0.003534	-1.563562
H	-0.225255	2.562930	-0.087546
H	0.139784	1.573892	1.361179
H	2.154916	2.811607	-0.607557
H	2.183223	2.913429	1.175267
C	-0.548586	0.032474	-1.014118
H	-0.344758	-0.874346	-1.584791
N	0.479432	0.596537	-0.468754
O	0.743684	-2.066711	0.211401
C	1.846441	-1.516946	-0.039314
O	3.008144	-1.994934	0.020332
C	-1.949033	0.507304	-0.907587
H	-2.007334	1.526106	-0.501595
C	-2.798385	-0.453242	-0.018559
H	-2.700657	-1.468270	-0.438293
H	-2.376599	0.503740	-1.923037
C	2.691557	0.925256	0.353399
H	3.714993	0.999729	-0.031568
H	2.737805	0.538018	1.382212
C	-2.278822	-0.469886	1.425502
H	-1.229403	-0.799114	1.462839
H	-2.353054	0.533549	1.875651
H	-2.875992	-1.162035	2.039250
C	-4.272991	-0.037959	-0.090461
H	-4.645009	-0.066094	-1.126374
H	-4.891973	-0.717319	0.516178
H	-4.409218	0.984820	0.297756

TS Endo-Oxazolidinone → *E*-Iminium

C	1.869402	0.260207	0.685741
C	1.171376	-1.721039	-0.490196
C	2.668194	-1.875528	-0.199531
H	1.967904	0.569222	1.736898
H	0.591943	-2.640550	-0.345605
H	0.995827	-1.335198	-1.508867
H	2.805833	-2.530624	0.672080
H	3.212643	-2.303800	-1.050294
C	-0.424074	-0.113857	0.550198
H	-0.597359	0.522973	1.420080
N	0.776156	-0.712192	0.518895
O	0.147272	1.504242	-0.423439
C	1.403939	1.514174	-0.126466
O	2.220033	2.406637	-0.422346
C	-1.611906	-0.708786	-0.141551
H	-1.498441	-0.548134	-1.227044
C	-2.969120	-0.166311	0.349461
H	-3.011690	-0.332726	1.440069
H	-1.571193	-1.799568	0.013288
C	3.133321	-0.437601	0.133457
H	3.953745	-0.427758	0.860566
H	3.472960	0.085956	-0.769947
C	-3.123751	1.338835	0.079747
H	-2.320836	1.920431	0.554546
H	-3.091241	1.541024	-1.003057

H	-4.088241	1.696074	0.471019
C	-4.113535	-0.962902	-0.296907
H	-4.038250	-2.035216	-0.060664
H	-5.087780	-0.597079	0.060030
H	-4.090438	-0.849867	-1.392805

TS *E*-Iminium → s-*Trans*-Enamine

C	-1.831377	0.106221	-0.732568
C	-1.032048	-1.575346	0.781181
C	-2.517798	-1.879524	0.562766
H	-1.919403	0.255150	-1.817735
H	-0.387158	-2.459853	0.850733
H	-0.879780	-0.945296	1.674675
C	0.519689	-0.404327	-0.757928
H	0.596293	0.115795	-1.719664
N	-0.707594	-0.819062	-0.439678
O	-0.423497	1.668453	0.551610
C	-1.551451	1.498631	-0.076451
O	-2.430187	2.363052	-0.199619
C	1.560463	-0.232331	0.174134
H	0.690484	0.811062	0.398571
C	2.959362	0.158481	-0.268642
H	2.864101	0.767450	-1.184161
H	1.493788	-0.782777	1.120248
C	-3.069535	-0.599587	-0.112403
H	-3.817443	-0.834199	-0.880214
H	-3.539826	0.066096	0.623189
C	3.650263	1.007081	0.811281
H	3.077859	1.923439	1.023111
H	3.743942	0.437212	1.750528
H	4.660905	1.299933	0.487251
C	3.788354	-1.093494	-0.610384
H	3.307170	-1.674069	-1.412830
H	4.799599	-0.812117	-0.944547
H	3.888217	-1.746184	0.272510
H	-2.619280	-2.743484	-0.110027
H	-3.032379	-2.111597	1.504259

s-T*rans* Enamine

C	1.697620	0.023013	-0.706452
C	0.582712	1.710967	0.651029
C	2.101001	1.941902	0.711761
H	1.578465	-0.263966	-1.762941
H	0.052786	2.545823	0.154408
H	0.133589	1.578394	1.649856
C	-0.758263	-0.123401	-0.373898
N	0.448388	0.489343	-0.139107
O	1.941740	-1.575309	1.145238
C	2.266401	-1.190297	0.036916
O	3.223194	-1.804698	-0.701812
C	2.628952	1.254130	-0.559750
H	2.485985	1.898126	-1.439227
H	3.689974	0.979865	-0.497488
C	-1.974421	0.280781	0.081795
C	-3.258840	-0.452644	-0.230025
H	-3.004778	-1.325937	-0.856692
H	-0.684402	-1.021417	-0.996531
C	-4.237238	0.434625	-1.027812
H	-4.505776	1.334157	-0.448443
H	-3.784043	0.764495	-1.975806
H	-5.167653	-0.109408	-1.260546
C	-3.936711	-0.972505	1.054279
H	-4.867890	-1.515013	0.820941
H	-3.268498	-1.654388	1.603238
H	-4.191291	-0.134076	1.724469
H	-2.057337	1.177396	0.707485
H	2.521352	1.460118	1.606989
H	2.358360	3.008933	0.744905
H	3.585691	-2.547879	-0.175343

Structures of Oxazolidinone + Proline Precomplexes and their Deprotonation TS

Exo-Oxa (Isopentanal) + Proline Precomplex

C	-3.208343	-1.349572	-0.138671
C	-1.853050	-1.525883	-0.842233
C	-0.772165	-0.512521	-0.379636
C	-0.918958	0.905907	-0.910059
N	0.199700	1.815769	-0.419485
C	0.663470	2.858276	-1.417455
C	1.178485	3.982587	-0.522263
C	0.159261	4.030170	0.636914
C	-0.363632	2.577081	0.754056
C	-1.871374	2.428910	0.565406
O	-2.107985	1.557475	-0.459825
O	-2.734212	2.993834	1.172487
O	2.508091	0.122715	-1.842992
C	3.006088	0.107798	-0.715027
O	2.504644	0.592472	0.369088
C	4.399035	-0.560985	-0.544660
C	4.424873	-2.065436	-0.865633
C	4.095703	-2.740563	0.477135
C	4.856196	-1.890674	1.497137
N	4.734402	-0.480191	0.946757
H	5.918702	-2.142983	1.521503
H	-0.919772	0.934111	-1.999981
H	-0.672273	4.703705	0.413369
H	0.605400	4.364237	1.574792
H	-0.061421	2.085310	1.681868
H	1.399331	2.389717	-2.072062
H	-0.208274	3.172281	-1.999213
H	-0.740026	-0.484783	0.717743
H	1.053857	1.256164	-0.117540
H	-1.454053	-2.501717	-0.533321
H	3.019924	-2.708503	0.679408
H	4.412073	-3.785232	0.516800
H	4.457434	-1.913321	2.512430
H	5.420697	-2.362424	-1.210247
H	3.712240	-2.296323	-1.659230
H	5.134246	0.011843	-1.113186
H	0.206561	-0.860127	-0.730034
H	3.889814	0.026895	1.312085
H	1.242058	4.930053	-1.062220
H	2.178904	3.738874	-0.150990
H	5.563997	0.082552	1.138818
H	-3.097876	-1.349550	0.951629
H	-3.702230	-0.417547	-0.426510
H	-3.875492	-2.176614	-0.401748
C	-2.008665	-1.562093	-2.371724
H	-2.501910	-0.660356	-2.753866
H	-1.043307	-1.668707	-2.880442
H	-2.632593	-2.410935	-2.666960

Endo-Oxa (Isopentanal) + Proline Precomplex

C	-1.150419	1.067561	0.071806
N	-0.713770	-0.333628	0.500631
C	-1.271801	-0.938376	1.789385
C	-2.197284	-2.080584	1.348783
C	-1.613895	-2.534110	0.000282
C	-1.175404	-1.217092	-0.638978
C	-2.338857	-0.417743	-1.230177
O	-2.334363	0.838684	-0.691870
O	-3.161234	-0.807328	-2.007332
O	1.630285	0.132452	-1.575526
C	2.361864	-0.051644	-0.598965
O	2.004207	-0.344882	0.603462
C	3.894975	0.087331	-0.807375
C	4.491786	-0.919119	-1.805801
C	4.848599	-2.137307	-0.936937
C	5.400349	-1.509265	0.345120
N	4.545409	-0.266773	0.532024
H	6.434463	-1.180078	0.221245
H	-2.337562	-3.049545	-0.634897
H	-0.748497	-3.189864	0.139383
H	-0.371933	-1.289059	-1.377191
H	-0.406450	-1.303429	2.346987
H	-1.765589	-0.168420	2.378407
H	0.348716	-0.333785	0.557678
H	3.958606	-2.736493	-0.717330
H	5.585448	-2.793211	-1.405760
H	5.325296	-2.131097	1.238381
H	5.390801	-0.502814	-2.271624
H	3.773126	-1.139267	-2.596934
H	4.120557	1.126132	-1.056529
H	-3.222333	-1.718272	1.218557
H	-2.221985	-2.880013	2.092641
H	5.073690	0.508015	0.935096
C	-1.376145	2.057676	1.199167
H	-2.332175	1.840964	1.691333
C	-1.342603	3.542539	0.761333
H	-0.392802	3.704292	0.229631
C	-1.340041	4.437176	2.011137
H	-0.496365	4.211077	2.673287
H	-1.269870	5.492032	1.729350
H	-2.264776	4.311355	2.587025
C	-2.493980	3.922695	-0.182507
H	-2.484733	3.345910	-1.110742
H	-3.465034	3.759710	0.299793
H	-2.427990	4.982886	-0.445678
H	-0.353907	1.397281	-0.603612
H	3.698067	-0.442105	1.126550
H	-0.578407	1.900613	1.937227

Exo-Oxa(Isopentanal) + Proline TS

C	2.101062	3.631451	1.095205
C	1.317711	2.982342	-0.036656
C	1.000915	1.498990	0.175099
C	1.710009	0.528756	-0.533566
N	1.300087	-0.892196	-0.348527
C	1.519652	-1.781966	-1.555404
C	1.437591	-3.184012	-0.961573
C	2.133964	-3.060742	0.415039
C	2.057143	-1.560793	0.788895
C	3.417083	-0.845131	0.844310
O	3.475628	0.180484	0.061248
O	4.312764	-1.266973	1.580425
O	-1.486434	1.365416	-0.728144
C	-2.059254	0.239028	-0.478465
O	-1.493854	-0.805067	-0.104320
C	-3.577821	0.248886	-0.677717
C	-4.342098	1.142265	0.328216
C	-4.759147	0.179918	1.452380
C	-5.119244	-1.101003	0.704603
N	-4.085131	-1.159353	-0.410597
H	-6.098392	-1.033915	0.229265
H	2.039208	0.743997	-1.544111
H	3.181938	-3.363874	0.362263
H	1.647531	-3.679399	1.170552
H	1.513516	-1.380021	1.718097
H	0.765243	-1.547305	-2.306756
H	2.513221	-1.553808	-1.946232
H	0.709855	1.234854	1.195637
H	0.273275	-0.899176	-0.145141
H	0.381169	3.539777	-0.158166
H	-3.932557	0.001288	2.147298
H	-5.609114	0.553934	2.026424
H	-5.054910	-2.018901	1.288160
H	-5.222516	1.563030	-0.164149
H	-3.718847	1.968557	0.672576
H	-3.789686	0.511990	-1.714905
H	-0.361269	1.350066	-0.431975
H	-3.256287	-1.707453	-0.126362
H	1.922959	-3.915268	-1.610896
H	0.391803	-3.482930	-0.843179
H	-4.460769	-1.596538	-1.254200
H	1.807069	3.196615	2.027613
H	3.147923	3.472062	0.941654
H	1.898954	4.682054	1.112138
C	2.086821	3.145452	-1.360841
H	3.085704	2.781299	-1.240323
H	1.594453	2.588238	-2.130248
H	2.114685	4.180148	-1.632001

Endo-Oxa(Isopentanal) + Proline TS

C	-1.314794	0.732367	-0.223623
N	-1.449429	-0.693113	0.155081
C	-2.122368	-0.971803	1.501305
C	-2.923512	-2.280020	1.306645
C	-2.628362	-2.751780	-0.135836
C	-2.266820	-1.468977	-0.870766
C	-3.492382	-0.560906	-1.219634
O	-3.333209	0.642713	-0.807709
O	-4.424448	-1.083939	-1.821227
O	1.770879	1.077680	0.624431
C	2.179038	-0.133286	0.439624
O	1.489746	-1.144197	0.255479
C	3.712133	-0.255692	0.464171
C	4.432497	0.475549	-0.691314
C	4.545870	-0.586809	-1.798075
C	4.862217	-1.868171	-1.028650
N	4.023504	-1.733489	0.241372
H	5.908641	-1.912410	-0.719686
H	-3.494608	-3.212887	-0.613636
H	-1.799558	-3.469530	-0.158351
H	-1.649253	-1.621919	-1.760989
H	-1.341122	-1.034251	2.260518
H	-2.767374	-0.119724	1.706631
H	-0.494647	-1.082698	0.186772
H	3.605324	-0.689398	-2.349821
H	5.330627	-0.355690	-2.521546
H	4.591822	-2.797970	-1.530636
H	5.424155	0.795658	-0.358227
H	3.880322	1.366588	-0.994192
H	4.071671	0.048574	1.449606
H	-3.988981	-2.070640	1.423594
H	-2.649730	-3.032584	2.049536
H	4.480230	-2.162148	1.049116
C	-0.950297	1.693893	0.677052
H	-1.163699	1.526493	1.734440
H	0.704434	1.200073	0.599069
C	-0.876553	3.160871	0.255567
H	-0.521614	3.199521	-0.784990
C	0.098185	3.966081	1.131962
H	1.128280	3.601159	1.059796
H	0.097090	5.018941	0.833701
H	-0.202415	3.924919	2.186103
C	-2.287427	3.785947	0.293304
H	-2.986191	3.227187	-0.334047
H	-2.680342	3.789770	1.317105
H	-2.251576	4.824609	-0.053051
H	-1.110671	0.859892	-1.280520
H	3.089304	-2.176525	0.133823

Exo-Oxa (3-Phenyl-Propanal) + Proline Precomplex

C	-4.153775	-1.419793	-1.201304
C	-3.060573	-1.815669	-0.421063
C	-3.293485	-2.221866	0.901784
C	-4.583579	-2.217287	1.435684
C	-5.665437	-1.811590	0.648740
C	-5.447399	-1.416378	-0.672506
C	-1.654948	-1.836178	-0.992771
C	-0.661861	-0.819314	-0.379654
C	-0.850625	0.607513	-0.873871
N	0.160240	1.563242	-0.255634
C	0.596739	2.701288	-1.156523
C	0.974428	3.797344	-0.163306
C	-0.096516	3.686979	0.945602
C	-0.544435	2.205376	0.912434
C	-2.019604	1.998391	0.567951
O	-2.109977	1.170184	-0.514980
O	-2.962340	2.497873	1.108905
O	2.580827	0.119942	-1.699218
C	3.062400	0.054449	-0.565386
O	2.513606	0.421471	0.541069
C	4.496013	-0.528492	-0.418708
C	4.635913	-1.990294	-0.876266
C	4.319960	-2.808649	0.387813
C	4.993324	-2.009375	1.505629
N	4.793478	-0.564005	1.081878
H	6.069167	-2.194320	1.543359
H	-0.756402	0.668842	-1.959816
H	-0.955331	4.332944	0.745719
H	0.292568	3.958259	1.928145
H	-0.302743	1.659262	1.827516
H	1.400704	2.332849	-1.794607
H	-0.263785	2.987361	-1.768566
H	-0.727277	-0.842366	0.715049
H	1.034842	1.048372	0.063336
H	-1.692014	-1.692533	-2.079367
H	-1.220138	-2.830599	-0.836153
H	3.239621	-2.866945	0.557669
H	4.706336	-3.829224	0.342048
H	4.568830	-2.151179	2.500622
H	5.658507	-2.186121	-1.214865
H	3.961384	-2.192663	-1.709917
H	5.199519	0.145158	-0.911982
H	0.357991	-1.105090	-0.658983
H	-3.995476	-1.110488	-2.231607
H	-6.282484	-1.105688	-1.293160
H	-6.669779	-1.810088	1.060942

H	-4.745891	-2.538739	2.460326
H	-2.463110	-2.560838	1.518707
H	3.911670	-0.143609	1.468630
H	0.985861	4.781750	-0.636628
H	1.973579	3.608356	0.241819
H	5.581655	0.028184	1.346170

Exo-Oxa (3-Phenyl-Propanal) + Proline TS

C	-3.771037	-1.258780	-0.201872
C	-2.687684	-2.103805	-0.490308
C	-2.734103	-3.437320	-0.062027
C	-3.841190	-3.925252	0.639016
C	-4.915429	-3.079009	0.921604
C	-4.876148	-1.746389	0.499090
C	-1.479453	-1.591455	-1.263259
C	-0.767269	-0.439582	-0.562957
C	-0.836696	0.838813	-1.042191
N	-0.139732	1.931543	-0.316027
C	0.134655	3.167772	-1.147947
C	0.458655	4.248283	-0.110582
C	-0.308032	3.834171	1.180155
C	-0.933243	2.464249	0.880846
C	-2.424353	2.520455	0.417109
O	-2.620357	1.887091	-0.679767
O	-3.206234	3.140193	1.130420
O	1.820728	-1.141881	-1.191954
C	2.737047	-0.451887	-0.594866
O	2.591504	0.610199	0.020820
C	4.133306	-1.085633	-0.707426
C	4.271833	-2.457103	-0.010379
C	4.718606	-2.107508	1.419392
C	5.698180	-0.953219	1.212764
N	5.077943	-0.163803	0.059586
H	6.676213	-1.301281	0.874272
H	-1.031309	1.049967	-2.085580
H	-1.116713	4.523060	1.433795
H	0.369718	3.791898	2.036993
H	-0.839555	1.747398	1.699865
H	0.937362	2.949430	-1.855465
H	-0.789315	3.372813	-1.690560
H	-0.589646	-0.576549	0.507078
H	0.765870	1.564285	0.010103
H	-1.783734	-1.263189	-2.265322
H	-0.788683	-2.431649	-1.410975
H	3.870255	-1.789056	2.034470
H	5.198677	-2.947568	1.925786
H	5.825151	-0.285534	2.065763
H	5.035258	-3.050997	-0.521703
H	3.333975	-3.013113	-0.052620
H	4.422956	-1.111830	-1.760378
H	0.843713	-0.742590	-1.036165
H	-3.748068	-0.218626	-0.516226
H	-5.707697	-1.081830	0.714008
H	-5.777505	-3.454428	1.464821
H	-3.864015	-4.963126	0.958647
H	-1.905223	-4.105332	-0.287434
H	4.463943	0.600626	0.404795
H	0.153982	5.230474	-0.478162
H	1.536538	4.291743	0.074985
H	5.789378	0.255220	-0.542829

Protontransfer TS *Z*-iminium+Water+DMSO → Enamine

C	1.647898	1.021330	0.908767
C	1.428267	1.348485	-1.501696
C	1.760926	2.704040	-0.842344
H	2.238171	0.380557	1.577476
H	2.138601	1.075382	-2.296198
H	0.409304	1.314599	-1.912244
C	1.532242	-0.951083	-0.631318
N	1.543465	0.358657	-0.406597
O	-0.224340	0.205089	2.186480
C	0.207438	1.196850	1.515176
O	-0.395627	2.263037	1.265026
C	2.331966	2.346369	0.548258
H	3.421708	2.194726	0.498019
H	2.112363	3.120693	1.292845
C	1.450080	-1.992272	0.309410
H	1.671917	-1.723843	1.352738
C	1.860009	-3.404350	-0.110534
H	1.508889	-3.558759	-1.147373
H	1.485137	-1.213483	-1.694685
C	1.186265	-4.460312	0.782624
H	1.488903	-4.321639	1.833371
H	0.090600	-4.383938	0.733864
H	1.480130	-5.476289	0.477544
C	3.392590	-3.570419	-0.098649
H	3.685384	-4.585600	-0.410827
H	3.871992	-2.846436	-0.775846
H	3.788216	-3.398243	0.915684
O	-1.134341	-1.716257	0.820886
H	-0.883608	-0.973458	1.490154
H	-1.504899	-1.192411	0.035476
H	0.044228	-1.946894	0.469440
H	2.473188	3.281121	-1.447697
H	0.846873	3.294816	-0.715423
S	-3.093593	0.792915	-0.960529
O	-1.895711	-0.190414	-1.165648
C	-2.378236	2.462623	-1.180096
H	-2.041583	2.519391	-2.222907
H	-3.175211	3.197607	-0.998329
H	-1.553278	2.573533	-0.459102
C	-3.372129	0.905970	0.845766
H	-4.166597	1.648549	1.006465
H	-3.707677	-0.085348	1.175180
H	-2.431339	1.207324	1.333234

Proton Transfer TS *E*-Iminium+Water+DMSO → Enamine

C	1.270295	1.991595	-1.937050
C	1.366614	0.454111	-1.856752
N	2.020137	0.199788	-0.555807
C	2.192917	1.449669	0.206526
C	2.280490	2.508252	-0.891995
C	2.126223	-0.999846	0.004765
C	1.497859	-2.180410	-0.442025
C	1.946225	-3.557591	0.053981
C	0.947652	1.626999	1.162398
O	0.364406	2.727039	1.156319
O	0.661546	0.591768	1.853476
H	3.094817	1.376427	0.832076
H	2.006379	3.494263	-0.500608
H	3.300034	2.544691	-1.307857
H	0.259285	2.310609	-1.650104
H	1.474423	2.361069	-2.950836
H	0.373894	-0.016790	-1.882349
H	1.990092	0.017969	-2.653544
H	0.309906	-1.817792	0.276395
H	-0.179566	-0.578259	1.394784
O	-0.668838	-1.356156	0.918548
H	1.070813	-4.224139	-0.040983
H	2.622048	-0.991699	0.977571
H	-1.237362	-0.872298	0.235499
H	1.132645	-2.171638	-1.477060
C	3.066017	-4.134632	-0.835044
H	3.968779	-3.505826	-0.765111
H	3.332607	-5.157234	-0.523249
H	2.756165	-4.167395	-1.891012
C	2.361614	-3.560020	1.534679
H	2.538898	-4.590225	1.877562
H	3.297498	-2.998612	1.689446
H	1.582862	-3.114332	2.171628
S	-2.834829	1.280557	-0.486701
O	-1.884752	0.107210	-0.875728
C	-4.490271	0.504084	-0.353390
H	-5.205610	1.255268	0.009801
H	-4.764602	0.167871	-1.360847
H	-4.419051	-0.347458	0.336843
C	-2.580575	1.625385	1.287590
H	-1.569421	2.056249	1.393805
H	-3.345488	2.357222	1.585207
H	-2.681223	0.689036	1.853255

Z-Iminium+Water+DMSO

C	1.565489	0.511127	0.584971
C	1.110540	0.604194	-1.812995
C	1.546770	1.985056	-1.302415
H	2.161583	-0.120243	1.254470
H	1.804825	0.190376	-2.558798
H	0.084295	0.593322	-2.200902
C	0.774213	-1.508132	-0.628693
N	1.170096	-0.269217	-0.603274
O	-0.538400	0.007012	1.645914
C	0.256172	0.954116	1.383596
O	0.172758	2.162786	1.671514
C	2.340072	1.681985	-0.017336
H	3.376597	1.386387	-0.248341
H	2.342247	2.525427	0.681933
C	0.939354	-2.485552	0.484079
H	0.989966	-1.970148	1.451506
C	2.187632	-3.386422	0.259399
H	2.108207	-3.828327	-0.750148
H	0.481485	-1.890377	-1.607522
C	2.179613	-4.531407	1.283615
H	2.231212	-4.131764	2.309053
H	1.263182	-5.134039	1.197672
H	3.044938	-5.194426	1.132002
C	3.495986	-2.583317	0.331984
H	4.361690	-3.232956	0.134904
H	3.515741	-1.764846	-0.404092
H	3.624795	-2.145695	1.335156
O	-1.638510	-1.387976	-0.390111
H	-1.326422	-0.968765	0.455792
H	-1.874733	-0.592952	-0.930260
H	0.038501	-3.114352	0.493589
H	2.133210	2.529298	-2.054168
H	0.661118	2.581222	-1.048999
S	-3.088938	1.989651	-0.870644
O	-2.067442	1.060800	-1.590932
C	-2.120568	3.409084	-0.236518
H	-1.716918	3.921880	-1.118925
H	-2.814944	4.073015	0.298328
H	-1.323877	3.042756	0.431196
C	-3.445335	1.219330	0.752963
H	-4.060827	1.926959	1.326239
H	-4.008587	0.300726	0.547346
H	-2.495259	0.996504	1.264603

E-Iminium+Water+DMSO

C	-0.760427	2.152983	-1.380368
C	0.711982	1.725350	-1.467349
N	1.122555	1.595124	-0.045366
C	0.074668	2.067670	0.865467
C	-0.858615	2.885004	-0.027801
C	2.136986	0.906555	0.378565
C	3.093082	0.190986	-0.512649
C	4.040942	-0.745095	0.264883
C	-0.623422	0.790011	1.547114
O	-1.793577	0.989140	1.921321
O	0.107467	-0.232047	1.651081
H	0.525299	2.636334	1.690490
H	-1.870345	2.875810	0.393155
H	-0.510921	3.927739	-0.108407
H	-1.397996	1.256656	-1.376375
H	-1.046693	2.783266	-2.232376
H	0.861191	0.757063	-1.961111
H	1.353075	2.491643	-1.931747
H	2.504279	-0.388886	-1.245509
H	0.332266	-1.138420	0.026072
O	0.376266	-1.425120	-0.912973
H	4.544090	-0.142213	1.043530
H	2.279503	0.889903	1.460260
H	-0.551223	-1.299719	-1.226579
H	3.673926	0.940407	-1.083662
C	3.250043	-1.872240	0.950685
H	2.741600	-2.492499	0.197161
H	3.925004	-2.513266	1.537427
H	2.475421	-1.477418	1.625274
C	5.117629	-1.305716	-0.675022
H	5.808913	-1.961744	-0.125311
H	4.654686	-1.899915	-1.479247
H	5.706904	-0.499400	-1.139902
S	-3.363057	-1.543426	-0.687208
O	-2.260228	-0.852773	-1.537792
C	-2.528718	-2.261315	0.779467
H	-3.306844	-2.693215	1.424847
H	-1.861831	-3.046810	0.403396
H	-1.963450	-1.476415	1.301518
C	-4.229247	-0.186828	0.188596
H	-4.701363	0.425702	-0.589937
H	-4.996189	-0.635044	0.836799
H	-3.489480	0.380748	0.773406

Energies and Conformations

	conformation	$\Delta G_{298,\ DMSO}$ CCSD(T)/CBS
No explicit solvent		
Exo-Oxazolidonone	1	-595.6334052
	2	-595.6353672
	3	-595.6328051
	4	-595.6354190
Z-Iminium	1	-595.6179021
	2	-595.6199908
	3	-595.6211282
	4	-595.6206091
TS *Exo*-Oxazolidinone → *Z*-Iminium	1	-595.6129714
	2	-595.6133678
	3	-595.6137328
	4	-595.6158822
TS *Z*-Iminium → s-*cis*-Enamine	1	-595.5983267
	2	-595.5991040
	3	-595.5971961
	4	-595.5975060
s-Cis-Enamine	1	-595.6253771
	2	-595.6228481
	3	-595.6252868
	4	-595.6253543
	5	-595.6245098
	6	-595.6234323
	7	-595.6251117
	8	-595.6241813
Endo-Oxazolidinone	1	-595.6319171
	2	-595.6296091
	3	-595.6320302
	4	-595.6346033

	conformation	$\Delta G_{298,\ DMSO}$ CCSD(T)/CBS
E-Iminium	1	-595.6226691
	2	-595.6214869
	3	-595.6243694
	4	-595.6230592
TS E*ndo*-Oxazolidinone → *E*-Iminium	1	-595.6154231
	2	-595.6201261
	3	-595.6209521
	4	-595.6162981
TS *E*-Iminium → s-*Trans*-Enamine	1	-595.5823850
	2	-595.5810490
	3	-595.5825425
	4	-595.5815788
s-Trans-Enamine	1	-595.6240801
	2	-595.6223638
	3	-595.6235759
	4	-595.6236832
	5	-595.6240331
	6	-595.6213151
	7	-595.6244361
	8	-595.6243830
Explicit solvent		
Exo-Oxazolidinone + DMSO	1	-1148.2222352
	2	-1148.2171407
	3	-1148.2166112
	4	-1148.2199993
	5	-1148.2181131
	6	-1148.2198209
	7	-1148.2205882
	8	-1148.2189650
Z-Iminium + DMSO	1	-1148.2066929
	2	-1148.2070667
	3	-1148.2085078

	conformation	$\Delta G_{298,\ DMSO}$ CCSD(T)/CBS
	4	-1148.2087050
	5	-1148.2108611
	6	-1148.2116255
	7	-1148.2068833
	8	-1148.2074366
TS *Exo*-Oxazolidinone → *Z*-Iminium	1	-1148.1983134
+ DMSO	2	-1148.1942436
	3	-1148.1961150
	4	-1148.1990654
	5	-1148.2035605
	6	-1148.1988073
	7	-1148.1992314
	8	-1148.1947389
TS *Z*-Iminium → s-*Cis*-Enamine	1	-1148.1832263
+ DMSO	2	-1148.1827905
	3	-1148.1809913
	4	-1148.1808515
s-Cis-Enamine + DMSO	1	-1148.2173842
	2	-1148.2141482
	3	-1148.2180885
	4	-1148.2148397
Endo-Oxazolidinone + DMSO	1	-1148.2173676
	2	-1148.2142418
	3	-1148.2188535
	4	-1148.2169128
	5	-1148.2161137
	6	-1148.2131395
	7	-1148.2143451
	8	-1148.2158859
E-Iminium + DMSO	1	-1148.2071481
	2	-1148.2061269

	conformation	$\Delta G_{298,\ DMSO}$ CCSD(T)/CBS
	3	-1148.2095367
	4	-1148.2102308
	5	-1148.2112163
	6	-1148.2103647
	7	-1148.2094084
	8	-1148.2068402
TS *Endo*-Oxazolidinone → *E*-iminium	1	-1148.2037801
+ DMSO	2	-1148.2015269
	3	-1148.2008682
TS *E*-Iminium → s-T*trans*-Enamine	1	-1148.1657183
+ DMSO	2	-1148.1646679
	3	-1148.1676511
	4	-1148.1647580
s-Trans-Enamine + DMSO	1	-1148.2143498
	2	-1148.2141469
	3	-1148.2127801
	4	-1148.2148148
Water assisted proton transfer		
Z-Iminium + H_2O	1	-672.0019984
	2	-672.0026881
	3	-672.0038734
	4	-672.0031674
Z-Iminium + H_2O + DMSO	1	-1224.5893533
TS *Z*-Iminium → s-*Cis*-Enamine	1	-671.9650844
+ H_2O	2	-671.9648687
TS Z-Iminium + H_2O + DMSO → s-*Cis*-Enamine	1	-1224.5599673

	conformation	**$\Delta G_{298,\ DMSO}$ CCSD(T)/CBS**
E-Iminium + H_2O	1	-672.0057588
	2	-672.0033417
	3	-672.0027311
	4	-672.0025326
E-Iminium + H_2O + DMSO	1	-1224.5947164
TS *E*-Iminium → s-*Trans*-Enamine	1	-671.9725998
+ H_2O	2	-671.9708971
TS E-Iminium + H_2O + DMSO → s-*Trans*-Enamine	1	-1224.5629288

2.5 References

(1) Pihko, P. M.; Majander, I.; Erkkilä, A. *Top. Curr. Chem.* **2009**, 291, 29.

(2) List, B. *Synlett* 2001, **2001**, 1675.

(3) Zhong, G.; Fan, J.; Barbas, C. F. *Tetrahedron Lett.* **2004**, 45, 5681.

(4) Hayashi, Y.; Itoh, T.; Aratake, S.; Ishikawa, H. *Angew. Chem. Int. Ed.* **2008**, 47, 2082.

(5) Enders, D.; Chow, S. Eur. *J. Org. Chem.* **2006**, 2006, 4578.

(6) Hayashi, Y.; Gotoh, H.; Hayashi, T.; Shoji, M. *Angew. Chem. Int. Ed.* **2005**, 44, 4212.

(7) Chi, Y.; Gellman, S. H. Org. Lett. **2005**, 7, 4253.

(8) Marigo, M.; Wabnitz, T. C.; Fielenbach, D.; Jørgensen, K. A. *Angew. Chem. Int. Ed.* **2005**, 44, 794.

(9) Palomo, C.; Mielgo, A. *Angew. Chem. Int. Ed.* **2006**, 45, 7876.

(10) Ramachary, D. B.; Reddy, Y. V. *Eur. J. Org. Chem.* **2012**, 2012, 865.

(11) Kumar, I.; Ramaraju, P.; Mir, N. A. *Org. Biomol. Chem.* **2013**, 11, 709.

(12) Dieckmann, A.; Breugst, M.; Houk, K. N. *J. Am. Chem. Soc.* **2013**, 135, 3237.

(13) Nicewicz, D. A.; MacMillan, D. W. C. *Science* **2008**, 322, 77.

(14) Neumann, M.; Füldner, S.; König, B.; Zeitler, K. *Angew. Chem. Int. Ed.* **2011**, 50, 951.

(15) Pirnot, M. T.; Rankic, D. A; Martin, D. B. C.; MacMillan, D. W. C. *Science* **2013**, 339, 1593.

(16) Seebach, D.; Boes, M.; Naef, R.; Schweizer, W. B. *J. Am. Chem. Soc.* **1983**, 105, 5390.

(17) Bock, D. A.; Lehmann, C. W.; List, B. *Proc. Natl. Acad. Sci. U. S. A.* **2010**, 107, 20636.

(18) List, B.; Hoang, L.; Martin, H. J. *Proc. Natl. Acad. Sci. U. S. A.* **2004**, 101, 5839.

(19) Iwamura, H.; Wells, D. H.; Mathew, S. P.; Klussmann, M.; Armstrong, A.; Blackmond, D. G. *J. Am. Chem. Soc.* **2004**, 126, 16312.

(20) Seebach, D.; Beck, A. K.; Badine, D. M.; Limbach, M.; Eschenmoser, A.; Treasurywala, A. M.; Hobi, R.; Prikoszovich, W.; Linder, B. *Helv. Chim. Acta* **2007**, 90, 425.

(21) Isart, C.; Burés, J.; Vilarrasa, J. *Tetrahedron Lett.* **2008**, 49, 5414.

(22) F. Orsini, F. Pelizzoni, M. Forte, M. Sisti, G. Bombieri, F. B. *J. Heterocycl. Chem.* **1989**, 26, 837.

(23) Schmid, M. B.; Zeitler, K.; Gschwind, R. M. *Angew. Chem. Int. Ed.* **2010**, 49, 4997.

(24) Schmid, M. B.; Zeitler, K.; Gschwind, R. M. *Chem. Eur. J.* **2012**, 18, 3362.

(25) Schmid, M. B.; Zeitler, K.; Gschwind, R. M. *J. Org. Chem.* **2011**, 76, 3005.

(26) Schmid, M. B.; Zeitler, K.; Gschwind, R. M. *J. Am. Chem. Soc.* **2011**, 133, 7065.

(27) Schmid, M. B.; Zeitler, K.; Gschwind, R. M. *Chem. Sci.* **2011**, 2, 1793.

(28) Bruice, P. Y.; Bruice, T. C. *J. Am. Chem. Soc.* **1978**, 100, 4793.

(29) Bruice, P. Y. *J. Am. Chem. Soc.* **1989**, 111, 962.

(30) Bruice, P. Y. *J. Am. Chem. Soc.* **1990**, 112, 7361.

(31) Schmid, M. B. Ph.D. Thesis, University of Regensburg, Regensburg-Germany, January 2011.

(32) Seegerer, A. Master Thesis, University of Regensburg, Regensburg-Germany, September 2014.

(33) Bahmanyar, S.; Houk, K. N.; Martin, H. J.; List, B. *J. Am. Chem. Soc.* **2003**, 125, 2475.

(34) List, B.; Lerner, R. A.; Barbas, C. F. *J. Am. Chem. Soc.* **2000**, 122, 2395.

(35) Sharma, A. K.; Sunoj, R. B. *Angew. Chem. Int. Ed.* **2010**, 49, 6373.

(37) Orrell, K. G.; Šik, V.; Stephenson, D. *Prog. Nucl. Magn. Reson. Spectrosc.* **1990**, 22, 141.

(38) Campbell, I. D.; Dobson, C. M.; Ratcliffe, R. G.; Williams, R. J. P. *J. Magn. Reson.* **1978**, 29, 397.

(39) Forsén, S.; Hoffman, R. A. *J. Chem. Phys.* **1963**, 39, 2892.

(40) Perrin, C. L.; Johnston, E. R. *J. Magn. Reson.* **1979**, 33, 619.

(41) *NMR Spectroscopy*, 3rd ed.; Wiley-VCH, Weinheim, 2013.

(42) Bain, A. D. *Prog. Nucl. Magn. Reson. Spectrosc.* **2003**, 43, 63.

(43) Aski, S. N.; Takacs, Z.; Kowalewski, *J. Magn. Reson. Chem.* **2008**, 46, 1135.

(44) Perrin, C. L.; Dwyer, T. J. *Chem. Rev.* **1990**, 90, 935.

(45) Kumar, A.; Wagner, G.; Ernst, R. R.; Wuethrich, K. *J. Am. Chem. Soc.* **1981**, 103, 3654.

(46) Nyberg, A. I.; Usano, A.; Pihko, P. M. *Synlett* **2004**, 11, 1891.

(47) Pihko, P. M.; Laurikainen, K. M.; Usano, A.; Nyberg, A. I.; Kaavi, J. A. *Tetrahedron* **2006**, 62, 317.

(48) Hein, J. E.; Burés, J.; Lam, Y.; Hughes, M.; Houk, K. N.; Armstrong, A.; Blackmond, D. G. *Org. Lett.* **2011**, 13, 5644.

(49) Bryantsev, V. S.; Diallo, M. S.; Goddard, W. A., III *J. Phys. Chem. B* **2008**, 112, 9709.

(50) Pliego, J. R.; Riveros, J. M. *J. Phys. Chem. A* **2001**, 105, 7241.

(51) Thar, J.; Zahn, S.; Kirchner, B. *J. Phys. Chem. B* **2008**, 112, 1456.

(53) Baidya, M.; Kobayashi, S.; Mayr, H. *J. Am. Chem. Soc.* **2010**, 132, 4796.

(54) Schäfer, A.; Huber, C.; Ahlrichs, R. *J. Chem. Phys.* **1994**, 100, 5829.

(55) Schäfer, A.; Horn, H.; Ahlrichs, R. *J. Chem. Phys.* **1992**, 97, 2571.

(56) Kendall, R. A.; Jr., Dunning, T. H.; Harrison, R. *J. Chem. Phys.* **1992**, 96, 6796.

(57) Woon, D. E.; Dunning, T. H. *J. Chem. Phys.* **1993**, 98, 1358.

(58) Tao, J.; Perdew, J. P.; Staroverov, V. N.; Scuseria, G. E. *Phys. Rev. Lett.* **2003**, 91, 146401.

(59) Grimme, S.; Ehrlich, S.; Goerigk, L. *J. Comput. Chem.* **2011**, 32, 1456.

(60) Riplinger, C.; Sandhoefer, B.; Hansen, A.; Neese, F. *J. Chem. Phys.* **2013**, 139, 134101.

(61) Riplinger, C.; Neese, F. *J. Chem. Phys.* **2013**, 138, 034106.

(62) Neese, F.; Wennmohs, F.; Hansen, A.; Becker, U. *Chem. Phys.* **2009**, 356, 98.

(63) Neese, F. *J. Comput. Chem.* **2003**, 24, 1740.

(64) Izsák, R.; Neese, F. *J. Chem. Phys.* **2011**, 135, 144105.

(65) Weigend, F.; Furche, F.; Ahlrichs, R. *J. Chem. Phys.* **2003**, 119, 12753.

(66) Neese, F. *Wiley Interdiscip. Rev. Comput. Mol. Sci.* **2012**, 2, 73.

(67) Klamt, A.; Schüürmann, G. *J. Chem. Soc., Perkin Trans. 2* **1993**, 799.

(68) Klamt, A. *Wiley Interdisciplinary Reviews: Computational Molecular Science* **2011**, 1, 699.

(69) Peiper, J. C.; Pitzer, K. S. *J. Chem. Thermodyn.* **1982**, 14, 613.

(70) Grechin, A. G.; Buschmann, H.-J.; Schollmeyer, E. *Thermochim. Acta* **2006**, 449, 67.

(71) Castro, E. A.; Aliaga, M.; Campodonico, P. R.; Leis, J. R.; García-Río, L.; Santos, J. G. *J. Phys. Org. Chem.* **2008**, 21, 102.

(72) Burkhard, R. K.; Sellers, D. E.; DeCou, F.; Lambert, J. L. *J. Org. Chem.* **1959**, 24, 767.

(73) TURBOMOLE V6.6 2014, a development of University of Karlsruhe and Forschungszentrum Karlsruhe GmbH, 1989-2007, TURBOMOLE GmBH, since 2007; available from http://turbomole.com.

(74) Marenich, A. V.; Cramer, C. J.; Truhlar, D. G. *J. Phys. Chem. B* **2009**, 113, 6378.

(75) Gaussian 09, Revision D.01, Frisch, M. J.; Trucks, G. W.; Schlegel, H. B.; Scuseria, G. E.; Robb, M. A.; Cheeseman, J. R.; Scalmani, G.; Barone, V.; Mennucci, B.; Petersson, G. A.; Nakatsuji, H.; Caricato, M.; Li, X.; Hratchian, H. P.; Izmaylov, A. F.; Bloino, J.; Zheng, G.; Sonnenberg, J. L.; Hada, M.; Ehara, M.; Toyota, K.; Fukuda, R.; Hasegawa, J.; Ishida, M.; Nakajima, T.; Honda, Y.; Kitao, O.; Nakai, H.; Vreven, T.; Montgomery, J. A., J.; Peralta, J. E.; Ogliaro, F.; Bearpark, M.; Heyd, J. J.; Brothers, E.; Kudin, K. N.; Staroverov, V. N.; Kobayashi, R.; Normand, J.; Raghavachari, K.; Rendell, A.; Burant, J. C.; Iyengar, S. S.; Tomasi, J.; Cossi, M.; Rega, N.; Millam, J. M.; Klene, M.; Knox, J. E.; Cross, J. B.; Bakken, V.; Adamo, C.; Jaramillo, J.; Gomperts, R.; Stratmann, R. E.; Yazyev, O.; Austin, A. J.; Cammi, R.; Pomelli, C.; Ochterski, J. W.; Martin, R. L.; Morokuma, K.; Zakrzewski, V. G.; Voth, G. A.; Salvador, P.; Dannenberg, J. J.; Dapprich, S.; Daniels, A. D.; Farkas, Ö.; Foresman, J. B.; Ortiz, J. V.; Cioslowski, J.; Fox, D. J. Gaussian Inc., Wallingford CT, 2009.

(76) Ho, J.; Klamt, A.; Coote, M. L. *J. Phys. Chem. A* **2010**, 114, 13442.

(77) Ribeiro, R. F.; Marenich, A. V.; Cramer, C. J.; Truhlar, D. G. *J. Phys. Chem. B* **2011**, 115, 14556.

(78) Sinnecker, S.; Rajendran, A.; Klamt, A.; Diedendorf, M.; Nesse, F. *J. Phys. Chem. A* **2006**, 110, 2235.

3 What Is Your Actual Catalyst? TMS Cleavage Rates of Diarylprolinol Silyl Ethers Studied by *in situ* NMR

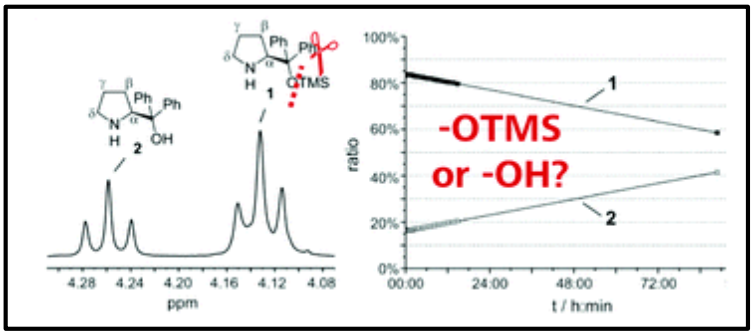

Initial NMR studies were performed by M. B. Schmid in close collaboration with K. Zeitler.

M. H. Haindl, M. B. Schmid, K. Zeitler, R. M. Gschwind,

RSC Advances. **2012**, *2*, 5941.

http://dx.doi.org/10.1039/C2RA20860A

3.1 Abstract

Diarylprolinol silyl ethers are excellent and broadly applicable organocatalysts for various enamine and iminium-type synthetic transformations. However, their undesired degradation to the corresponding diarylprolinols and the subsequent formation of oxazolidines during reaction with aldehydes may significantly affect their catalytic performance. Therefore, *in situ* NMR was used to examine the TMS cleavage rate of diarylprolinol silyl ethers as a function of solvent properties, acidic/basic additives and the presence of water. Highly polar solvents with strong hydrogen bond acceptor properties and especially moderate acidic additives with pK_a (DMSO) values around 10 accelerate the deprotection significantly, whereas basic and highly acidic additives are not detrimental. Additional mechanistic studies reveal that the substitution reaction takes places at the silicon atom.

3.2 Manuscript

Introduction

Jørgensen–Hayashi-type diarylprolinol silyl ethers have demonstrated an excellent performance in a variety of asymmetric organocatalytic transformations.[1–7] Even multi-component domino reactions have been developed allowing for one pot synthesis of complex organic molecules with many stereocenters.[8–12] Recently, different additives have been reported to be highly beneficial in organocatalysis.[13–17] For diarylprolinol silyl ethers, especially, benzoic acid has successfully been used to increase both yields and the catalytic activity.[13–15] However, a critical shortcoming of diarylprolinol silyl ethers is the potential loss of the TMS group leading to the formation of diarylprolinol catalysts. Although both catalyst classes, diarylprolinol silyl ethers and their deprotected analogues, share excellent stereocontrolling properties leading to high *ee* values, diarylprolinols are known to be less active.[18–21] Recently, we have been able to monitor for the first time the deprotection of a diarylprolinol silyl ether by *in situ* NMR.[20] Further extensive spectroscopic studies of the enamine intermediates revealed different preferred conformations of the diarylprolinol silyl ether enamines and diarylprolinol enamines.[22] In addition, the lower reactivity of diarylprolinols could be correlated to the hardly reversible formation of oxazolidines with carbonyl species and strongly reduced amounts of enamine intermediates being present during the reaction with aldehydes.[20] Since typical reaction times in diarylprolinol silyl ether catalysis vary from hours to days, the stability of the TMS protecting group under particular reaction conditions (solvents and additives) is of utmost importance. Herein we present a systematic study on the cleavage conditions for the TMS protecting group of diarylprolinol silyl ethers **1** and **3** (see Fig. 29) in solution by means of modern *in situ* NMR experiments.

Results and Discussion

NMR Spectroscopic Analysis. The NMR spectroscopic analysis of the mixtures of **1** and its desilylated analogue **2** as well as of **3** and its free-OH analogue **4** in solution reveals different chemical shifts for the pyrrolidine protons of **1** and **2**, and of **3** and **4**, respectively (for the ^{1}H NMR chemical shift assignments see chapter 3.3.1). Based on this, the identification of the silylated and desilylated species can be accomplished either *via* their different diffusion coefficients in DOSY spectra or via NOE contacts between the pyrrolidine protons and the TMS protons or the OH proton (the latter being detectable in DMSO, data not shown). In this study, the ^{1}H NMR signals originating from the α-protons of species **1**–**4**, which are clearly separated from other ^{1}H NMR resonances (see Fig. 30A), are used as a probe to monitor the kinetics of the TMS cleavage reaction.

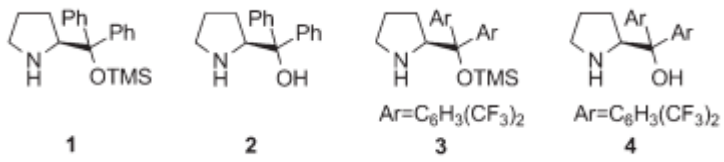

Fig. 29: The diarylprolinol silyl ethers **1** and **3** used as model systems and their desilylated analogues **2** and **4**.

Here, our first surprising observation was that the commercially purchased catalysts **1** and **3** contained at least 10–15% of their deprotected analogues **2** and **4** (see Fig. 29). Since typically the activity of diarylprolinol catalysts is low in comparison with diarylprolinol silyl ethers[6] and stereocontrol might follow different modes with possible opposite stereoinduction, the observed purity grade of the purchased catalysts may not satisfy the needs of synthetic organic chemists. A simple ^{1}H NMR experiment and integration of the well separated α-proton resonances of **1** and **2** (see Fig. 30A) and of **3** and **4**, respectively, may be used to decide if purification of the catalyst is necessary prior to its application (for chemical shift assignments of **1** and **2** in various solvents see chapter 3.3.1).

Influence of Solvent Properties

In order to examine the influence of solvent properties (*i.e.* polarity, as expressed by the dielectric constant ε_r[23] and hydrogenbond acceptor properties as expressed by the Kamlet–Taft parameter β[23]) on the TMS cleavage of **1**, we performed a solvent screening at room temperature using cyclohexane-d_{12}, chloroform-d_1, THF-d_8, acetone-d_6, MeOH-d_4, acetonitrile-d_3, DMF-d_7 and DMSO-d_6. For example, the ^{1}H reaction profiles of **1** and **2** in MeOH-d_4 are presented in Fig. 30B. The negative slope of the deprotection of **1** represents the cleavage rate per hour (c.r.) in Fig. 30C. The fastest cleavage rates were observed in the polar solvents DMF-d_7 (c.r. = 0.84% h^{-1}), MeOH-d_4 (c.r. = 0.27% h^{-1}) and DMSO-d_6 (c.r. = 0.15% h^{-1}). Virtually no cleavage was monitored in the non-polar solvents cyclohexane-d_{12} (c.r. = 0.0001% h^{-1}) and chloroform-d_1 (c.r. = 0.0003% h^{-1}) and only very slow deprotection was observed in acetone-d_6 (c.r. = 0.006% h^{-1}) and acetonitrile-d_3 (c.r. = 0.005% h^{-1}). Considering that the typical reaction times of **1** in DMF at room temperature range from hours to a few days[24–27] the deprotected analogue **2** should be present in high amounts and should compete with **1** as the active organocatalyst. In fact, this could explain some of the reported drawbacks of such solvent–catalyst combinations.[24–27] Interestingly, the cleavage rate of **1** only correlates roughly with the solvent parameters ε_r and β (Fig. 2C). However, clearly a combination of high polarity and strong hydrogen bond acceptor properties (DMF-d_7, MeOH-d_4 and DMSO-d_6) leads to a relevant cleavage

rate with an exceptionally high rate in DMF-d_7. Solvents lacking one of these properties (THF-d_8: large β, small ε_r; MeCN-d_3: small β, large ε_r) show significantly slower cleavage tendencies.

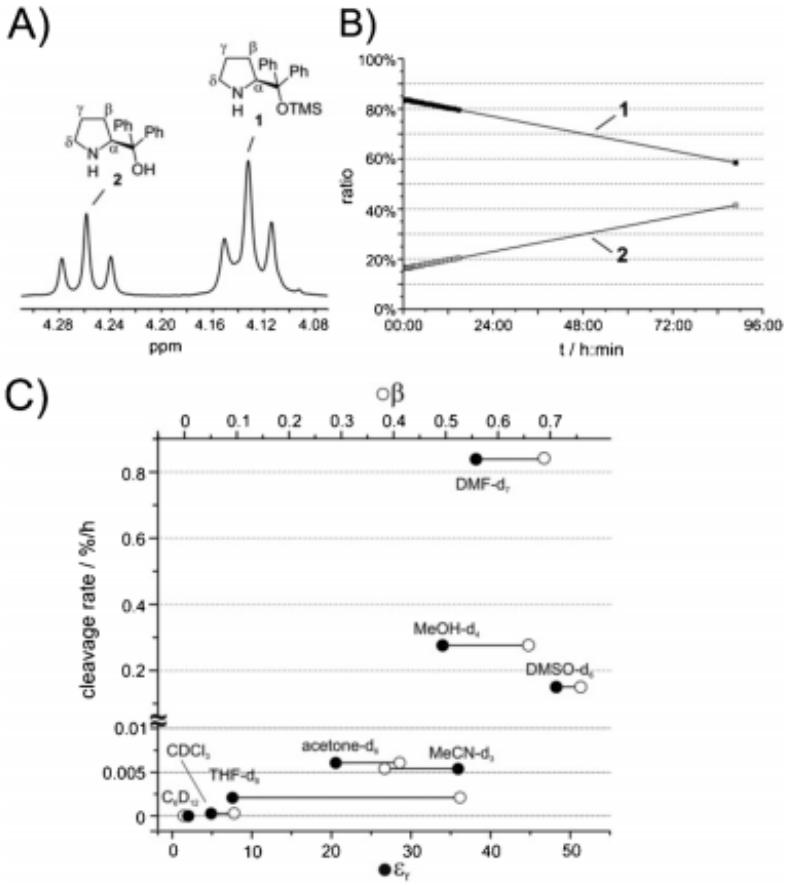

Fig. 30: (A) ^{1}H NMR resonances of the α-protons of **1** and **2**, respectively, in DMSO-d_6 at room temperature at 600 MHz. (B) Reaction profile of **1** and **2** during the TMS cleavage reaction in MeOH-d_4 at room temperature. (C) Experimental cleavage rate (c.r.) of **1** in different solvents correlated with the dielectric constants ε_r (•) and hydrogen bond acceptor properties β (○) (Kamlet–Taft parameter) of these solvents.

Acidic and Basic Additives

We continued our study with an investigation of the influence of various acidic and basic additives on the cleavage reaction and selected DMSO-d_6 as the model solvent for that purpose (see Fig. 31A). Benzoic acid as a typical additive for diarylprolinol silyl ethers was tested with all the solvents used in the additive free study (see above). To cover a broad pK_a range, acids with pK_a values in DMSO varying from 0 to 11.1 were selected (see Fig. 31A). Along with the acidic additives picric acid (I), HCl aq. (II), TFA (trifluoroacetic acid) (III), tetrazole (IV), succinic acid (V), *p*-nitrophenol (VI) and benzoic acid (VII) we also applied the basic additives DABCO (1,4-diazabicyclo[2.2.2]octane), DMAP (4-dimethylaminopyridine) and DBU (1,8-diazabicycloundec-7-ene).

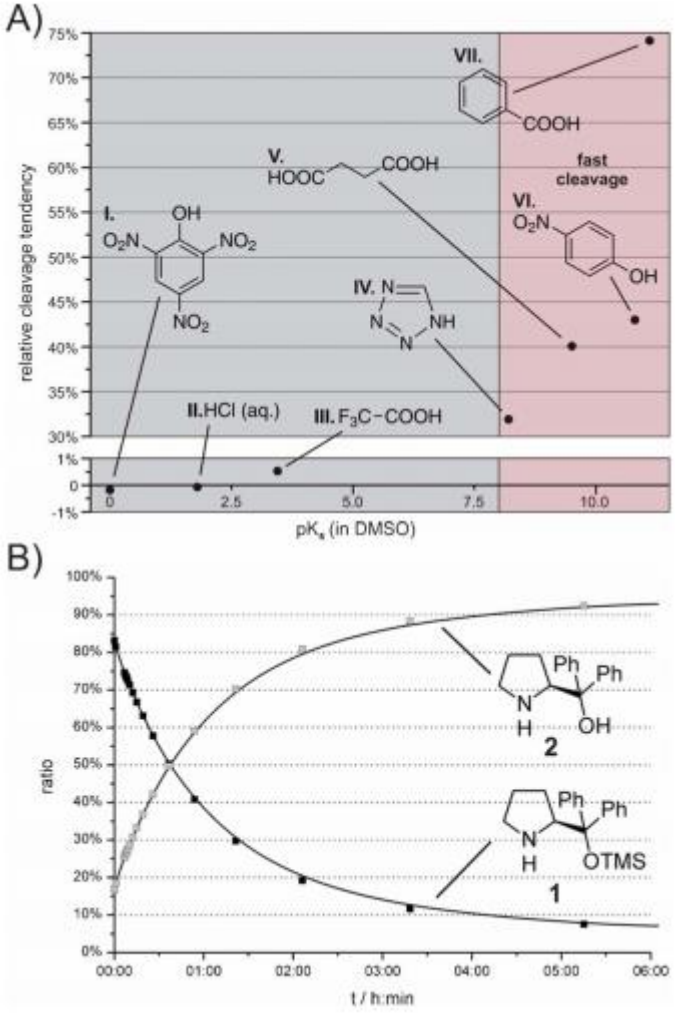

Fig. 31: Relative cleavage tendency (the amount of the TMS-group cleaved after 5 h minus the corresponding amount cleaved in pure DMSO-d_6) of **1** with acidic additives (100 mol%, 50 mM) in DMSO-d_6 at room temperature as a function of their pK_a(DMSO) values.[28–31] (B) ^{1}H reaction monitoring of **1** and **2** in DMSO-d_6 with benzoic acid as additive at room temperature.

As expected, the basic additives such as DBU pK_{aH} (acetonitrile) = 23.9,[32] DMAP pK_{aH} (acetonitrile) = 18.18[33] or DABCO pK_{aH} (DMSO) = 8.93[28] only show a minor effect. Most strikingly, all the tested acidic additives with pK_a values above 7.5 strongly accelerated the cleavage reaction (see Fig. 31A). The fastest deprotection was observed with benzoic acid. In this case, the amount of **1** decreased exponentially from about 84% at the beginning to less than 10% after 6 h (see Fig. 31B). Under these ''fastest cleavage conditions'', the progress of deprotection can easily be detected by the crystallisation of the benzoate salt of **2** after a few hours (for crystal structure see chapter 3.3.3). Surprisingly, Enders *et al.*[9] described an enantioselective Michael addition–α-alkylation cascade reaction in which a 1:1 mixture of catalyst **1** and benzoic acid in DMSO was successfully applied during reaction times from one to four days. However, our experimental findings suggest that after a few hours **1** should not

be the predominant catalytic species in the described reaction any longer. Interestingly, strong acids such as picric acid pK_{aH}(DMSO) = 0,[29] hydrochloric acid pK_a(DMSO) = 1.8[29] and TFA pK_a(DMSO) = 3.45[29] also have only a negligible effect on the desilylation rate (see Fig. 31A).

Solvents + Benzoic Acid

Since benzoic acid shows the highest acceleration rate and is broadly applied as an additive in combination with diarylprolinol silyl ethers, we examined the deprotection rates with this additive also in other solvents (cyclohexane-d_{12}, chloroform-d_1, THF-d_8, acetone-d_6, MeOH-d_4, acetonitrile-d_3, DMF-d_7 and DMSO-d_6). A strong acceleration effect of benzoic acid was only observed in DMSO-d_6 and DMF-d_7.

Investigation of the Cleavage Mechanism

We then investigated the cleavage mechanism of the TMS deprotection in an attempt to better understand the difference between benzoic acid and strong acids. Apart from the expected hydrolysis product TMS–OH **5** and its condensation product TMS–O–TMS **6** (see Fig. 32) we observed the formation of silyl benzoate **7** after an induction period as a result of the nucleophilic attack of $PhCOO^-$ at the Si atom. This product could be fully suppressed if additional water (up to 16 vol%) was used. Unlike using dry conditions, the TMS cleavage is decelerated (stopped at about 35%) and only silyl ester **7** is formed (for the reaction profile and the chemical shift assignments of **7**, see chapter 3.3.2). Further experiments using methanol as a competing nucleophile and the resulting exclusive formation of methoxytrimethylsilane during the TMS cleavage also revealed that the nucleophilic attack occurred at the electrophilic silicon atom.

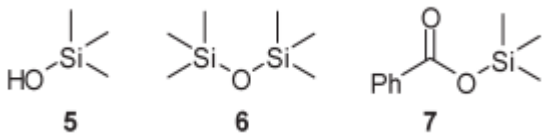

5 **6** **7**

Fig. 32: The detected silyl products **5**, **6** and **7** during the TMS cleavage of silylether **1** in the presence of benzoic acid.

Unlike weak acids (pK_a(DMSO) > 7.5, see Fig. 31A), which tend to greatly accelerate the TMS deprotection in DMSO with increasing pK_a, strong acids (pK_a(DMSO) < 5, see Fig. 31A: TFA, HCl etc.), featuring a full protonation of the catalyst's pyrrolidine nitrogen as detected by NMR (for spectra see chapter 3.3.4),[c] are ineffective for the TMS cleavage. For the ammonium species of **2** two separated NH signals

[c] The corresponding trifluoroacetic acid and perchlorate salts of **3** have been isolated by Hayashi *et al.*: Y. Hayashi, S. Samanta, H. Gotoh and H. Ishikawa, *Angew. Chem. Int. Ed.* **2008**, 47, 6634.

($\Delta\delta \geq 0.38$ ppm) were detected indicating an intramolecular hydrogen bond between one NH proton and the ether oxygen atom.[d] For the ammonium form of **1** only one broad signal could be observed. Hence shifting the equilibrium from 50%:50%[e] amine R_2NH vs. protonated analogue $R_2NH_2^+$ to ≈ 100% of the corresponding ammonium species $R_2NH_2^+$ of **1** (respectively **3**) with decreasing pK_a, mirrors the diminishing cleavage tendency. Cleavage ''protection'' by full protonation may arise from both a steric and an electrostatic shielding of the silicon atom against nucleophilic attack by the closely attached counterion of the acid.

Conclusion

Our extensive NMR spectroscopic studies on the TMS cleavage rates of diarylprolinol silyl ethers in various solvents and with different additives reveal that the experimental conditions for this important and widely applied catalyst have to be chosen with care as significant catalyst degradation might occur during the reaction. In polar solvents with strong H-bond acceptor properties cleavage rates up to 0.84% h^{-1} are observed and weak acidic additives (pK_a(DMSO) ≈ 10) even result in more than 90% of the desilylated catalyst within 5 h. In contrast, non-polar solvents and basic or strongly acidic additives as well as benzoic acid in non-polar solvents are not detrimental. We expect our findings to aid chemists working with diarylprolinol silyl ethers in choosing optimal reaction conditions and designing new reactions.

Acknowledgements

This work was supported by the DFG (SPP 1179).

[d]In experiments with diphenylprolinol methyl ether a similar signal pattern ($\Delta\delta$ = 2.94 ppm) was detected in DMSO-d_6 with 100 mol% TFA where NOESY data show that the proton in proximity to the methoxy group has the higher chemical shift (downfield).

[e]As an estimation for the pK_a values of the ammonium species $R_2NH_2^+$ the pK_a value of pyrrolidinium pK_a(DMSO)=11.1 was used: M. R. Crampton and I. A. Robotham, *J. Chem. Res. Synop.* **1997**, 22.

3.3 Supporting Information

3.3.1 Chemical Shift Assignments of Pyrrolidine Protons of 1 and 2 in Different Solvents

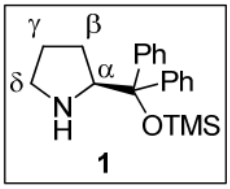

1

1	THF-d_8	MeOH-d_4	acetone-d_6	DMSO-d_6	DMF-d_7	cyclohexane-d_{12}	$CDCl_3$	MeCN-d_3
α	4.12	4.13	4.19	4.14	4.23	3.97	3.94	4.13
β	1.54	1.75	1.54	1.46	1.53	1.52	1.47	1.51
	1.54	1.75	1.54	1.35	1.53	1.52	1.47	1.51
γ	1.35	1.59	1.38	1.28	1.37	1.35	1.47	1.37
	1.35	1.33	1.38	1.45	1.37	1.35	1.28	1.37
δ	2.81	2.73	2.93	2.61	2.96	2.87	2.74	2.88
	2.92	2.57	2.80	2.86	2.75	2.87	2.69	2.77

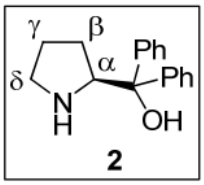

2

2	THF-d_8	MeOH-d_4	acetone-d_6	DMSO-d_6	DMF-d_7	cyclohexane-d_{12}	$CDCl_3$	MeCN-d_3
α	4.29	4.32	4.42	4.26	4.43	4.17	4.25	4.37
β	1.66	1.64	1.38	1.45	1.53	1.65	1.64	1.50
	1.66	1.64	1.38	1.39	1.53	1.65	1.58	1.50
γ	1.57	1.75	1.68	1.58	1.67	1.70	1.73	1.68
	1.44	1.75	1.68	1.58	1.67	1.65	1.73	1.68
δ	2.95	3.00	3.62	2.86	2.96	3.01	3.03	2.92
	2.95	2.87	3.52	2.82	2.75	2.89	2.95	2.92

Fig. 33: The chemical shift (ppm) assignements of the pyrrolidine protons of the catalysts **1** (with TMS group) and **2** (without TMS group in various deuterated solvents is shown.

Fig. 33 shows a comprehensive list of chemical shifts of the ring protons of the TMS-protected **1** and deprotected **2** catalysts in different deuterated solvents.

3.3.2 Silyl Degradation Products – $^{1}H/^{29}Si$ Chemical Shifts, Reaction Profile

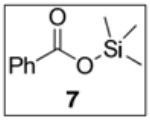

7	*in situ* (DMSO-d_6)	synthesized compound following a literature procedure (DMSO-d_6)	literature assignment (CCl_4)	literature assignment (C_6D_6)
^{1}H: CH_3	0.36-0.37	0.36	0.21 ,0.31 ,0.43	0.57
^{29}Si	24.4	24.4	23.6	-

Fig. 34: ^{1}H and ^{29}Si chemical shifts (ppm) of the possible degradation product, silyl ester **7**. Values are shown from the *in situ* detection, from synthesized compound **7** and from the literature.

The presumably detected silyl degradation product silyl ester **7** is shown in Fig. 34 together with ^{1}H and ^{29}Si chemical shifts from its *in situ* detection, from the synthesis of compound **7** according to a literature procedure[34] and from the literature. The values from the synthesized compound (^{1}H: 0.36-0.37 ppm; ^{29}Si: 24.4 ppm) perfectly match the *in situ* detected chemical shifts (^{1}H: 0.36 ppm, ^{29}Si: 24.4 ppm). Since literature chemical shifts are not available in DMSO-d_6, values in CCl_4 and C_6D_6 were used instead. The determined proton chemical shift of 0.36 ppm is in good agreement with literature values in CCl_4 (0.21 ppm, 0.31 ppm, 0.43 ppm)[35–37] and in rough agreement with a literature value in C_6D_6 (23.6 ppm)[38]. Additionally, a literature ^{29}Si chemical shift of 23.6 ppm[37] in CCl_4 also fits to the *in situ* detected species (24.4 ppm). Overall the data above suggests, the assignment of the detected silyl degradation product to silyl ester **7**.

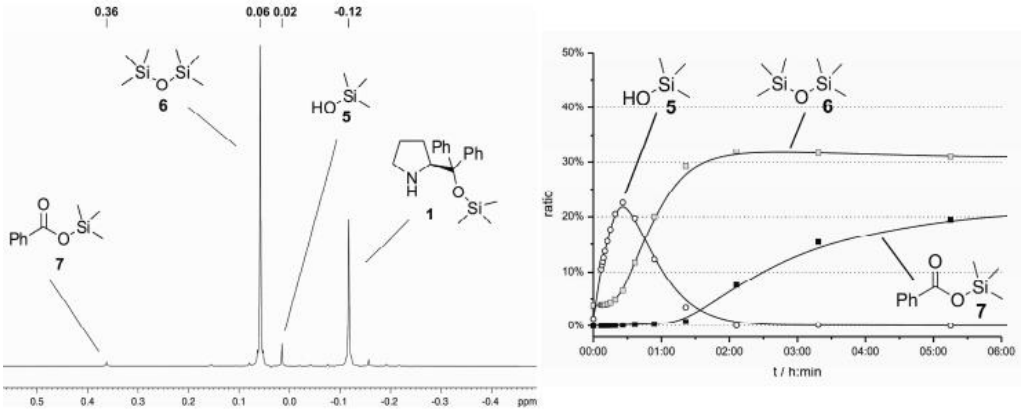

Fig. 35: The ^{1}H reaction profile (right) is shown of the silyl degradation products **5**, **6** and **7** determined from the reaction of **1** and benzoic acid (100 mol%) in DMSO-d_6 at room temperature and a proton resonance frequency of 600 MHz. The silyl slice (-0.5 – 0.5 ppm) of one ^{1}H spectrum of this reaction profile is shown on the left.

In Fig. 35 the ^{1}H reaction profile of all *in situ* detected silyl degradation products together with a slice of one proton spectra used for the construction of the profile is shown. Only when TMS-OH **5** is completely consumed, silyl ester **7** is formed.

3.3.3 Crystal Structure of the Benzoate Salt of 2, Crystallized in DMSO-d_6

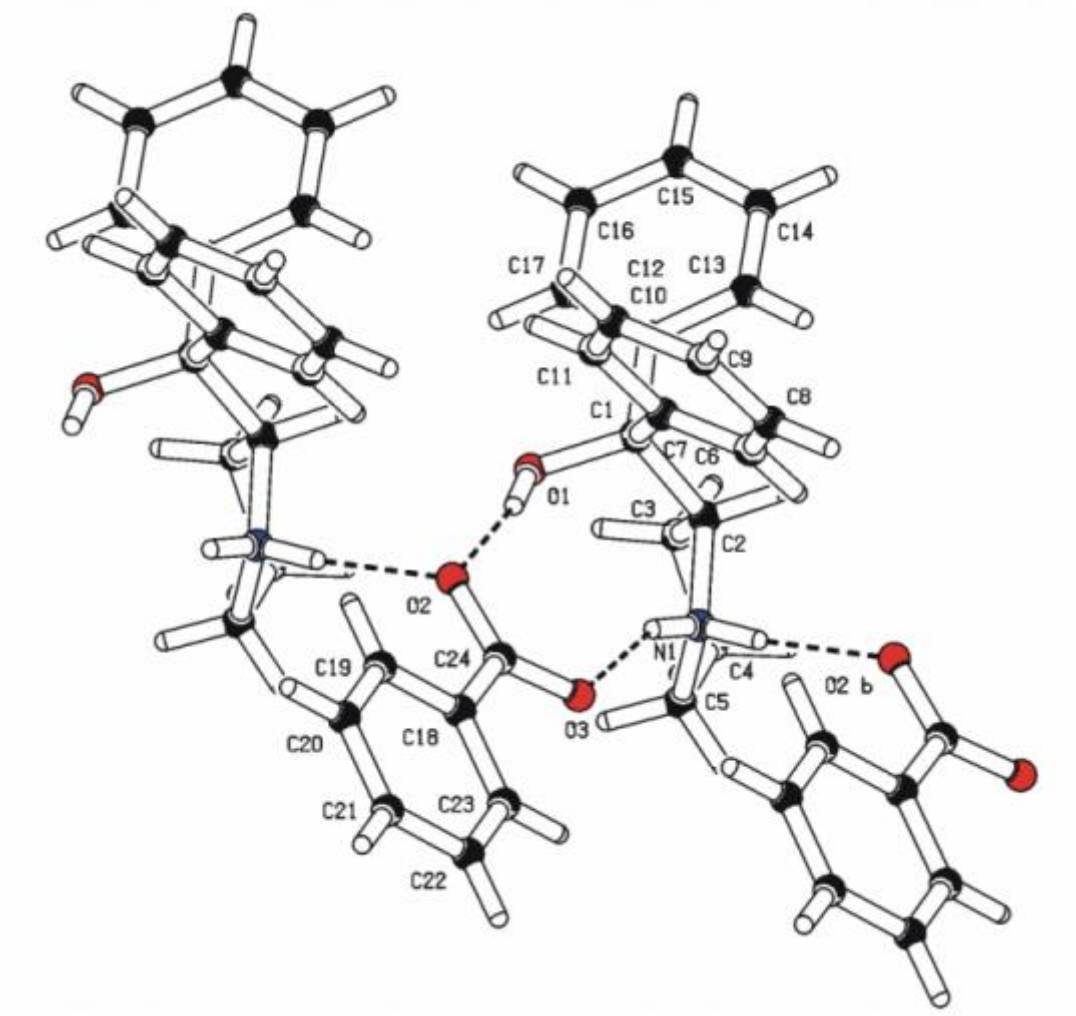

Fig. 36: The 2D projection of the crystal structure of the benzoate salt of **2**, crystallized in DMSO-d_6 is shown. Crystallographic data (CCDC 869742) can be obtained free of charge from The Cambridge Crystallographic Data Centre via http://www.ccdc.cam.ac.us/data request/cif.

A 2D projection of the crystal structure of the benzoate salt of **2** is shown in Fig. 36.

3.3.4 Influence of Strong Acids – Formation of Secondary Ammonium Ions, Equilibria

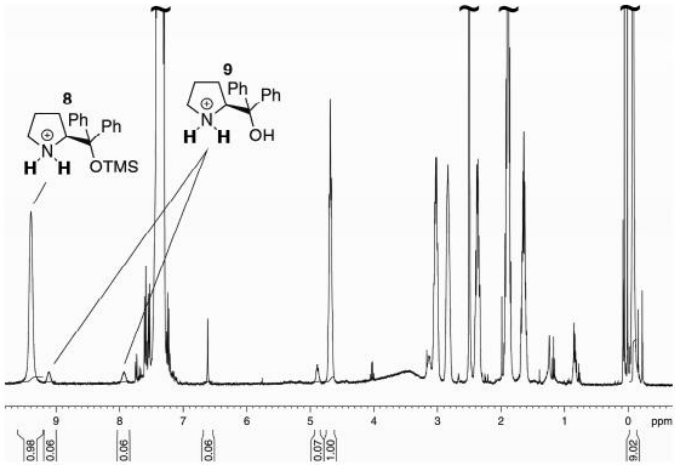

Fig. 37: ^{1}H spectrum of **1** and **2** with 100 mol% TFA in DMSO-d_6 is shown measured at room temperature and a proton resonance frequency of 600 MHz. NH signals of the formed secondary ammonium ions **8** and **9** are highlighted.

Strong acids (*e.g.* TFA, picric acid) lead to protonation of the amine nitrogen of amines **1** and **2** to form the ammonium ions **8** and **9**. The corresponding NH proton signals of **8** and **9** become visible (in contrast to that of **1** and **2**) presumably because the exchange with other exchangeable protons (*e.g.* water) is slowed down. Chemical shifts of these NH protons were detected to lie roughly between 7.5 ppm and 10 ppm (see Fig. 37). The amount of ammonium ion **8** relative to amine **1** is connected to the rate of the loss of the TMS protecting group of **1**. The equilibria between **1** and **8** as well as **2** and **9** depending on the acidity of the acid is shown in Fig. 38. Stronger acids (like picric acid) lead to higher amounts of ammonium ion **8** and slower TMS cleavage rates, whereas weaker acids do not show detectable amounts of **8** and the determined cleavage rates are fast (see manuscript).

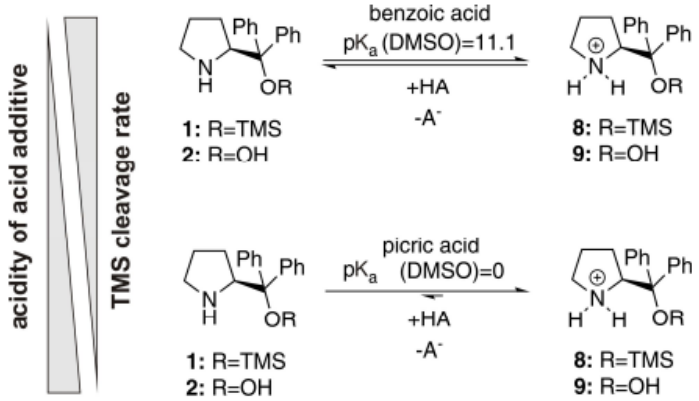

Fig. 38: The equilibria between free amine and protonated ammonium ion of catalysts **1** and **2** in DMSO depending on the acidity of the added acid is shown. Strong acids favor ammonium ion formation and decelerate the loss of the TMS protecting group of **1**.

3.4 References

(1) Marigo, M.; Fielenbach, D.; Braunton, A.; Kjaersgaard, A.; Jørgensen, K. A. *Angew. Chem. Int. Ed.* **2005**, 44, 3703.

(2) Marigo, M.; Wabnitz, T. C.; Fielenbach, D.; Jørgensen, K. A. *Angew. Chem. Int. Ed.* **2005**, 44, 794.

(3) Hayashi, Y.; Gotoh, H.; Hayashi, T.; Shoji, M. *Angew. Chem. Int. Ed.* **2005**, 44, 4212.

(4) Marigo, M.; Franzén, J.; Poulsen, T. B.; Zhuang, W.; Jørgensen, K. A. *J. Am. Chem. Soc.* **2005**, 127, 6964.

(5) Mielgo, A.; Palomo, C. *Chem. Asian J.* **2008**, 3, 922.

(6) Palomo, C.; Mielgo, A. *Angew. Chem. Int. Ed.* **2006**, 45, 7876.

(7) Xu, L.-W.; Li, L.; Shi, Z.-H. *Adv. Synth. Catal.* **2010**, 352, 243.

(8) Enders, D.; Grondal, C.; Hüttl, M. R. M. *Angew. Chem. Int. Ed.* **2007**, 46, 1570.

(9) Enders, D.; Wang, C.; Bats, J. W. *Angew. Chem. Int. Ed.* **2008**, 47, 7539.

(10) Marigo, M.; Bertelsen, S.; Landa, A.; Jørgensen, K. A. *J. Am. Chem. Soc.* **2006**, 128, 5475.

(11) Marigo, M.; Schulte, T.; Franzén, J.; Jørgensen, K. A. *J. Am. Chem. Soc.* **2005**, 127, 15710.

(12) Wang, W.; Li, H.; Wang, J.; Zu, L. *J. Am. Chem. Soc.* **2006**, 128, 10354.

(13) Li, J.-L.; Kang, T.-R.; Zhou, S.-L.; Li, R.; Wu, L.; Chen, Y.-C. *Angew. Chem. Int. Ed.* **2010**, 49, 6418.

(14) Brandau, S.; Maerten, E.; Jørgensen, K. A. *J. Am. Chem. Soc.* **2006**, 128, 14986.

(15) Cabrera, S.; Alemán, J.; Bolze, P.; Bertelsen, S.; Jørgensen, K. A. *Angew. Chem. Int. Ed.* **2008**, 47, 121.

(16) Hein, J. E.; Burés, J.; Lam, Y.; Hughes, M.; Houk, K. N.; Armstrong, A.; Blackmond, D. G. *Org. Lett.* **2011**, 13, 5644.

(17) Schmid, M. B.; Zeitler, K.; Gschwind, R. M. *Chem. Eur. J.* **2012**, 18, 3362.

(18) Alza, E.; Pericas, M. A. *Adv. Synth. Catal.* **2009**, 351, 3051.

(19) Seebach, D.; Badine, D. M.; Schweizer, W. B.; Beck, A. K.; Krossing, I.; Klose, P.; Hayashi, Y.; Uchimaru, T. *Helv. Chim. Acta* **2009**, 92, 1225.

(20) Schmid, M. B.; Zeitler, K.; Gschwind, R. M. *J. Am. Chem. Soc.* **2011**, 133, 7065.

(21) Varela, M. C.; Dixon, S. M.; Lam, K. S.; Schore, N. E. *Tetrahedron* **2008**, 64, 10087.

(22) Schmid, M. B.; Zeitler, K.; Gschwind, R. M. *Chem. Sci.* **2011**, 2, 1793.

(23) *Chemistry in Alternative Reaction Media*; John Wiley & Sons Ltd., Chichester, 2003.

(24) García-García, P.; Ladépêche, A.; Halder, R.; List, B. *Angew. Chem. Int. Ed.* **2008**, 47, 4719.

(25) Franzén, J.; Fisher, A. *Angew. Chem. Int. Ed.* **2009**, 48, 787.

(26) Govender, T.; Hojabri, L.; Moghaddam, F. M.; Arvidsson, P. I. *Tetrahedron: Asymmetry* **2006**, 17, 1763.

(27) Ibrahem, I.; Zhao, G.-L.; Rios, R.; Vesely, J.; Sundén, H.; Dziedzic, P.; Córdova, A. *Chem. Eur. J.* **2008**, 14, 7867.

(28) Benoit, R. L.; Lefebvre, D.; Fréchette, M. *Can. J. Chem.* **1987**, 65, 996.
(29) Bordwell, G. *Acc. Chem. Res.* **1988**, 21, 456.
(30) Kolthoff, I. M.; Chantooni, M. K. *J. Am. Chem. Soc.* **1976**, 98, 5063.
(31) Kolthoff, I. M.; Chantooni, M. K.; Bhowmik, S. *J. Am. Chem. Soc.* **1968**, 90, 23.
(32) Leffek, K. T.; Pruszynski, P.; Thanapaalasingham, K. *Can. J. Chem.* **1989**, 67, 590.
(33) Augustin-Nowacka, D.; Makowski, M.; Chmurzynski, L. *Anal. Chim. Acta* **2000**, 418, 233.
(34) Morita, T.; Okamoto, Y.; Sakurai, H. *Tetrahedron Lett.* **1980**, 21, 835.
(35) Chang, Y. H.; Chiu, F.-T.; Zon, G. *J. Org. Chem.* **1981**, 46, 342.
(36) Tacke, R.; Lange, H. *Chem. Ber.* **1983**, 116, 3685.
(37) McFarlane, W.; Seaby, J. M. *J. Chem. Soc. Perkin Trans. 2* **1972**, 1561.
(38) Yam, C. M.; Kakkar, A. K. *J. Chem. Soc. Chem. Commun.* **1995**, 907.

4 Conformational Preferences in Small Peptide Models – The Relevance of Cis/Trans Conformations

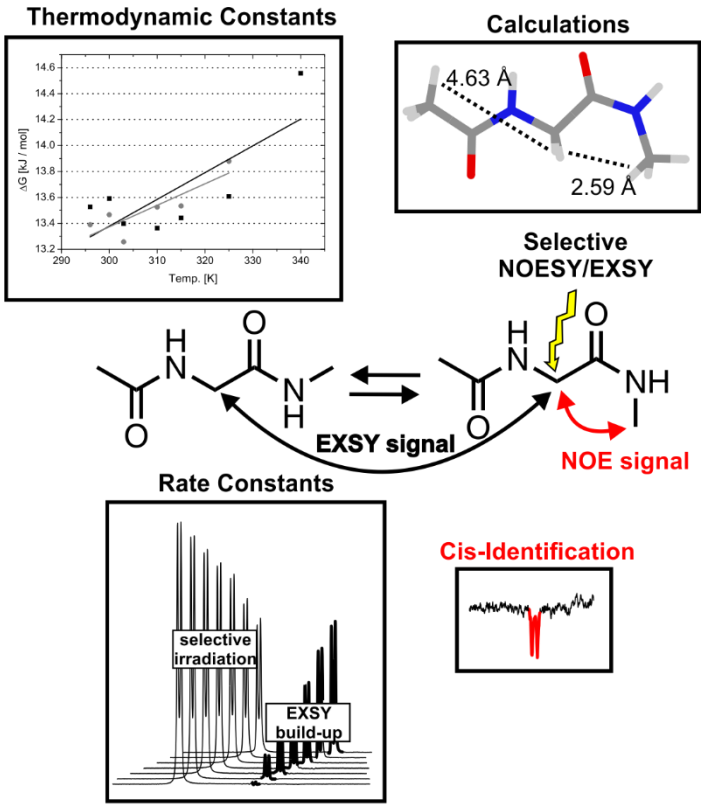

All theoretical calculations were performed by H. Jangra and J. Hioe. Synthesis of **1** was performed by F. Achrainer.

H. Jangra[1], M. H. Haindl[2], F. Achrainer[1], J. Hioe[2], R. M. Gschwind[2] and H. Zipse[1],

to be submitted.

[1] Department of Chemistry, LMU München, D-81377 München, Germany

[2] Institut für Organische Chemie, Universität Regensburg, D-93053 Regensburg, Germany

4.1 Abstract

A comprehensive conformational analysis of dipeptide model Ace-Gly-NMe has been carried out using a combination of theoretical (thermochemistry and isotropic shielding) calculations and experimental (^{1}H & ^{13}C NMR and NOESY/EXSY) spectroscopic measurements. Particular attention has been paid to the identification of the most stable conformer and the relevance of very low populated *cis*-peptide conformers. Relative to the global minimum **C7_tt** conformation featuring two amide groups with trans conformation, **tc** and **ct** conformations containing one of the amide groups in *cis*-conformation are located 10.7 and 16.5 kJ mol^{-1} higher in energy, respectively, in the gas phase. NMR measurements in DMSO solution point toward a linear nature of the global minimum, in line with theoretical prediction of extended **C5_tt** as the most stable conformer in DMSO. The calculated *cis*-peptide structures **C5_ct** and **C5_tc** are almost isoenergetic at around 12 kJ mol^{-1}, which is in close agreement with the NMR experimental value of 13.0 ± 2 kJ mol^{-1}.

4.2 Manuscript

Introduction

Conformational preferences in peptides and proteins are of outstanding relevance for practically all aspects of protein chemistry and biology. The correct prediction of these preferences by molecular mechanics-based theoretical approaches is thus of fundamental importance for the applicability of these methods. Several recently developed force fields for peptide and protein modelling have therefore been derived with reference to accurate structural and energetic data obtained in *ab initio* studies on small peptide models.[1–13] One important reference compound is N-methyl-acetamide (**NMA**), whose *cis*/*trans* energy difference has been studied extensively by experimental and theoretical means (see Fig. 39A). Almost irrespective of the choice of solvent, the *trans*-conformation (**NMA_t**) is preferred over the *cis*-conformation (**NMA_c**) by 8.5 - 10.5 kJ mol^{-1}.[14–16] Experimental studies are challenged by both, the low population of *cis*-conformer **NMA_c** as well as the high *trans*/*cis* isomerization barrier of more than 80 kJ mol^{-1}.[17–23] That the *cis*/*trans* energy difference shows little solvent dependence is surprising in light of the large absolute solvation energies of peptides in polar media.[23] Glycine derivative 2-acetamino-N-methylacetamide **1** has been studied as the smallest dipeptide model featuring peptide-like conformational properties.[3,4,13,24–27] In a recent exploration of the stability of peptide radicals, we calculated an enthalpy difference of 10.7 kJ mol^{-1} between the global minimum (C_7) and the lowest lying *cis*-peptide conformer of dipeptide model **1** (Fig. 39B).

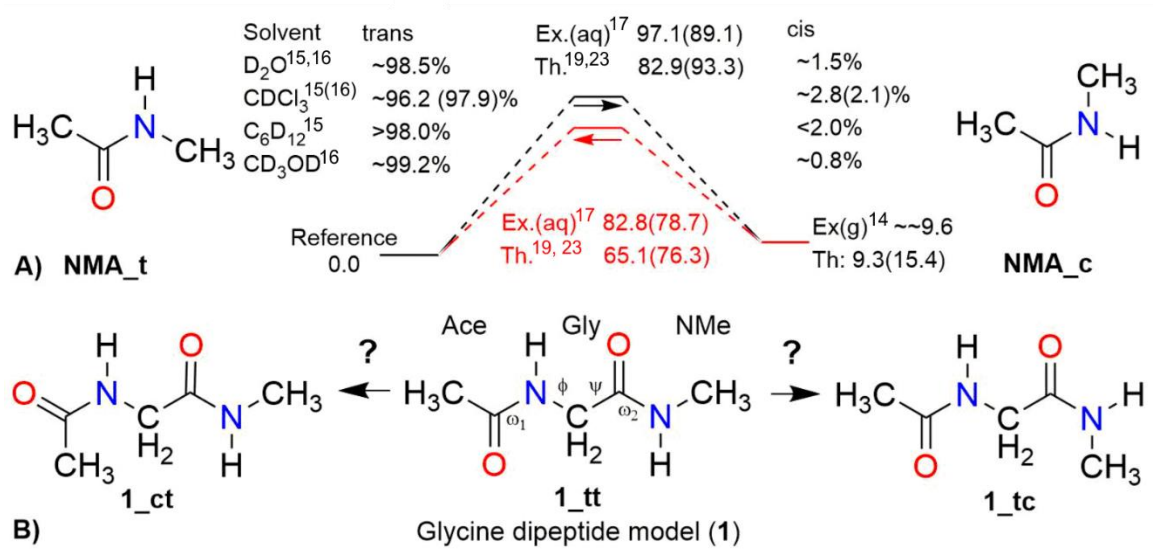

Fig. 39: A) N-methylacetamide (**NMA**): experimental and theoretical data on the relative stability and *trans*/*cis* isomerization barrier shown in terms of ΔH (ΔG) in kJ mol^{-1}; and **B**) 2-Acetamino-N-methylacetamide **1**, where glycine (Gly) is capped with acetyl (Ace) at the N-terminal and as N-methyl amide (NMe) at the C-terminal side.

Unfortunately, experimental studies on this energy difference appear not to exist. A larger number of theoretical studies have been performed on small (di)peptide models, often aiding the development of more accurate protein force fields. However, in practically all these studies *cis*-peptide conformations have been excluded on the basis of their unfavorable stability.[28–30] The *cis*/*trans* isomerization occurs quite frequently at proline residues and this issue has already been addressed in a number of previous studies.[31] Still, *cis*-peptide structures also occur at other residues at a low rate.[32–39]

Numerous surveys and statistical analyses of the PDB database revealed that *cis*-peptide conformations occur as much as 50 times less than expected (for non-proline residues) and a systematic increase is observed with increasing resolution of the protein structures.[31–36,38] Some of the very recent analyses of PBD structures concern the potentially incorrect assignment of peptide plane conformations.[39] These findings, together with the debate on *cis*/*trans* isomerism in side-chain amide bonds,[40] implies that the structural assignment of *cis*-peptide bonds in larger systems by NMR spectroscopy or X-ray analysis is challenged by technical complications. The recent advancement in theory and experiment make it possible to study the scarcely populated *cis*-peptide conformers with better accuracy and confidence. In the present work we use an array of different quantum chemical methods together with ^{1}H & ^{13}C NMR and NOESY/EXSY measurements to explore the conformational preferences of **1** and the relevance of sparsely populated *cis*/*trans* (**tc** and **ct**) conformers. ^{1}H and ^{13}C chemical shift assignments of conformers of **1** are based on a combination of ^{1}H spectra, standard 2D NMR experiments (^{1}H-^{1}H COSY, ^{1}H-^{1}H NOESY, ^{1}H-^{13}C HSQC, ^{1}H-^{13}C HMBC) and 1D selective ^{1}H-^{1}H NOESY experiments. The latter enabled the unambiguous detection of key NOE contacts for minor *cis*-conformer assignments. This was not possible with the standard 2D NOESY experiment due to the strong T1 noise of the large signals of the main *trans*-*trans* (**tt**) conformer. In addition, also from 1D selective NOESY experiments (also called EXSY experiments in this context) rate constants *k* were determined.

Results and Discussions

Gas Phase Conformational Distribution of Glycine Dipeptide 1. The conformational space of **1** was explored using a systematic search with defined variations in the four most relevant dihedral angles (Φ, Ψ, ω_1 and ω_2) as shown in Fig. 39B to obtain starting geometries that were subsequently optimized at B3LYP/6-31G(d) level of theory (for details see chapter 4.3.3). This strategy locates the 14 structures shown in Fig. 40. Conformational ordering as reflected in relative enthalpies at 298.15 K (ΔH_{298}) shows little dependence on the particular theoretical method and is practically identical at

the previously used G3(MP2)-RAD and the slightly more elaborate G3B3 and CCSD(T)/CBS methods (Table 5). We will therefore continue to discuss the G3(MP2)-RAD results, if not mentioned otherwise. Perusal of the gas phase enthalpy data in Fig. 40 shows that the best conformation for **1** corresponds to **C7_tt**, very much in line with most of the previous theoretical studies of this system. The extended **C5_tt** is located only 4.2 kJ mol^{-1} higher in energy and thus represents the 2nd best conformation. Rotation around the C-terminal amide bond leads to the **C5_tc** conformer, which is located +10.7 kJ mol^{-1} above the global minimum and represents the 3rd best conformation overall. This is followed by the all-*trans* conformation **β2_tt** at +11.5 kJ mol^{-1}. The first N-terminal *cis*-conformer **αR_ct** is found as the 5th best conformer at +16.5 kJ mol^{-1}. The most stable *di-cis* amide conformer **C5_cc** occurs at 30.3 kJ mol^{-1} relative to the global minimum, which implies that the energetic effort of rotating the amide bonds on the N- or C-terminal side of **1** into the *cis*-conformation is quite independent of other conformational settings.

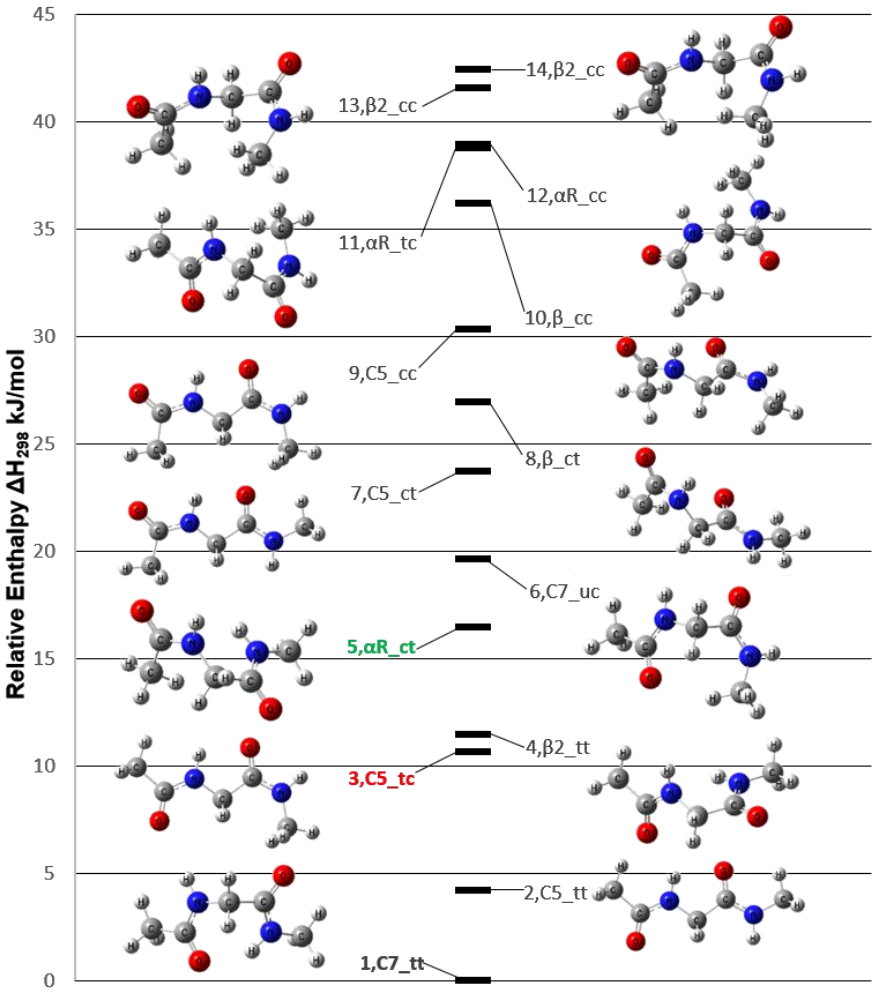

Fig. 40: The structures of gas phase minima obtained at B3LYP/6-31G(d) level and ΔH_{298} calculated at G3(MP2)-RAD level.

Table 5: Relative enthalpies ΔH_{298} (kJ mol^{-1}) for conformers of glycine dipeptide model **1** at different QM theoretical levels. "*" Please refer to chapter 4.3.3, Table 10 for conformational nomenclature. "**" 'u' indicates a peptide bond conformation deviating more than 15° from the idealized dihedral angles of 0° (*cis*, c) and 180° (*trans*, t). For **C7_ut** the dihedral angle amounts to 164.4°.

SI	Conf.*	B3LYP/6-31G(d)	B2PLYP/G3M2LARGE	G3(MP2)-RAD	G3B3	CCSD(T)/CBS
1	C7_tt	0.0	0.0	0.0	0.0	0.0
2	C5_tt	2.0	1.3	4.2	4.7	2.7
3	C5_tc	9.8	8.5	10.7	11.2	9.7
4	β2_tt	10.1	9.7	11.5	11.8	10.9
5	αR_ct	17.9	16.2	16.5	16.9	16.1
6	C7_uc**	20.1	19.6	19.6	19.8	19.6
7	C5_ct	20.7	21.0	23.7	24.3	22.2
8	β_ct	26.2	26.7	26.9	27.3	26.4
9	C5_cc	28.5	28.4	30.3	30.9	29.4
10	β_cc	37.0	36.9	36.2	36.6	36.0
11	αR_tc	42.7	40.1	38.8	39.0	39.7
12	αR_cc	40.9	40.0	39.0	39.4	39.4
13	β2_cc	44.5	42.3	41.6	42.1	42.4
14	β2_cc	44.2	42.8	42.5	43.0	43.1

In free energy terms (ΔG_{298}) the extended **C5_tt** conformation represents the global minimum, followed by **C7_tt** at +2.7 kJ mol^{-1} (the first column in Fig. 41). This flip can be understood in terms of the entropic cost of the internal hydrogen bond present in **C7_tt** as compared to the extended **C5_tt** structure. The order and relative stability for the rest of the conformers is not changed much. The **C5_tc** structure remains the 3rd best conformer and appears at 8.8 kJ mol^{-1}, while the first conformation with a *cis*-amide on the N-terminal side **αR_ct** occurs at 18.8 kJ mol^{-1}, *i.e.* 10 kJ mol^{-1} higher than **C5_tc**. In summary all gas phase results predict a close competition of **C5_tt** and **C7_tt** conformations, followed by the **C5_tc** conformation as the lowest lying *cis*-amide structure. The best conformation of **ct** type is at all levels significantly less stable than that of **tc** type. The effects of solvation were explored for DMSO as one of the often used polar solvents for NMR spectroscopy. Building on the gas phase geometries and energies shown in Fig. 40, solvation free energies were calculated using the IEF-PCM and COSMO-SAC continuum solvation models. Combining the gas phase free energies with the solvation free energies yields the conformational distribution shown in Fig. 41. Irrespective of the solvation model the **C5_tt** conformation is predicted as the global minimum, followed by **β2_tt** as the 2nd best and the

C7_tt conformation as the 3rd best *trans-trans* conformer. The **C5_ct** and **C5_tc** conformations are almost isoenergetic now and they are 12 kJ mol^{-1} above the global minimum using COSMO-SAC solvation energies. This is in close agreement with the experimental measurements predicting energy differences of 13.0 ± 2 kJ mol^{-1} (see below).

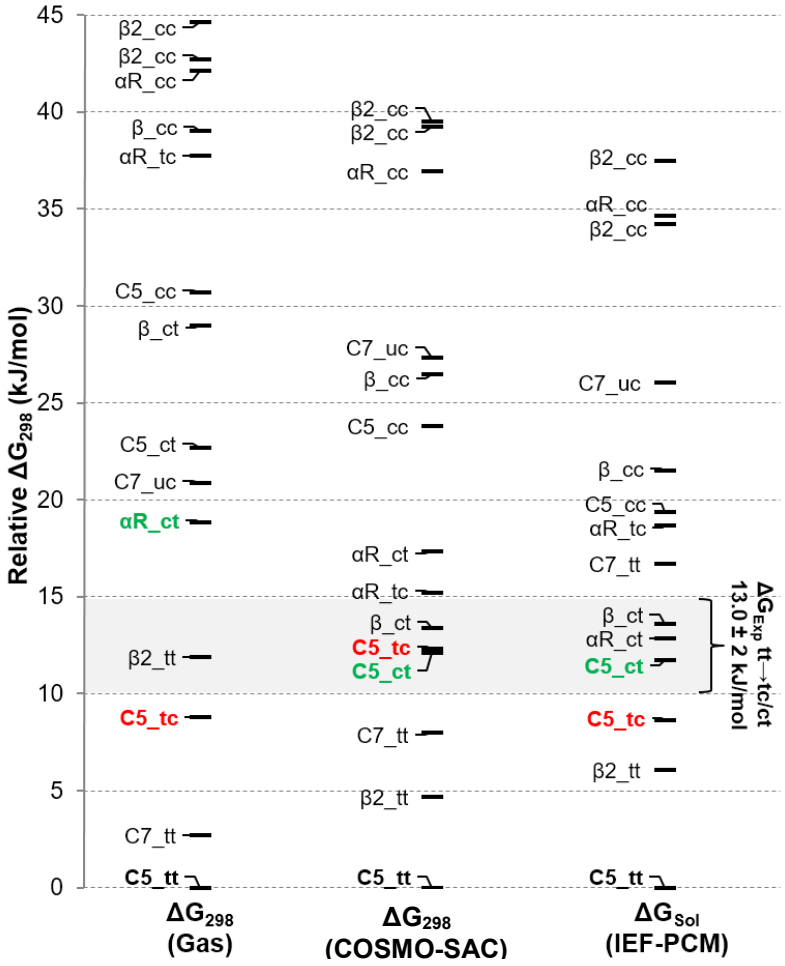

Fig. 41: Gas phase and solution phase (DMSO) free energy differences (ΔG_{298}, kJ mol^{-1}) for conformers of glycine dipeptide model **1**.

Experimental Results

The four characteristic regions of the ^{1}H NMR spectra of **1** (NH, Hα, Ace, and NMe see Fig. 42A) reveal signal sets of the main conformer **1_tt** as well as of the two very low populated *cis*-conformers **1_ct** and **1_tc**. At 600 MHz some of the *cis*-conformer signals partially overlap with the large resonances of the main conformer, but several signals of **1_ct** and **1_tc** are even base-line separated and enable a highly reliable integration. In Fig. 42B, the ^{1}H chemical shifts of **1_tt**, **1_ct** and **1_tc** in DMSO-d_6 at 305 K are depicted (for 2D assignment spectra and ^{13}C chemical shift assignment

please refer to chapter 4.3.1). The population of the *cis*-conformers is in the order of the ^{13}C satellites of the main conformer **1_tt** (see Fig. 42A), *i.e.* about 0.5% each.

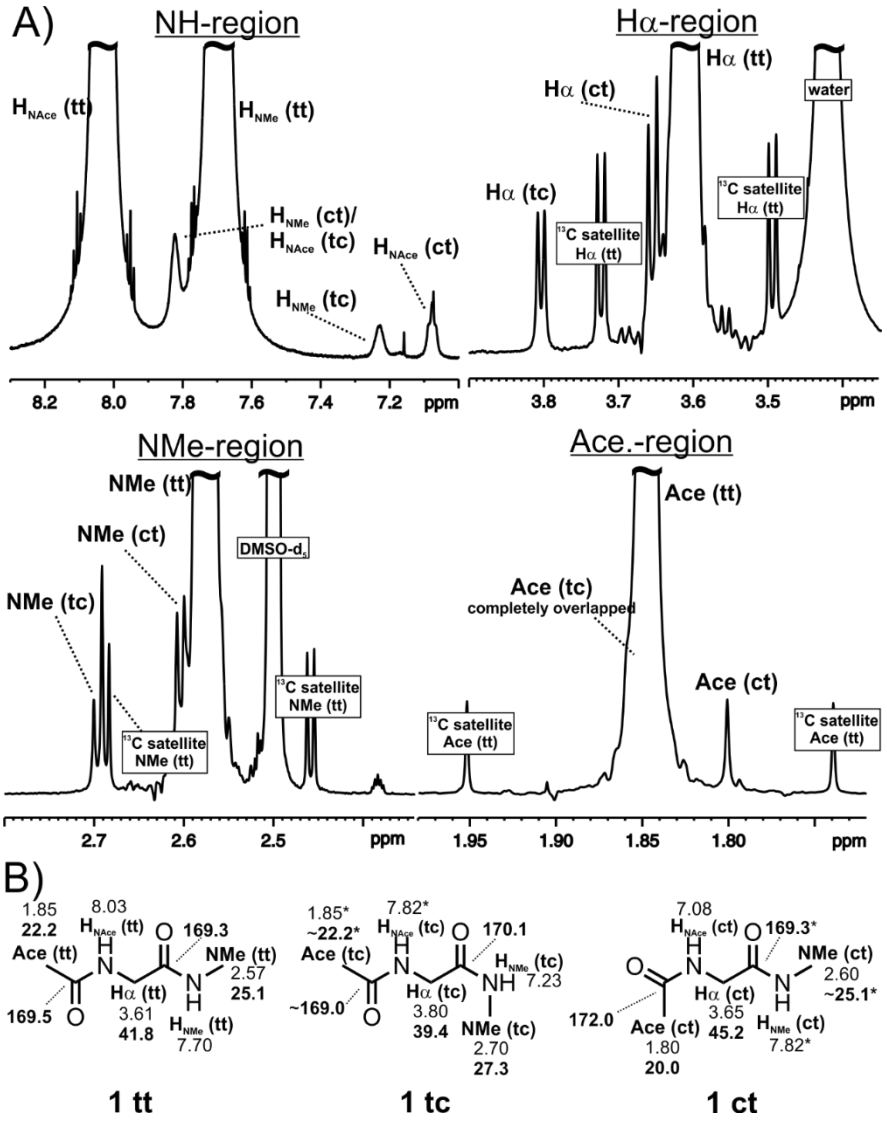

Fig. 42: **A**) Four characteristic ^{1}H NMR-regions (of one spectrum) of dipeptide **1** and all signals of the three distinguishable conformers (see B) at 305 K are shown. The signals of the main conformer **1_tt** are truncated. **B**) ^{1}H (normal font) and ^{13}C (bold font) chemical shift assignment (in ppm) of conformers **1_tt**, **1_tc** and **1_ct** are depicted. "*" marks signals which strongly overlap, and "~" marks approximate assignments with some uncertainty.

The amide protons of the *cis*-conformers (H_{NAce} and H_{NMe} of **1_ct** and **1_tc**) were identified unambiguously using magnetisation transfer *via* chemical exchange (EXSY) in 1D selective NOESY experiments. Selective irradiation of H_{NAce} or H_{NMe} in **1_tt** results in an EXSY signal build-up of the corresponding signals in **1_ct** and **1_tc** (for details see chapter 4.3.1) and thus differentiates these signals from possible impurities.

Intramolecular NOE contacts of Hα (**tc**) and NMe (**tc**) as well as Hα (**ct**) and Ace (**ct**) detected by 1D selective NOESY experiments prove *cis*-conformations in **1_ct** and **1_tc**

(see Fig. 43). The intensity of the nuclear Overhauser effect (NOE) is directly proportional to the inverse sixth power of the corresponding, weighted proton-proton distance. In high concentrated samples up-to-date NMR equipment allows for NOE detection up to a distance of roughly 5 Å. In very low concentrated samples or in the case of minor conformers such as **1_ct** and **1_tc** the individual cut off distance can be significantly shorter, due to sensitivity problems. Thus, in the applied setup for the *cis*-conformer **1_tc**, even a distance of 3.69 Å (Hα-H_{NMe}) was not detected by NOESY experiments (see chapter 4.3.1). As a result the detected NOE contacts of Hα (**tc**) and NMe (**tc**) as well as Hα (**ct**) and Ace (**ct**) indicate considerably shorter distances, which is in agreement with the theoretical Hα-Ace and Hα-NMe distances of **1_tc** and **1_ct** (2.69 Å and 2.59 Å). In contrast, in all calculated *trans*-isomer geometries, these distances are larger than 4.5 Å (see Fig. 43C). Thus, the detected NOE contacts shown in Fig. 43 fully support the population of *cis*-conformers of peptide **1** in DMSO. Additionally, a comparison of the assigned structures (see Fig. 43C) shows that only in the **ct**-conformer the N-terminal carbonyl group is pointing away from the Cα group and therefore exclusively in this conformer the Cα carbon should not sense a significant shielding effect of the carbonyl π-system. If the assignments of **1_tt**, **1_tc** and **1_ct** are correct, this must result in a considerably higher ^{13}C chemical shift of Cα (**ct**) compared to Cα (**tt**) and Cα (**tc**) conformers. Indeed, the experimental ^{13}C chemical shift of Cα (**ct**) (45.2 ppm) is more than 3 ppm higher than in conformers **tt** (41.8 ppm) and **ct** (39.4 ppm) which further supports the conformer assignments. Due to signal overlap *cis*-*cis* conformations cannot be excluded experimentally (for details refer to chapter 4.3.1). However, theoretical considerations make the population of double *cis*-peptide **1_cc** very unlikely.

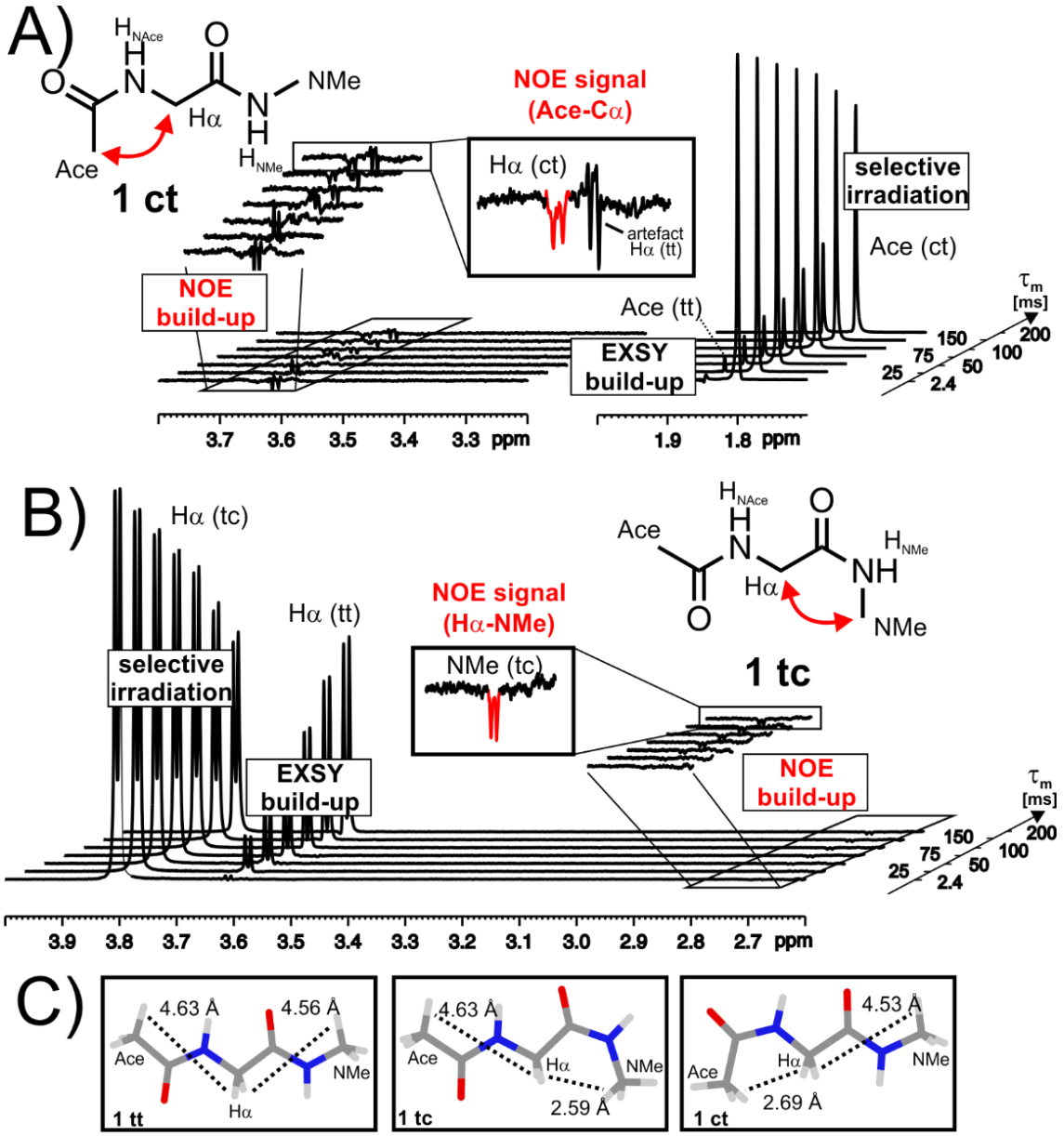

Fig. 43: Assignment and structure determination is shown of *cis*-conformers *via* 1D selective NOESY/EXSY spectra. Stacked plots of 1D selective NOESY spectra of **1** at 303 K with increasing mixing time (τ_m) reveal both unambiguous assignments by EXSY signals as well as distance information within the *cis*-conformers by NOESY signals. This is shown for selective irradiation of Ace (**ct**) (see A) and of Hα (**tc**) (see B). C) Calculated peptide **1** conformer geometries (B3LYP/6-31G(d)) with key distances are shown. For the high populated main-conformer **1_tt** both depicted distances (4.63 Å, 4.56 Å) lead to detectable NOE signals (data not shown). In contrast, only the short distances depicted within the *cis*-conformers **1_tc** (2.59 Å) and **1_ct** (2.69 Å) allow for NOE signal detection (see A and B) with this NMR setup and *cis*-conformer populations of about 0.5%.

Next the thermodynamic constants ΔG_T (change in Gibbs free energy), ΔH (change in enthalpy) and ΔS (change in entropy) of the equilibrium between the conformers **tt** and **ct** as well as **tt** and **tc** of peptide **1** (see Fig. 44) were calculated based on the temperature dependent population changes monitored by proton NMR spectroscopy (for details see chapter 4.3.1).

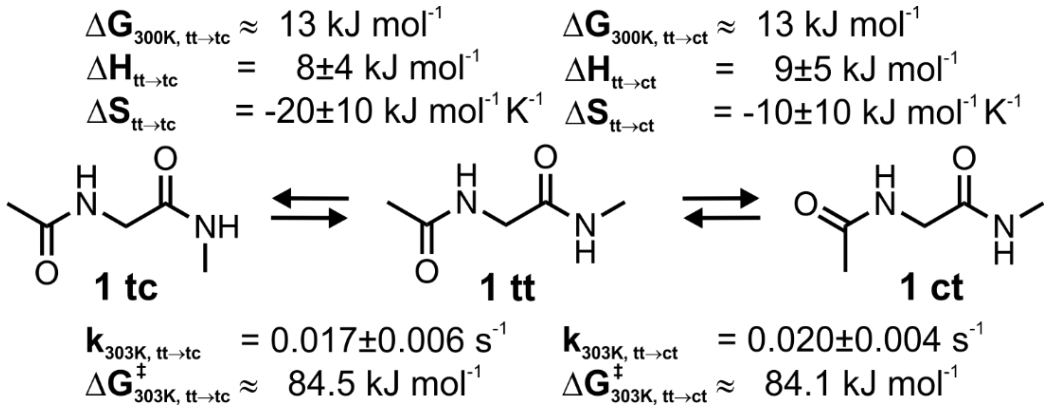

Fig. 44: Conformer equilibria and NMR spectroscopically determined thermodynamic and kinetic constants. (DMSO-d_6, 303 K).

To check the reliability of the data originating from a combination of very small and very large integrals for each of the two equilibria two independent sets of signals were chosen (NH: H_{NAce} (**tt**), H_{NMe} (**tc**), H_{NAce} (**ct**) / aliphatic: ^{13}C satellite of Hα (**tt**), Hα (**tc**), Ace (**ct**)). The temperature dependence of ΔG_T for **1_tt** → **1_tc** is presented in Fig. 45, the thermodynamic and kinetic constants are summarized in Fig. 44. For both *cis*-conformers, the experimentally determined ΔH values are very similar ($\Delta H_{tt\rightarrow tc}$ = 8±4 kJ mol^{-1} and $\Delta H_{tt\rightarrow ct}$ = 9±5 kJ mol^{-1}) and the ΔS values are small ($\Delta S_{tt\rightarrow tc}$ = -20±10 J mol^{-1} K^{-1}, $\Delta S_{tt\rightarrow ct}$ = -10±10 J mol^{-1} K^{-1}) as expected for a conformer equilibrium. The experimentally determined ΔG_{300K} values for both equilibria (both about 13 kJ mol^{-1}) are extremely close to the theoretically calculated values for **C5_ct** and **C5_tc** conformations using COSMO-SAC, which are both about 12 kJ/mol above the global minimum (see above).

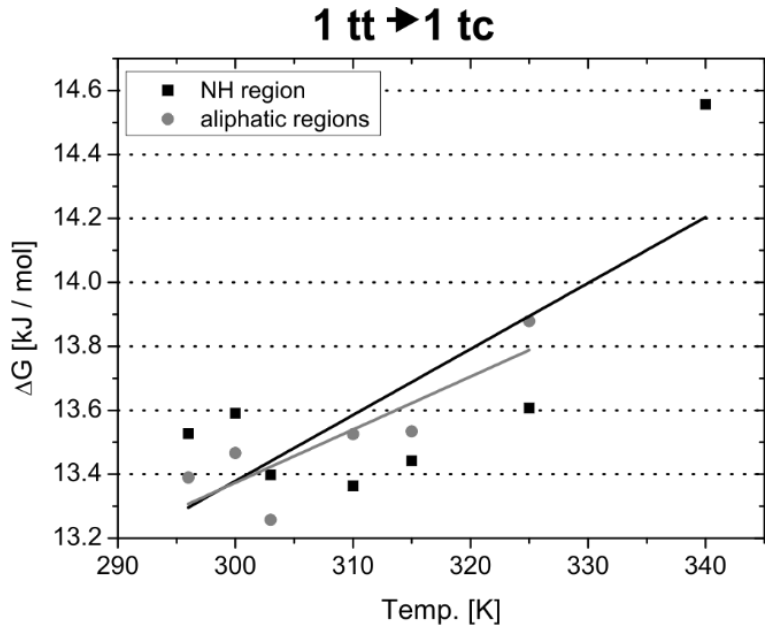

Fig. 45 Plots of ΔG against T for two signal sets (NH, aliphatic) of the equilibrium **1_tt** -> **1_tc**. R^2 values are 0.51 (NH) and 0.66 (aliphatic).

Rate constants *k* were determined by 1D selective NOESY/EXSY spectra in combination with the initial rate approximation as applied recently for investigations on the formation mechanism of the central organocatlytic enamine intermediate.[41] This method is based on work[42,43] of Perrin and Dwyer and makes use of the NOESY experiment and the chemical exchange during the chosen mixing time τ_m (for details, additional results applying a 2D NOESY approach as well as a rate constant cross-check, see chapter 4.3.1). Peptide **1** *cis*-conformer formation rate constants determined by 1D selective NOESY and the initial rate approximation in DMSO-d_6 at 303K[f] are $k_{tt\text{-}tc}$ = 0.017±0.006 s^{-1} and $k_{tt\text{-}ct}$ = 0.020±0.004 s^{-1}, respectively. In the actual sample at a total concentration of peptide **1** of 380 mM, this translates to *cis*-conformer formation rates of about 0.008 mol L^{-1} s^{-1}. In other words, within 1 min reaction time, a number of molecules exceeding the whole population of the main conformer **1_tt** reacts once to a minor *cis*-conformer. Therefore, even if the population of the *cis*-conformers **1_tc** and **1_ct** is extremely low, kinetically they are very much accessible.

Collective Analysis of Experimental and Theoretical Data

The spectral data discussed in the previous section results from averaging over different conformers, thus making it difficult to determine the contribution of an individual conformer or a sub-group of conformers to the overall signals. The overlapping signals (see Fig. 42) further add to an already complicated scenario. QM-derived isotropic shieldings, energetics and structural properties were used to aid the analysis of the experimental spectral data of **1** with respect to the following points:

The Best Conformation for 1. In terms of ΔG_{Sol} (COSMO-SAC and IEF-PCM), **C5_tt** is predicted as the best conformer followed by **β2_tt** (see Fig. 41). To investigate this further, the structural information is extracted from proton-proton NOE integrals in 2D NOESY spectra between the corresponding protons (see Fig. 46A). The NOE integrals of signals between Hα protons to amide protons (H_{NAce} and H_{NMe}) of **1_tt** were used to determine a distance ratio of 1.03 ($r_{Hα\text{-}HNMe}/r_{Hα\text{-}HNAce}$). A closely similar value of 1.06 was obtained using the theoretical average distance ratio calculated over **C7_tt**, **β2_tt** and **C5_tt** gas phase geometries using weighted distances between Cα and amide protons (H_{NAce} and H_{NMe}). An individual conformer analysis reveals that **C5_tt** has a distance ratio of 1.11, while **β2_tt** and **C7_tt** have distance ratios of 0.82 and 0.95, respectively. A very similar conclusion can be drawn from analysis of the ^{1}H chemical shifts of the amide protons of **1**. These can be observed for the all-*trans* conformer at 8.03 ppm (H_{NAce} proton), 0.33 ppm downfield from the H_{NMe} proton at 7.7 ppm. Calculated ^{1}H chemical shifts (B3LYP/PCS4, DMSO//B3LYP/6-31G(d), gas)

[f] Rate constants were determined at elevated temperature (303 K) in order to increase the exchange rates and thereby improve the signal to noise ratios.

for the all-*trans* conformers indicate that only for the **C5_tt** conformer the H_{NAce} signals occur downfield from the H_{NMe} signals, while the reverse order is predicted for the **β2_tt** and **C7_tt** conformers (Fig. 46B). Taken together the energetics, structural and chemical shift analysis indicates that **C5_tt** is the most preferred conformation for **1** in DMSO.

The ^{13}C Spectral Trends in 1. The experimental ^{13}C signals for the **tt**, **tc** and **ct** conformers strongly overlap in a number of instances, which makes the assignments for the **tc** and **ct** isomers challenging. Using the theoretically calculated ^{13}C chemical shifts shown in Fig. 46D, the assignment of the *cis*-peptide conformers can be aided substantially.

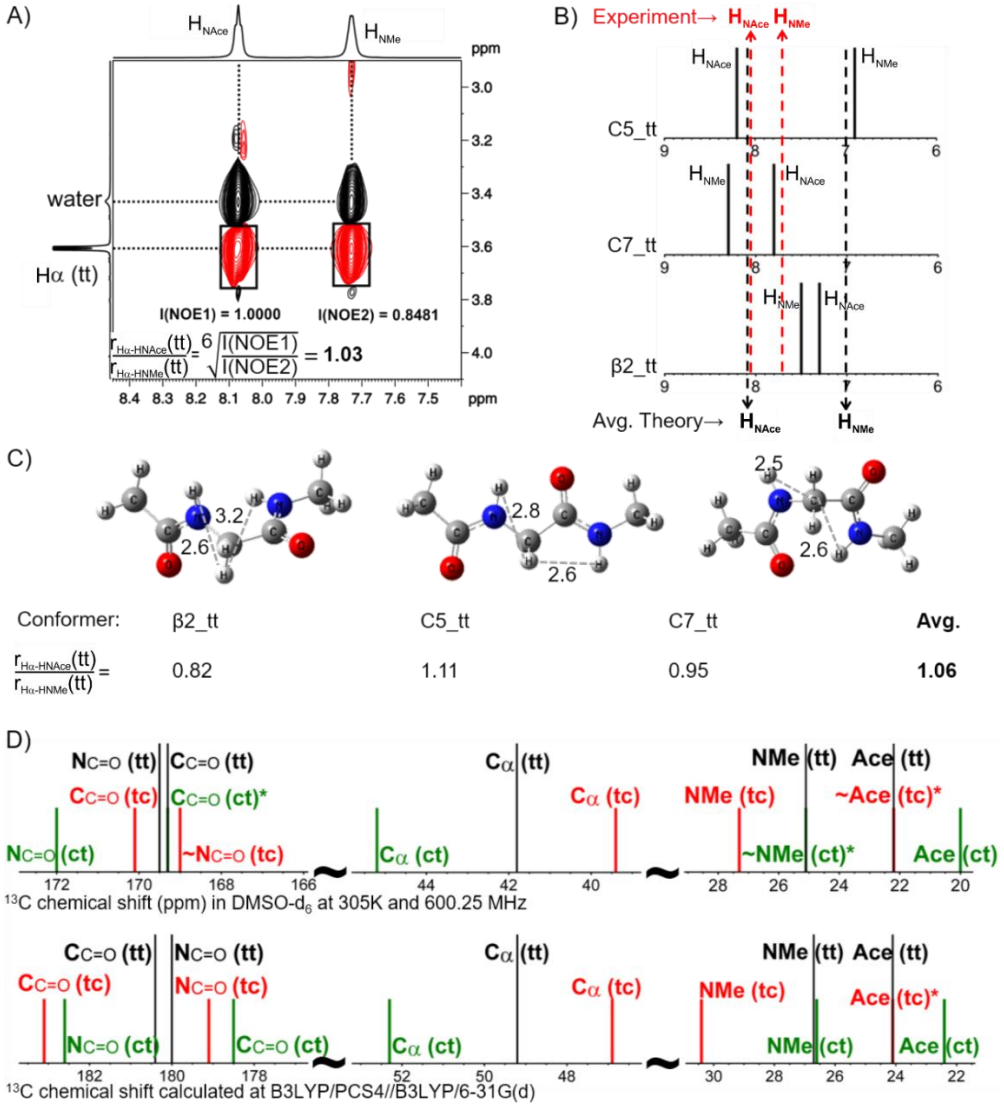

Fig. 46: A) Section of the 2D NOESY spectrum of **1** (380 mM) in DMSO-d_6 at 300 K with a mixing time of 250 ms. B) Comparison of experimentally measured and theoretically calculated ^{1}H chemical shifts for the amide protons in the all-*trans* conformer of **1**. C) Weighted distance ratios ($r_{Hα\text{-}HNMe}/r_{Hα\text{-}HNAce}$) for all-*trans* conformers of **1** using gas phase geometries optimized at B3LYP/6-31G(d) level. D) Comparison of experimentally measured and theoretically calculated ^{13}C chemical shifts of **1**.

Calculated *absolute* ^{13}C shifts deviate from the experimental values by 2-10 ppm, and the three most relevant regions of the calculated ^{13}C NMR spectrum for **1** in Fig. 46D with signals for the carbonyl carbon (c=o), Cα and terminal methyl carbons (Ace and NMe) are therefore shifted such that best alignment is obtained for the **tt** signals.

The theoretical prediction of ^{13}C shifts for Ace, NMe and Cα carbon of **tt**, **tc** and **ct** conformers relative to each other matches the experimentally observed trends. The calculated values verify the overlapping behaviour of Ace (**tc**→**tt**) and NMe(**ct**→**tt**) signals. The Cα shifts for **tc** and **ct** relative to **tt** are also supported by the theoretical results. The ^{13}C shifts calculated for carbonyl carbons show slightly less satisfactory agreement in an absolute sense, but again show the proper relative order of signals for each individual conformer.

Conclusion

QM-derived thermochemical data predict an extended **C5_tt** conformation for dipeptide model **1** as the preferred conformation. Isomerization of the N- or C-terminal amide bond are both found to be endergonic by 12 kJ mol^{-1} at 300 K, leading to the occurrence of the *trans-cis* (**tc**) and *cis-trans* (**ct**) conformations as detectable species by NMR measurements in DMSO-d_6. An NOE integral-based distance analysis reveals that **1_tt** is mainly populated by the **C5_tt** conformer. Complete assignments of ^{1}H and ^{13}C chemical shifts as well as experimental distance ratios generated from NOE cross signals deliver data that was supported by theoretical calculations. The trends of calculated ^{13}C and ^{1}H isotropic chemical shifts agree well with experimental observations. Temperature-dependent ^{1}H NMR measurements indicate that the *cis-trans* energy difference is mainly of enthalpic origin, which is again in line with theoretical predictions. In addition, the experimentally determined rate constants for *cis*-conformer formation at 303 K of roughly 0.02 s^{-1} and the deduced rates of 8 mmol L^{-1} s^{-1} show that, despite the rather low absolute population of *cis*-conformers, they are easily accessible kinetically.

Experimental Details

The pseudo-dipeptide **1** (2-acetamino-N-methylacetamide, 380 mM) sample was prepared inside a melt-sealed standard 5 mm NMR tube in DMSO-d_6. NMR spectra were recorded on a Bruker Avance DRX 600 (600.13 MHz) and on a Bruker Avance III 600 (600.25 MHz) spectrometer, the latter equipped with a TCI cryoprobe with z-gradient. All spectra were referenced to the DMSO residual peaks (^{1}H: 2.50 ppm, ^{13}C: 39.5 ppm).

Computational Details

The geometries of all the conformers of **1** were optimized at B3LYP/6-31G(d) level of theory in gas phase.[44,45] The frequency calculations were performed at the same level of theory and all minima were confirmed with all positive frequencies. Single point calculations were done at double hybrid B2-PLYP/G3MP2LARGE,[46] composite methods G3(MP3)-RAD,[47] G3B3[48] and CCSD(T)/CBS.[49,50] For CCSD(T)/CBS, extrapolations to the complete-basis-set (CBS) limit were carried out based on the MP2 single-point energies by the two-point extrapolation scheme using cc-pVTZ and cc-pVQZ basis set (see chapter 4.3.2 for a detailed description).[51] The energies were calculated for a temperature of 298.15 K in the gas phase and the thermal corrections to the enthalpy and Gibb's free energy were obtained at the B3LYP/6-31G(d) level of theory. The solvent correction for ΔG_{solv} was calculated using IEFPCM[52] and COSMO-SAC[53] models in DMSO and were subsequently added to the single point energy. For chemical shieldings the specifically optimized pcS-4 basis set developed by Jensen was used with B3LYP in the gas phase and DMSO.[54] The IEFPCM is used for modelling implicit DMSO. The solvation energies using COSMO-SAC were calculated using COSMO-RS module implemented in ADF2014[55-56] with Gaussian09 generated COSMO potential and all other calculations were performed using Gaussian09, Rev. D.01.[57]

4.3 Supporting Information

4.3.1 Structural Identification and Determination of Thermodynamic Constants and Rate Constants by NMR

Here, NMR experimental evidence is presented for the existence of two different low populated *cis*-conformers of pseudo-dipeptide **1** in DMSO-d_6 at room temperature. The complete set of ^{1}H and ^{13}C chemical shifts together with experimental distance ratios, as well as thermodynamic constants and rate constants of *cis*-conformer formation were determined. This unprecedented large pool of experimental results on an elusive *cis*-peptide in solution is most suitable for the optimization and verification of theoretical calculations. Additionally, it is shown that although populations of *cis*-conformers of **1** are very low, they are easily accessible kinetically.

Differentiation of NH Protons. In Fig. 47A a stacked plot of 1D selective NOESY spectra of pseudo-dipeptide **1** in DMSO-d_6 is shown with selective irradiation of proton H_{NAce} of the main conformer **1_tt**. As expected, the spectra reveals a NOE contact of this proton and the second NH proton H_{NMe} in the same molecule.

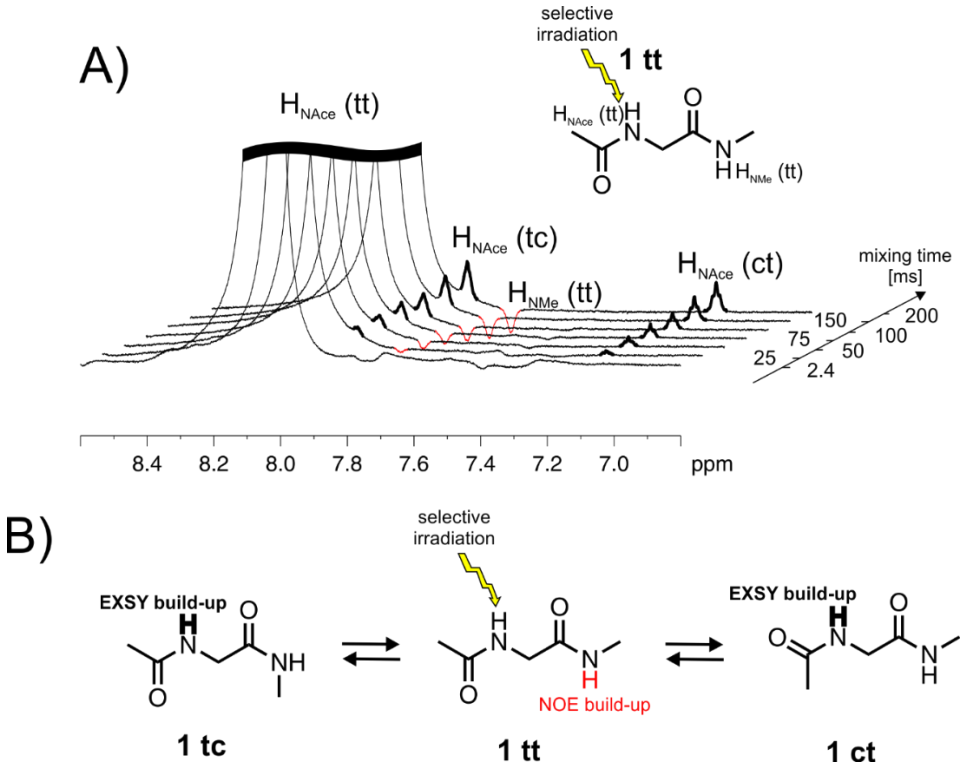

Fig. 47: A) Shows stacked plots of 1D selective NOESY spectra of peptide **1** in DMSO-d_6 with increasing mixing time and selective irradiation of the NH proton resonance H_{NAce} of the main conformer **1_tt**. Only the NH chemical shift window is shown. The signals of the irradiated resonance are truncated. EXSY build-up (positive phase, stems from chemical exchange with the irradiated molecule) is shown in black, NOE build-up (negative phase, stems from NOE contact over space with the irradiated proton) is shown in red. B) Shows the equilibrium between the main conformer **1_tt** and the two side conformers later identified as **1_tc** and **1_ct**. The proton corresponding to the signals which are building-up in the spectra are highlighted. Spectra were recorded at a proton resonance frequency of 600.25 MHz and a temperature of 303 K and were referenced to the solvent residual peak (2.50 ppm).

In addition, two EXSY signals occur. Since pseudo-dipeptide **1** is stable in DMSO, this means that under the applied conditions, the main conformer is in an equilibrium with two side conformers and the protons which show the EXSY build-up are also H_{NMe} protons of these conformers. The equilibrium between the three conformers is shown in Fig. 47B. The identity of the two side conformers as **1_tc** and **1_ct** cannot be extracted from these spectra. The data for its identification is shown below.

In Fig. 48A a stacked plot of 1D selective NOESY spectra of pseudo-peptide **1** in DMSO-d_6, now with selective irradiation of proton H_{NMe} of the main conformer **1_tt** (see Fig. 48B) is shown. Again the second NH signal H_{NAce} of **1_tt** has a NOE contact with the irradiated proton. As expected, also the irradiated H_{NMe} proton of the main conformer is exchanging with the H_{NMe} protons of the two side conformers as evidenced by the EXSY build-up of their resonances. The resonance of H_{NMe} (**ct**) is overlapped by the irradiated signal but the overlap is not complete and the signal can be identified anyway especially at the highest mixing time of 200 ms (see Fig. 48A, right-hand side). It can be excluded that the H_{NMe} (**ct**) resonance is irradiated together with the H_{NMe} (**tt**) conformer because in the spectra with low mixing times the H_{NMe} (**ct**) resonance does not show up.

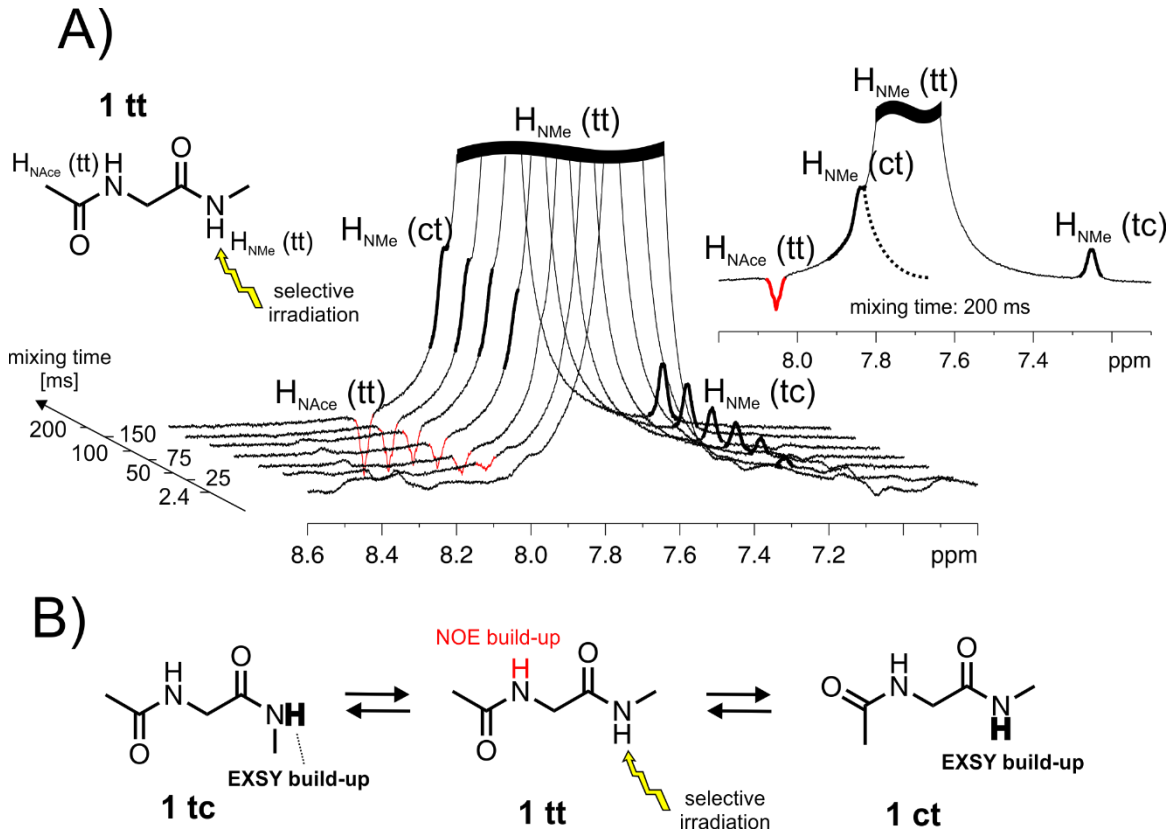

Fig. 48: Same as Fig. 47 but the irradiated NH proton resonance is now H_{NMe} of the main conformer **1_tt**. The exchanging H_{NMe} (**ct**) signal is overlapped by the large signal of the irradiated resonance. Nevertheless, it can be clearly identified.

¹H and ¹³C Chemical Shift Assignment. ¹H and ¹³C chemical shift assignment in DMSO-d_6 of the three distinguishable conformers of peptide **1**, *i.e.* **1_tt**, **1_tc** and **1_ct**, is shown in Fig. 49. Assignments are based on 1D ¹H, selective 1D ¹H NOESY/EXSY, 2D ¹H-¹H COSY, 2D ¹H-¹H NOESY, 2D ¹H-¹³C HSQC and 2D ¹H-¹³C HMBC NMR experiments. Proton spectra of **1** can be divided into four characteristic regions – the NH-region, the Hα-region, the Ace-region and the NMe-region (as shown in Fig. 42 in the manuscript).

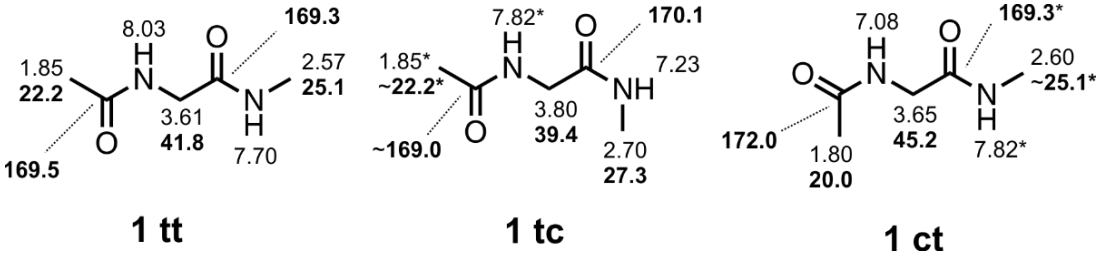

Fig. 49: ¹H (normal font) and ¹³C (bold font) chemical shift assignment (in ppm) of the three distinguishable conformers of peptide **1**, **1_tt** (*trans-trans*), **1_tc** (*trans-cis*) and **1_ct** (*cis-trans*) based on ¹H, selective ¹H NOESY/EXSY, ¹H-¹H COSY, ¹H-¹H NOESY, ¹H-¹³CHSQC and ¹H-¹³C HMBC experiments. Chemical shifts are in DMSO-d_6 at 305 K and referenced to the solvent residual peak (2.50 ppm). The proton resonance frequency is 600.25 MHz. * Marks signals which are strongly overlayed. ~ Marks rough assignments with some uncertainty remaining.

In the NH-region broad NH signals of the three conformers show up. One NH signal of both side isomers (H_{NMe} (**tc**) and H_{NAce} (**ct**)), respectively, is fully baseline separated without signal overlay. Signal integration for the determination of thermodynamic and kinetic constants is possible. In contrast, the resonances of H_{NMe} (**ct**) and H_{NAce} (**tc**) are completely overlaid. Notably, the NH resonances of the *cis*-conjugated part of the side conformers H_{NAce} (**ct**) (7.08 ppm) and H_{NMe} (**tc**) (7.23 ppm) are both high field shifted in comparison to their *trans*-conjugated counterparts in the other conformers. This can be explained by the shorter distance of these NH protons to the π-system of the neighboring carbonyl oxygen atom and the stronger shielding effect of the carbonyl π-electrons on these NH protons. In the Hα-region, the Hα (**ct**) resonance is baseline separated, but the signal of the second *cis*-isomer Hα (**tc**) is partly overlapped by the corresponding signal of the **tt**-conformer. Only the integral of the Hα (**tc**) signal can therefore be used for the extraction of thermodynamic constants. The situation in the Ace-region is similar. Here the resonance of the **ct**-isomer is fully baseline separated, but the signal Ace (**tc**) is completely overlaid by the corresponding signal of the main isomer **1_tt**. In the NMe-region, no *cis*-conformer shows a non-overlaid signal. NMe (**ct**) is overlaid with NMe (**tt**), and NMe (**tc**) is partly overlaid by a ¹³C satellite of NMe (**tt**). In summary, a reliable integration of signals of the *cis*-isomers **ct** and **tc** is only possible for two NH signals (H_{NMe} (**tc**) and H_{NAce} (**ct**)) and for two aliphatic signals in the Hα and the Ace-region (Hα (**tc**) and Ace (**ct**)).

Standard 2D NMR experiments were used in the structure identification and chemical shift assignment process. ^{1}H-^{13}C HSQC experiments reveal ^{1}J couplings between carbons and directly attached protons. The HSQC shown in Fig. 50 is DEPT-135 edited meaning that signals from CH_2 groups show a negative phase (red) whereas signals from CH and CH_3 groups show a positive phase (black).

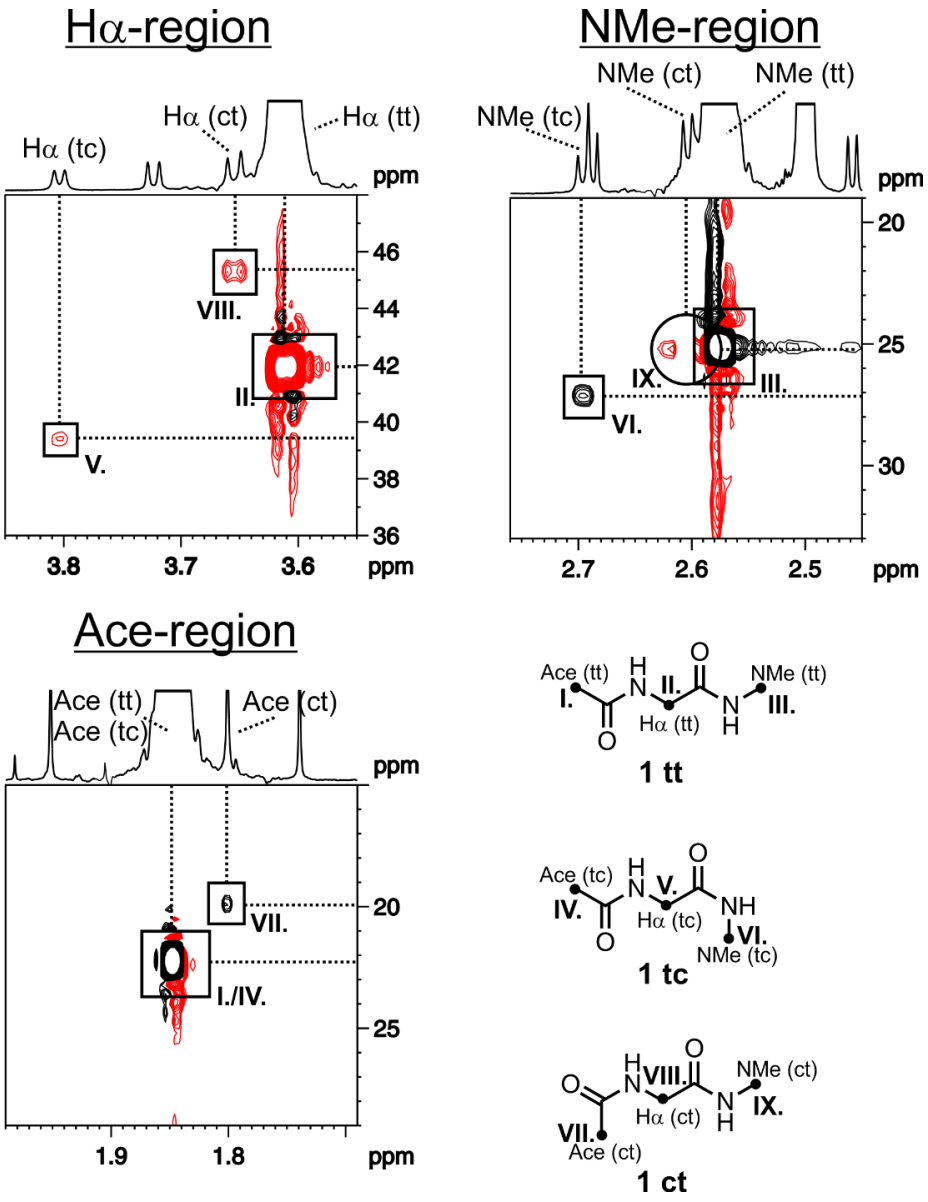

Fig. 50: Slices of a DEPT-135 edited ^{1}H-^{13}C HSQC spectrum of peptide **1** (380 mM) is shown, acquired in DMSO-d_6 at 305 K. Relevant cross signals and the corresponding carbon atoms in the conformers **1_tt**, **1_tc** and **1_ct** are highlighted and numbered in roman numerals. The spectrum is referenced to the solvent residual peak (^{1}H: 2.50 ppm, ^{13}C: 39.5 ppm).

All conformers show clean, cross signals in the Hα-region without any signal overlap. The negative phased (red) cross signals **II**, **V** and **VIII** can clearly be assigned to the ^{13}C resonances directly attached to the protons Hα (**tt**), Hα (**tc**) and Hα (**ct**). The Cα resonances show the largest difference in ^{13}C chemical shifts in between the three

conformers (about 5 ppm) which is useful for the validation of NMR shielding calculations (see manuscript). This large difference can be explained by the position of the N-terminal carbonyl group and the shielding effect of its π-electrons.

In the NMe-region cross signals of NMe (**tt**) **III** and NMe (**tt**) **VI** were doubtlessly assigned to the ^{13}C resonances of the corresponding CH_3 groups. The cross signal of NMe (**ct**) **IX** (circled signal) suffers from signal overlap with the **tt** isomer and a little uncertainty remains with its assignment. Actually, the lack of any signal in the center of the circled part of the spectrum indicates the cross signal. This lack of signal arises from the overlap of the NMe (**ct**) cross signal (positive phase, black color) with the T2 noise (negative phase, red color) stemming from cross signal **III**. Both effects are cancelling out each other resulting in the white spot in the center of the circled area. The remaining negative phased spot on the left-hand side of the circle stems from the T2 noise which is lying left of the cross signal and therefore is not cancelled out.

In the Ace-region assignment of the cross signals Ace (**tt**) **I** and Ace (**ct**) **VII** is straight forward. The signal of Ace (**tc**) **IV** is completely overlapped by the Ace (**tt)** cross signal **I** making the ^{13}C assignment a rough estimation. The existence of the Ace (**tc**) proton signal underneath the **tt** signal is proven by a NOE with the H_{NAce} (**tc**) proton (see below). Since no other HSQC cross signal was detected it is very likely that the rough ^{13}C assignment of the Ace (**tc**) methyl group is correct.

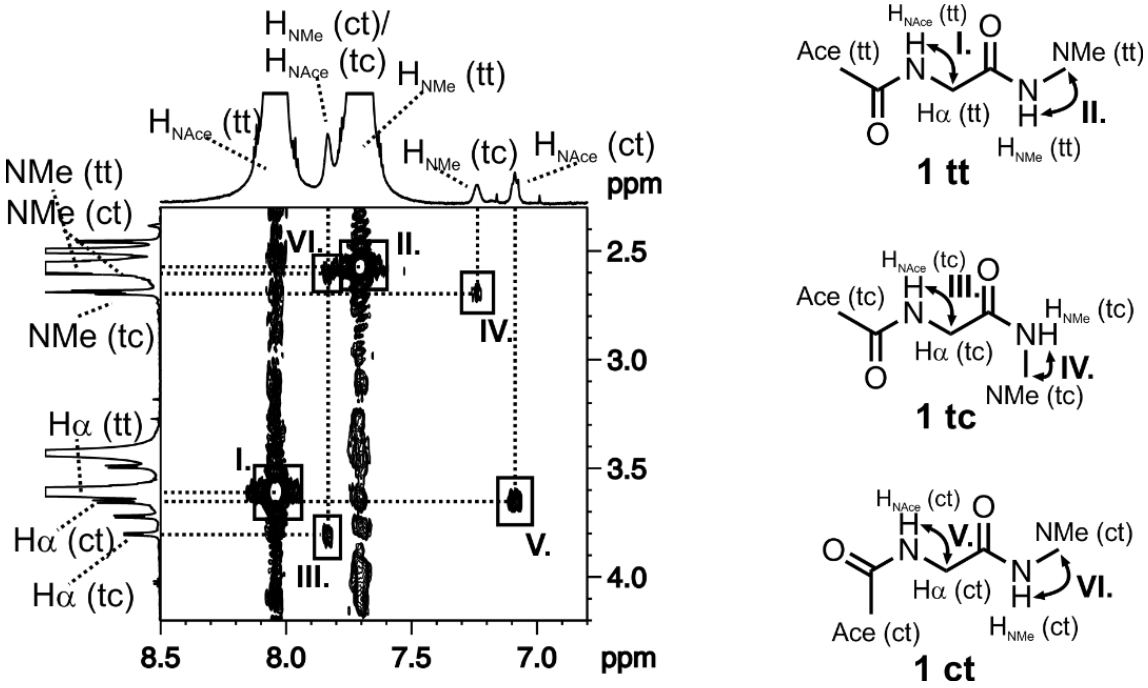

Fig. 51: A slice of a ^1H-^1H COSY spectrum of peptide **1** (380 mM) acquired in DMSO-d_6 at 305 K shows cross signals stemming from ^3J scalar couplings between the H_{NAce} protons and the Hα protons as well as the H_{NMe} protons and the NMe protons of conformers **tt**, **ct** and **tc**. Cross signals and the corresponding connectivities in the molecules are highlighted and numbered in roman numerals. The spectrum is referenced to the solvent residual peak (^1H: 2.50 ppm).

In the ^{1}H-^{1}H COSY spectrum shown in Fig. 51 cross signals stemming from ^{3}J proton-proton scalar couplings and the corresponding connectivities in conformers **1_tt**, **1_tc** and **1_ct** are presented. All signals are well separated and the resolution allows for doubtless assignments. The H_{NAce}-Hα connectivities are proven by cross signals **I** (**tt**), **III** (**tc**) and **V** (**ct**) whereas the H_{NMe}–NMe connectivities are proven by cross signals **II** (**tt**), **IV** (**tc**) and **VI** (**ct**). This spectrum also reveals the overlap of proton resonances H_{NMe} (**ct**) and H_{NAce} (**tc**) since cross peaks into both regions NMe and Hα (**VI** and **III**) are visible exclusively for H_{NMe} (**ct**) / H_{NAce} (**tc**) NH proton signals.

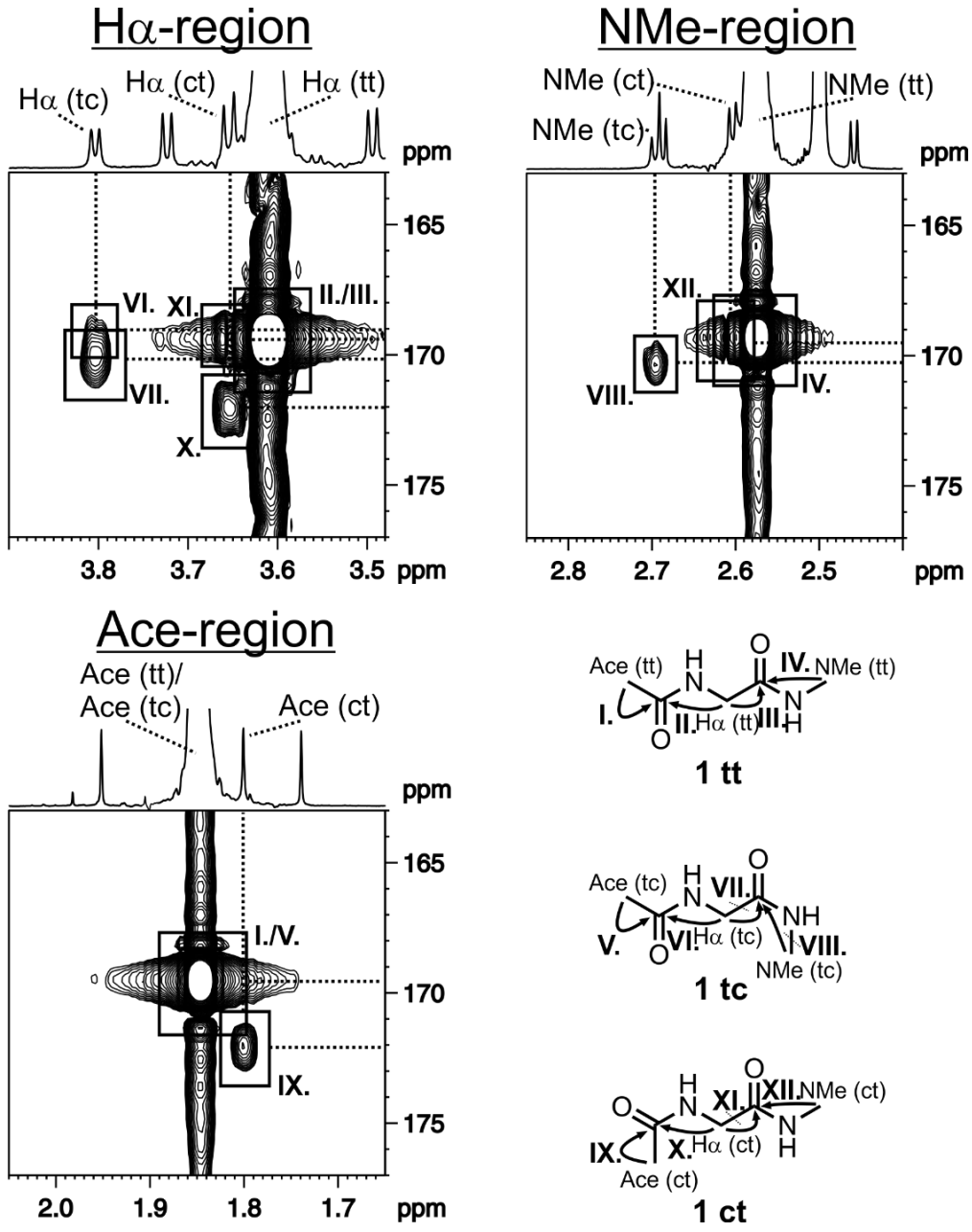

Fig. 52: Slices of a ^{1}H-^{13}C HMBC spectrum of peptide **1** (380 mM) acquired in DMSO-d_6 at 305 K show cross signals stemming from ^{2}J and ^{3}J proton-carbon scalar couplings of conformers **tt**, **c**t and **tc**. Cross signals and the corresponding connectivities in the molecules are highlighted and numbered in roman numerals. The spectrum is referenced to the solvent residual peak (^{1}H: 2.50 ppm, ^{13}C: 39.5 ppm).

Slices of a ^{1}H-^{13}C HMBC spectrum are presented in Fig. 52. The highlighted cross peaks are indicative for ^{2}J and ^{3}J proton-carbon scalar couplings and proof the connectivities in conformers **1_tt**, **1_tc** and **1_ct** as drawn in black arrows. The HMBC experiment shows the connectivity of the carbonyl groups with the other parts of the molecule.

In the Hα-region, cross peaks **II**/**III**, **VII** and **X** proof unambiguously the ^{3}J connectivity of Hα (**tt**) with both **tt** carbonyl carbon atoms, the connection of Hα (**tc**) with the C-terminal carbonyl group as well as the connectivity of Cα (**ct**) with the N-terminal carbonyl group of **ct**. Cross peaks **VI** and **XI** are partly overlaid but can still be assigned to ^{3}J couplings of Hα (**tc**) with the N-terminal carbonyl carbon atom of the **tc**-isomer and Hα (**ct**) with the C-terminal carbonyl carbon atom of the **ct**-isomer.

The NMe-region allows for the proof of connectivity of all NMe groups NMe (**tt**), NMe (**tc**) and NMe (**ct**) with their C-terminal carbonyl carbon atom counterparts (cross signals **IV**, **VIII** and **XII**) at which cross signal **XII** identification is based on a dispersive part in the T2 noise of cross signal **IV** and therefore contains some uncertainty.

HMBC cross signals in the Ace-region indicate the proton-carbon ^{2}J connectivity of the Ace groups with the N-terminal carbonyl groups. The Ace (**tt**) and Ace (**ct**) cross signals (**I** and **IX**) are clearly separated whereas the Ace (**tc**) cross peak is assumed to be completely overlaid by the **tt** signal and therefore cannot be assigned doubtlessly. However, the connectivity of Ace (**tc**) with the rest of the **tc** molecule is additionally proven by intramolecular NOEs (see below).

In slices of a ^{1}H-^{1}H NOESY spectrum (Fig. 53), proton-proton NOE cross signals are presented which are indicative for a short corresponding proton-proton distance. For the main conformer **1_tt**, a chain connectivity over space from the molecule group Ace to H_{NAce} (cross signal **I**), to Hα (cross signal **II**), over H_{NMe} (cross signal **III**) to NMe (cross signal **IV**) was proven. The same connectivity pattern was proven for isomer **1_tc** (Ace-H_{NAce}-Hα-NMe) by cross signals **V**, **VI** and **VII** and for the Hα (**tc**)-NMe (**tc**) connection by selective 1D NOESY experiments described below. For isomer **1_ct**, the NOESY experiments proved the connectivity chain over space NMe-H_{NMe}-Hα-H_{NAce} by cross peaks **X**, **IX**, and **VIII.** The Ace (**ct**)–Hα (**ct**) connectivity is again shown by selective 1D NOESY experiments described below.

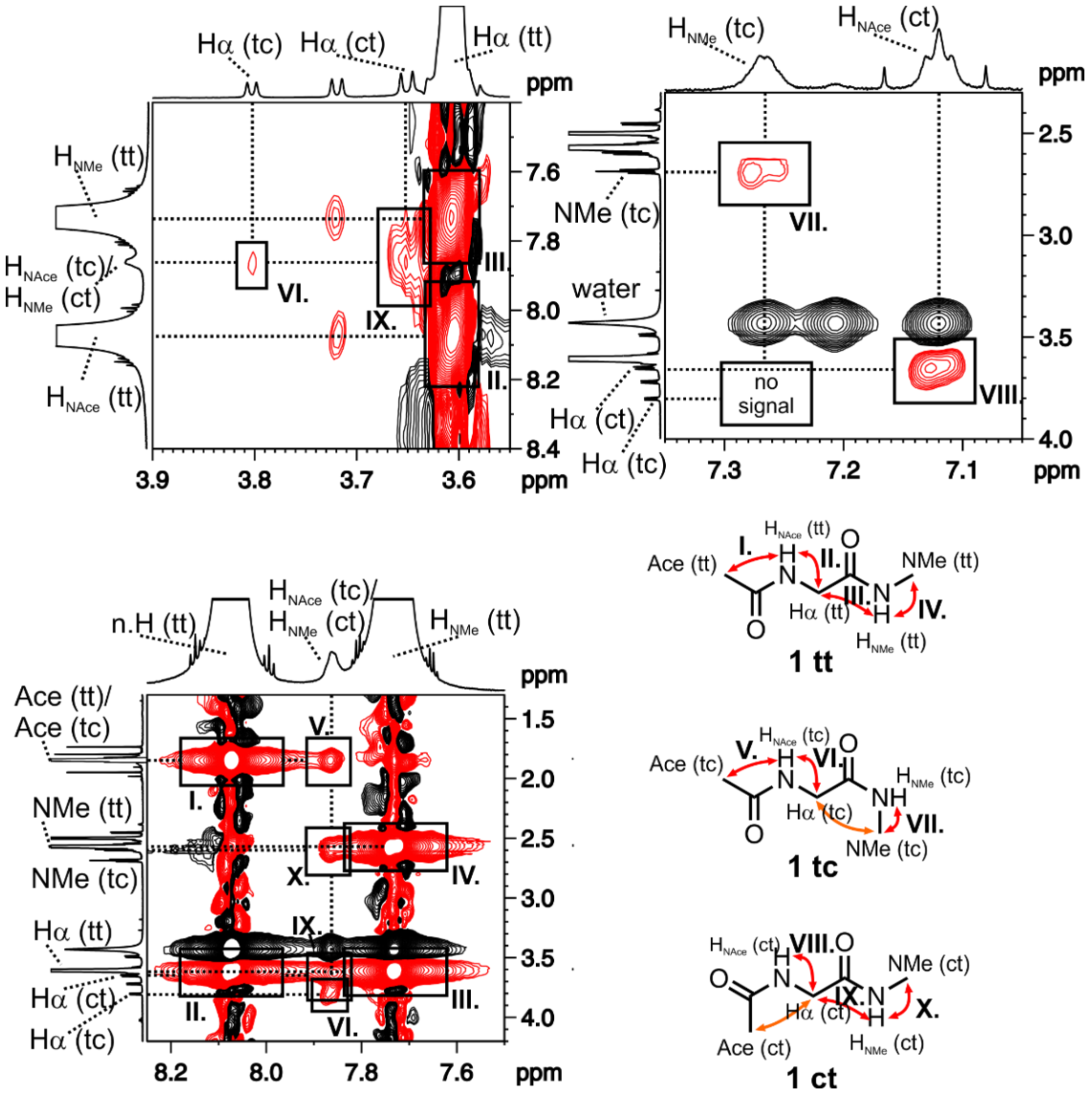

Fig. 53: Slices of a ^{1}H-^{1}H NOESY spectrum of peptide **1** (380 mM) acquired in DMSO-d_6 at 298 K with a mixing time of 250 ms show NOE cross signals (red) stemming from proton-proton dipole-dipole cross relaxation *via* space. Cross signals and the corresponding connectivities in the molecules (red arrows) are highlighted and numbered in roman numerals. The spectrum is referenced to the solvent residual peak (^{1}H: 2.50 ppm). Orange arrows represent connectivities revealed by selective 1D NOESY experiments as shown below.

Conformer Identification - Introduction. The calculated geometries of **1_tt**, **1_tc** and **1_ct** as well as the extracted averaged proton-proton distances Hα-Ace and Hα-NMe are presented in Fig. 54. Based on theoretical calculations conformers **1_tc** and **1_ct** are among the most probable occurring side conformers of pseudo-peptide **1**. In the NMR experiments above, two side conformers of dipeptide **1** were detected. In order to assign these conformers to theoretical structures, NOE contacts can be exploited.

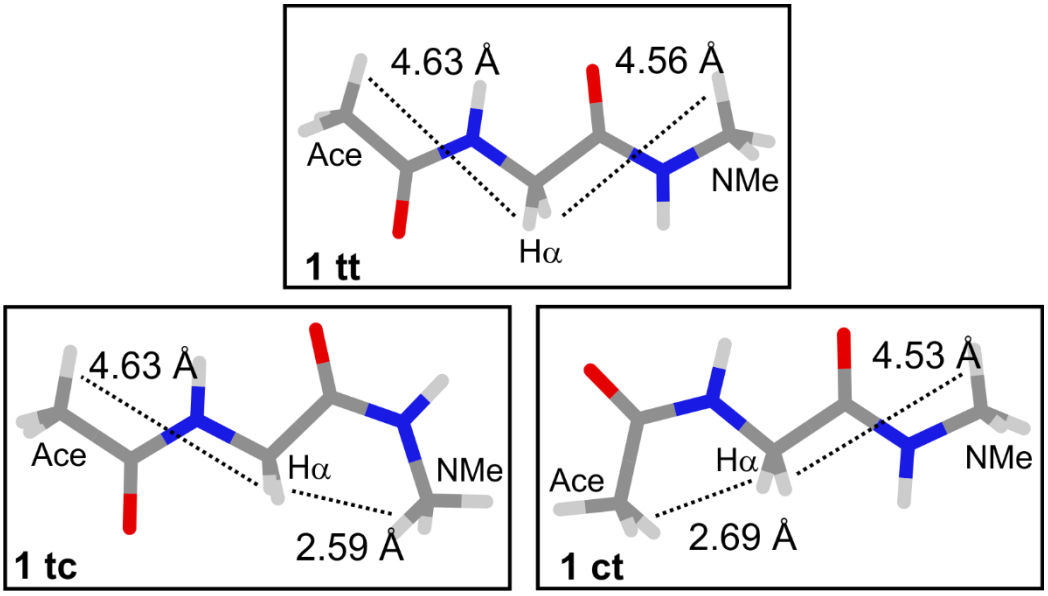

Fig. 54: Calculated Geometries are presented of the three conformers **1_tt**, **1_tc** and **1_ct**. (B3LYP/6-31G(d)) together with averaged proton-proton distances (each single distance is weighted with r^{-6}) of Hα-Ace and Hα-NMe.

Conformer Identification – Main Conformer 1_tt. In NMR theory, NOE signal intensities between two protons are direct proportional to the sixth inverse power of the corresponding proton-proton distance. In general, in order to detect a NOE contact with modern NMR equipment, a rule of thumb says that the underlying proton-proton distance must be shorter than 5 Å. However, for NOE detection of protons which are more than 4 Å away from each other, additionally high concentrated samples are necessary. The concentration of the main conformer of pseudo-peptide **1**, **1_tt** is very high (380 mM) and in deed, a Hα (**tt**)-Ace (**tt**) and Hα (**tt**)-NMe (**tt**) (theoretical distance of 4.63 Å and 4.56 Å) NOE is just detectable (see Fig. 55, on the left-hand side).

These NOEs can be used to validate the calculated theoretical geometries of the main conformer by determining the experimental distance ratio $r_{Hα\text{-}NMe}(tt)/r_{Hα\text{-}Ace}(tt)$ (see Fig. 55, on the right-hand side) and comparing it with the according distance ratio from calculations (see manuscript).

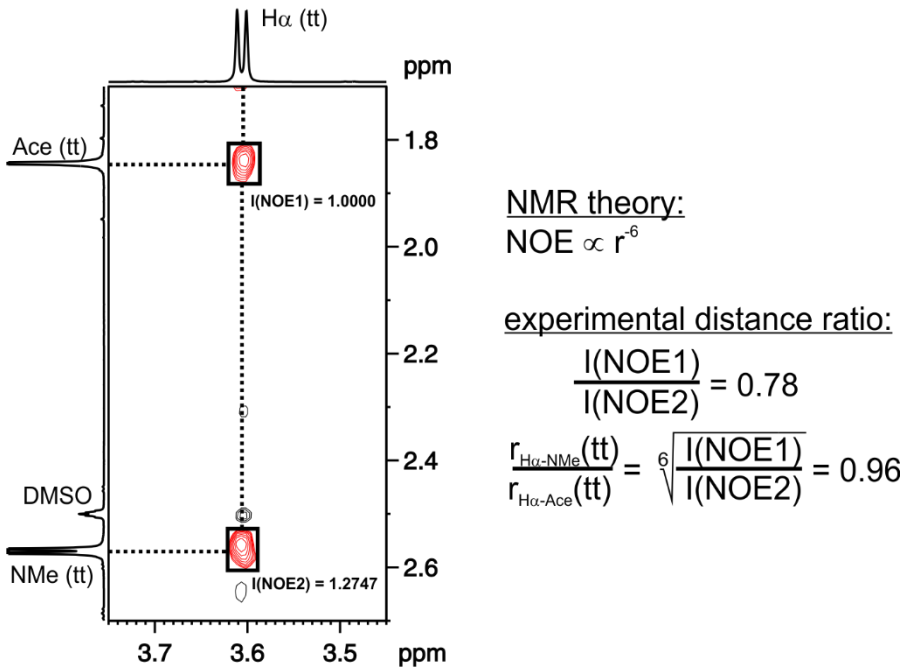

Fig. 55: A slice of a 2D NOESY spectrum of dipeptide **1** (380 mM) in DMSO-d_6 at 296 K and a mixing time of 400 ms is showing NOE signals (red) in between the Hα (**tt**) and Ace (**tt**) as well as Hα (**tt**) and NMe (**tt**) together with the corresponding integrals I(NOE1) and I(NOE2). On the right-hand side, the NMR theoretical dependence of the NOE intensity on the proton-proton distance r, the NOE ratio I(NOE1)/I(NOE2) and the experimental distance ratio $r_{Hα\text{-}NMe}(tt)/r_{Hα\text{-}Ace}(tt)$ calculated thereof are shown.

Conformer Identification – Cis-Conformers 1_tc and 1_ct. In contrast to the main conformer **tt**, the concentration of the *cis*-conformers (**tc** and **ct**; roughly 0.5%, ~1.9 mM) is way too low to allow for an NOE detection based on a proton-proton distance of more than 4 Å in the applied setup. Therefore, if NOE contacts in between protons of side conformers can be detected, the corresponding averaged proton-proton distance must be lower than 4 Å. As can be seen in Fig. 54 in the **tc**-conformer the Hα-NMe distance (2.59 Å) is short enough for NOE detection, whereas the Hα-Ace distance (4.63 Å) is too large. Exactly the opposite is shown for the **ct**-conformer. Here the Hα-Ace distance (2.69 Å) is short enough for NOE detection whereas the Hα-NMe distance (4.53 Å) is too high. Since the most probable candidate structures for the experimentally detected, low populated side conformers are **1_tc** and **1_ct**, experimentally detectable NOE contacts of Hα-NMe or Hα-Ace in these side conformers allows for the assignment of their structures to the corresponding *cis*-isomers. Therefore, if a Hα-NMe or Hα-Ace NOE contact is detected, the corresponding protons can be assigned to **1_tc** or **1_ct**.

In Fig. 56 the stacked plot of 1D selective NOESY spectra of peptide **1** with a selective irradiation of the Hα (**tc**) resonance is shown. With increasing mixing time a NOE build-up of the NMe (**tc**) resonance is detected. The strongest Hα-NMe NOE signal at

a mixing time of 200 ms is magnified and highlighted in red. As stated above, this NOE contact is indicative for a Hα-NMe distance (see Fig. 56 red arrow) below 4 Å and therefore a *cis*-conformation at this part of the molecule. The corresponding signal set can be assigned to **1_tc**. We note here that a Hα-Ace NOE contact cannot be totally excluded. The Ace (**tc**) chemical shift region is showing a overlap with the Ace signal of the high concentrated main conformer **1_tt** (region of the spectra not shown). A potential tiny NOE signal between NMe (**tc**) and Ace (**tc**) may be buried underneath that signal. However, assuming such an NOE contact would mean that the structure assigned here to **1_tc** is in fact the double *cis*-conformer **1_cc** and the probability for the occurrence of that isomer is assumed to be very low.

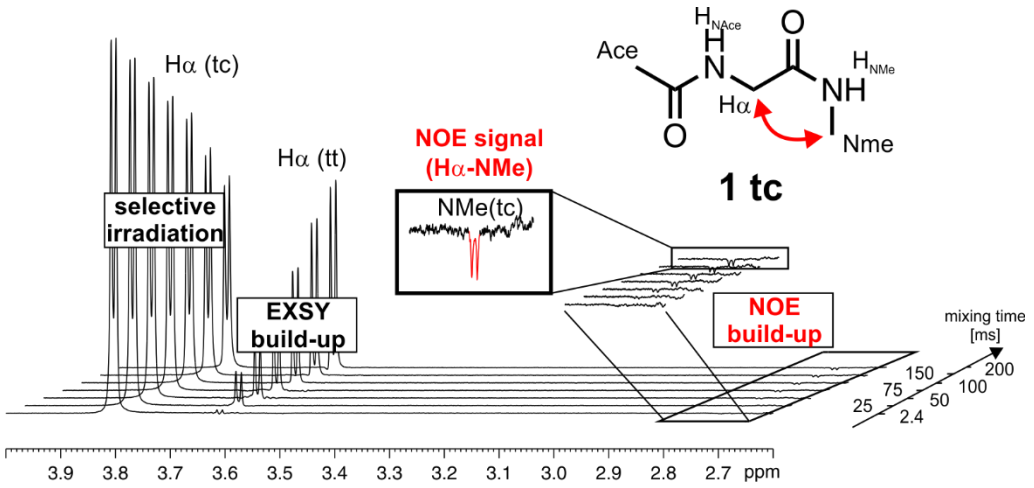

Fig. 56: Stacked plot of 1D selective NOESY spectra of peptide **1** (380 mM) in DMSO-d_6 with increasing mixing time (2.4-200 ms) and selective irradiation of the Hα resonance of the conformer **tc**. Magnified and highlighted in red is the NOE signal build-up of the NMe (**tc**) signal indicative for a short (below 4 Å) Hα-NMe distance which fits to the corresponding distance in the **tc** isomer (red arrows). In addition, the expected EXSY build-up of the exchanging Hα (**tt**) resonance is shown. The spectra were measured at 303 K and are referenced to the solvent residual peak (2.50 ppm).

Fig. 57 shows the stacked plot of 1D selective NOESY spectra of peptide **1** with a selective irradiation of the Ace (**ct**) resonance. Here, with increasing mixing time a NOE build-up of the Hα (**ct**) resonance is detected. The strongest Ace (**ct**)-Hα (**ct**) NOE signal at a mixing time of 200 ms is magnified and highlighted in red. Again, as stated above, this NOE contact is indicative for a Hα-Ace distance below 4 Å (see red arrow in Fig. 57) and therefore a *cis*-conformation at this part of the molecule. The corresponding signal set can be assigned to **1_ct**. A NMe-Hα NOE contact cannot be excluded because both the NMe (**ct**) resonance as well as the Hα (**ct**) resonance is overlaid by the corresponding signal of the *trans-trans* isomer and therefore couldn't be irradiated selectively. However, should there actually be a NOE contact, the molecule assigned here as **1_ct** would be in fact again **1_cc** and again the occurrence of this isomer is assumed to be unlikely.

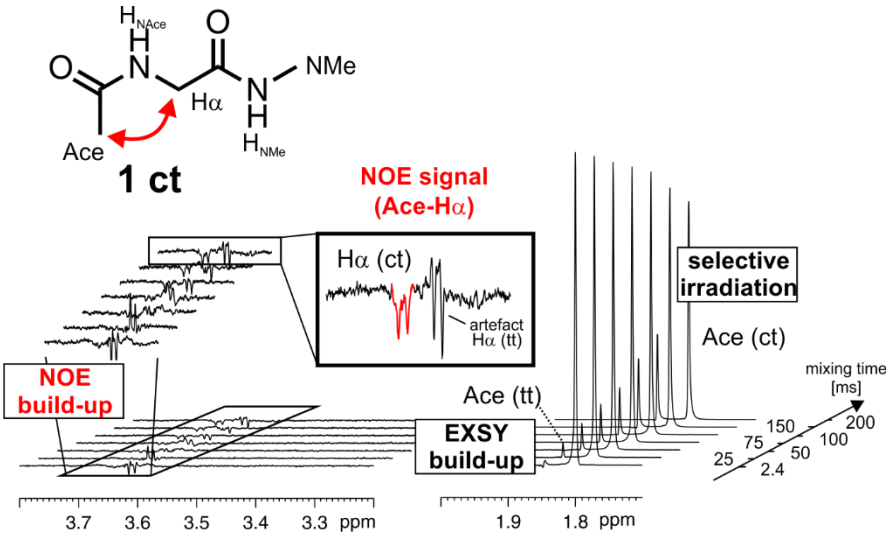

Fig. 57: Stacked plot of 1D selective NOESY spectra of peptide **1** (380 mM) in DMSO-d_6 with increasing mixing times (2.4-200 ms) and selective irradiation of the Ace resonance of the conformer **ct**. Magnified and highlighted in red is the NOE signal build-up of the Hα (**ct**) signal indicative for a short (below 4 Å) Ace-Hα distance which fits to the corresponding distance in the **ct**-isomer (red arrows). In addition, the expected EXSY build-up of the exchanging Ace (**tt**) resonance is shown. The spectra were measured at 303 K and are referenced to the solvent residual peak (2.50 ppm).

The lack of a distinct 2D NOE signal between Hα (**tc**) and H_{NMe} (**tc**) (see Fig. 53 top right-hand side, "no signal") is supporting the *cis*-assignment at the C-terminal part of this molecule because in contrast, in the conformers **ct** and **tt**, strong Hα-H_{NMe} NOEs were detected (see Fig. 53, cross signals VIII and IX). Since only in the **tc** conformer the H_{NMe} proton points away from the Hα protons, the weighted Hα-H_{NMe} distance is maximal for the **tc**-conformer (**tc**: 3.69 Å, **ct**: 2.53 Å and **tt**: 2.55 Å in the B3LYP/6-31G(d) optimized structures depicted in Fig. 54). Therefore, the lack of NOE signal for that distance in the **tc**-conformer is completely in line with the conformer assignments and additionally emphasizes, that for the very low populated *cis*-peptides and with the applied experimental setup, close proton-proton distances (even below 3.69 Å) are necessary for NOE detection.

Additionally, experimentally detected shielding effects of the N-terminal carbonyl group are supportive for the *cis*-conformer assignments. A comparison of the theoretical structures of the assigned conformers (see Fig. 54) shows that only in the **ct**-conformer the N-terminal carbonyl group is pointing away from Cα. In contrast, in the **tc**-conformer and **tt**-conformer it is pointing in the same direction as Cα. Therefore exclusively in the **ct**-conformer the Cα carbon should not sense a significant shielding effect of the N-terminal carbonyl π-system. If the assignments of **1_tt**, **1_tc** and **1_ct** are correct, this must result in a considerably higher ^{13}C chemical shift of Cα (**ct**) compared to Cα (**tt**) and Cα (**tc**). Indeed, the experimental ^{13}C chemical shift of Cα (**ct**) (45.2 ppm) is more than 3 ppm higher than in conformers **tt** (41.8 ppm) and **ct** (39.4 ppm) which further supports the *cis*-conformer assignments.

Thermodynamic and Rate Constants – Overview. In Fig. 58 the summarized results of the NMR spectroscopic determination of thermodynamic and rate constants between conformers **1_tt** and **1_ct** as well as **1_tt** and **1_tc** are presented. Thermodynamic constants were extracted from temperature dependent ^{1}H integrals. The change in Gibbs free energy at 300 K was determined at about 13 kJ mol^{-1} for both processes. Change in enthalpy is roughly 10 kJ mol^{-1} for the formation of both cis-conformers which are very low populated at a ratio of approximately 0.5% each. Free entropy of these processes is low (between -30 and 0 kJ mol^{-1} K^{-1}) as expected for such conformer equilibria.

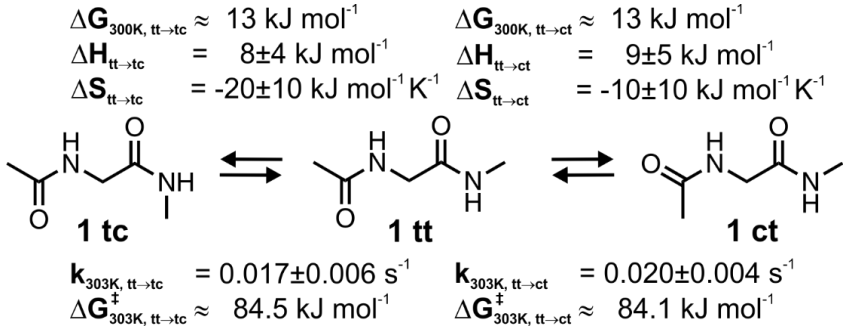

Fig. 58: Conformer equilibria and NMR spectroscopically determined thermodynamic and kinetic constants of *cis*-conformer formations **1_tc** and **1_ct** from the all-*trans* conformer **1_tt** are shown.

The rate constants were determined at 303 K by the robust 1D selective NOESY initial rate approximation approach and show the following trends. Both, the *cis-trans* conformer (**1_ct**) as well as the *trans-cis* conformer (**1_tc**) are formed from the main all-*trans* (**1_tt**) conformer with a rate constant of roughly 0.02 s^{-1}. Accordingly, in the actual sample of 0.38 M total concentration of pseudo-dipeptide **1** in DMSO with a molar fraction of about 0.99 (see below) of the main conformer (**tt**), the formation rate of the low populated *cis*-conformers at 303 K is about 0.008 mol L^{-1} s^{-1}. In other words, within 1 min reaction time, a number of molecules exceeding the whole population of the main all-*trans*-conformer reacts once to a minor *cis*-conformer. Therefore, even if the population of the *cis*-conformers **1_tc** and **1_ct** is extremely low, kinetically, they are very accessible.

Determination of Thermodynamic Constants. Thermodynamic constants ΔG_T (change in Gibbs free energy), ΔH (change in enthalpy) and ΔS (change in entropy) of the equilibra between the conformers **tt**, **ct** and **tc** of pseudo-dipeptide **1** (see Fig. 58) were extracted from proton integrals of **1** in DMSO-d_6 at temperatures from 296 K to 340 K as follows. $I_{normalized}$ (integral normalized by the corresponding number of protons) values were translated into X (molar fraction) according to Equation 11 and from thereof K (equilibrium constant) was derived as shown in Equation 12. Finally, Equation 13 was applied to generate ΔG_T and according to Equation 14 slope

and y-axis intercept of the plot of ΔG_T against T (temperature) correspond to constants ΔS and ΔH, respectively.

$$X_i = \frac{I_{normalized,i}}{\sum_i I_{normalized,i}} \qquad \textbf{Equation 11}$$

$$K_{i\to j} = \frac{X_j}{X_i} \qquad \textbf{Equation 12}$$

$$\Delta G_{T,i\to j} = -RT\ ln(K_{i\to i}) \qquad \textbf{Equation 13}$$

$$\Delta G_{T,i\to j} = \Delta H - T\Delta S \qquad \textbf{Equation 14}$$

In order to perform an accurate ^{1}H integration, the signals should be free from any overlap. This is of special importance if the corresponding signal intensity is low, as it is the case for the minor conformers **ct** and **tc** of pseudo-dipeptide **1** in DMSO-d_6. Only a few resonances fulfill that requirement and in some cases minor overlap cannot be avoided. Therefore two sets of integrals were extracted and final values of the thermodynamic constants were obtained by averaging.

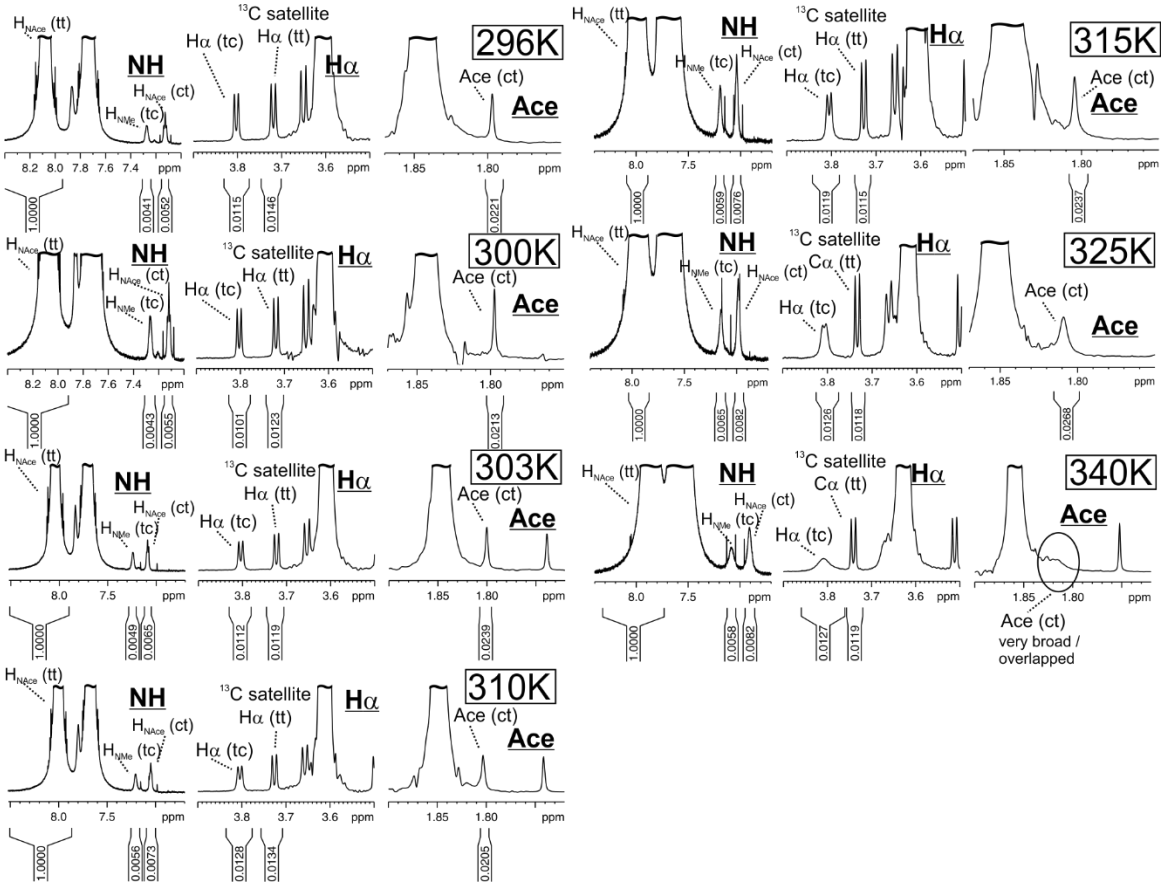

Fig. 59: The NH-region, Hα-region and Ace-region of ^{1}H spectra of peptide **1** (380 mM) at temperatures from 296 K to 340 K in DMSO-d_6 are shown, together with all signal integrals used for the determination of thermodynamic constants. The Hα and Ace signals show a decent broadening with increasing temperature. Spectra are referenced to the solvent residual peak (2.50 ppm).

The first set consist of three NH signals *i.e.* H_{NAce} (**tt**), H_{NMe} (**tc**) and H_{NAce} (**ct**) (see Fig. 59). The chemical shift of the minor conformers slightly changes with temperature changes. Therefore only in few cases H_{NAce} (**ct**) is overlaid by a very narrow impurity signal with very low intensity. The H_{NMe} (**tc**) resonance does not suffer from any overlay and the overlay of H_{NAce} (**tt**) with the second **tt** amine signal can be neglected.

Table 6: X (molar fraction), K (equilibrium constant) and ΔG_T (change in Gibbs free energy) are presented of the thermodynamic equilibria between conformers **1_tt** and **1_tc** as well as **1_tt** and **1_ct** in DMSO-d_6 at different temperatures extracted from NMR proton integrals of the NH region (H_{NAce} (**tt**), H_{NMe} (**tc**) and H_{NAce} (**ct**)) depicted in Fig. 59.

T [K]	X_{tt}	X_{tc}	X_{ct}	$K_{tt\rightarrow tc}$	$K_{tt\rightarrow ct}$	$\Delta G_{T,tt\rightarrow tc}$ [kJ mol^{-1}]	$\Delta G_{T,tt\rightarrow ct}$ [kJ mol^{-1}]
296	0.9908	0.0041	0.0052	0.0041	0.0052	13.53	12.94
300	0.9903	0.0043	0.0054	0.0043	0.0055	13.59	12.98
303	0.9887	0.0048	0.0064	0.0049	0.0065	13.40	12.69
310	0.9873	0.0055	0.0072	0.0056	0.0073	13.36	12.68
315	0.9867	0.0058	0.0075	0.0059	0.0076	13.44	12.78
325	0.9855	0.0064	0.0081	0.0065	0.0082	13.61	12.98
340	0.9862	0.0057	0.0081	0.0058	0.0082	14.56	13.58

The second aliphatic signal set consist of the ^{13}C satellite signal of Hα (**tt**), Hα (**tc**) and Ace (**ct**) (see Fig. 59). The satellite signal was used, because the corresponding main signal is strongly overlapped and the half of the ^{13}C natural abundance (0.5 x 1.109%) was applied as a weighting factor for the normalized integrals to account for the intensity difference. Both signals, ^{13}C satellite of Hα (**tt**) as well as Hα (**tc**) are not overlapped even at higher temperatures where a strong broadening of the signals occurs. The broadening itself is an error source for the Hα (**tc**) integrals, because parts of the signals are hidden below the baseline level and therefore cannot be integrated. However, the broadening is not severe enough to make this effect significant except for the indeed very broad signal at 340 K. In contrast, for the Ace (**ct**) signal, broadening is accompanied by an increasing signal overlap which gets worse with increasing temperatures and which makes a reliable integration at 340 K impossible. The data points for the second signal set at 340 K were therefore omitted.

Table 7: X (molar fraction), K (equilibrium constant) and ΔG_T (change in Gibbs free energy) of the thermodynamic equilibrium between conformers **1_tt** and **1_tc** as well as **1_tt** and **1_ct** in DMSO-d_6 at different temperatures extracted from NMR proton integrals of the aliphatic regions (^{13}C satellite of Hα (**tt**), Hα (**tc**) and Ace (**ct**)) as depicted in Fig. 59. "*" outlier.

T [K]	X_{tt}	X_{tc}	X_{ct}	$K_{tt->tc}$	$K_{tt->ct}$	$\Delta G_{T,tt->tc}$ [kJ mol^{-1}]	$\Delta G_{T,tt->ct}$ [kJ mol^{-1}]
296	0.9902	0.0043	0.0055	0.0043	0.0056	13.39	12.78
300	0.9892	0.0045	0.0063	0.0045	0.0064	13.47	12.62
303	0.9876	0.0051	0.0073	0.0052	0.0074	13.26	12.37
310	0.9892	0.0052	0.0056*	0.0053	0.0056*	13.53	13.36*
315	0.9869	0.0056	0.0075	0.0057	0.0076	13.53	12.79
325	0.9860	0.0058	0.0082	0.0059	0.0083	13.88	12.94

The values of X, K and ΔG_T calculated from the proton integrals are listed in Table 6 (NH signal set) and Table 7 (aliphatic signal set). Thereof generated plots of ΔG_T against the temperature as well as linear fits and the resulting averaged values for ΔH and ΔS are shown in Fig. 60. Quality of these fits is medium to low (R^2 values from 0.66 to 0.12) because of the integration problems mainly due to signal overlap and low signal intensity (see above). Nevertheless, the resulting change in enthalpy ΔH from the main *trans-trans* (**1_tt**) conformer to the *cis-trans* (**1_ct**) and *trans-cis* (**1_tc**) side conformers can be determined to be approximately 10 kJ mol^{-1} each. The reason for such a high energy difference being detectable by NMR is the excellent solubility of peptide **1** in DMSO. As expected for a conformer equilibrium the difference in free entropy is low (between -30 J mol^{-1} K^{-1} and 0 J mol^{-1} K^{-1}).

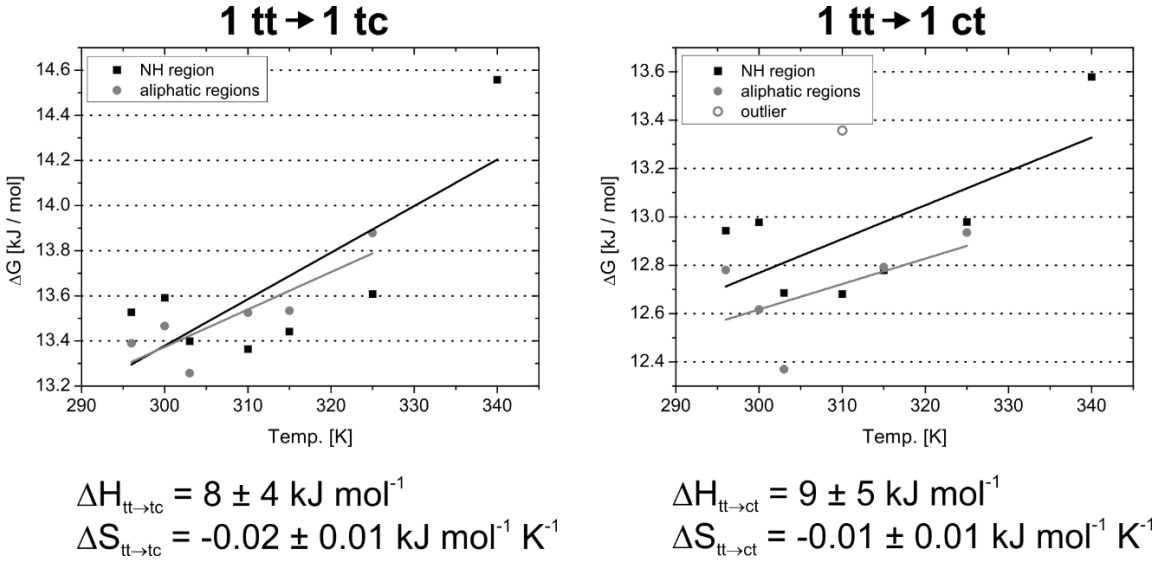

Fig. 60: The plots of ΔG (change in Gibbs free energy) against the temperature are shown for the thermodynamic equilibrium between conformers **1_tt** and **1_tc** as well as **1_tt** and **1_ct** from a sample of **1** (380 mM) in DMSO-d_6 as well as the thereof generated values of ΔH (change in enthalpy) and ΔS (change in entropy). The depicted outlier was omitted. R^2 values for the fit of **1_tt** → **1_tc** are 0.51 (NH) and 0.66 (aliphatic). R^2 values for the fit of **1_tt** → **1_ct** are 0.40 (NH) and 0.12 (aliphatic).

Determination of Rate Constants - Overview. Rate constants of the conformer equilibrium between **1_tt** and **1_tc** as well as **1_tt** and **1_ct** (see Fig. 61) were determined by application of two different approaches. Both methods base on work of Perrin and Dwyer and make use of the NOESY experiment and the chemical exchange during the chosen mixing time τ_m.[43]

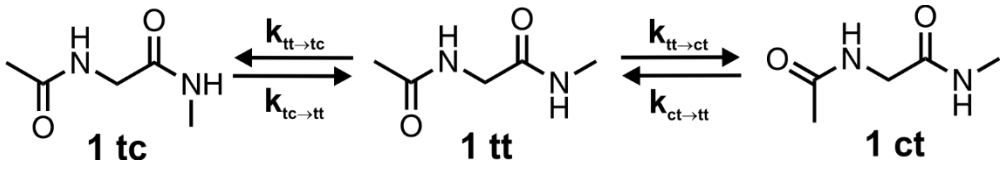

Fig. 61: Equilibria as well as the corresponding determined rate constants are shown between conformers **1_tt**, **1_tc** and **1_ct**.

The 1st method applies the 2D ^{1}H-^{1}H NOESY experiment and uses integrals of the diagonal signal as well as of the cross signals in both dimensions. It simultaneously determines rate constants of the forth and back reaction which can be seen as a disadvantage, because it does not allow for a rate cross-check. (Rates of forth and back reactions must be equal by definition.) This method was already applied for the investigation of small peptide kinetics by focusing on NH-resonances.[58] It is a simplified version of a more complex matrix method, first presented by Perrin and Gipe[42] and in principal it is only applicable on two-site exchanges. Results for more complicated systems must therefore be interpreted with special care. Especially the integral extraction of diagonal signals is prone to errors/uncertainties due to the necessity of choosing imperfect 2D integration areas.

The second approach is called the initial rate approximation[59] and was combined with 1D selective ^{1}H-NOESY experiments as recently applied in investigations on the formation mechanism of the central organocatlytic enamine intermediate.[41] Here the possibility of selective irradiation of resonances is exploited and therefore just one signal of the starting molecule is required to be free from overlap in the ^{1}H spectrum. Integration is much more reliable because the resulting 1D ^{1}H-EXSY signals are typically very clean. Therefore this method is considerably less prone to integration errors. In addition, single rate constants are determined which adds the possibility of result validation by a rate cross-check. In order to give exact rates, for the initial rate approximation, mixing times must be chosen with care. They must be in the initial linear region of EXSY signal build-up. Higher mixing times distort the results, because active multistep exchange processes deplete the EXSY integrals.

Determination of Rate Constants – Simplified 2D NOESY Approach. The NH-slice of a 2D NOESY spectrum in Fig. 62 shows all chosen integral areas of diagonal signals and cross (EXSY) signals applied for rate constant determination. Exemplarily, for the exchange between the main conformer **1_tt** and the low populated conformer **1_ct**, the total exchange rate k_{total} (here k is **not** a rate constant!) is defined as:

$$k = \frac{1}{\tau_m} ln \frac{r+1}{r-1}$$ **Equation 15**

where τ_m is the chosen mixing time and r is a term which describes the unequal population of the conformers as:

$$r = 4X_{tt}X_{ct}\frac{I_{tt1}+I_{ct}}{I_{tt1\rightarrow ct}+I_{ct\rightarrow tt1}} - (X_{tt} - X_{ct})^2,$$ **Equation 16**

where X_{tt} and X_{ct} are the molar fractions of the conformers **1_tt** and **1_ct**. I_{tt1} and I_{ct} are the diagonal signal integrals whereas $I_{tt1\rightarrow ct}$ and $I_{ct\rightarrow tt1}$ are the cross (EXSY) signal integrals as shown in Fig. 62. The **1_tt** ↔ **1_ct** total exchange rate k_{total} is connected with the rate constants $k_{tt\rightarrow ct}$ and $k_{ct\rightarrow tt}$ as well as the equilibrium constant K by the following equations:

$$k_{total} = k_{tt\rightarrow ct} + k_{ct\rightarrow tt}$$ **Equation 17**

and

$$K = \frac{k_{tt\rightarrow ct}}{k_{ct\rightarrow tt}}$$ **Equation 18**

and accordingly

$$k_{tt\rightarrow ct} = \frac{k_{total}K}{K+1}.$$ **Equation 19**

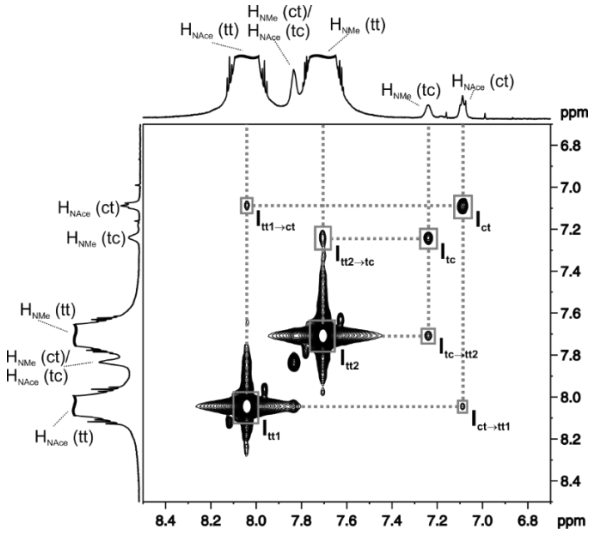

Fig. 62: NH-slice of a 2D NOESY spectrum of peptide **1** (380 mM) in DMSO-d_6 showing chosen integration areas of diagonal signals and EXSY cross signals applied for rate constant determination by the simplified 2D NOESY approach. The spectrum was measured at 303 K with a mixing time of 150 ms and is referenced to the solvent residual peak (^{1}H: 2.50 ppm).

The equilibrium constant K was calculated by proton resonance integration (see Fig. 59). Analogous, rate constants of the equilibrium **1_tt** ↔ **1_tc** were determined. The results of rate constant extraction by the simplified 2D NOESY approach applied on the NH-region of pseudo-dipeptide **1** in DMSO-d_6 at 303 K are presented in Table 8. The rate constants for the formation of minor *cis*-conformers **1_ct** and **1_tc** from the main all-*trans* conformer **1_tt** are similar ($k_{tt\text{-}ct}$ = 0.009s^{-1}, $k_{tt\text{-}tc}$ = 0.020s^{-1}). Although, the 2D method actually is only exact for simple two-site exchanges, these rate constants are qualitatively in agreement with those determined by the 1D selective NOESY initial rate approximation approach ($k_{tt\text{-}ct}$ = 0.020±0.004 s^{-1}, $k_{tt\text{-}tc}$ = 0.017±0.006s^{-1}). However, comparison of the back reaction rate constants (**1_ct** → **1_tt** and **1_tc** → **1_tt**) reveals the low accuracy of the simplified 2D method if it is applied on multi-site exchanges. $k_{tc\text{-}tt}$ (4.012 s^{-1}) is more than three times larger than $k_{ct\text{-}tt}$ (1.255 s^{-1}) although the population of the two side conformers is very similar (see molar fractions in Table 6 and Table 7). It seems that the order of magnitude of the results generated by the 2D method is supprisingly accurate, but the exact numbers contain, as expected, significant errors.

As already mentioned, rate constants of forth and back reaction cannot be determined independently for the simplified 2D NOESY approach and therefore a validation by rate cross-check is not possible.

Table 8: Results are presented of rate constant (k) determination of peptide **1** conformer isomerization in DMSO-d_6 at 303 K *via* the simplified 2D NOESY approach.

Reaction	r	k_{total} [s^{-1}]	k [s^{-1}]
1_tt → **1_ct**	10.581	1.264	0.009
1_ct → **1_tt**	10.581	1.264	1.255
1_tt → **1_tc**	3.407	4.032	0.020
1_tc → **1_tt**	3.407	4.032	4.012

Determination of Rate Constants – Selective 1D Initial Rate Approximation Approach. In Fig. 63 a stacked plot of 1D selective NOESY spectra (also called 1D selective EXSY spectra in this context) with selective irradiation of the Hα resonance of conformer **1_tc** shows the EXSY signal build-up of the resonance Hα (**tt**) and the plot of integrals of the irradiated and the build-up resonances. The initial linear region in that EXSY build-up plot is used for extraction of rate constant $k_{tc\text{-}tt}$ as follows.

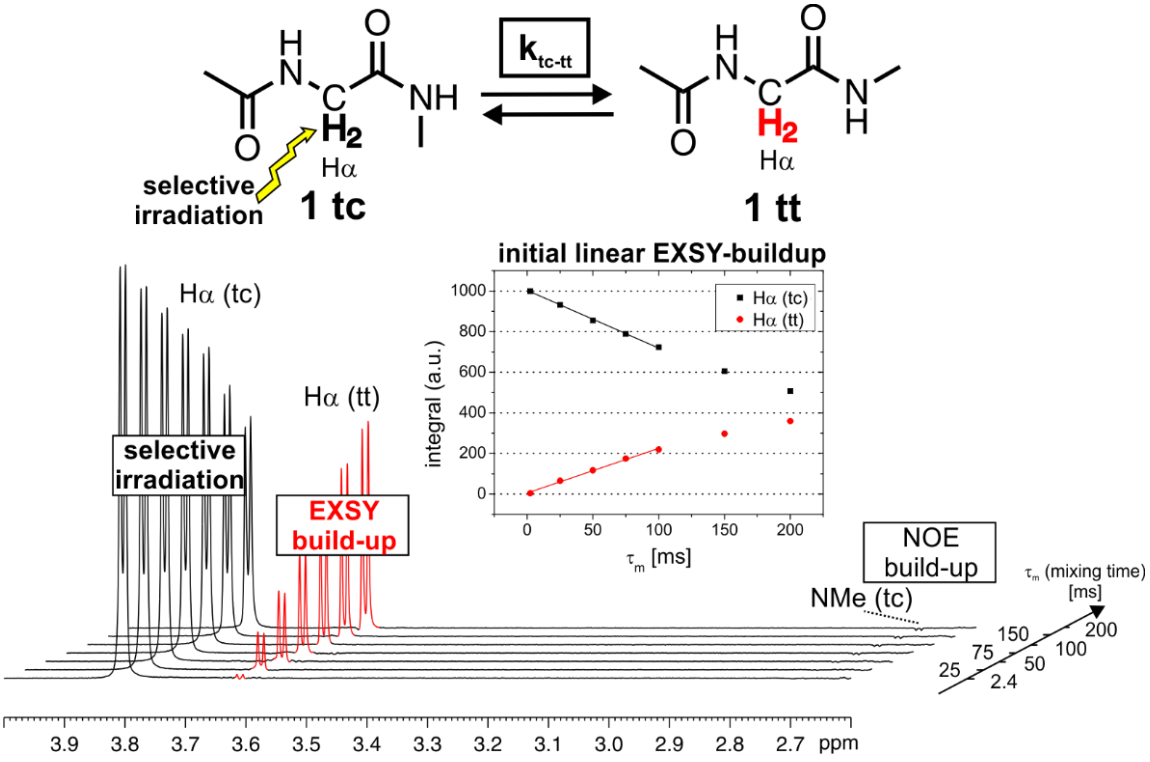

Fig. 63: The equilibrium between the *trans-cis* and all-*trans* conformer of peptide **1** (380 mM) as well as a stacked plot of slices of 1D selective ^{1}H NOESY spectra in DMSO-d_6 at 303 K with selective irradiation of the Hα (**tc**) resonance of **1_tc** and different mixing times (2.4-200 ms) is presented. EXSY signal buildup of the Hα (**tt**) resonance is highlighted in red. The resulting integral plot shows the initial linearity of the EXSY build-up. EXSY integrals in this initial area can be used for rate constant extraction. Additionally, NOE build-up of the NMe (**tc**) resonance is highlighted. The spectra are referenced to the solvent residual peak (^{1}H: 2.50 ppm)

For an unimolecular reaction, the reaction rate equals the corresponding rate constant times the equilibrium concentration of the starting material. Exemplarily, this translates to Equation 20 for the conformer equilibrium **1_tc** → **1_tt**. The initial rate approximation in this equilibrium is described by Equation 21, and says that the rate ($r_{tc\text{-}tt}$) normalized by the equilibrium concentration of the starting material ([tc]) equals the EXSY integral ($I_{\tau m}$(Hα **tt**)) at a chosen mixing time τ_m (τ_m has to lie within the linear region of the EXSY build-up) divided by that chosen mixing time τ_m times the integral of the irradiated resonance of the starting material at a mixing time of zero I_0(Hα **tc**). (Since the lowest mixing time applied is 2.4 ms, the value for 0 ms is calculated by linear back-extrapolation.) By combination of Equation 20 and Equation 21 the rate constant $k_{tc\text{-}tt}$ was calculated (see Equation 22). Analogous, the rate constants $k_{tt\text{-}tc}$, $k_{ct\text{-}tt}$ and $k_{tt\text{-}ct}$ were determined.

$$r_{tc-tt} = k_{tc-tt}\,[tc] \qquad \textbf{Equation 20}$$

$$\frac{I_{\tau_m}(H\alpha\ tt)}{\tau_m\, I_0(H\alpha\ tc)} = \frac{r_{tc-tt}}{[tc]} \qquad \textbf{Equation 21}$$

$$k_{tc-tt} = \frac{I_{\tau_m}(H\alpha\ tt)}{\tau_m\, I_0(H\alpha\ tc)} \qquad \textbf{Equation 22}$$

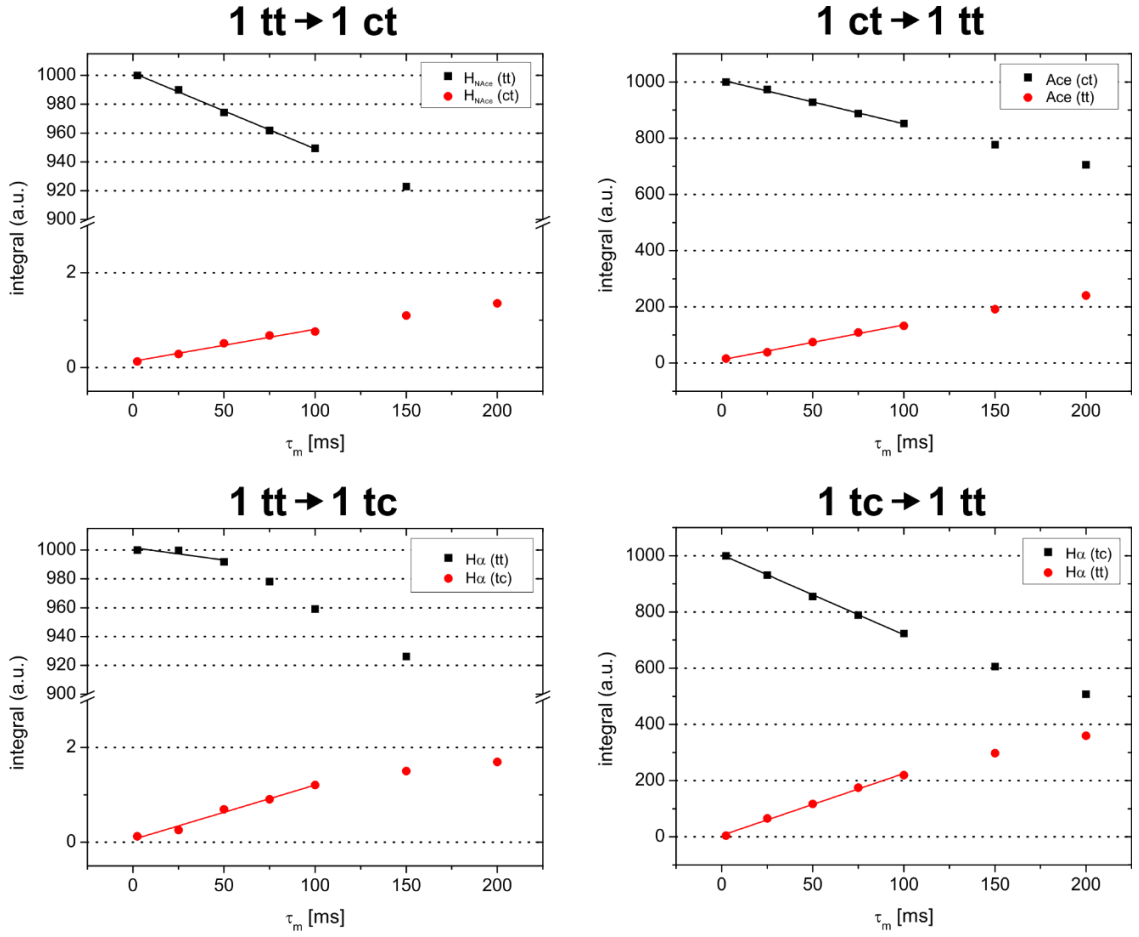

Fig. 64: EXSY build-up curves (red) and curves of the selectively irradiated resonance (black) are presented derived from integrals of the build-up and the irradiated resonance of rows of 1D selective ^{1}H NOESY experiments of peptide **1** (380 mM) with mixing times from 2.4 ms to 200 ms. Spectra were measured in DMSO-d_6 at 303 K. Drawn lines represent the linear fits applied for the extraction of I_o and I_{1oms}. R^2 values of the fit functions in a clockwise direction are H_{NAce} (tt): 0.997, H_{NAce} (ct): 0.972, Ace (ct): 0.996, Ace (tt): 0.993, Hα (tc): 0.998, Hα (tt): 0.994, Hα (tt): 0.594, Hα (tc): 0.978.

The extracted EXSY build-up curves (red) in Fig. 64 show a perfect linearity at the chosen mixing time of 10 ms. Also, the integral plots of the irradiated resonances show a very good initial linearity except for the case of Hα (**tt**) irradiation (see Fig. 64, bottom left-hand side). However, for the purpose of I_o extraction (back-extrapolation from τ_m = 2.4 ms to τ_m = 0 ms) the quality of this fit is considered sufficient and the error introduced thereof into the rate constant calculation is negligible.

Table 9: Results are presented of rate constant (k) determination of peptide **1** conformer isomerizations in DMSO-d_6 at 303 K *via* the initial rate approximation approach. The resonance used is indicated in brackets.

Isomerization Process (Resonance)	I_o (a.u.)	I_{1oms} (a.u.)	k [s^{-1}]
1_tt → **1_ct** (H_{NAce})	1001.7±0.9	0.20±0.04	0.020±0.004
1_tt → **1_tc** (Hα)	1002±8	0.17±0.06	0.017±0.006
1_tc → **1_tt** (Hα)	1003±4	27±6	2.7±0.6
1_ct → **1_tt** (Ace)	1007±3	24±4	2.4±0.4

All rate constants of the equilibria between the main all-*trans* conformer and the two side conformers **ct** and **tc** of pseudo-dipeptide **1** could be extracted and the results are presented in Table 9. Side conformers **1_ct** and **1_tc** are formed from the main conformer **1_tt** with similar rate constants of about 0.02 s^{-1}. These results are in good agreement with the less accurate simplified 2D NOESY approach (see above). In contrast to the 2D method, also the backwards rate constants **1_tt** → **1_ct** and **1_tt** → **1_tc** are reasonably close to each other ($k_{tc\text{-}tt}$ = 2.7±0.6 $s^{-}1$, $k_{ct\text{-}tt}$ = 2.4±0.4 s^{-1}) considering the similar population of both *cis*-conformers. This shows the higher accuracy of the selective 1D method.

Rate Constant Cross-Check. In order to further validate the kinetic results, rates were calculated according to Equation 20. In kinetic theory, equilibrium rates of forth and back reactions have to be equal because net concentrations do not change. Indeed, the results of the so called rate cross-check (see Fig. 65) show, that as the theory is demanding, within the error bars the calculated rates r of the forth and back isomerization processes **1_tt** ↔ **1_ct** and **1_tt** ↔ **1_tc** are equal. This internal validation is not possible for the simplified 2D approach, because there rate constants of forth and back isomerization are intrinsically linked and cannot be determined separately.

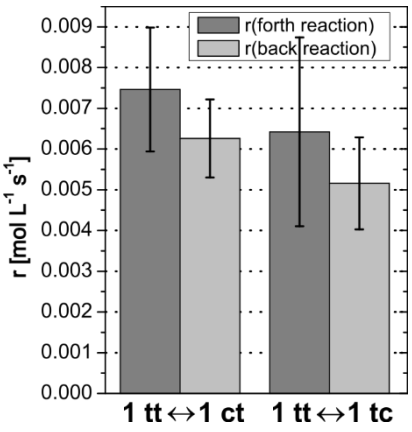

Fig. 65: Rate constant cross-check shows equal rates (within the error bars) for the forth and back isomerization processes **1_tt** ↔ **1_ct** and **1_tt** ↔ **1_tc**. Rates were calculated as defined by Equation 20.

Experimental Energy Diagram. From the extracted rate constants k, energy barriers $\Delta G^{\ddagger}$ were calculated according to the transition state theory (Equation 23 and Equation 24).

$$\Delta G^{\ddagger} = RTln\left(\frac{k}{k^{\ddagger}}\right) \qquad \textbf{Equation 23}$$

$$k^{\ddagger} = \frac{k_B T}{h} \qquad \textbf{Equation 24}$$

The resulting energy diagram including experimentally determined free energy differences (see above) and activation barriers at 303 K is shown in Fig. 66.

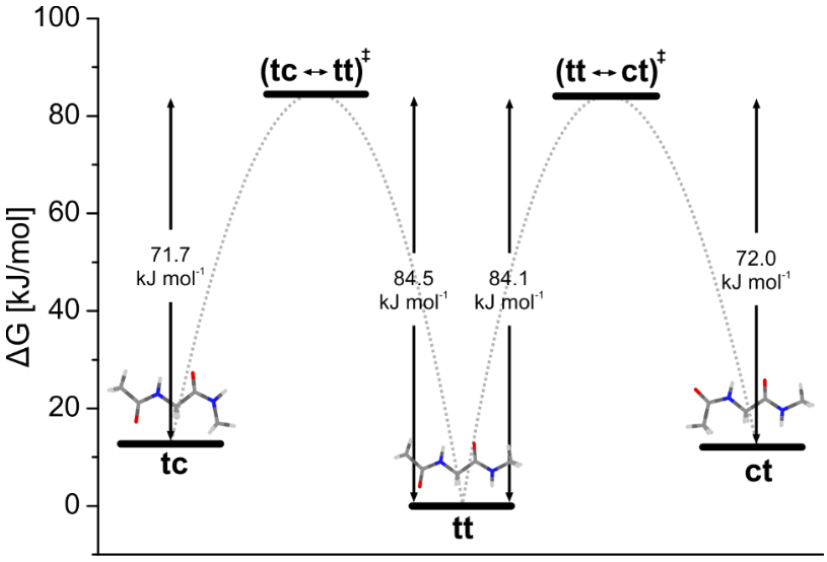

Fig. 66: Energy diagram of the conformer isomerization of pseudo-dipeptide **1** containing experimentally determined energy barriers (calculated from rate constants) and free energies (calculated from ^{1}H integrals) at 303 K in DMSO-d_6. Free energy of main conformer **1_tt** was set to zero.

4.3.2 Technical Details

Force Field Based Calculation. The Maestro 10.2, MacroModel[60] and Tinker 7.1[61] were employed for molecular mechanics (MM) based conformational search using Amber 94, Amber99sb, MM3*, OPLS_2005, MMFFs, Charmm22 and Charmm22cmap force field (FF) parameters.

Quantum Chemical Calculation. The geometries of all the conformers of 2-acetamino-N-methylacetamide were optimized at B3LYP/6-31G(d) level of theory in gas phase.[44,45] The frequency calculations were performed at the same level of theory and all minima were confirmed with all positive frequencies. Single point calculations were done at double hybrid B2-PLYP/G3MP2LARGE,[46] composite methods G3(MP3)-RAD,[47] G3B3[48] and CCSD(T)/CBS[49,50] on B3LYP/6-31G(d) optimized geometries.

G3(MP2)-RAD Scheme.

$$E(G3(MP2)-RAD) = E(CCSD(T)/6-31G(d)) + (MP2/G3MP2large - MP2(FC)/6-31G(d)) \quad \textbf{Equation 25}$$

G3B3 Scheme.

$$E(G3B3) = E(QCISD/6-31G(d)) + DE(+) + DE(2df,p) + DE(G3large) \quad \textbf{Equation 26}$$

$$DE(+) = E(MP4/6-31+G(d)) - E(MP4/6-31G(d)) \quad \textbf{Equation 27}$$

$$DE(2df,p) = E(MP4/6-31G(2df,p)) - E(MP4/6-31G(d)) \quad \textbf{Equation 28}$$

$$DE(G3large) = E(MP2/G3large) - E(MP2/6-31G(2df,p)) - E(MP2/6-31+G(d)) + E(MP2/6-31G(d)) \quad \textbf{Equation 29}$$

CCSD(T)/CBS Scheme. Extrapolations to the complete-basis-set (CBS) limit for CCSD(T) were carried out *via* separate extrapolation of HF and MP2 correlation energies by the two-point extrapolation scheme using cc-pVTZ and cc-pVQZ basis set.[51]

$$E(HF\backslash CBS) = \frac{E(HF\backslash cc\text{-}pVTZ)\,3^5 - E(HF\backslash cc\text{-}pVQZ)\,4^5}{3^5 - 4^5} \qquad \textbf{Equation 30}$$

$$Ec(MP2\backslash CBS) = \frac{Ec(MP2\backslash cc\text{-}pVTZ - HF\backslash cc\text{-}pVTZ)\,3^3 - Ec(MP2\backslash cc\text{-}pVQZ - HF\backslash cc\text{-}pVQZ)\,4^3}{3^3 - 4^3} \qquad \textbf{Equation 31}$$

$$E(MP2\backslash CBS) = Ec(MP2\backslash CBS) + E(HF\backslash CBS) \qquad \textbf{Equation 32}$$

$$E(CCSD(T)\backslash CBS) = E(MP2\backslash CBS) + E(CCSD(T)\backslash cc\text{-}pVDZ) - E(MP2\backslash cc\text{-}pVDZ) \qquad \textbf{Equation 33}$$

The energies were calculated for a temperature of 298.15 K in the gas phase and the thermal corrections to the enthalpy and Gibb's free energy were obtained at the B3LYP/6-31G(d) level of theory. ZPE corrections were scaled by factor 0.9806 and 0.9600 for G3(MP2)-RAD and G3B3, respectively.

For chemical shieldings the specifically optimized pcS-4 basis set developed by Jensen was used with B3LYP in the gas phase and DMSO.[54] The pcS-n series basis sets were designed for rapid convergence at the DFT level. The IEFPCM is used for modelling implicit DMSO.

The solvent correction for ΔG_{solv} was calculated at using IEFPCM[52] and COSMO-SAC[53,55,56] models in DMSO and subsequently added to the single point energy. The isotropic chemical shielding values were calculated at B3LYP/PCS4 level of theory in gas and DMSO. IEFPCM is used for modelling implicit DMSO. The solvation energies using COSMO-SAC were calculated using COSMO-RS implemented in ADF2014[56] and all other calculation are performed using Gaussian09, Rev. D.01.[57]

4.3.3 Procedure for Conformational Search

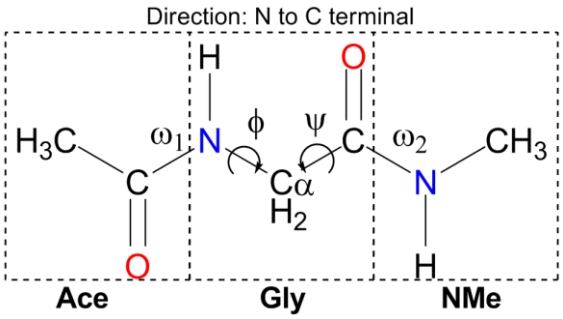

Fig. 67: The systemic diagram of pseudo-dipeptide **1** (2-acetamino-N-methylacetamide) is shown.

Table 10: Definitions and markers used for the nomenclature in classifying the peptide geometry are shown.

PHI (ϕ)	PSI (ψ)	Backbone C alpha(Cα) geometry marker
0.0° – 120.0°	0.0° – 120.0°	α_L
120.0° – 240.0°	0.0° – 120.0°	β_2
240.0° – 360.0°	0.0° – 120.0°	$C_{7,eq}$
0.0° – 120.0°	120.0° – 240.0°	α_D
120.0° – 240.0°	120.0° – 240.0°	C_5
240.0° – 360.0°	120.0° – 240.0°	β
0.0° – 120.0°	240.0° – 360.0°	$C_{7,ax}$
120.0° – 240.0°	240.0° – 360.0°	α
240.0° – 360.0°	240.0° – 360.0°	α_R
In case of glycine dipeptide $C_{7,eq} = C_{7,ax} = C_7$, $\alpha' = \beta_2$, $\alpha_D = \beta$, $\alpha_L = \alpha_D$;		
Peptide bond conformation marker : Trans (t) = 180° ±15° & Cis (c)= 0° ±15°		

Systematic Search Procedure. To explore the conformation space of glycine pseudo-dipeptide **1** in a systematic manner, four dihedral angles as mentioned in Fig. 67 *i.e.* Φ (phi, CNCαC), Ψ (psi, NCCαN), ω_1 (N terminal peptide bond) and ω_2 (C terminal peptide bond) were varied systematically. To obtain initial geometries, dihedral angle Φ was varied from 0° to 180° with a 10° interval, for each value of Φ, dihedral angle Ψ was varied from 0° to 180° with a 10° interval and finally for each combination of Φ and Ψ, four combinations of ω_1 and ω_2 were used [(180°, 180°), (180,0°), (0°, 180°) and (0°, 0°)]. All other distances, angles, and dihedrals needed to define the complete geometry of **1** were taken from the extended C5, all-*trans* conformer that is optimized at B3LYP/6-31G(d). The above specified steps of systematic variations, generated 1444 ($\Phi^*\Psi^*\omega_1^*\omega_2$, 19*19*2*2) initial geometries. All these structures were subjected to optimization at B3LYP/6-31G(d). This led to 30 unique conformers, after removing duplicate and other modified structures resulted from different bond formation during optimization. 29 structures were further screened using frequencies calculated at B3LYP/6-31G(d), to characterize these stationary points into true minima, transitional states and saddle points of different order. Finally, this whole exercise led to 14 unique true minima in PES of glycine pseudo-dipeptide **1** and 15 other stationary points as listed in Table 10.

Force Field Based Approach. Maestro 10.2.011, MacroModel, and Tinker 7.1 were employed for molecular mechanics (MM) based conformational searches using Amber 94, Amber99sb, MM3*, OPLS_2005, MMFFs, Charmm22 and Charmm22cmap force field (FF) parameters. For MacroModel the mixed torsional/low-mode sampling method with extended torsion sampling options was chosen for conformational sampling. An energy window of 63 kJ mol^{-1} (~15 kcal mol^{-1}) was used for exploring the potential energy surface of glycine pseudo-dipeptide **1**. Scheme 1 depicts the strategy

to explore the conformational space using force field based molecular mechanics. For Tinker, the protein module is used to generate initial structures that were later subjected to conformational searches using the scan module with an energy window of 20 kcal mol^{-1}. Other criteria were set as follows: automatic selection of torsion angle (0), search direction is set to 5 with a convergence criterion of 0.0001 kcal mol^{-1}. A collective pool of different structures was obtained with the Amber 94, MM3*, OPLS_2005 and MMFFs force fields based conformation search. All conformers were then subjected to optimization with the B3LYP/6-31G(d) hybrid functional. To get the final conformational space, duplicate minima were removed from the optimized conformation pool obtained in the last step. Table 12 lists the various conformations for the Ace-Gly-NMe dipeptide model **1**. Many FF structures converged to a TS and were modified in order to converge to true minima. In most of the cases, the optimized transition states resulted from torsions in the N-terminal capping group acetyl (Ace).

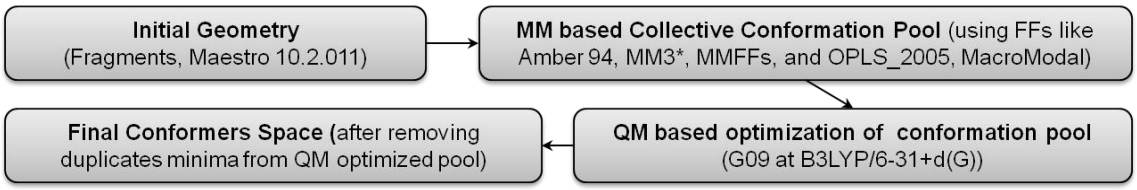

Scheme 1: Strategy for the forcefield based conformation search is shown.

4.3.4 Calculated Energies and Structural Parameters of 1

Gas Phase Calculations. All calculated gas phase energies and structural parameters for pseudo-dipeptide **1** are shown below.

Table 11: List of minima, transitional state and other saddle points on PES of **1** at B3LYP/6-31G(d) in gas phase is shown, located by systemic conformational search. "*" The notation specifies the starting geometry in following manner: Gly_ Φ_ Ψ _ ω_1_ ω_2.

Marker	Molecule*	Low Frequency			Cor. δH	Cor. δG	B3LYP\6-31G(d)	Φ	Ψ	ω_1	ω_2	Cα	Peptide	Rel. ΔE
1	Gly_0_30_180_180	-8	-6	0	0.170862	0.122111	-456.5375163	82.2	291.5	173.5	183.5	C7	tt	0.0
2	Gly_20_160_180_180	-10	-3	-3	0.170286	0.118913	-456.5361652	180.0	180.0	180.0	180.0	C5	tt	3.5
3	Gly_0_40_180_180	0	0	0	0.170546	0.120943	-456.5333573	122.8	338.1	188.4	176.4	β2	tt	10.9
4	Gly_0_160_180_0	-5	0	0	0.170278	0.119786	-456.5331903	180.3	179.8	179.7	3.9	C5	tc	11.4
5	Gly_20_40_0_180	-4	0	0	0.170461	0.121583	-456.5302838	94.4	1.8	6.3	182.0	αR	ct	19.0
6	Gly_50_0_180_0	-9	-5	-3	0.170901	0.121606	-456.5298830	93.9	242.8	164.4	0.9	C7	uc	20.0
7	Gly_180_90_0_180	0	0	0	0.170076	0.119908	-456.5288423	180.0	180.0	360.0	180.0	C5	ct	22.8
8	Gly_20_180_0_180	-8	-4	0	0.170384	0.121386	-456.5270436	74.8	151.8	348.8	178.3	β	ct	27.5
9	Gly_180_130_0_0	-12	-11	-2	0.16994	0.120317	-456.5257541	180.4	179.5	359.7	3.5	C5	cc	30.9
10	Gly_40_170_0_0	-9	-8	0	0.170227	0.121536	-456.5227786	70.7	169.9	347.3	3.2	β	cc	38.7
11	Gly_20_60_0_0	-12	0	0	0.170463	0.121897	-456.5215423	77.0	70.8	358.2	6.1	αR	cc	41.9
12	Gly_20_40_180_0	-14	-2	0	0.170221	0.120072	-456.5206067	69.8	43.4	185.8	4.2	αR	tc	44.4
13	Gly_180_60_0_0	-4	0	0	0.17049	0.121543	-456.5203164	196.6	64.0	350.2	355.7	β2	cc	45.2
14	Gly_170_20_0_0	-10	-3	0	0.170403	0.121061	-456.5200926	207.7	64.5	351.3	3.7	β2	cc	45.7
15	Gly_180_90_180_180	-69	-5	0	0.169275	0.11976	-456.5357220	180.3	180.0	180.1	179.8	C5	tt	4.7
16	Gly_180_180_180_180	-81	-76	-9	0.168186	0.120092	-456.5352684	180.0	180.0	180.0	180.0	C5	tt	5.9
17	Gly_170_170_180_0	-46	0	0	0.169311	0.120974	-456.5331646	180.0	179.9	179.9	0.6	C5	tc	11.4
18	Gly_180_180_180_0	-81	-69	-11	0.168162	0.121473	-456.5326820	180.0	180.0	180.0	0.0	C5	tc	12.7
19	Gly_10_90_0_180	-80	-5	0	0.169433	0.122116	-456.5296714	94.0	1.9	6.0	181.7	αR	ct	20.6
20	Gly_130_140_0_180	-78	-2	0	0.169048	0.120586	-456.5284072	180.0	179.9	359.9	179.7	C5	ct	23.9
21	Gly_120_80_0_180	-89	-6	-4	0.169378	0.122048	-456.5265477	74.7	151.1	348.8	178.5	β	ct	28.8

Marker	Molecule*	Low Frequency			Cor. δH	Cor. δG	B3LYP\6-31G(d)	Φ	Ψ	ω_1	ω_2	Cα	Peptide	Rel. ΔE
22	Gly_0_0_180_180	-130	-79	-28	0.167814	0.124644	-456.5252378	0.0	0.0	180.0	180.0	null	tt	32.2
23	Gly_180_0_180_180	-420	-103	-75	0.166059	0.122015	-456.5210412	180.0	0.0	180.0	180.0	β2	tt	43.3
24	Gly_180_0_0_180	-314	-87	-52	0.167018	0.122085	-456.5191699	180.0	0.0	0.0	180.0	β2	ct	48.2
25	Gly_180_0_180_0	-210	-96	-69	0.167276	0.123123	-456.5132478	180.0	0.0	180.0	0.0	null	tc	63.7
26	Gly_180_0_0_0	-130	-71	-8	0.168414	0.123479	-456.5108552	180.0	0.0	0.0	0.0	null	cc	70.0
27	Gly_0_180_0_180	-190	-79	-64	0.167406	0.123642	-456.5073842	0.0	180.0	0.0	180.0	null	ct	79.1
28	Gly_0_180_0_0	-173	-39	-14	0.168287	0.121387	-456.5042735	0.0	180.0	0.0	0.0	null	cc	87.3
29	Gly_0_180_180_180	-170	-112	-85	0.165885	0.123087	-456.5010418	360.0	180.0	180.0	180.0	β	tt	95.8
30	Gly_0_180_180_0	-153	-44	-35	0.165893	0.124115	-456.4976694	0.0	180.0	180.0	360.0	β	tc	104.6

Table 12: Force field based conformational search of the Ace-Gly-NMe is shown.

		Force Field Geometries								B3LYP\6-31G(d) optimized								Match
Force field	No.	Φ	Ψ	ω_1	ω_2	Potential Energy	Low Frequency			B3LYP\6-31G(d)	Φ	Ψ	ω_1	ω_2	Conf. FF	Conf. QM	Rel. ΔE-FF	Rel. ΔE-QM	Systemic Search
Amber 94	1	284.3	59.5	181.5	178.6	-149.424	-9	-6	0	-456.5375163	277.8	68.5	186.5	176.5	C7_tt	C7_tt	0.0	0.0	1
Amber 94	2	180.0	180.0	180.0	180.0	-141.434	-11	-3	-3	-456.5361652	179.8	180.0	179.9	180.0	C5_tt	C5_tt	8.0	3.5	2
Amber 94	3	180.0	180.0	180.0	0.0	-131.453	-5	0	0	-456.5331903	179.9	179.8	179.4	3.9	C5_tc	C5_tc	18.0	11.4	4
Amber 94	4	279.1	355.6	356.2	179.9	-126.820	-4	0	0	-456.5302837	265.6	358.3	353.7	178.0	αR_ct	αR_ct	22.6	19.0	5
Amber 94	5	109.3	274.0	178.8	0.6	-124.102	-8	-5	-3	-456.5298829	93.9	242.7	164.4	0.9	C7_tc	C7_uc	25.3	20.0	6
Amber 94	6	180.1	180.0	0.0	180.0	-116.829	0	0	0	-456.5288423	180.1	180.0	0.0	180.0	C5_ct	C5_ct	32.6	22.8	7
Amber 94	7	283.9	179.1	4.9	180.1	-109.529	-8	-5	0	-456.5270434	285.2	208.3	11.2	181.7	β_ct	β_ct	39.9	27.5	8
Amber 94	8	180.0	180.0	360.0	0.0	-107.998	-12	-12	-2	-456.5257541	180.4	179.5	359.7	3.5	C5_cc	C5_cc	41.4	30.9	9
Amber 94	9	297.1	303.6	358.2	359.6	-103.567	-12	0	0	-456.5215422	283.0	289.2	1.9	353.9	αR_cc	αR_cc	45.9	41.9	11
Amber 94	10	165.4	292.2	2.8	359.8	-101.664	-4	0	0	-456.5203164	163.4	296.1	9.8	4.3	β2_cc	β2_cc	47.8	45.2	13
Amber 94	11	283.6	179.3	4.7	359.8	-100.740	-10	-8	0	-456.5227777	289.3	190.0	12.7	356.7	β_cc	β_cc	48.7	38.7	10
MM3*	1	278.5	60.0	185.2	180.3	-0.042	-9	-6	0	-456.5375163	277.8	68.6	186.5	176.5	C7_tt	C7_tt	0.0	0.0	1

		Force Field Geometries									B3LYP\6-31G(d) optimized								Match
Force field	No.	Φ	Ψ	ω_1	ω_2	Potential Energy	Low Frequency			B3LYP\6-31G(d)	Φ	Ψ	ω_1	ω_2	Conf. FF	Conf. QM	Rel. ΔE-FF	Rel. ΔE-QM	Systemic Search
MM3*	2	167.6	215.9	182.4	179.4	5.206	-11	-3	-3	-456.5361652	180.0	180.0	180.0	180.0	C5_tt	C5_tt	5.2	3.5	2
MM3*	3	180.0	180.0	180.0	180.0	11.078	-10	-4	-3	-456.5361651	180.7	179.9	180.3	180.0	C5_tt	C5_tt	11.1	3.5	2
MM3*	4	175.8	192.0	181.0	358.9	14.205	-5	0	0	-456.5331903	179.7	180.2	180.3	356.1	C5_tc	C5_tc	14.2	11.4	4
MM3*	5	273.6	1.7	358.7	181.6	15.483	-4	0	0	-456.5302836	265.4	358.3	353.6	178.0	C7_ct	αR_ct	15.5	19.0	5
MM3*	6	134.8	263.8	180.1	1.8	17.245	-8	-5	-3	-456.5298829	93.9	242.7	164.4	0.9	β2_tc	C7_uc	17.3	20.0	6
MM3*	7	188.3	131.4	356.8	179.4	25.822	0	0	0	-456.5288423	180.0	180.0	0.0	180.0	C5_ct	C5_ct	25.9	22.8	7
MM3*	8	176.4	196.9	1.5	358.5	34.676	-13	-12	-2	-456.5257541	179.8	180.5	0.4	356.5	C5_cc	C5_cc	34.7	30.9	9
MM3*	9	165.8	278.1	3.7	1.4	35.227	-4	0	0	-456.5203163	163.3	296.1	9.8	4.4	β2_cc	β2_cc	35.3	45.2	13
MM3*	10	170.0	242.1	3.4	0.3	35.931	-12	-12	-2	-456.5257541	179.6	180.5	0.3	356.5	β2_cc	C5_cc	36.0	30.9	9
MM3*	11	262.5	257.8	4.7	181.4	36.094	-8	-4	0	-456.5270434	285.1	208.3	11.2	181.7	αR_ct	β_ct	36.1	27.5	8
MM3*	12	285.4	329.5	356.6	356.8	39.502	-12	0	0	-456.5215422	283.0	289.2	1.9	353.9	αR_cc	αR_cc	39.5	41.9	11
MM3*	13	265.3	268.8	3.9	0.4	44.843	-12	0	0	-456.5215422	283.0	289.2	1.8	353.9	αR_cc	αR_cc	44.9	41.9	11
MMFFs	1	82.6	286.8	173.0	188.4	-84.112	-9	-6	0	-456.5375163	82.2	291.5	173.4	183.4	C7_tt	C7_tt	0.0	0.0	1
MMFFs	2	179.8	180.3	181.1	180.0	-78.261	-10	-4	-3	-456.5361651	180.7	179.9	180.3	180.0	C5_tt	C5_tt	5.9	3.5	2
MMFFs	3	180.1	179.9	179.0	0.0	-72.403	-5	0	0	-456.5331903	180.2	180.2	180.7	356.1	C5_tc	C5_tc	11.7	11.4	4
MMFFs	4	271.8	351.9	357.4	181.3	-67.793	-4	0	0	-456.5302837	265.5	358.3	353.7	178.0	αR_ct	αR_ct	16.3	19.0	5
MMFFs	5	98.8	238.2	170.4	0.2	-65.845	-8	-5	-3	-456.5298828	93.9	242.8	164.4	0.9	β_tc	C7_uc	18.3	20.0	6
MMFFs	6	105.6	211.8	169.3	357.1	-65.566	-5	0	0	-456.5331903	179.7	180.2	180.3	356.1	β_tc	C5_tc	18.5	11.4	4
MMFFs	7	179.9	180.4	0.0	180.0	-55.234	0	0	0	-456.5288423	180.0	179.9	360.0	180.0	C5_ct	C5_ct	28.9	22.8	7
MMFFs	8	180.0	180.1	0.0	360.0	-49.982	-13	-11	-2	-456.5257540	180.4	179.6	359.8	3.4	C5_cc	C5_cc	34.1	30.9	9
MMFFs	9	264.6	135.7	5.7	179.7	-48.341	0	0	0	-456.5288423	180.0	180.0	360.0	180.0	β_ct	C5_ct	35.8	22.8	7
MMFFs	10	270.9	208.6	5.1	179.3	-47.319	-8	-4	0	-456.5270434	285.1	208.3	11.2	181.7	β_ct	β_ct	36.8	27.5	8
MMFFs	11	282.6	324.1	177.5	351.8	-43.013	-14	-2	0	-456.5206065	290.1	316.6	174.2	355.9	αR_tc	αR_tc	41.1	44.4	12
MMFFs	12	90.9	197.4	353.5	357.7	-41.514	-10	-8	0	-456.5227778	70.6	169.9	347.3	3.2	β_cc	β_cc	42.6	38.7	10

4.3 Supporting Information

		Force Field Geometries								B3LYP\6-31G(d) optimized								Match
Force field	No.	Φ	Ψ	ω_1	ω_2	Potential Energy	Low Frequency			B3LYP\6-31G(d)	Φ	Ψ	ω_1	ω_2	Conf. FF	Conf. QM	Rel. ΔE-FF	Rel. ΔE-QM	Systemic Search
MMFFs	13	87.4	171.5	354.2	1.4	-41.316	-10	-9	0	-456.5227772	70.7	169.9	347.3	3.2	β_cc	β_cc	42.8	38.7	10
MMFFs	14	282.0	315.2	357.8	354.2	-40.813	-12	0	0	-456.5215422	282.8	289.3	1.7	354.0	αR_cc	αR_cc	43.3	41.9	11
MMFFs	15	165.6	306.9	3.8	355.0	-40.254	-10	-3	0	-456.5200925	152.3	295.6	8.7	356.3	β2_cc	β2_cc	43.9	45.7	14
MMFFs	16	90.2	90.0	357.5	358.1	-38.967	-12	0	0	-456.5215422	77.0	70.8	358.2	6.1	αR_cc	αR_cc	45.1	41.9	11
OPLS_2005	1	282.3	51.8	183.6	180.1	-185.101	-9	-6	0	-456.5375163	277.8	68.5	186.4	176.5	C7_tt	C7_tt	0.0	0.0	1
OPLS_2005	2	179.7	180.3	180.0	180.0	-180.418	-11	-3	-3	-456.5361652	179.6	180.1	179.8	180.0	C5_tt	C5_tt	4.7	3.5	2
OPLS_2005	3	275.3	356.9	357.5	180.7	-170.862	-4	-2	0	-456.5302837	265.5	358.4	353.7	177.9	αR_ct	αR_ct	14.2	19.0	5
OPLS_2005	4	180.0	180.0	180.0	360.0	-168.906	-5	0	0	-456.5331902	179.2	180.2	180.1	356.1	C5_tc	C5_tc	16.2	11.4	4
OPLS_2005	5	92.8	236.8	173.7	359.2	-164.756	-8	-5	-3	-456.5298829	93.9	242.7	164.4	0.9	β_tc	C7_uc	20.3	20.0	6
OPLS_2005	6	180.2	179.7	0.0	180.0	-159.606	0	0	0	-456.5288423	180.0	180.1	0.0	180.0	C5_ct	C5_ct	25.5	22.8	7
OPLS_2005	7	87.7	216.5	352.9	179.6	-156.123	0	0	0	-456.5288423	180.0	180.0	0.0	180.0	β_ct	C5_ct	29.0	22.8	7
OPLS_2005	8	180.1	180.1	0.0	360.0	-148.802	-12	-12	-2	-456.5257541	180.4	179.6	359.7	3.5	C5_cc	C5_cc	36.3	30.9	9
OPLS_2005	9	275.5	166.8	6.9	0.6	-144.347	-10	-9	0	-456.5227773	289.3	190.1	12.7	356.8	β_cc	β_cc	40.8	38.7	10
OPLS_2005	10	72.6	34.7	180.3	3.7	-141.159	-14	-2	0	-456.5206065	69.9	43.4	185.8	4.1	αR_tc	αR_tc	43.9	44.4	12
OPLS_2005	11	71.0	49.8	0.7	0.7	-140.798	-12	0	0	-456.5215422	77.1	70.7	358.3	6.0	αR_cc	αR_cc	44.3	41.9	11

Effect of Solvent on Conformational Preference of Glycine Dipeptide. 30 conformations that are located using systemic search approach as describe in previous section, were subject to re-optimization at B3LYP\6-31G(d) under implicit solvent conditions. DMSO is used as solvent, IEFPCM model and uahf radii. Table 17 lists the conformations obtained by reoptimization of the gas phase stationary points in implicit solvation conditions. Only true minima (stationary points with imaginary frequency) were reported, marker entries in tables could be used to trace the starting gas phase stationary points that later converge to respective minima under implicit solvation reoptimization.

Table 13: Solvation energies [kcal mol^{-1}] for **1** are shown with implicit DMSO using COSMO-SAC and IEFPCM solvation models.

SI	Molecule	Conf.	COSMO-SAC	HF/6-31G(d), IEFPCM, uahf radii
1	Gly_0_30_180_180	C7_tt	-10.90	-27.37
2	Gly_20_160_180_180	C5_tt	-12.17	-30.72
3	Gly_0_40_180_180	β2_tt	-13.90	-32.11
4	Gly_0_160_180_0	C5_tc	-11.32	-30.75
5	Gly_20_40_0_180	αR_ct	-12.52	-32.14
6	Gly_50_0_180_0	C7_uc	-10.63	-29.48
7	Gly_180_90_0_180	C5_ct	-14.70	-33.34
8	Gly_20_180_0_180	β_ct	-15.90	-34.39
9	Gly_180_130_0_0	C5_cc	-13.82	-33.43
10	Gly_40_170_0_0	β_cc	-15.17	-34.9
11	Gly_20_60_0_0	αR_cc	-13.40	-32.51
12	Gly_20_40_180_0	αR_tc	-17.56	-35.28
13	Gly_180_60_0_0	β2_cc	-13.39	-32.43
14	Gly_170_20_0_0	β2_cc	-13.00	-32.74

Table 14: Values of individual calculation steps are shown, used in G3(MP2)-RAD schemes and B2PYLP/GTMP2LARGE for conformers of **1** using geometries optimized in gas phase at B3LYP/6-31G(d).

Marker	Corr. G	Corr. H	B2PLYP/ GTMP2large	MP2/6-31G(d)	MP2/ GTMP2large	CCSD(T)/ 6-31G(d)
1	0.118867	0.167899	-456.3390006	-455.1384248	-455.6694253	-455.2418268
2	0.115681	0.167339	-456.3379461	-455.1356747	-455.6672543	-455.2390848
3	0.117705	0.167593	-456.3350005	-455.1336602	-455.6649422	-455.2368703
4	0.116553	0.167330	-456.3351775	-455.1327635	-455.6647549	-455.2362051
5	0.118346	0.167508	-456.3324459	-455.1315928	-455.6630796	-455.2346772
6	0.118361	0.167939	-456.3315732	-455.1304870	-455.6617431	-455.2341418
7	0.116679	0.167133	-456.3302348	-455.1282114	-455.6596501	-455.2315874
8	0.118152	0.167434	-456.3283393	-455.1279843	-455.6585398	-455.2315460
9	0.117090	0.166999	-456.3272692	-455.1252250	-455.6569789	-455.2286275
10	0.118304	0.167280	-456.3243049	-455.1239951	-455.6548148	-455.2276073
11	0.118661	0.167511	-456.3233668	-455.1227556	-455.6540212	-455.2263377

Marker	Corr. G	Corr. H	B2PLYP/ GTMP2large	MP2/6-31G(d)	MP2/ GTMP2large	CCSD(T)/ 6-31G(d)
12	0.116840	0.167278	-456.3230715	-455.1219919	-455.6539986	-455.2254317
13	0.118306	0.167536	-456.3223302	-455.1213059	-455.6527592	-455.2248413
14	0.117826	0.167451	-456.3224366	-455.1211410	-455.6529938	-455.2246934

Table 15: Values of calculation of pseudo-dipeptide **1** is are shown at B3LYP/6-31G(d) and B2PLYP/GTMP2large in gas phase, obtained through optimization in implicit DMSO solvent using iefpcm model at B3LYP\6-31G(d).

Marker	Corr. G	Corr. H	B3LYP/6-31G(d)	B2PLYP/ GTMP2large
1	0.121227	0.168370	-456.5293107	-456.3303915
2	0.122011	0.168720	-456.5254870	-456.3271376
3	0.121958	0.168646	-456.5235681	-456.3260989
4	0.122302	0.168490	-456.5195618	-456.3205051
5	0.121325	0.168025	-456.5216971	-456.3224911
6	0.121624	0.168636	-456.5228366	-456.3246759
7	0.121841	0.168665	-456.5232964	-456.3245711
8	0.121725	0.168349	-456.5192355	-456.3206419
9	0.122323	0.168686	-456.5138893	-456.3154251
10	0.122563	0.168900	-456.5150862	-456.3161291
11	0.122146	0.168596	-456.5133547	-456.3150285

Table 16: Values of individual calculation steps are shown, used in G3(MP2)-RAD schemes for conformers of **1** obtained through optimization in implicit DMSO solvent using iefpcm model at B3LYP\6-31G(d).

Marker	Corr. G	Corr. H	MP2/6-31G(d)	MP2/ GTMP2large	CCSD(T)/ 6-31G(d)
1	0.118031	0.165443	-455.1295083	-455.6599408	-455.2335944
2	0.118808	0.165785	-455.1268802	-455.6575844	-455.2305823
3	0.118757	0.165715	-455.1252349	-455.6565431	-455.2292988
4	0.119104	0.165560	-455.1216386	-455.6512752	-455.2256491
5	0.118136	0.165105	-455.1220606	-455.6523502	-455.2260420
6	0.118424	0.165702	-455.1249703	-455.6556543	-455.2285967
7	0.118639	0.165729	-455.1250688	-455.6552993	-455.2287304
8	0.118530	0.165421	-455.1202924	-455.6507760	-455.2244982
9	0.119121	0.165752	-455.1167062	-455.6471359	-455.2204810
10	0.119357	0.165960	-455.1171627	-455.6471994	-455.2212050
11	0.118946	0.165663	-455.1154757	-455.6461891	-455.2194641

Table 17: A list of calculated conformers of **1** is shown, obtained through optimization in implicit DMSO using iefpcm model at B3LYP\6-31G(d) and solvation energy calculated at HF/6-31G(d) using UAHF radii.

SI.	Marker	Molecule	Low Frequency			Cor. δG	Cor. δH	B3LYP\ 6-31G(d)	Φ	Ψ	ω_1	ω_2	Cα	Peptide	Rel. ΔE	DeltaG DMSO
1	2	Gly_20_160_180_180	-28	-11	0	0.107843	0.157875	-456.5839816	176.0	190.1	182.1	178.8	C5	tt	0.0	-161.4
2	1	Gly_0_30_180_180	-9	-6	0	0.107994	0.158714	-456.5832014	103.4	355.8	181.8	178.0	C7	tt	2.0	-172.8
3	29	Gly_0_180_180_180	-27	-14	0	0.108546	0.158937	-456.5825903	289.6	158.7	184.7	179.1	β	tt	3.7	-175.6
4	21	Gly_120_80_0_180	-24	0	0	0.109720	0.158241	-456.5804155	75.8	161.2	351.8	180.0	β	ct	9.4	-180.9
5	20	Gly_130_140_0_180	-21	0	0	0.107811	0.157156	-456.5798522	178.1	190.6	2.5	181.8	C5	ct	10.8	-173.8
6	19	Gly_10_90_0_180	-23	0	0	0.109231	0.158380	-456.5797128	94.4	357.7	359.5	181.5	C7	ct	11.2	-170.8
7	5	Gly_20_40_0_180	-24	0	0	0.108939	0.158412	-456.5795049	95.4	356.4	359.3	180.4	C7	ct	11.8	-168.5
8	30	Gly_0_180_180_0	-26	-10	0	0.107895	0.157558	-456.5794362	272.2	186.3	186.4	359.4	β	tc	11.9	-178.7
9	12	Gly_20_40_180_0	-34	-19	0	0.110652	0.159108	-456.5747284	64.8	49.4	178.8	2.8	αR	tc	24.3	-182.1
10	11	Gly_20_60_0_0	-26	0	0	0.111984	0.159377	-456.5718606	81.5	72.2	357.5	4.9	αR	cc	31.8	-168.2
11	14	Gly_170_20_0_0	-25	0	0	0.110660	0.158653	-456.5698569	213.3	56.9	354.4	2.8	β2	cc	37.1	-169.4

Table 18: Values of individual calculation steps are shown, used in G3T3 schemes for conformers of **1** obtained through geometries optimized in gas phase at B3LYP/6-31G(d).

Marker	Cor. δH	Cor. δG	MP2/ 6-31G(d)	MP2/ 6-31+G(d)	MP2/ 6-31G(2df,p)	MP4/ 6-31G(d)	MP4/ 6-31+G(d)	MP4/ 6-31G(2df,p)	MP2/ G3large	QCISD(T)/ 6-31G(d)
1	0.115416	0.164758	-455.1384248	-455.1712761	-455.4809959	-455.2480958	-455.2833665	-455.6124128	-456.0684496	-455.243816
2	0.112241	0.164214	-455.1356747	-455.1677541	-455.4782975	-455.2451506	-455.2794888	-455.6094685	-456.0663605	-455.2410183
3	0.11426	0.164462	-455.1336602	-455.1666214	-455.4760686	-455.2432927	-455.2786043	-455.6074208	-456.0639465	-455.2388426
4	0.113114	0.164205	-455.1327635	-455.1655496	-455.4751412	-455.2423206	-455.2774013	-455.606371	-456.0638586	-455.2381404
5	0.114904	0.164378	-455.1315928	-455.1649456	-455.4739327	-455.2412385	-455.2770007	-455.6052232	-456.0620903	-455.2366464
6	0.114909	0.164798	-455.130487	-455.1638067	-455.4726896	-455.2404441	-455.2762121	-455.6043509	-456.060726	-455.2361281
7	0.113244	0.164013	-455.1282114	-455.1597029	-455.4713744	-455.2380326	-455.2718123	-455.6028382	-456.0587118	-455.2335604
8	0.11471	0.164306	-455.1279843	-455.1600149	-455.4707585	-455.2380202	-455.2725299	-455.6024234	-456.0575069	-455.2335183
9	0.113658	0.163881	-455.125225	-455.1573405	-455.4681645	-455.2351313	-455.2695609	-455.599691	-456.0560437	-455.2306033
10	0.114866	0.164157	-455.1239951	-455.15666	-455.4664958	-455.2341111	-455.2692825	-455.598225	-456.0537836	-455.2295735
11	0.115218	0.164381	-455.1227556	-455.1555854	-455.4652607	-455.2328025	-455.2681087	-455.5969195	-456.0529782	-455.2283128

Marker	Cor. δH	Cor. δG	MP2/ 6-31G(d)	MP2/ 6-31+G(d)	MP2/ 6-31G(2df,p)	MP4/ 6-31G(d)	MP4/ 6-31+G(d)	MP4/ 6-31G(2df,p)	MP2/ G3large	QCISD(T)/ 6-31G(d)
12	0.113402	0.164157	-455.1219919	-455.1553382	-455.4650873	-455.2318956	-455.2677675	-455.5966195	-456.0529838	-455.2274066
13	0.114862	0.164405	-455.1213059	-455.1548243	-455.4635935	-455.231313	-455.26728	-455.5952264	-456.051687	-455.2268144
14	0.114384	0.164323	-455.121141	-455.1547061	-455.4635522	-455.2311722	-455.2671811	-455.5952042	-456.0519402	-455.2266702

Table 19: Values of individual calculation steps are shown, used in G3T3 schemes for conformers of **1** obtained through optimization in implicit DMSO solvent using iefpcm model at B3LYP\6-31G(d).

Marker	Cor. δH	Cor. δG	MP2/ 6-31G(d)	MP2/ 6-31+G(d)	MP2/ 6-31G(2df,p)	MP4/ 6-31G(d)	MP4/ 6-31+G(d)	MP4/ 6-31G(2df,p)	MP2/ G3large	QCISD(T)/ 6-31G(d)
1	0.162341	0.114632	-455.1295083	-455.1631376	-455.4703692	-455.2399214	-455.2758531	-455.6021436	-456.0586505	-455.2355615
2	0.162674	0.115402	-455.1268802	-455.1616004	-455.4676769	-455.2373462	-455.2744656	-455.5995385	-456.0562798	-455.2325872
3	0.162608	0.115352	-455.1252349	-455.1603179	-455.4665537	-455.2358618	-455.2734735	-455.5985613	-456.0552272	-455.2312939
4	0.162454	0.115702	-455.1216386	-455.1552002	-455.4628241	-455.2325051	-455.2685819	-455.5949948	-456.0499207	-455.2276562
5	0.162010	0.114744	-455.1220606	-455.1551521	-455.4633683	-455.2328407	-455.2682578	-455.5954556	-456.0510312	-455.2280551
6	0.162592	0.115019	-455.1249703	-455.1599176	-455.4657414	-455.2354653	-455.2728429	-455.5975629	-456.0543381	-455.2305955
7	0.162618	0.115234	-455.1250688	-455.1593971	-455.4659535	-455.2356664	-455.2724114	-455.5978821	-456.0539718	-455.2307460
8	0.162318	0.115131	-455.1202924	-455.1547642	-455.4613284	-455.2312128	-455.2681852	-455.5935845	-456.0494327	-455.2265113
9	0.162642	0.115715	-455.1167062	-455.1506990	-455.4583809	-455.2275083	-455.2640585	-455.5905317	-456.0457998	-455.2225115
10	0.162843	0.115947	-455.1171627	-455.1507556	-455.4583141	-455.2281004	-455.2641803	-455.5905770	-456.0458267	-455.2232272
11	0.162554	0.115542	-455.1154757	-455.1499867	-455.4565923	-455.2263760	-455.2633387	-455.5887947	-456.0448212	-455.2214834

Table 20: Values of individual calculation steps are shown, used in CCSD(T)/CBS for conformers of **1** obtained through geometries optimized in gas phase at B3LYP/6-31G(d).

Marker	Molecule	HF\CC-pVDZ	HF\CC-pVTZ	HF\CC-pVQZ	MP2\CC-pVDZ	MP2\CC-pVTZ	MP2\CC-pVQZ	CCSD(T)\CC-pVDZ
1	Gly_0_30_180_180	-453.8588691	-453.9878468	-454.0202995	-455.2370266	-455.6979364	-455.8485102	-455.3504362
2	Gly_20_160_180_180	-453.8598875	-453.9896268	-454.022242	-455.2343439	-455.6957687	-455.8467183	-455.3477447
3	Gly_0_40_180_180	-453.8563077	-453.9853149	-454.0177316	-455.2329443	-455.6937976	-455.8443495	-455.3460649
4	Gly_0_160_180_0	-453.8561169	-453.9862652	-454.0189353	-455.2312599	-455.6930369	-455.8440487	-455.3446283
5	Gly_20_40_0_180	-453.853048	-453.9822214	-454.0145928	-455.231067	-455.6919077	-455.8424859	-455.343933

Marker	Molecule	HF\CC-pVDZ	HF\CC-pVTZ	HF\CC-pVQZ	MP2\CC-pVDZ	MP2\CC-pVTZ	MP2\CC-pVQZ	CCSD(T)\CC-pVDZ
6	Gly_50_0_180_0	-453.8521164	-453.9816131	-454.0140206	-455.2294149	-455.6902561	-455.8408473	-455.3430283
7	Gly_180_90_0_180	-453.8512085	-453.9808218	-454.0133487	-455.2278622	-455.6885564	-455.8393208	-455.341096
8	Gly_20_180_0_180	-453.850615	-453.9792957	-454.0115883	-455.2278981	-455.6875785	-455.837992	-455.3413568
9	Gly_180_130_0_0	-453.8472496	-453.9772614	-454.0098253	-455.2246558	-455.685674	-455.8364938	-455.3378436
10	Gly_40_170_0_0	-453.8460703	-453.9751943	-454.0075448	-455.2236526	-455.6835915	-455.8341085	-455.337099
11	Gly_20_60_0_0	-453.8439955	-453.9731767	-454.0055063	-455.2226185	-455.6828333	-455.8332187	-455.3360085
12	Gly_20_40_180_0	-453.8439426	-453.9732403	-454.0055915	-455.2218611	-455.6826461	-455.832986	-455.3351766
13	Gly_180_60_0_0	-453.8424199	-453.9717392	-454.0041849	-455.221441	-455.6815162	-455.8319352	-455.3347364
14	Gly_170_20_0_0	-453.842282	-453.9718408	-454.0043193	-455.2211746	-455.681596	-455.83209	-455.3344641

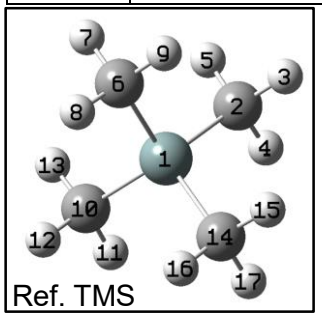

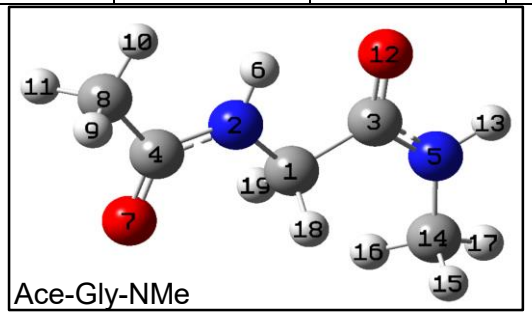

Fig. 68: Diagrams of Tetramethylsilane (TMS) and dipeptide model **1** (Ace-Gly-NMe) are shown. Atoms are marked with numeric label. TMS is used as reference for calculation of chemical shifts.

Table 21: Isotropic shielding values for TMS are shown at different levels of theory as specified in first column over B3LYP/6-31G(d) geometries in gas phase. See Fig. 68 for labels.

Label	1	2	6	10	14	3	4	5	7	8	9	11	12	13	15	16	17	Avg. Signal	
Symbol	Si	C	C	C	C	H	H	H	H	H	H	H	H	H	H	H	H	**C**	**H**
B3LYP/PCS4, Gas	321.9	179.6	179.6	179.6	179.6	31.5	31.5	31.4	31.4	31.5	31.5	31.4	31.5	31.4	31.5	31.4	31.4	**179.6**	**31.4**
B3LYP/PCS4, DMSO	321.6	180.9	180.8	180.8	180.8	31.4	31.4	31.4	31.4	31.4	31.4	31.4	31.4	31.4	31.4	31.4	31.4	**180.8**	**31.4**
MP2/PCS2, Gas	358.4	196.2	196.1	196.2	196.2	31.4	31.4	31.4	31.4	31.4	31.4	31.4	31.4	31.4	31.4	31.4	31.4	**196.2**	**31.4**
MP2/PCS2, DMSO	358.1	197.3	197.3	197.3	197.3	31.3	31.3	31.3	31.3	31.3	31.3	31.3	31.3	31.3	31.3	31.3	31.3	**197.3**	**31.3**

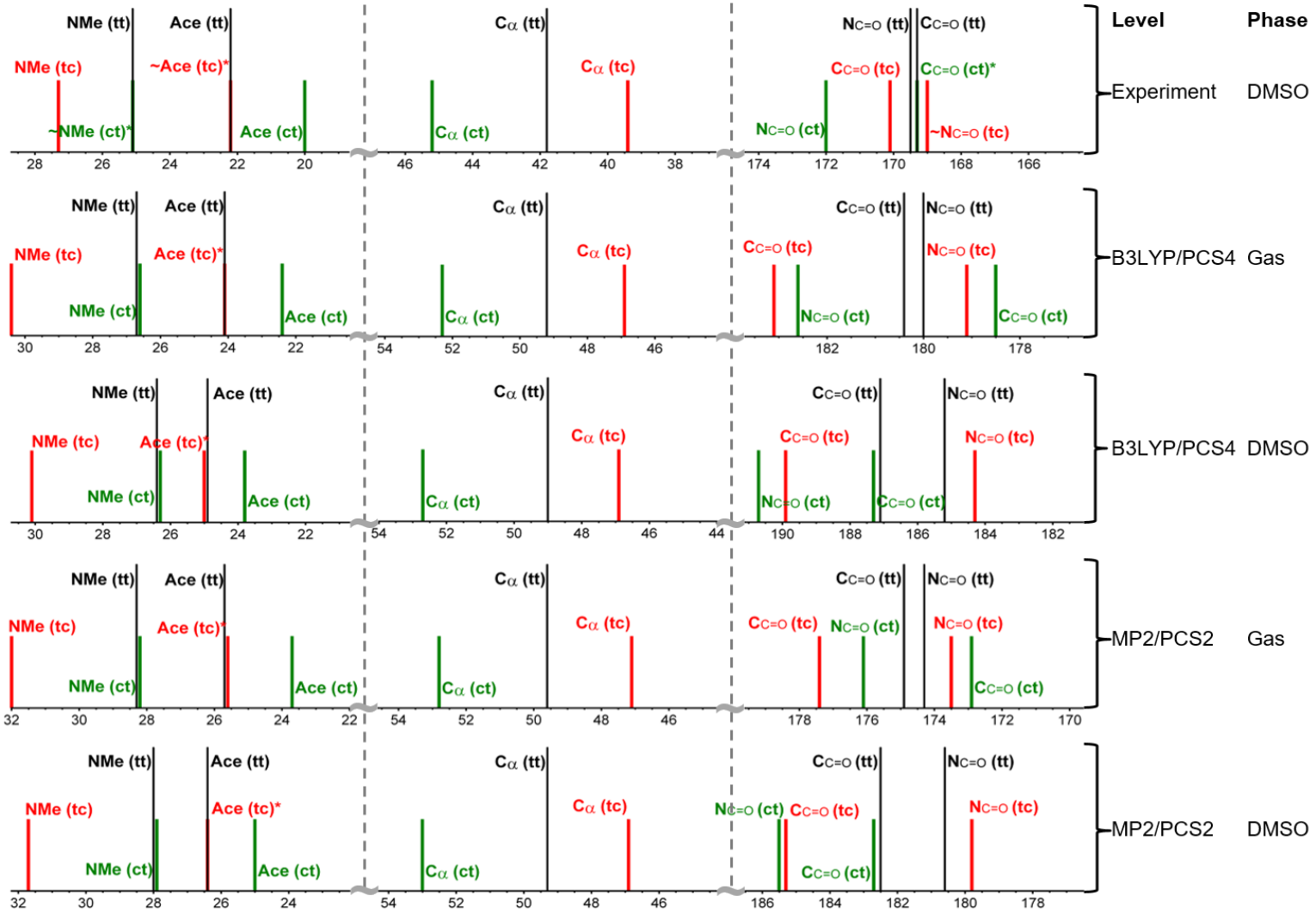

Fig. 69: A comparison of experimentally measured and theoretically calculated ^{13}C chemical shifts for **1** (Ace-Gly-NMe) are shown at different levels of theory using geometries optimized at B3LYP/6-31G(d) in the gas phase. The conformers are weighted using population dependent Boltzmann averaging based on ΔG_{298} at G3(MP2)-RAD.

Table 22: The isotropic shielding values for dipeptide **1** (Ace-Gly-NMe) are shown, calculated at B3LYP/PCS4//B3LYP/6-31G(d) gas. See Fig. 68 for labels.

	Label->	1	2	3	4	5	6	7	8	9	10	11	12	13	14	15	16	17	18	19
FileName	Conf.	C	N	C	C	N	H	O	C	H	H	H	O	H	C	H	H	H	H	H
Gly_0_30_180_180	C7_tt	126.8	115.2	-1.3	-3.7	127.8	25.6	-74.3	155.1	29.4	30.0	29.4	-81.3	24.0	153.4	27.3	29.2	29.2	28.5	27.0
Gly_0_40_180_180	β2_tt	131.0	117.9	0.1	-0.5	138.0	26.2	-94.0	154.9	29.3	30.0	29.4	-70.7	25.7	153.2	27.1	29.2	29.2	28.3	26.4
Gly_20_160_180_180	C5_tt	131.6	125.4	-0.6	0.7	136.2	24.7	-94.4	155.6	29.8	29.5	29.5	-60.5	26.7	152.7	29.1	27.0	29.1	27.6	27.6
Gly_0_160_180_0	C5_tc	132.7	124.1	-3.5	0.5	137.5	24.5	-94.3	155.5	29.5	29.8	29.5	-72.2	26.5	149.2	28.6	28.5	28.8	27.6	27.5
Gly_20_40_180_0	αR_tc	128.0	122.1	-0.3	0.1	138.3	26.1	-112.7	155.9	29.4	30.0	29.5	-106.4	26.7	146.2	28.3	28.5	28.8	28.1	27.3
Gly_50_0_180_0	C7_uc	136.6	116.9	-4.9	-2.4	134.4	25.5	-86.0	154.9	29.5	29.9	29.5	-74.6	26.7	147.6	27.1	28.9	28.6	28.7	26.6
Gly_180_90_0_180	C5_ct	129.7	131.6	1.6	1.2	137.3	25.3	-109.3	155.4	29.6	29.6	29.6	-68.5	26.9	152.4	27.0	29.1	29.1	27.6	27.6
Gly_20_180_0_180	β_ct	127.4	125.7	-1.2	-5.5	137.5	26.8	-127.0	157.7	29.0	29.7	29.6	-77.9	26.7	152.5	27.1	29.1	29.1	28.2	27.6
Gly_20_40_0_180	αR_ct	126.8	124.0	1.0	-3.9	135.8	26.4	-123.0	157.5	29.6	29.5	29.6	-59.6	25.2	153.1	29.1	27.1	29.1	27.9	27.6
Gly_170_20_0_0	β2_cc	125.6	125.5	-1.2	-2.0	134.3	26.8	-120.9	156.7	29.5	29.5	29.5	-113.7	26.6	146.6	28.3	28.5	28.8	27.3	27.7
Gly_180_130_0_0	C5_cc	130.7	130.0	-1.2	1.0	139.4	25.2	-110.4	155.3	29.5	29.5	29.5	-81.0	26.5	149.3	28.6	28.6	28.7	27.6	27.5
Gly_180_60_0_0	β2_cc	125.4	125.3	-2.1	-2.8	133.7	26.7	-125.8	156.7	29.6	29.5	29.5	-119.9	26.7	148.5	27.9	28.6	28.8	27.5	27.8
Gly_20_60_0_0	αR_cc	128.3	126.8	-2.7	-3.9	135.4	26.4	-117.4	156.6	28.8	29.5	29.7	-111.2	26.7	147.1	28.3	28.5	28.7	27.7	27.6
Gly_40_170_0_0	β_cc	129.8	130.7	-2.9	-5.5	140.5	26.8	-127.9	158.0	29.4	29.7	29.6	-97.1	26.6	148.5	28.5	28.5	28.7	27.8	27.6

Table 23: The isotropic shielding values for dipeptide model **1** (Ace-Gly-NMe) are shown, calculated at B3LYP/PCS4, DMSO//B3LYP/6-31G(d) gas. IEFPCM is used to model implicit DMSO. See Fig. 68 for labels.

	Label->	1	2	3	4	5	6	7	8	9	10	11	12	13	14	15	16	17	18	19
FileName	Conf.	C	N	C	C	N	H	O	C	H	H	H	O	H	C	H	H	H	H	H
Gly_0_30_180_180	C7_tt	128.7	107.4	-8.5	-7.7	120.7	23.6	-27.1	155.8	29.4	29.5	29.4	-22.2	23.1	154.9	27.6	28.9	29.0	27.5	26.1
Gly_0_40_180_180	β2_tt	131.6	108.6	-7.5	-6.5	129.4	24.1	-26.6	155.4	29.3	29.4	29.5	-2.4	23.9	154.7	27.4	29.0	28.9	27.3	25.8
Gly_20_160_180_180	C5_tt	132.9	113.2	-5.5	-3.2	130.5	23.2	-26.8	155.9	29.4	29.5	29.5	-6.0	24.5	154.2	28.9	27.3	28.9	26.6	26.6
Gly_0_160_180_0	C5_tc	133.9	112.6	-9.0	-3.5	128.6	23.1	-27.6	155.8	29.5	29.4	29.5	-11.5	24.8	150.7	28.5	28.3	28.5	26.5	26.4
Gly_20_40_180_0	αR_tc	129.0	109.5	-9.7	-6.6	125.5	23.8	-35.3	156.2	29.4	29.4	29.5	-24.0	25.0	148.0	28.3	28.2	28.6	26.5	26.8

	Label->	1	2	3	4	5	6	7	8	9	10	11	12	13	14	15	16	17	18	19
FileName	Conf.	C	N	C	C	N	H	O	C	H	H	H	O	H	C	H	H	H	H	H
Gly_50_0_180_0	C7_uc	137.8	110.3	-11.2	-7.2	125.7	23.7	-37.8	155.4	29.5	29.4	29.4	-11.0	25.0	148.3	27.4	28.6	28.3	27.5	25.8
Gly_180_90_0_180	C5_ct	131.3	117.8	-4.8	-5.5	132.1	24.2	-28.3	155.4	29.2	29.2	29.8	-6.1	24.6	154.1	27.4	28.9	28.9	26.4	26.4
Gly_20_180_0_180	β_ct	129.6	112.4	-7.6	-13.5	130.8	25.1	-52.4	157.0	28.9	29.0	29.9	-12.0	24.5	154.2	27.4	28.9	28.9	26.7	26.4
Gly_20_40_0_180	αR_ct	127.4	111.2	-6.8	-10.7	128.2	24.6	-45.9	157.3	29.3	29.1	29.9	9.2	23.6	154.7	28.9	27.4	28.9	26.8	26.6
Gly_170_20_0_0	β2_cc	127.1	113.8	-9.0	-9.0	123.2	25.1	-43.6	156.5	29.2	28.9	29.8	-35.7	24.9	148.4	28.4	28.2	28.5	26.0	27.0
Gly_180_130_0_0	C5_cc	132.1	117.0	-8.2	-5.8	130.2	24.1	-29.5	155.3	29.1	29.1	29.8	-11.3	24.8	150.8	28.5	28.4	28.5	26.3	26.2
Gly_180_60_0_0	β2_cc	126.9	113.5	-10.1	-9.8	123.5	25.1	-47.5	156.5	29.2	29.0	29.8	-42.0	25.0	149.6	27.8	28.4	28.6	26.2	27.1
Gly_20_60_0_0	αR_cc	130.4	112.5	-9.8	-10.0	124.3	24.5	-44.0	156.6	28.7	29.0	29.9	-42.0	25.0	148.8	28.4	28.1	28.5	26.3	26.8
Gly_40_170_0_0	β_cc	131.3	116.6	-10.4	-13.9	130.9	25.1	-52.5	157.3	29.3	29.1	29.9	-20.0	24.9	150.1	28.4	28.3	28.5	26.4	26.3

Table 24: The isotropic shielding values for dipeptide model **1** (Ace-Gly-NMe) are shown, calculated at MP2/PCS2, gas//B3LYP/6-31G(d) gas for **tt**, **tc** and **ct** conformers. See Fig. 68 for labels.

Label->	1	2	3	4	5	6	7	8	9	10	11	12	13	14	15	16	17	18	19
Conf.	C	N	C	C	N	H	O	C	H	H	H	O	H	C	H	H	H	H	H
C7_tt	142.4	143.6	20.6	18.8	157.7	25.7	-26.0	170.2	29.4	30.1	29.4	-27.6	24.3	168.4	29.1	27.4	29.2	28.5	27.1
C5_tt	148.0	154.3	21.5	22.9	165.7	25.0	-41.7	170.6	29.9	29.5	29.5	-10.4	26.7	167.7	29.0	27.1	29.0	27.8	27.8
B2_tt	147.2	147.6	22.4	22.5	167.6	26.5	-41.3	170.1	29.4	29.3	30.1	-19.0	25.9	168.2	29.1	29.1	27.2	28.3	26.5
C5_tc	149.1	153.1	18.8	22.7	166.8	24.9	-41.5	170.5	29.5	29.9	29.5	-22.1	26.5	164.2	28.7	28.5	28.6	27.7	27.6
C7_tc	151.9	146.2	17.1	20.1	164.1	25.6	-35.9	170.1	29.5	30.0	29.5	-24.3	26.8	162.5	28.9	27.2	28.6	26.7	28.7
aR_tc	143.8	150.9	22.2	23.0	168.3	26.4	-57.8	170.9	30.1	29.4	29.4	-53.2	26.8	161.2	28.4	28.8	28.5	28.0	27.4
aR_ct	142.8	154.2	23.1	19.3	165.7	26.5	-69.4	172.8	29.6	29.5	29.7	-8.6	25.4	168.1	29.1	27.2	29.0	28.0	27.7
C5_ct	146.1	161.6	23.8	23.6	167.0	25.5	-56.6	170.7	29.6	29.6	29.6	-16.3	26.9	167.5	29.0	29.0	27.1	27.8	27.8
B_ct	143.2	155.7	21.3	17.8	166.9	26.9	-73.8	172.8	29.7	29.6	29.1	-24.6	26.9	167.6	29.1	29.1	27.1	27.7	28.3

Table 25: The isotropic shielding values for dipeptide model **1** (Ace-Gly-NMe) are shown, calculated at MP2/PCS2, DMSO//B3LYP/6-31G(d) gas for **tt**, **tc** and **ct** conformers. See Fig. 68 for labels.

Label->	1	2	3	4	5	6	7	8	9	10	11	12	13	14	15	16	17	18	19
Conf.	C	N	C	C	N	H	O	C	H	H	H	O	H	C	H	H	H	H	H
C7_tt	144.3	135.6	12.6	13.8	150.0	23.7	14.9	170.9	29.4	29.5	29.4	20.7	23.3	169.7	28.8	27.6	28.9	27.4	26.2
C5_tt	149.3	142.1	15.6	17.7	159.1	23.4	16.6	171.0	29.5	29.5	29.5	36.1	24.5	169.1	28.8	27.3	28.8	26.7	26.7
B2_tt	147.8	138.1	13.8	15.1	158.2	24.3	15.8	170.5	29.5	29.3	29.5	38.7	24.0	169.5	28.9	28.8	27.4	27.3	25.9
C5_tc	150.3	141.7	12.1	17.5	157.3	23.4	16.1	170.9	29.4	29.5	29.4	30.3	24.8	165.6	28.4	28.3	28.5	26.6	26.4
C7_tc	153.1	139.6	9.8	14.3	154.5	23.8	4.5	170.6	29.5	29.5	29.4	30.7	25.0	163.2	28.5	27.5	28.3	25.9	27.5
aR_tc	144.9	138.2	11.4	14.9	155.2	24.0	8.0	171.2	29.5	29.4	29.5	16.7	25.0	162.8	28.3	28.5	28.2	26.4	26.9
aR_ct	143.6	141.6	14.3	11.1	157.1	24.6	-4.8	172.7	29.8	29.1	29.3	49.9	23.7	169.5	28.8	27.4	28.8	26.8	26.7
C5_ct	147.6	147.9	16.3	15.5	160.7	24.4	12.3	170.8	29.8	29.1	29.1	36.3	24.6	169.0	28.8	28.8	27.4	26.5	26.5
B_ct	145.4	142.8	13.6	8.4	159.1	25.1	-11.7	172.3	29.0	29.8	28.9	31.9	24.6	169.1	28.9	28.8	27.4	26.5	26.8

4.3.5 Structural Data of Dipeptide Model 1

Minima.

Gly_0_160_180_0.log

1\1\GINC-T3\FOpt\RB3LYP\6-31G(d)\C5H10N2O2\HARISH\27-Mar-2015\0\\#p b3
lyp/6-31g(d) opt freq geom=connectivity\\Gly_0_160_180_0\\0,1\C,0.3244
795365,-0.8551171489,0.0940031504\N,0.6127907847,-0.3586818182,1.41465
99413\C,0.6783706255,0.2351621159,-0.9171732619\C,0.3998736924,-1.1215
621024,2.5215827566\N,0.4709214315,-0.0655761196,-2.2287118915\H,0.972
6184009,0.5877668455,1.4513889142\O,-0.0425250086,-2.26414929,2.449026
2819\C,0.7464887823,-0.4646282373,3.8493343188\H,1.4907107581,-1.07994
84206,4.3644154425\H,1.1344967875,0.5535023925,3.7474044807\H,-0.14940
68589,-0.4433923946,4.4776576149\O,1.1140768376,1.3264500299,-0.558778
4282\H,0.7664446722,0.6635773474,-2.8650984639\C,0.0730790975,-1.35217
88597,-2.7791021078\H,0.8795991934,-2.0965591742,-2.7394292485\H,-0.79
64895803,-1.7535372549,-2.2496365191\H,-0.2112143818,-1.2098583041,-3.
8240938178\H,0.8941338959,-1.7720031243,-0.1137559529\H,-0.7353740608,
-1.1329974082,0.0023285591\\Version=AM64L-G09RevC.01\State=1-A\HF=-456
.5331903\RMSD=5.497e-09\RMSF=1.090e-05\Dipole=0.0538121,0.1782634,-1.3
382159\Quadrupole=-1.3566431,-8.1492803,9.5059234,-2.2816548,2.7322589
,6.50475\PG=C01 [X(C5H10N2O2)]\\@

Gly_0_30_180_180.log

1\1\GINC-HP1\FOpt\RB3LYP\6-31G(d)\C5H10N2O2\ROOT\27-Mar-2015\0\\#p b3l
yp/6-31g(d) opt freq geom=connectivity\\Gly_0_30_180_180\\0,1\C,0.2341
082079,-0.0223711722,0.0762185937\N,0.2048827186,-0.4954635168,1.45766
17446\C,1.268746269,-0.744317626,-0.8119246329\C,1.0876469843,-0.05892
66536,2.3969307501\N,2.5587699505,-0.4672312368,-0.4845771607\H,-0.449
3811286,-1.2263925692,1.6962035291\O,1.9841758911,0.7442142712,2.13038
05311\C,0.9002038849,-0.6070472634,3.8004198132\H,0.7507625538,0.23278
91025,4.4858797572\H,0.0568089829,-1.2975481708,3.8961153976\H,1.81779
34732,-1.1183422933,4.1073313359\O,0.9190105241,-1.4831781869,-1.72616
07739\H,2.7145901658,0.1201810428,0.3311267131\C,3.6841750663,-1.08275
75891,-1.1624159674\H,3.2929716869,-1.6557924134,-2.0044181351\H,4.377
8826485,-0.3208211638,-1.5360073094\H,4.2346190566,-1.7585158495,-0.49
53995672\H,-0.7464712352,-0.1904681833,-0.3706506381\H,0.4430215116,1.
0521570761,0.0959140513\\Version=AM64L-G09RevC.01\State=1-A\HF=-456.53
75163\RMSD=6.063e-09\RMSF=6.894e-06\Dipole=-0.3653417,-0.1878539,1.191
2408\Quadrupole=4.719894,-2.378322,-2.3415719,-1.549243,-5.4757807,-5.
749555\PG=C01 [X(C5H10N2O2)]\\@

Gly_0_40_180_180.log

1\1\GINC-HP1\FOpt\RB3LYP\6-31G(d)\C5H10N2O2\ROOT\27-Mar-2015\0\\#p b3l
yp/6-31g(d) opt freq geom=connectivity\\Gly_0_40_180_180\\0,1\C,0.4249
500558,0.0114408309,0.0927575668\N,0.6324511139,-0.5192695373,1.430548
015\C,1.3830646634,-0.5120656741,-0.9859077076\C,0.8760012463,0.298584
2457,2.5139757724\N,2.5602575143,-1.0176025597,-0.5257768977\H,0.34093
27061,-1.4706730957,1.6086792499\O,1.0860295576,1.4967737234,2.3997021
714\C,0.874233932,-0.399067976,3.8657578374\H,-0.0027940165,-0.0688904
843,4.4328391434\H,0.8583988515,-1.4916112393,3.7992603184\H,1.7599781
337,-0.0855358101,4.4246231043\O,1.0769485725,-0.4387707296,-2.1694162
075\H,2.7254210888,-0.9759172338,0.4700996195\C,3.6202026731,-1.459511
7332,-1.4125020702\H,3.2190698231,-1.4558010389,-2.4271582382\H,4.4861
735562,-0.7872646132,-1.3706320992\H,3.9481052046,-2.4734286894,-1.156
1597921\H,-0.5914657439,-0.1867011782,-0.262789768\H,0.5487850493,1.09
64745914,0.1659901194\\Version=AM64L-G09RevC.01\State=1-A\HF=-456.5333
573\RMSD=4.696e-09\RMSF=8.908e-06\Dipole=0.2955888,-1.4512968,1.225804
1\Quadrupole=5.6494589,-1.5696108,-4.079848,-0.2018793,-3.7203013,-3.9
52774\PG=C01 [X(C5H10N2O2)]\\@

Gly_170_20_0_0.log

1\1\GINC-HP1\FOpt\RB3LYP\6-31G(d)\C5H10N2O2\ROOT\30-Mar-2015\0\\#p b3l
yp/6-31g(d) opt freq geom=connectivity\\Gly_170_20_0_0\\0,1\C,0.109460
9846,0.5803365943,-0.2193756555\N,-0.0363422291,1.0498039529,1.1509113
398\C,1.5872945965,0.4562409672,-0.6219440279\C,-1.0758167989,0.804688
6123,2.0235407909\N,2.3467258686,-0.4647721406,0.0428398216\H,0.504836
9932,1.8670346846,1.4124015682\O,-1.1720764487,1.4328764476,3.06777407
21\C,-2.0639833574,-0.2873464342,1.6400332437\H,-2.6016551354,-0.03701
12255,0.7181151426\H,-1.5683105471,-1.252885343,1.4840632443\H,-2.7819
800211,-0.3852237498,2.454799185\O,2.0547851245,1.1597077451,-1.508575
8698\H,3.3195644725,-0.4482102252,-0.2366098043\C,1.9671319013,-1.3389
264353,1.1418721586\H,1.9616426496,-0.8251901319,2.110375354\H,0.97413
91734,-1.7662801665,0.9749969935\H,2.6783891259,-2.1680423848,1.185885
4646\H,-0.3876098504,-0.3892843458,-0.3168836114\H,-0.3391467128,1.266
941608,-0.9469513379\\Version=AM64L-G09RevC.01\State=1-A\HF=-456.52009
26\RMSD=6.255e-09\RMSF=4.093e-06\Dipole=0.1706858,-1.4498248,-0.146508
5\Quadrupole=5.5652454,3.4593275,-9.0245728,-1.1485297,7.4491585,-0.86
28391\PG=C01 [X(C5H10N2O2)]\\@

Gly_180_130_0_0.log

1\1\GINC-T4\FOpt\RB3LYP\6-31G(d)\C5H10N2O2\HARISH\30-Mar-2015\0\\#p b3
lyp/6-31g(d) opt freq geom=connectivity\\Gly_180_130_0_0\\0,1\C,-0.051
5873001,-0.392355141,0.0388076352\N,-0.0728454054,0.2129655088,1.34444
74465\C,1.4026801402,-0.4328579746,-0.4510233125\C,-1.1593545258,0.438
6093945,2.1475407796\N,1.6065317203,-0.9892014405,-1.6782415638\H,0.83
30420975,0.5108848496,1.6943117752\O,-1.044948937,0.9711204812,3.24313
21114\C,-2.5063717443,-0.0114565103,1.5969286617\H,-2.7452785408,0.497
9835863,0.6552336012\H,-2.5196974101,-1.0905426145,1.4002044534\H,-3.2
724172575,0.2263264914,2.3356781866\O,2.3197986179,0.0217916144,0.2218
82697\H,2.5815065185,-1.0373141385,-1.9446576752\C,0.6213905839,-1.652
1726867,-2.5177018318\H,0.2923660624,-2.6149326735,-2.1038178155\H,-0.
2592325262,-1.0194212942,-2.6713295059\H,1.0693408933,-1.8374468361,-3
.4962199173\H,-0.4526780501,-1.4178137445,0.0479091075\H,-0.6545862532
,0.1697250664,-0.6919296862\\Version=AM64L-G09RevC.01\State=1-A\HF=-45
6.5257541\RMSD=5.895e-09\RMSF=5.848e-06\Dipole=-0.3814655,-1.3569772,-

2.5945025\Quadrupole=0.4648822,0.9103464,-1.3752286,-0.7678541,-0.6413
133,-1.0938925\PG=C01 [X(C5H10N2O2)]\\@

Gly_180_60_0_0.log

1\1\GINC-HP2\FOpt\RB3LYP\6-31G(d)\C5H10N2O2\HARISH\30-Mar-2015\0\\#p b
3lyp/6-31g(d) opt freq geom=connectivity\\Gly_180_60_0_0\\0,1\C,0.0605
019443,0.2766925452,-0.1180750313\N,0.0456657856,0.3254518624,1.339269
0653\C,1.4841153302,0.0802156176,-0.6623268107\C,-1.0555856136,0.17154
86887,2.158668965\N,2.1213296345,-1.0892031866,-0.3538985242\H,0.78694
75567,0.857042701,1.7835278948\O,-1.0047876394,0.4898522779,3.33723944
73\C,-2.3001330395,-0.4379086387,1.5309791753\H,-2.704640642,0.2047228
48,0.740202607\H,-2.0939816738,-1.4191800674,1.0872985948\H,-3.0487847
573,-0.5512219627,2.3155827701\O,2.0247912055,0.9565536573,-1.32454472
88\H,3.0337498095,-1.1622454233,-0.7877168645\C,1.5483905264,-2.292673
2336,0.2305161086\H,0.8742443349,-2.0275427025,1.0470134086\H,1.004976
0994,-2.9030877407,-0.5048325756\H,2.356381405,-2.9000324424,0.6471231
432\H,-0.5819213574,-0.5443338605,-0.4529967014\H,-0.3047128557,1.2045
060535,-0.5741417972\\Version=AM64L-G09RevC.01\State=1-A\HF=-456.52031
64\RMSD=9.283e-09\RMSF=1.071e-05\Dipole=-0.118995,-1.4251875,-0.708024
7\Quadrupole=5.2544623,3.601374,-8.8558363,-3.667954,5.4891638,2.03921
75\PG=C01 [X(C5H10N2O2)]\\@

Gly_180_90_0_180.log

1\1\GINC-HP2\FOpt\RB3LYP\6-31G(d)\C5H10N2O2\HARISH\30-Mar-2015\0\\#p b
3lyp/6-31g(d) opt freq geom=connectivity\\Gly_180_90_0_180\\0,1\C,0.07
15683315,-0.4638471981,0.1071856122\N,-0.117401986,0.4045531007,1.2398
090913\C,1.535450093,-0.3538507614,-0.3543212475\C,-1.2653786809,0.611
3716709,1.9577874788\N,1.8457861084,-1.1325084066,-1.4259093171\H,0.70
93999448,0.9190419043,1.5288071958\O,-1.2957485172,1.3824037583,2.9072
883538\C,-2.4901938949,-0.1719808021,1.5034589709\H,-2.7589236365,0.06
90803603,0.4675939021\H,-2.3164278374,-1.2538444874,1.5555023845\H,-3.
3226760161,0.087913447,2.1580796672\O,2.3351088321,0.3804459146,0.2121
778204\H,1.121216289,-1.7086964743,-1.8312408871\C,3.1745150474,-1.172
280464,-2.0150661582\H,3.8059963131,-0.4911594082,-1.4438105386\H,3.59
79351638,-2.1818879931,-1.9645875172\H,3.151621864,-0.8479384909,-3.06
17039295\H,-0.1408883487,-1.5167728978,0.3501342047\H,-0.5828071373,-0
.1951724812,-0.7368699298\\Version=AM64L-G09RevC.01\State=1-A\HF=-456.
5288423\RMSD=2.876e-09\RMSF=3.477e-06\Dipole=0.0182999,-1.8098948,-2.2
068727\Quadrupole=1.062512,0.0854916,-1.1480036,0.6776997,0.8866317,-1
.6422323\PG=C01 [X(C5H10N2O2)]\\@

Gly_20_160_180_180.log

1\1\GINC-S5\FOpt\RB3LYP\6-31G(d)\C5H10N2O2\HARISH\27-Mar-2015\0\\#p b3
lyp/6-31g(d) opt freq geom=connectivity\\Gly_20_160_180_180\\0,1\C,0.4
816971663,1.5056813903,-0.2042460441\N,0.6058705963,1.081579772,1.1666
372208\C,1.1544872173,0.4608423254,-1.0998202771\C,0.0959116071,1.8221
719459,2.1884110787\N,1.1086224789,0.7414326304,-2.4294253155\H,1.0939
677823,0.2047136971,1.305460809\O,-0.4915589105,2.8819178571,1.9929473
86\C,0.3027565078,1.2496247336,3.5827262771\H,0.8441179663,0.298573972
2,3.5909585828\H,0.8531465537,1.9783558042,4.1858828819\H,-0.674281404
,1.1077794544,4.0550091472\O,1.6863895156,-0.5422010707,-0.6320594223\
H,0.6492116785,1.5915675746,-2.7255711513\C,1.6894122619,-0.1243519557
,-3.441961569\H,2.4694617466,0.3979655133,-4.0077542176\H,2.1321887205
,-0.9777237908,-2.9273361349\H,0.9246309483,-0.4834793372,-4.140214794
7\H,-0.5749645885,1.6211087597,-0.4845261099\H,0.9481892944,2.48978487
6,-0.3537240264\\Version=AM64L-G09RevC.01\State=1-A\HF=-456.5361652\RM
SD=5.732e-09\RMSF=2.210e-06\Dipole=0.2881217,-0.3181049,-1.2436805\Qua
drupole=-2.9673673,-7.0508841,10.0182515,4.2248516,1.9452477,-4.978819
\PG=C01 [X(C5H10N2O2)]\\@

Gly_20_180_0_180.log

1\1\GINC-P3\FOpt\RB3LYP\6-31G(d)\C5H10N2O2\HARISH\27-Mar-2015\0\\#p b3
lyp/6-31g(d) opt freq geom=connectivity\\Gly_20_180_0_180\\0,1\C,0.421
9242395,0.359755596,-0.0443516\N,0.4532745323,-0.1617820108,1.30082485
59\C,1.5936233025,-0.118638607,-0.929648452\C,1.2998444402,0.241359003
8,2.3201325298\N,1.3078207462,-0.1726787352,-2.2624070557\H,0.15568441
46,-1.123290571,1.4220507926\O,1.4347672913,-0.4540710974,3.3147970423
\C,1.9894739482,1.5843499887,2.1573768806\H,2.7268139419,1.5302326482,
1.3503070807\H,1.2777920007,2.3856846524,1.9250911406\H,2.494969483,1.
8168412362,3.0953236464\O,2.6911562316,-0.3812037644,-0.4573151877\H,0
.3672729977,0.035537744,-2.5665687014\C,2.2992961788,-0.5210040292,-3.
2668187185\H,3.2330794737,-0.7282983418,-2.7426870508\H,1.996617831,-1
.4132372659,-3.8266947908\H,2.4570793539,0.3039060315,-3.9715380934\H,
-0.5413343573,0.0982256817,-0.4996626316\H,0.4601847667,1.4546014823,-
0.0114080744\\Version=AM64L-G09RevC.01\State=1-A\HF=-456.5270436\RMSD=
4.380e-09\RMSF=8.483e-06\Dipole=-1.1494639,0.6498186,-2.3424817\Quadru
pole=0.6105283,1.6827339,-2.2932622,1.5376146,1.7836054,3.5690861\PG=C
01 [X(C5H10N2O2)]\\@

Gly_20_40_0_180.log

1\1\GINC-S6\FOpt\RB3LYP\6-31G(d)\C5H10N2O2\HARISH\27-Mar-2015\0\\#p b3
lyp/6-31g(d) opt freq geom=connectivity\\Gly_20_40_0_180\\0,1\C,0.4912
12026,0.4845198152,-0.1141692153\N,0.5633434166,-0.1248683463,1.204140
0662\C,1.5810648943,0.0864170342,-1.128769468\C,1.1609604279,0.3891675
593,2.3403539428\N,2.4831692651,-0.8302699621,-0.6916394189\H,-0.04344
70533,-0.9119204634,1.4012811227\O,1.0284418872,-0.170596095,3.4181860
545\C,1.9857759607,1.6535559222,2.1645329994\H,2.6895200337,1.57368198
45,1.3292594535\H,1.3379121363,2.5175536133,1.9725834203\H,2.533832018
1,1.8287288576,3.0908291815\O,1.5841199711,0.5966591066,-2.2420964795\
H,2.3542314452,-1.2000566232,0.2403452324\C,3.5553971589,-1.3357623616
,-1.5292802249\H,3.4320282116,-2.4065006106,-1.7314451202\H,3.51862832
46,-0.788688627,-2.4726487202\H,4.5310221493,-1.1764644536,-1.05639621
71\H,-0.4707274251,0.2321631713,-0.5713725069\H,0.5139329285,1.5756574
353,-0.0427178991\\Version=AM64L-G09RevC.01\State=1-A\HF=-456.5302838\
RMSD=4.558e-09\RMSF=8.058e-06\Dipole=0.1611042,-0.3426822,-0.1180045\Q
uadrupole=7.2750558,6.272092,-13.5471479,-0.9289897,0.5770612,5.317765
7\PG=C01 [X(C5H10N2O2)]\\@

Gly_20_40_180_0.log

1\1\GINC-T1\FOpt\RB3LYP\6-31G(d)\C5H10N2O2\HARISH\27-Mar-2015\0\\#p b3
lyp/6-31g(d) opt freq geom=connectivity\\Gly_20_40_180_0\\0,1\C,0.2318
878035,-0.1175425104,0.0852597116\N,0.3803308472,-0.2488027051,1.52657
93821\C,1.5226699725,-0.1532715724,-0.7526647655\C,0.9451105275,0.7545
634824,2.2730689706\N,2.4799636744,-1.0853300478,-0.4541974542\H,-0.09
83841502,-1.000938675,1.9991387549\O,1.4451416155,1.7409649067,1.75327
93443\C,0.90500822,0.5553780056,3.7818223774\H,0.2502312846,1.31486167
27,4.2219212889\H,0.5518524417,-0.434138878,4.0901218887\H,1.908531282
,0.7182455927,4.1845038622\O,1.6484828389,0.6037565486,-1.7041054078\H
,3.2884557438,-1.0101693363,-1.0578448023\C,2.4662958179,-2.1552812162
,0.5278181144\H,2.7392883584,-1.8161296751,1.5344419978\H,1.4836102442
,-2.6353117978,0.5803389013\H,3.1845794167,-2.9183968325,0.2142112907\
H,-0.427983873,-0.9230377624,-0.2570893948\H,-0.2351019313,0.837873739
8,-0.1667625609\\Version=AM64L-G09RevC.01\State=1-A\HF=-456.5206067\RM
SD=3.361e-09\RMSF=6.749e-06\Dipole=-0.48858,-2.1848498,1.3229947\Quadr
upole=4.6966983,-2.1585176,-2.5381808,-2.0085216,-1.8181569,2.495009\P
G=C01 [X(C5H10N2O2)]\\@

Gly_20_60_0_0.log

1\1\GINC-P3\FOpt\RB3LYP\6-31G(d)\C5H10N2O2\HARISH\27-Mar-2015\0\\#p b3
lyp/6-31g(d) opt freq geom=connectivity\\Gly_20_60_0_0\\0,1\C,0.599852
0351,0.2071679297,-0.0596959892\N,0.7356209958,0.0430745235,1.37972138
82\C,1.8490062948,-0.2089114046,-0.8586254949\C,1.4229148927,0.8567204
783,2.2588824183\N,2.1389884909,-1.5432425223,-0.9311466098\H,0.389712
3585,-0.8047904996,1.8101288916\O,1.5310648892,0.5364860669,3.43399665
82\C,1.9835117115,2.1517420468,1.6967405007\H,2.560336289,1.9935233544
,0.7804334333\H,1.1673428029,2.845239181,1.4569505886\H,2.612630546,2.
6059758237,2.4630173762\O,2.5533473957,0.6308390528,-1.4086462475\H,3.
0234152093,-1.7286721772,-1.388911931\C,1.5132292091,-2.6380578481,-0.
2082931494\H,1.8570641216,-2.7131703484,0.8320935938\H,0.4239707137,-2
.5330742341,-0.2107125675\H,1.7485389839,-3.5758812948,-0.718261581\H,
-0.2780429953,-0.3607029846,-0.3865549123\H,0.4215609354,1.2551999824,
-0.3078702863\\Version=AM64L-G09RevC.01\State=1-A\HF=-456.5215423\RMSD
=5.781e-09\RMSF=1.756e-05\Dipole=-0.697057,-1.2884815,-0.8760659\Quadr
upole=2.9681859,8.0402177,-11.0084037,-1.4987377,1.4366048,3.0550012\P
G=C01 [X(C5H10N2O2)]\\@

Gly_40_170_0_0.log

1\1\GINC-T5\FOpt\RB3LYP\6-31G(d)\C5H10N2O2\HARISH\29-Mar-2015\0\\#p b3
lyp/6-31g(d) opt freq geom=connectivity\\Gly_40_170_0_0\\0,1\C,0.13249
19649,0.2130384436,-0.0399992747\N,0.2322782523,0.1251761778,1.3962691
557\C,1.3600111849,-0.3534042932,-0.7866860207\C,1.0754440437,0.868125
5428,2.2048248548\N,1.2261396527,-0.4896287692,-2.1406350241\H,0.02315
07626,-0.7769500534,1.8080456789\O,1.285162425,0.5235793566,3.35715968
35\C,1.6677094438,2.1325470141,1.6067968528\H,2.4119757198,1.872855762
4,0.8466029787\H,0.9044039828,2.7673054374,1.1414360184\H,2.1545524848
,2.6875645808,2.4094136128\O,2.3991202198,-0.631371551,-0.2056619715\H
,2.0420162334,-0.8852066458,-2.5903675429\C,0.0285960884,-0.2791118173
,-2.9388350217\H,-0.7322248073,-1.0553912,-2.7779000391\H,-0.422801765
4,0.697203445,-2.7328984416\H,0.3089595008,-0.295197739,-3.9944961232\
H,-0.7761837723,-0.3125014723,-0.3550651792\H,-0.0058252816,1.25859953
33,-0.3415925431\\Version=AM64L-G09RevC.01\State=1-A\HF=-456.5227786\R
MSD=8.152e-09\RMSF=1.146e-05\Dipole=-1.2151528,0.1248151,-2.5544333\Qu
adrupole=-0.5210321,2.7603255,-2.2392934,2.4810393,-0.3200917,1.609597
\PG=C01 [X(C5H10N2O2)]\\@

Gly_50_0_180_0.log

1\1\GINC-T1\FOpt\RB3LYP\6-31G(d)\C5H10N2O2\HARISH\29-Mar-2015\0\\#p b3
lyp/6-31g(d) opt freq geom=connectivity\\Gly_50_0_180_0\\0,1\C,0.58536
77386,0.3179910768,0.2490817783\N,-0.1410308298,0.2259746986,1.5062767
743\C,1.3839826646,-0.9704247192,0.0005948061\C,0.3962814849,0.7161248
467,2.667473609\N,2.7403426231,-0.8844103878,-0.0624176661\H,-0.830876
8495,-0.5115711507,1.5645106986\O,1.4184586506,1.3956130149,2.68978244
59\C,-0.3763797652,0.3863686661,3.9341096379\H,-0.5444487612,1.3113627
543,4.4926687599\H,-1.3384734522,-0.0994985654,3.7460739137\H,0.235773
1616,-0.2689856757,4.5627966092\O,0.7851417144,-2.0354089416,-0.124140
8214\H,3.1885789732,-1.7759758292,-0.2343737726\C,3.5861845091,0.27674
93405,0.1994635388\H,3.2206347991,0.8360707686,1.0648732394\H,4.594678
1359,-0.0794925421,0.4239580779\H,3.6498963854,0.9472041351,-0.6676904
983\H,-0.1344694833,0.4095560791,-0.5704896599\H,1.1929078855,1.220684
1804,0.2873045776\\Version=AM64L-G09RevC.01\State=1-A\HF=-456.529883\R
MSD=4.880e-09\RMSF=8.475e-06\Dipole=0.1055208,0.1318994,-0.0280409\Qua
drupole=6.3493792,-6.8253498,0.4759705,-3.1046713,-5.3516945,-4.838159
4\PG=C01 [X(C5H10N2O2)]\\@

Saddle Points.

Gly_0_0_180_180.log

1\1\GINC-P3\FOpt\RB3LYP\6-31G(d)\C5H10N2O2\HARISH\27-Mar-2015\0\\#p b3
lyp/6-31g(d) opt freq geom=connectivity\\Gly_0_0_180_180\\0,1\C,0.2991
851771,0.0000000002,0.1662036157\N,0.3440434766,-0.0000000145,1.643484
9171\C,1.5031063762,0.0000000225,-0.8043007719\C,1.3274649486,-0.00000
0014,2.5844752868\N,2.7646043769,0.0000000308,-0.3478417196\H,-0.59028
26078,-0.0000000281,2.0327348976\O,2.5400170264,0.0000000006,2.3678128
459\C,0.7996493603,-0.0000000341,4.0165350751\H,0.1854523366,0.8866867
037,4.2120318384\H,0.1854523548,-0.8866867886,4.2120318202\H,1.6514799
485,-0.0000000323,4.6967764475\O,1.1991918799,0.0000000315,-1.99606557
07\H,2.9210663323,0.000000022,0.6624504941\C,3.8775711223,0.0000000518
,-1.2817349937\H,3.8496536641,-0.8845708087,-1.9275774995\H,3.84965364
59,0.8845709249,-1.9275774814\H,4.8092244571,0.0000000555,-0.711574388
1\H,-0.284566743,-0.8754350826,-0.1407443471\H,-0.284566761,0.87543507
72,-0.1407443291\\Version=AM64L-G09RevC.01\State=1-A'\HF=-456.5252378\
RMSD=3.270e-09\RMSF=3.782e-05\Dipole=-0.8561978,0.,1.4978213\Quadrupol
e=5.44707,-0.0723306,-5.3747394,0.0000001,-7.4084153,0.\PG=CS [SG(C5H4
N2O2),X(H6)]\\@

Gly_0_180_0_0.log

1\1\GINC-P4\FOpt\RB3LYP\6-31G(d)\C5H10N2O2\HARISH\27-Mar-2015\0\\#p b3
lyp/6-31g(d) opt freq geom=connectivity\\Gly_0_180_0_0\\0,1\C,0.218576
5876,-0.0000000207,-0.1791876762\N,0.345237043,-0.0000000289,1.2723980
646\C,1.4358726837,0.0000000037,-1.1048097921\C,1.2849665189,-0.000000
0221,2.2961951224\N,1.0999487253,0.0000000079,-2.4352440384\H,-0.56823
08171,-0.0000000454,1.7133185161\O,0.8461286193,-0.0000000365,3.442200
4995\C,2.773679206,0.0000000017,2.0375774662\H,3.0832902279,-0.8737428
815,1.4612857994\H,3.0832902021,0.8737429019,1.4612858115\H,3.25819021
89,0.000000002,3.0153047258\O,2.6075517748,0.0000000186,-0.7604041192\
H,1.91019261,0.0000000241,-3.0407532768\C,-0.2204191313,-0.0000000073,
-3.0428582375\H,-0.8021485696,-0.8900682558,-2.7712971839\H,-0.8021485
959,0.8900682202,-2.7712971716\H,-0.0982116325,0.000000002,-4.12794653
94\H,-0.3851707673,-0.8748382074,-0.4687571938\H,-0.3851707931,0.87483
81522,-0.4687571816\\Version=AM64L-G09RevC.01\State=1-A'\HF=-456.50427
35\RMSD=6.064e-09\RMSF=2.338e-05\Dipole=-1.0717775,0.,-2.4993987\Quadr
upole=2.0428668,0.7065167,-2.7493836,0.,3.9305805,0.\PG=CS [SG(C5H4N2O
2),X(H6)]\\@

Gly_0_180_0_180.log

1\1\GINC-HP1\FOpt\RB3LYP\6-31G(d)\C5H10N2O2\ROOT\27-Mar-2015\0\\#p b3l
yp/6-31g(d) opt freq geom=connectivity\\Gly_0_180_0_180\\0,1\C,0.27732
1882,-0.0000000643,-0.1872552977\N,0.3164538431,-0.0000000405,1.269700
0127\C,1.5497487234,-0.0000000573,-1.0485676969\C,1.1992258887,-0.0000
000092,2.3421074059\N,1.254067155,-0.0000000833,-2.382253105\H,-0.6207
665929,-0.0000000496,1.6575581164\O,0.7017648738,0.0000000006,3.463847
1653\C,2.6991313878,0.0000000123,2.1588844811\H,3.0375503219,-0.873781
618,1.5988688984\H,3.0375502935,0.8737816358,1.5988688707\H,3.13422736
2,0.0000000353,3.1595761146\O,2.7048276706,-0.0000000323,-0.6528725888
\H,0.2924437013,-0.0000001038,-2.6891498838\C,2.3118013644,-0.00000008
2,-3.3818597447\H,2.9469763662,0.8857276477,-3.2781305949\H,2.94697639
5,-0.8857277879,-3.2781305668\H,1.8557133242,-0.0000001052,-4.37411981
41\H,-0.3032462681,-0.8778003793,-0.5122837392\H,-0.3032462966,0.87780
02215,-0.5122837671\\Version=AM64L-G09RevC.01\State=1-A'\HF=-456.50738
42\RMSD=7.498e-09\RMSF=2.418e-05\Dipole=-0.8721448,0.,-2.5042361\Quadr
upole=2.7206527,0.7009305,-3.4215832,0.0000001,5.1041514,0.\PG=CS [SG(
C5H4N2O2),X(H6)]\\@

Gly_0_180_180_0.log

1\1\GINC-HP1\FOpt\RB3LYP\6-31G(d)\C5H10N2O2\ROOT\27-Mar-2015\0\\#p b3l
yp/6-31g(d) opt freq geom=connectivity\\Gly_0_180_180_0\\0,1\C,0.33739
72456,0.0001111542,-0.0032607666\N,0.4660663165,0.0000352533,1.4502443
744\C,1.5581522739,0.0001612244,-0.9380729853\C,1.5075715132,-0.000009
5495,2.3643561354\N,1.1842001243,0.000024459,-2.2679730484\H,-0.445765
33,0.0000196595,1.8870493047\O,2.6956069093,-0.0000163565,2.1215455573
\C,0.9791692752,-0.0000441516,3.8059202971\H,0.3662963198,0.8867950556
,4.0087599921\H,0.3662733139,-0.8868791776,4.0087085076\H,1.836374185,
-0.000074698,4.479592669\O,2.7309531553,0.0000475607,-0.6256639496\H,1
.9823511137,-0.0000420114,-2.8887022746\C,-0.1449836934,-0.0000533144,
-2.8520107334\H,-0.7253560479,-0.8898712044,-2.5734088832\H,-0.7253716
043,0.8898165525,-2.5736072831\H,-0.0421102409,-0.0001736605,-3.939511
9342\H,-0.2657403483,-0.8754584101,-0.2888821206\H,-0.2657296373,0.875
7176614,-0.2887886361\\Version=AM64L-G09RevC.01\State=1-A\HF=-456.4976
694\RMSD=9.345e-09\RMSF=1.198e-05\Dipole=-2.5325545,0.0000099,-0.86830
77\Quadrupole=-5.6958886,-2.4036706,8.0995592,0.0000431,-2.2874618,0.0
002705\PG=C01 [X(C5H10N2O2)]\\@

Gly_0_180_180_180.log

1\1\GINC-P7\FOpt\RB3LYP\6-31G(d)\C5H10N2O2\HARISH\26-Mar-2015\0\\#p b3
lyp/6-31g(d) opt freq geom=connectivity\\Gly_0_180_180_180\\0,1\C,0.41
21488862,-0.0000002141,0.0492887408\N,0.470506666,0.0000022249,1.50730
34747\C,1.6774355685,-0.0000015422,-0.838401515\C,1.4744849544,-0.0000
002794,2.4610759403\N,1.3243110262,-0.0000015443,-2.1664360183\H,-0.45
96692754,0.0000043654,1.9037459555\O,2.6706712202,-0.0000037483,2.2606
948315\C,0.8933981465,0.0000002637,3.8816556805\H,0.2735963651,0.88690
85922,4.0617807279\H,0.2735937467,-0.8869063503,4.0617802013\H,1.72541
89942,-0.0000012024,4.5862723054\O,2.8404281771,0.0000028061,-0.490778
5075\H,0.3533095912,-0.0000035967,-2.4410824421\C,2.346252363,0.000000
9954,-3.2008028825\H,2.9860619958,0.8851106596,-3.119338698\H,2.986064
9206,-0.8851067055,-3.1193401995\H,1.8569307725,0.0000010325,-4.177639
5492\H,-0.1717578861,-0.8785980954,-0.26514742\H,-0.1717577005,0.87859
68593,-0.2651499924\\Version=AM64L-G09RevC.01\State=1-A\HF=-456.501041
8\RMSD=7.424e-09\RMSF=2.249e-05\Dipole=-2.4730525,0.,-0.9085802\Quadru
pole=-3.1678848,-3.0727364,6.2406212,0.0000004,-2.6922875,0.0000157\PG
=C01 [X(C5H10N2O2)]\\@

Gly_10_90_0_180.log

1\1\GINC-P4\FOpt\RB3LYP\6-31G(d)\C5H10N2O2\HARISH\27-Mar-2015\0\\#p b3
lyp/6-31g(d) opt freq geom=connectivity\\Gly_10_90_0_180\\0,1\C,0.4097
213849,0.3125864801,-0.1141760867\N,0.4724526832,-0.4691726533,1.11039
16587\C,1.3309491042,-0.1278276748,-1.2680698958\C,1.2429375015,-0.223
3548663,2.2314715096\N,2.0840178509,-1.231984385,-1.0407755134\H,-0.24
26134817,-1.1690147917,1.269372537\O,1.1039555114,-0.8985389078,3.2403
363296\C,2.2596496865,0.9015531516,2.1267129005\H,2.873499485,0.818510
5358,1.2235398668\H,1.7601797697,1.8777040762,2.1011866601\H,2.8986337
445,0.8601672185,3.0093401106\O,1.3496743537,0.5081144975,-2.314762466
1\H,1.9815386494,-1.7053156182,-0.1545666543\C,2.9742736555,-1.7624771
832,-2.0602078603\H,2.4242060591,-1.966897852,-2.9844775618\H,3.771135
7374,-1.0484493085,-2.294453548\H,3.4207327684,-2.6889677516,-1.692978
7094\H,-0.6141843886,0.288249138,-0.5004852253\H,0.632412154,1.3652304
05,0.0824199468\\Version=AM64L-G09RevC.01\State=1-A\HF=-456.5296714\RM
SD=4.400e-09\RMSF=1.627e-05\Dipole=0.0911571,-0.3653631,-0.1614671\Qua
drupole=7.0564617,5.077564,-12.1340257,-0.7495923,-0.1183109,7.7744945
\PG=C01 [X(C5H10N2O2)]\\@

Gly_120_80_0_180.log

1\1\GINC-T3\FOpt\RB3LYP\6-31G(d)\C5H10N2O2\HARISH\29-Mar-2015\0\\#p b3
lyp/6-31g(d) opt freq geom=connectivity\\Gly_120_80_0_180\\0,1\C,-0.08

05505318,-0.4008719713,0.1890266511\N,-0.3608285231,0.0082990564,1.544
7664407\C,1.3608849197,-0.0939589512,-0.271591439\C,-0.5645339108,1.30
48752475,1.9871317839\N,1.8583960422,-0.9421452189,-1.2123184863\H,0.0
033944704,-0.5841118791,2.2824371504\O,-0.5067154753,1.560859695,3.179
7758721\C,-0.906205755,2.3487798445,0.9387645576\H,-0.0370259767,2.534
4527713,0.2999860596\H,-1.7435261411,2.0345691004,0.3041310957\H,-1.17
75746217,3.2684772369,1.4582554722\O,1.9886154944,0.8676932438,0.15145
03479\H,1.3085909634,-1.7337622774,-1.5118636517\C,3.1726249843,-0.730
1283477,-1.8019379776\H,3.207462923,0.2162507638,-2.3522396472\H,3.941
2434966,-0.6968741753,-1.0236710781\H,3.3892416436,-1.5521284209,-2.48
75332047\H,-0.3001747874,-1.4714292992,0.0930671111\H,-0.7628593584,0.
1162946562,-0.4952015145\\Version=AM64L-G09RevC.01\State=1-A\HF=-456.5
265477\RMSD=9.027e-09\RMSF=1.351e-05\Dipole=-0.0174057,-1.7146495,-2.1
132518\Quadrupole=0.152707,3.9541984,-4.1069054,-2.1020872,1.1622034,-
0.8046168\PG=C01 [X(C5H10N2O2)]\\@

Gly_130_140_0_180.log

1\1\GINC-S1\FOpt\RB3LYP\6-31G(d)\C5H10N2O2\HARISH\30-Mar-2015\0\\#p b3
lyp/6-31g(d) opt freq geom=connectivity\\Gly_130_140_0_180\\0,1\C,0.11
59240312,0.4650631623,-0.1508334934\N,0.2406094466,0.7006281731,1.2640
382416\C,1.4378256061,-0.1335675262,-0.6618108236\C,-0.6966376379,1.22
2988984,2.1152660863\N,1.4675429911,-0.4124830326,-1.9899231401\H,1.13
9014054,0.4452589921,1.6637510439\O,-0.4643993494,1.3751316436,3.30686
85663\C,-2.0340103165,1.5987462683,1.4903361866\H,-1.9117825332,2.3572
818136,0.7073985906\H,-2.5215229744,0.728929125,1.0330777955\H,-2.6770
933766,1.9966934123,2.2759454828\O,2.3890020428,-0.3390053263,0.082286
4061\H,0.6521972625,-0.2272212375,-2.5557759609\C,2.6510426601,-0.9852
719343,-2.61635884\H,3.516132206,-0.3282303753,-2.4824930325\H,2.89201
9891,-1.9585746092,-2.1768357506\H,2.4570962476,-1.11110677,-3.6834833
189\H,-0.700945069,-0.2351412684,-0.3858646337\H,-0.0897192847,1.39088
01512,-0.7106760875\\Version=AM64L-G09RevC.01\State=1-A\HF=-456.528407
2\RMSD=7.354e-09\RMSF=8.435e-06\Dipole=-0.5986667,-0.3424043,-2.803188
8\Quadrupole=1.1269889,0.9809193,-2.1079082,0.0549197,0.2702902,-0.727
3245\PG=C01 [X(C5H10N2O2)]\\@

Gly_170_170_180_0.log

1\1\GINC-P7\FOpt\RB3LYP\6-31G(d)\C5H10N2O2\HARISH\29-Mar-2015\0\\#p b3
lyp/6-31g(d) opt freq geom=connectivity\\Gly_170_170_180_0\\0,1\C,-0.2
369895017,-0.0792284475,-0.0500944347\N,-0.1530059814,0.0855220878,1.3
778904679\C,1.1756319258,0.0005623521,-0.627464119\C,-1.2650601252,0.0
592746702,2.162260328\N,1.2819995793,-0.1387853597,-1.9769041176\H,0.7
823312346,0.2228849831,1.7423921115\O,-2.3875357121,-0.1064802636,1.69
42590723\C,-1.0230687246,0.2481767922,3.6523957916\H,-1.4133626191,-0.
6233551109,4.1871324155\H,0.0313199405,0.3830969832,3.9123434027\H,-1.
588991412,1.1202058602,3.9946449506\O,2.1554940183,0.1822679963,0.0910
382975\H,2.2312812133,-0.0884688978,-2.3223594976\C,0.1992739354,-0.37
40968426,-2.9200235682\H,-0.3110004752,-1.3266804684,-2.7320216176\H,-
0.5456763863,0.4298423378,-2.8939375573\H,0.6212226585,-0.4093275125,-
3.9263063189\H,-0.7033001908,-1.0408535185,-0.308144226\H,-0.878308735
1,0.6935620086,-0.4977635812\\Version=AM64L-G09RevC.01\State=1-A\HF=-4
56.5331646\RMSD=7.842e-09\RMSF=9.249e-06\Dipole=0.6265424,-0.0820609,-
1.2062046\Quadrupole=-11.1628019,-0.6804035,11.8432054,-1.1414454,-0.3
118881,1.4200605\PG=C01 [X(C5H10N2O2)]\\@

Gly_180_0_0_0.log

1\1\GINC-S3\FOpt\RB3LYP\6-31G(d)\C5H10N2O2\HARISH\30-Mar-2015\0\\#p b3
lyp/6-31g(d) opt freq geom=connectivity\\Gly_180_0_0_0\\0,1\C,-0.06174
24812,0.0000000049,0.0105672502\N,-0.1806605612,-0.0000000091,1.459232
7219\C,1.3201437324,0.0000000074,-0.6631249292\C,-1.3502000627,-0.0000
000127,2.1829882174\N,2.5084704896,-0.0000000031,0.0153337444\H,0.6378
45396,-0.0000000175,2.045289144\O,-1.3258272088,-0.000000025,3.4069394
685\C,-2.6436707827,-0.0000000008,1.3856752993\H,-2.716475963,0.883378
9952,0.7401978301\H,-2.7164759685,-0.8833789834,0.7401978125\H,-3.4764
055124,-0.0000000052,2.0894801342\O,1.3173530307,0.0000000196,-1.88857
24984\H,3.2808668275,0.0000000011,-0.6393810175\C,2.8530458209,-0.0000
000182,1.4309251712\H,2.4938267365,0.8963169929,1.9505928664\H,2.49382
67309,-0.8963170375,1.9505928485\H,3.9425833181,-0.0000000224,1.505348
9961\H,-0.5640690189,-0.8760148278,-0.4194904079\H,-0.5640690135,0.876
0148494,-0.4194903905\\Version=AM64L-G09RevC.01\State=1-A'\HF=-456.510
8552\RMSD=6.808e-09\RMSF=1.424e-05\Dipole=0.9099639,0.,-0.0600654\Quad
rupole=11.1213105,2.6710385,-13.792349,0.,7.036691,0.0000001\PG=CS [SG
(C5H4N2O2),X(H6)]\\@

Gly_180_0_0_180.log

1\1\GINC-S3\FOpt\RB3LYP\6-31G(d)\C5H10N2O2\HARISH\30-Mar-2015\0\\#p b3
lyp/6-31g(d) opt freq geom=connectivity\\Gly_180_0_0_180\\0,1\C,-0.026
3037667,-0.0000126578,-0.08360979\N,-0.0496242871,-0.000020173,1.37102
13194\C,1.3400408598,0.0000097783,-0.7832493245\C,-1.1621621663,-0.000
0380497,2.1810365187\N,2.4779876419,0.000003919,-0.0401328352\H,0.8048
873037,-0.0000086877,1.9094164759\O,-1.0460912178,0.0000159722,3.39898
94706\C,-2.5095523035,0.0000036812,1.4796148561\H,-2.6285757379,0.8835
745676,0.8413308239\H,-2.6286382132,-0.8835726432,0.8413501717\H,-3.28
89732949,0.0000396664,2.2420217132\O,1.362703174,-0.0000011408,-2.0074
067804\H,2.4515058473,-0.0000043187,0.9663185899\C,3.7814157588,0.0000
073355,-0.6919040898\H,3.8973860492,-0.8855413268,-1.3245049092\H,3.89
73882011,0.8855655825,-1.3244911097\H,4.5572629003,0.0000003662,0.0764
888166\H,-0.5493119578,-0.8786303775,-0.4821717647\H,-0.5493360643,0.8
785943424,-0.4821636222\\Version=AM64L-G09RevC.01\State=1-A\HF=-456.51
91699\RMSD=5.953e-09\RMSF=3.739e-05\Dipole=0.672551,-0.0000201,-0.1174
94\Quadrupole=11.0304037,2.9358475,-13.9662512,0.0000714,5.8437376,-0.
0001283\PG=C01 [X(C5H10N2O2)]\\@

Gly_180_0_180_0.log

1\1\GINC-HP2\FOpt\RB3LYP\6-31G(d)\C5H10N2O2\HARISH\30-Mar-2015\0\\#p b
3lyp/6-31g(d) opt freq geom=connectivity\\Gly_180_0_180_0\\0,1\C,-0.05
9445305,0.00000003,0.0597599785\N,-0.1479019144,0.0000000269,1.5131682
978\C,1.2990563336,0.0000000052,-0.6473297019\C,-1.3764949067,0.000000
0494,2.1204280067\N,2.5095040716,-0.0000000212,0.0003304008\H,0.676894

0649,0.0000000085,2.0864369282\O,-2.4163417502,0.0000000723,1.47582365
48\C,-1.3402203094,0.0000000436,3.6439091487\H,-0.8210838992,-0.886384
1784,4.0278787784\H,-0.8210838638,0.8863842423,4.0278787843\H,-2.36543
08766,0.0000000628,4.0156562895\O,1.2746321062,0.0000000097,-1.8720455
278\H,3.2644373167,-0.000000034,-0.674183883\C,2.8869926097,-0.0000000
334,1.4042324448\H,2.5407025007,0.8969687172,1.9339059636\H,2.54070246
48,-0.8969687737,1.9339059576\H,3.977986968,-0.0000000554,1.4567924256
\H,-0.5949235974,-0.8699937398,-0.3377242092\H,-0.5949235627,0.8699938
237,-0.3377242034\\Version=AM64L-G09RevC.01\State=1-A'\HF=-456.5132478
\RMSD=9.127e-09\RMSF=1.732e-05\Dipole=1.8993771,0.,1.7797103\Quadrupol
e=0.7730057,2.0336091,-2.8066148,0.,1.4778906,0.\PG=CS [SG(C5H4N2O2),X
(H6)]\\@

Gly_180_0_180_180.log

1\1\GINC-R2\FOpt\RB3LYP\6-31G(d)\C5H10N2O2\HARISH\30-Mar-2015\0\\#p b3
lyp/6-31g(d) opt freq geom=connectivity\\Gly_180_0_180_180\\0,1\C,-0.0
241521946,0.0000148345,-0.025464658\N,-0.0421579349,0.0000171409,1.431
7526382\C,1.3299034248,0.0000379545,-0.7359596606\C,-1.2344740285,-0.0
000029747,2.1100858237\N,2.4817600177,0.0000166328,-0.0066850089\H,0.8
095705381,0.0000325708,1.9697193594\O,-2.3077404162,-0.0000367002,1.52
45543526\C,-1.110377582,-0.0000127288,3.6286615429\H,-0.5702587478,-0.
8866210758,3.981960467\H,-0.5703054933,0.8866182285,3.9819751223\H,-2.
1125374147,-0.0000427024,4.0586389207\O,1.3491679834,-0.0000338792,-1.
9600630774\H,2.473317219,0.0000222888,0.9999220495\C,3.7748105071,-0.0
000183901,-0.6784611793\H,3.8813857178,-0.8852462818,-1.3132856749\H,3
.8814276436,0.8851967505,-1.3132964389\H,4.5632138902,-0.0000326053,0.
0774848369\H,-0.5712455345,-0.8728996246,-0.3995596633\H,-0.5712753517
,0.8729088209,-0.3995634565\\Version=AM64L-G09RevC.01\State=1-A\HF=-45
6.5210412\RMSD=9.076e-09\RMSF=3.549e-05\Dipole=1.770772,0.0000634,1.70
873\Quadrupole=-0.9250517,2.0496452,-1.1245935,-0.0000975,2.1156905,-0
.0001044\PG=C01 [X(C5H10N2O2)]\\@

Gly_180_180_180_0.log

1\1\GINC-S3\FOpt\RB3LYP\6-31G(d)\C5H10N2O2\HARISH\30-Mar-2015\0\\#p b3
lyp/6-31g(d) opt freq geom=connectivity\\Gly_180_180_180_0\\0,1\C,-0.2
505145712,0.0000000273,-0.0600113854\N,-0.1726071089,0.0000000169,1.37
76627593\C,1.171089895,0.0000000108,-0.6202629019\C,-1.2936623069,0.00
00000278,2.1520542551\N,1.2813393778,0.000000018,-1.9766397792\H,0.766
2897945,0.0000000012,1.7598748032\O,-2.4188131635,0.0000000469,1.66289
08385\C,-1.0376708154,0.0000000145,3.6531960275\H,-0.4652498645,-0.885
046388,3.9547511214\H,-0.4652498395,0.8850463968,3.9547511329\H,-1.997
4621267,0.0000000247,4.1713414669\O,2.1545080166,-0.0000000078,0.11591
47261\H,2.2354355126,0.0000000067,-2.312311997\C,0.1932120173,0.000000
0397,-2.94268522\H,-0.4404810205,-0.8897812561,-2.8456785246\H,-0.4404
809953,0.8897813522,-2.8456785131\H,0.6237502011,0.0000000401,-3.94592
6003\H,-0.8048576813,-0.8768009873,-0.424777348\H,-0.8048576565,0.8768
010624,-0.4247773367\\Version=AM64L-G09RevC.01\State=1-A'\HF=-456.5326
82\RMSD=6.431e-09\RMSF=5.143e-05\Dipole=0.6491338,0.,-1.1958349\Quadru
pole=-11.2450507,-0.720502,11.9655526,0.0000002,-0.2535042,0.\PG=CS [S
G(C5H4N2O2),X(H6)]\\@

Gly_180_180_180_180.log

1\1\GINC-T3\FOpt\RB3LYP\6-31G(d)\C5H10N2O2\HARISH\30-Mar-2015\0\\#p b3
lyp/6-31g(d) opt freq geom=connectivity\\Gly_180_180_180_180\\0,1\C,-0
.2038092643,-0.0000000118,-0.1311888326\N,-0.1348277654,0.0000000139,1
.307341679\C,1.2242559798,-0.0000000177,-0.6843837545\C,-1.2594640779,
0.0000000244,2.0765104709\N,1.3218624512,-0.0000000413,-2.037506187\H,
0.8019955512,0.0000000233,1.6948543232\O,-2.3820511962,0.0000000126,1.
5816328231\C,-1.010512447,0.0000000516,3.5788637055\H,-0.4395935286,-0
.8851315618,3.8829667941\H,-0.4395935335,0.885131679,3.8829667628\H,-1
.9727398753,0.0000000581,4.0924715165\O,2.2080804663,-0.000000002,0.05
08947078\H,0.4792954997,-0.0000000535,-2.5938957859\C,2.6152900582,-0.
0000000496,-2.7053721235\H,3.1958382128,0.8860763716,-2.4288158616\H,3
.1958382177,-0.8860764579,-2.4288158302\H,2.4530181251,-0.0000000692,-
3.7851547504\H,-0.7520769735,-0.8792331064,-0.4988131699\H,-0.75207697
83,0.8792330668,-0.498813201\\Version=AM64L-G09RevC.01\State=1-A'\HF=-
456.5352684\RMSD=5.173e-09\RMSF=4.371e-05\Dipole=0.7321032,0.,-1.12749
6\Quadrupole=-11.2781277,-0.4230482,11.7011758,0.,-0.0076229,0.0000002
\PG=CS [SG(C5H4N2O2),X(H6)]\\@

Gly_180_90_180_180.log

1\1\GINC-T5\FOpt\RB3LYP\6-31G(d)\C5H10N2O2\HARISH\30-Mar-2015\0\\#p b3
lyp/6-31g(d) opt freq geom=connectivity\\Gly_180_90_180_180\\0,1\C,0.1
584922771,-0.3404965828,0.1647791102\N,0.0448431592,0.1333093116,1.520
3193893\C,1.6395125872,-0.3391735856,-0.2250250493\C,-1.1629574767,0.2
340437772,2.1396537293\N,1.9084294759,-0.7646842164,-1.4847917092\H,0.
9207559232,0.3777650879,1.967235022\O,-2.2098483641,-0.0708335559,1.57
62493963\C,-1.127053481,0.7478958111,3.5712478781\H,-0.1190021346,0.97
72794491,3.9301867626\H,-1.7432708542,1.6498487363,3.6385394258\H,-1.5
768555516,-0.0033860667,4.2277969299\O,2.5172283664,0.0238660808,0.553
8342026\H,1.1473241773,-1.0541618052,-2.0818140224\C,3.2713526593,-0.8
187584228,-1.993151752\H,3.7335297198,0.1733808589,-1.9713515599\H,3.8
863068498,-1.4932458708,-1.3884741419\H,3.2479719351,-1.1810778095,-3.
0229307947\H,-0.2595605184,-1.3524488699,0.0670412904\H,-0.4158223826,
0.2964832017,-0.5228674444\\Version=AM64L-G09RevC.01\State=1-A\HF=-456
.535722\RMSD=7.778e-09\RMSF=3.022e-06\Dipole=0.8507152,-0.2763574,-1.0
005506\Quadrupole=-10.7622145,0.6405811,10.1216334,-1.9617579,-2.65719
11,3.5292807\PG=C01 [X(C5H10N2O2)]\\@

4.4 References

(1) Beachy, M. D.; Chasman, D.; Murphy, R. B.; Halgren, T. A.; Friesner, R. A. *J. Am. Chem. Soc.* **1997**, *119*, 5908.

(2) Cornell, W. D.; Cieplak, P.; Bayly, C. I.; Gould, I. R.; Merz, K. M.; Ferguson, D. M.; Spellmeyer, D. C.; Fox, T.; Caldwell, J. W.; Kollman, P. A. *J. Am. Chem. Soc.* **1995**, *117*, 5179.

(3) Cornell, W. D.; Gould, I. R.; Kollman, P. A. *J. Mol. Struct. (THEOCHEM)* **1997**, *392*, 101.

(4) Fujitani, H.; Matsuura, A.; Sakai, S.; Sato, H.; Tanida, Y. *J. Chem. Theory Comput.* **2009**, *5*, 1155.

(5) Gould, I. R.; Cornell, W. D.; Hillier, I. H. *J. Am. Chem. Soc.* **1994**, *116*, 9250.

(6) Gould, I. R.; Kollman, P. A. *J. Phys. Chem.* **1992**, *96*, 9255.

(7) Halgren, T. A. *J. Comput. Chem.* **1996**, *17*, 490.

(8) Head-Gordon, T.; Head-Gordon, M.; Frisch, M. J.; Brooks, C. L.; Pople, J. A. *J. Am. Chem. Soc.* **1991**, *113*, 5989.

(9) Hioe, J.; Savasci, G.; Brand, H.; Zipse, H. *Chem. Eur. J.* **2011**, *17*, 3781.

(10) Hioe, J.; Mosch, M.; Smith, D. M.; Zipse, H. *RSC Adv.* **2013**, *3*, 12403.

(11) Hu, H.; Elstner, M.; Hermans, J. *Proteins Struct. Funct. Bioinforma.* **2003**, *50*, 451.

(12) Jiang, J.; Wu, Y.; Wang, Z.-X.; Wu, C. *J. Chem. Theory Comput.* **2010**, *6*, 1199.

(13) Kaminský, J.; Jensen, F. *J. Chem. Theory Comput.* **2007**, *3*, 1774.

(14) Ataka, S.; Takeuchi, H.; Tasumi, M. *J. Mol. Struct.* **1984**, *113*, 147.

(15) Radzicka, A.; Pedersen, L.; Wolfenden, R. *Biochemistry* **1988**, *27*, 4538.

(16) Martínez, A. G.; Vilar, E. T.; Fraile, A. G.; Martínez-Ruiz, P. *J. Phys. Chem. A* **2002**, *106*, 4942.

(17) Drakenberg, T.; Forsén, S. *J. Chem. Soc. D Chem. Commun.* **1971**, 1404.

(18) Jorgensen, W. L.; Gao, J. *J. Am. Chem. Soc.* **1988**, *110*, 4212.

(19) Villani, V.; Alagona, G.; Ghio, C. *Mol. Eng.* **1998**, *8*, 135.

(20) Kang, Y. K.; Park, H. S. *J. Mol. Struct. (THEOCHEM)* **2004**, *676*, 171.

(21) Mantz, Y. A.; Gerard, H.; Iftimie, R.; Martyna, G. J. *J. Am. Chem. Soc.* **2004**, *126*, 4080.

(22) Mantz, Y. A.; Gerard, H.; Iftimie, R.; Martyna, G. J. *J. Phys. Chem. B* **2006**, *110*, 13523.

(23) Mantz, Y. A.; Branduardi, D.; Bussi, G.; Parrinello, M. *J. Phys. Chem. B* **2009**, *113*, 12521.

(24) Schäfer, L.; Alsenoy, C. Van; Scarsdale, J. N. *J. Chem. Phys.* **1982**, *76*, 1439.

(25) Bisetty, K.; Catalan, J. G.; Kruger, H. G.; Perez, J. J. *J. Mol. Struct. (THEOCHEM)* **2005**, *731*, 127.

(26) Pohl, G.; Perczel, A.; Vass, E.; Magyarfalvi, G.; Tarczay, G. *Phys. Chem. Chem. Phys.* **2007**, *9*, 4698.

(27) Cormanich, R. A.; Rittner, R.; Bühl, M. *RSC Adv.* **2015**, *5*, 13052.

(28) Neuman, R. C.; Jonas, V.; Anderson, K.; Barry, R. *Biochem. Biophys. Res. Commun.* **1971**, *44*, 1156.

(29) Mathieu, S.; Poteau, R.; Trinquier, G. *J. Phys. Chem. B* **2008**, *112*, 7894.

(30) Nguyen, K.; Iskandar, M.; Rabenstein, D. L. *J. Phys. Chem. B* **2010**, *114*, 3387.

(31) Doshi, U.; Hamelberg, D. *J. Phys. Chem. B* **2009**, *113*, 16590.

(32) Stewart, D. E.; Sarkar, A.; Wampler, J. E. *J. Mol. Biol.* **1990**, *214*, 253.

(33) Weiss, M. S.; Jabs, A.; Hilgenfeld, R. *Nat. Struct. Mol. Biol.* **1998**, *5*, 676.

(34) He, X.-L.; Li, H.-M.; Zeng, Z.-H.; Liu, X.-Q.; Wang, M.; Wang, D.-C. *J. Mol. Biol.* **1999**, *292*, 125.

(35) Jabs, A.; Weiss, M. S.; Hilgenfeld, R. *J. Mol. Biol.* **1999**, *286*, 291.

(36) Weiss, M. S.; Hilgenfeld, R. *Biopolymers* **1999**, *50*, 536.

(37) *cis-trans Isomerization in Biochemistry*; Dugave, C., Ed.; Wiley-VCH, Weinheim, 2006.

(38) Pal, D.; Chakrabarti, P. *J. Mol. Biol.* **1999**, *294*, 271.

(39) Touw, W. G.; Joosten, R. P.; Vriend, G. *Acta Crystallogr. Sect. D Biol. Crystallogr.* **2015**, *71*, 1604.

(40) Genshaft, A.; Moser, J.-A. S.; D'Antonio, E. L.; Bowman, C. M.; Christianson, D. W. *Proteins Struct. Funct. Bioinforma.* **2013**, *81*, 1051.

(41) Haindl, M. H.; Hioe, J.; Gschwind, R. M. *J. Am. Chem. Soc.* **2015**, *137*, 12835.

(42) Perrin, C. L.; Gipe, R. K. *J. Am. Chem. Soc.* **1984**, *106*, 4036.

(43) Perrin, C. L.; Dwyer, T. J. *Chem. Rev.* **1990**, *90*, 935.

(44) Becke, A. D. *J. Chem. Phys.* **1993**, *98*, 5648.

(45) Hariharan, P. C.; Pople, J. A. *Theor. Chim. Acta* **1973**, *28*, 213.

(46) Graham, D. C.; Menon, A. S.; Goerigk, L.; Grimme, S.; Radom, L. *J. Phys. Chem. A* **2009**, *113*, 9861.

(47) Henry, D. J.; Parkinson, C. J.; Radom, L. *J. Phys. Chem. A* **2002**, *106*, 7927.

(48) Baboul, A. G.; Curtiss, L. A.; Redfern, P. C.; Raghavachari, K. *J. Chem. Phys.* **1999**, *110*, 7650.

(49) Halkier, A.; Helgaker, T.; Jørgensen, P.; Klopper, W.; Koch, H.; Olsen, J.; Wilson, A. K. *Chem. Phys. Lett.* **1998**, *286*, 243.

(50) Goerigk, L.; Karton, A.; Martin, J. M. L.; Radom, L. *Phys. Chem. Chem. Phys.* **2013**, *15*, 7028.

(51) Dunning, T. H. *J. Chem. Phys.* **1989**, *90*, 1007.

(52) Miertuš, S.; Scrocco, E.; Tomasi, J. *Chem. Phys.* **1981**, *55*, 117.

(53) Xiong, R.; Sandler, S. I.; Burnett, R. I. *Ind. Eng. Chem. Res.* **2014**, 8265.

(54) Jensen, F. *J. Chem. Theory Comput.* **2008**, *4*, 719.

(55) Pye, C. C.; Ziegler, T.; van Lenthe, E.; Louwen, J. N. *Can. J. Chem.* **2009**, 790.

(56) ADF2014 COSMO-RS, SCM, Theoretical Chemistry, Vrije Universiteit, Amsterdam, http://www.scm.com.

(57) Gaussian 09, Revision D.01, Frisch, M. J.; Trucks, G. W.; Schlegel, H. B.; Scuseria, G. E.; Robb, M. A.; Cheeseman, J. R.; Scalmani, G.; Barone, V.; Mennucci, B.; Petersson, G. A.; Nakatsuji, H.; Caricato, M.; Li, X.; Hratchian, H. P.; Izmaylov, A. F.; Bloino, J.; Zheng, G.; Sonnenberg, J. L.; Hada, M.; Ehara, M.; Toyota, K.; Fukuda, R.; Hasegawa, J.; Ishida, M.; Nakajima, T.; Honda, Y.; Kitao, O.; Nakai, H.; Vreven, T.; Montgomery, J. A., J.; Peralta, J. E.; Ogliaro, F.;

Bearpark, M.; Heyd, J. J.; Brothers, E.; Kudin, K. N.; Staroverov, V. N.; Kobayashi, R.; Normand, J.; Raghavachari, K.; Rendell, A.; Burant, J. C.; Iyengar, S. S.; Tomasi, J.; Cossi, M.; Rega, N.; Millam, J. M.; Klene, M.; Knox, J. E.; Cross, J. B.; Bakken, V.; Adamo, C.; Jaramillo, J.; Gomperts, R.; Stratmann, R. E.; Yazyev, O.; Austin, A. J.; Cammi, R.; Pomelli, C.; Ochterski, J. W.; Martin, R. L.; Morokuma, K.; Zakrzewski, V. G.; Voth, G. A.; Salvador, P.; Dannenberg, J. J.; Dapprich, S.; Daniels, A. D.; Farkas, Ö.; Foresman, J. B.; Ortiz, J. V.; Cioslowski, J.; Fox, D. J. Gaussian Inc., Wallingford CT, 2009.

(58) Zhang, J.; Germann, M. W. *Biopolymers* **2011**, *95*, 755.

(59) Kumar, A.; Wagner, G.; Ernst, R. R.; Wuethrich, K. *J. Am. Chem. Soc.* **1981**, *103*, 3654.

(60) Schrödinger Release 2015-2: MacroModel, version 10.8, Schrödinger LLC, New York, 2015.

(61) Ponder, J. Tinker Software Tools for Molecular Design 7.1, 2015.

5 Organocatalytic One-Pot Nitroalkene Dimerization-Rearrangement to Enynes and Cyclic Nitronates: a NMR Study

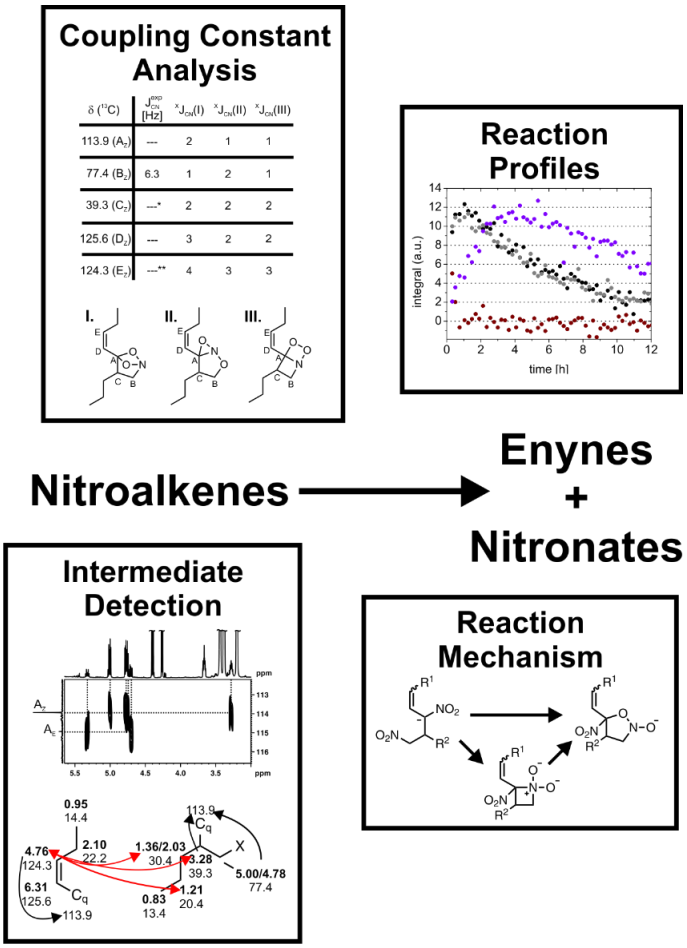

Initial NMR studies were performed by M. B. Schmid in close collaboration with K. Zeitler and also in part by F. v. Rekowski. Synthesis of **5a** and **2a**$_{15N}$ was performed by F. Morana and P. Renzi. Synthesis of **2f** and **2e** was performed by A. Zimmermann.

M. H. Haindl, M. B. Schmid, F. Morana, P. Renzi, F. v. Rekowski, A. Zimmermann, K. Zeitler, R. M. Gschwind,

to be submitted.

5.1 Abstract

NMR mechanistic investigations on a new organocatalytic nitroalkene dimerization followed by a base induced fragmentation to enynes or rearrangement to cyclic nitronates *via* a central uncommon bicyclic intermediate are presented. Product distribution is determined by the base strength and by the addition of benzoic acid as additive. Stronger bases favor the formation of a new bicyclic intermediate common to both products (enynes and nitronates), while the addition of benzoic acid suppresses the formation of cyclic nitronates and selectively enynes are formed. *In situ* NMR in combination with ^{13}C and ^{15}N labelling, allowed to detect key intermediate species - *e.g.* nitroalkene-catalyst adduct, nitroalkene dimer and a uncommon bicyclic intermediate – and unprecedented side products - *e.g.* molecular dinitrogen, carbon dioxide and water. Considering the importance of nitronates and conjugated enynes structural motifs, this mechanistic study should allow for a new entry to access these compounds from simple nitroalkenes. Since the structural motif of conjugated enynes occurs in many natural products and metal-free procedures are rare, an optimized enyne formation procedure is very valuable for organic synthesis.

5.2 Manuscript

Introduction

Nitroalkenes are valuable and versatile starting materials, especially for organocatalytic transformations.[1] Because of their high electrophilicity ("super-electrophiles"),[2] in fact, they belong to the most widely used acceptor species in organocatalytic Michael reactions. In this field, in particular in the direct catalytic asymmetric addition of aldehydes to nitroalkenes[3,4], mechanistic studies, recently, revealed, 4-membered cyclobutanes, 6-membered dihydro-oxazine *N*-oxide derivatives and linear nitro enamines, derived from γ-nitro aldehydes, as intermediate species. [5–7] In contrast, under the influence of bases, nitroalkanes are well-known to act as α-nucleophiles, for instance, in the addition to carbonyl species (Henry or Nitro-Aldol reaction) or to electron-poor alkenes.[8,9] In particular, the addition of nitroalkanes to nitroalkenes, promoted by bases,[10] (bis(oxazoline) and bis(thiazoline) zinc complexes,[11] cinchona alkaloids,[12] ammonium bifluorides,[13] or bifunctional amine-thiourea catalysts[14,15]) has been used to synthesize valuable 1,3-dinitro-compounds. On the other hand, according to the Baylis-Hillman reaction scheme, α-nucleophilic reactivity is also known for nitroalkenes under the influence of tertiary amine bases.[16] Additionally, in Rauhut-Currier type reactions, nitroalkenes were successfully used as α-nucleophiles together with α,β-unsaturated carbonyl compounds as electron deficient alkenes.[17,18] This chameleon-like reaction option of nitroalkenes, to act as α-nucleophiles and as β-electrophiles at the same time, is presumably also responsible for the formation of a nitroalkene-dimer as a by-product during the synthesis of β-nitronitriles in the presence of cyanide[19] and for the known tendency of nitroalkenes to polymerize,[2,8] especially under basic conditions.

The structural motif of a conjugated enyne occurs in many natural products and pharmaceuticals *e.g.* Dynemicin A[20], Terbinafine[21,22] (Lamisil®), Ponatinib[23] (Iclusig®) or Neocarzinostatin[24]. Synthetically, the most established methods for enyne formation are metal catalyzed cross-couplings, and especially the Pd^0 catalyzed versions (*e.g.* Hiyama coupling[25,26], Negishi coupling[27], Sonogashira coupling[28,29], Stille coupling[21] and Suzuki coupling[30]) are applied most frequently. Although metal free procedures to conjugated enynes would be very valuable for organic synthesis, in the literature they are rare.[31] Especially, organocatalytic methods for the synthesis of such enynes are to best of our knowledge unknown so far. On the other side, different organocatalytic approaches have been, recently, developed to access cyclic nitronates (isoxazoline-*N*-oxides).[32–36] This valuable compounds belong, in fact, to a class of versatile building-blocks which have been applied for the synthesis of

biologically active compounds[37,38], drug candidates[39–41] and natural products such as amino acids and amino sugars derivatives.[32]

We present here our NMR study on the metal free amine-catalyzed dimerization of nitroalkenes, followed, depending on the reaction conditions, by an unexpected fragmentation to conjugated enynes **3** or by the rearrangement to 5-membered cyclic nitronates **5**[42] (see Scheme 2). The mechanistic pathway leading to the dimerization was investigated by *in situ* NMR starting from nitroalkenes **1**. For an in depths investigation of the second part of the reaction, *i.e.* the rearrangement of the nitroalkene dimer **2** to enyne **3** or cyclic nitronate **5,** compound **2** was synthesized and used as starting material. Both of the mechanistic pathways from dimer **2** have a central, so far unknown, bicyclic intermediate **6** in common, which has not yet been discussed in the context of the commonly accepted reaction mechanism for the formation of cyclic nitronates.[43]

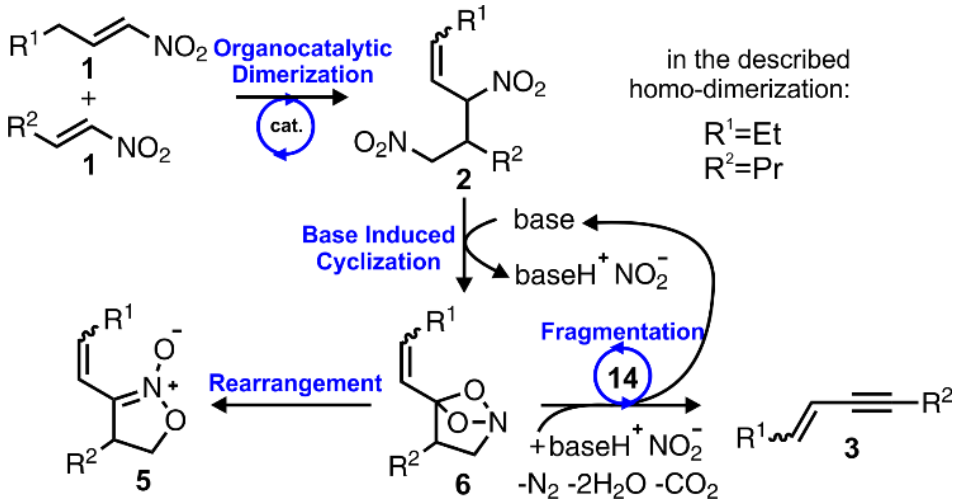

Scheme 2: An overview is provided for the formation of enyne **3** and cyclic nitronate **5** starting from two molecules of nitroalkene **1**. Detected key intermediate species (nitroalkene dimer **2** and bicyclic intermediate **6**) as well as detected side products (molecular dinitrogen, water and carbon dioxide) are included. cat.: catalyst, **14**: benzoic acid.

Model System

The mechanistic investigations were performed in DMSO-d_6 at room temperature unless otherwise indicated. For insights into the nitroalkene dimerization, nitropentene **1a** (also isotopically labeled **1a^{15}N** and **1a^{13}C**), 1-nitro-2-(2-nitrovinyl)benzene **1b** as well as 3-methylnitrobutene **1c** were selected as nitroalkenes. L-proline **10**, prolinol **11**, diphenylprolinol (DPP) **12** and the Jørgensen-Hayashi catalyst **13** were employed as catalysts, whereas benzoic acid **14** as well as *p*-nitrophenol **15** as acidic additives (see Fig. 70). For the cyclization, fragmentation and rearrangement reactions, nitroalkene dimers 5-nitro-6-(nitromethyl)non-3-ene **2a** (also completely ^{15}N labelled **2a^{15}N**), 1-(5-methyl-1,3-dinitrohex-4-en-2-yl)-2-nitrobenzene **2b** and 1-methoxy-2-

(5-methyl-1,3-dinitrohex-4-en-2-yl)benzene **2c** were chosen (see Figure 1). As bases DPP **12**, DBU **16** and triethylamine **17** and as additives benzoic acid **14** and *p*-nitrophenol **15** were tested. Direct enyne formation from nitroalkenes **1** could also be conducted in DMF-d_7 allowing for low temperature NMR investigations and simplified detection of intermediates towards dimer **2** due to lower reaction rates (see chapter 5.3.1).

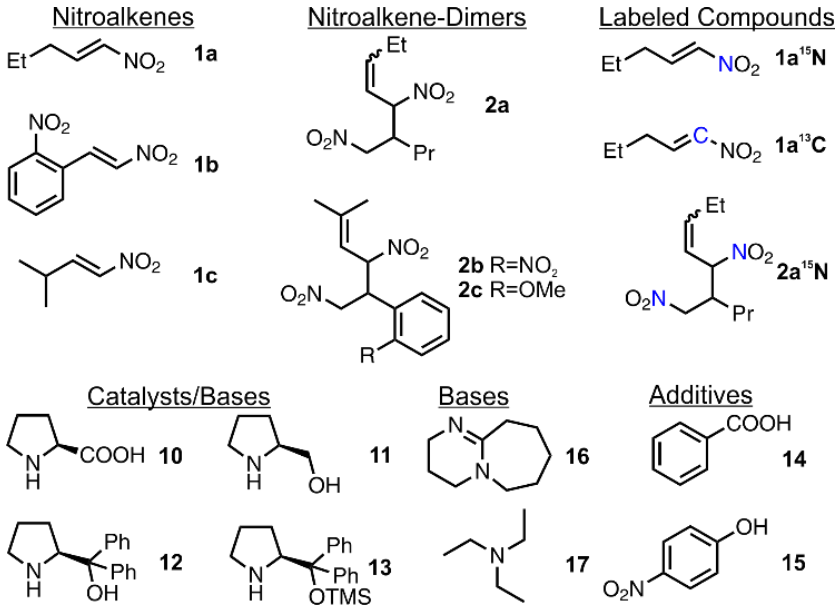

Fig. 70: All compounds applied in this study are shown. Blue atoms indicate isotopic labelling with NMR active isotopes (^{15}N, ^{13}C).

Results and Discussion

Enyne **3** as well as nitronate **5** formation from nitroalkenes **1** are multi-step processes (see Scheme 2). The first common step in both pathways is a dimerization reaction (Baylis-Hillman-Type) of nitroalkene **1** to its dimer **2** catalyzed by a secondary amine (see Fig. 71A). First, the nitrogen lone pair of the catalyst attacks the highly electrophilic β-carbon of **1**, resulting in the catalyst-nitroalkene adduct **18**. Using *e.g.* nitropentene **1a** as starting material, DPP **12** as catalyst and benzoic acid **14** as additive (see Fig. 71B), this adduct was detected and could be characterized by *in situ* NMR (for chemical shifts see chapter 5.3.2). Upon deprotonation in α-position to the nitro group, the α-carbon can attack another molecule of **1**. From the resulting catalyst-nitroalkene-nitroalkene adduct, the catalyst is released and the C-C double bond is reconstituted. Similar to the MBH reaction, the process rate increases with the addition of acids therefore a similar mechanism can be assumed. Notably, compared to the original nitroalkene **1a**, the double bond is now shifted and a deconjugated nitroalkene-dimer **2a** is formed. This shift of the double bond is in line with early reports that the ratio of deconjugated nitroalkenes is increased by α-substitution.[44]

In addition, the same regiochemical outcome was reported for the amine base-catalyzed addition of α,β-unsaturated nitroalkenes to aldehydes,[9] for the DBU-induced Baylis-Hillman reaction using nitroalkenes,[45] and for the tetramethylguanidine-catalyzed Michael addition of α,β-unsaturated nitroalkenes to electron-deficient olefins, such as α,β-unsaturated ketones, esters, nitriles, or sulfones.[9] Moreover, the unexpected preference of the *Z*-configuration of the nitroalkene-dimer is in line with a previous report on the observation of the dimer of 1-nitro-hept-1-ene.[19] The conditions in Fig. 71B led to the subsequent formation of enyne **3a** (final *E*/*Z* ratio of 5.6/1) as the major product and cyclic nitronate **5a** as a very low concentrated side product. The same intermediates and products *e.g.* nitroalkene-catalyst adduct **18**, nitroalkene-dimer **2** and enyne **3** were detected in the homo-dimerization of nitroalkene **1c** and also in the hetero-dimerization of nitroalkenes **1b** and **1c**. Applying secondary amine **13** as catalysts together with nitroalkene **1a** it was observed the same outcome in terms of products and detected intermediates as with catalyst **12.** On the other hand, with prolinol **11** no enyne **3** but only nitronate **5** was formed as the final product. With proline **10** the reaction stopped at the dimer **2**.

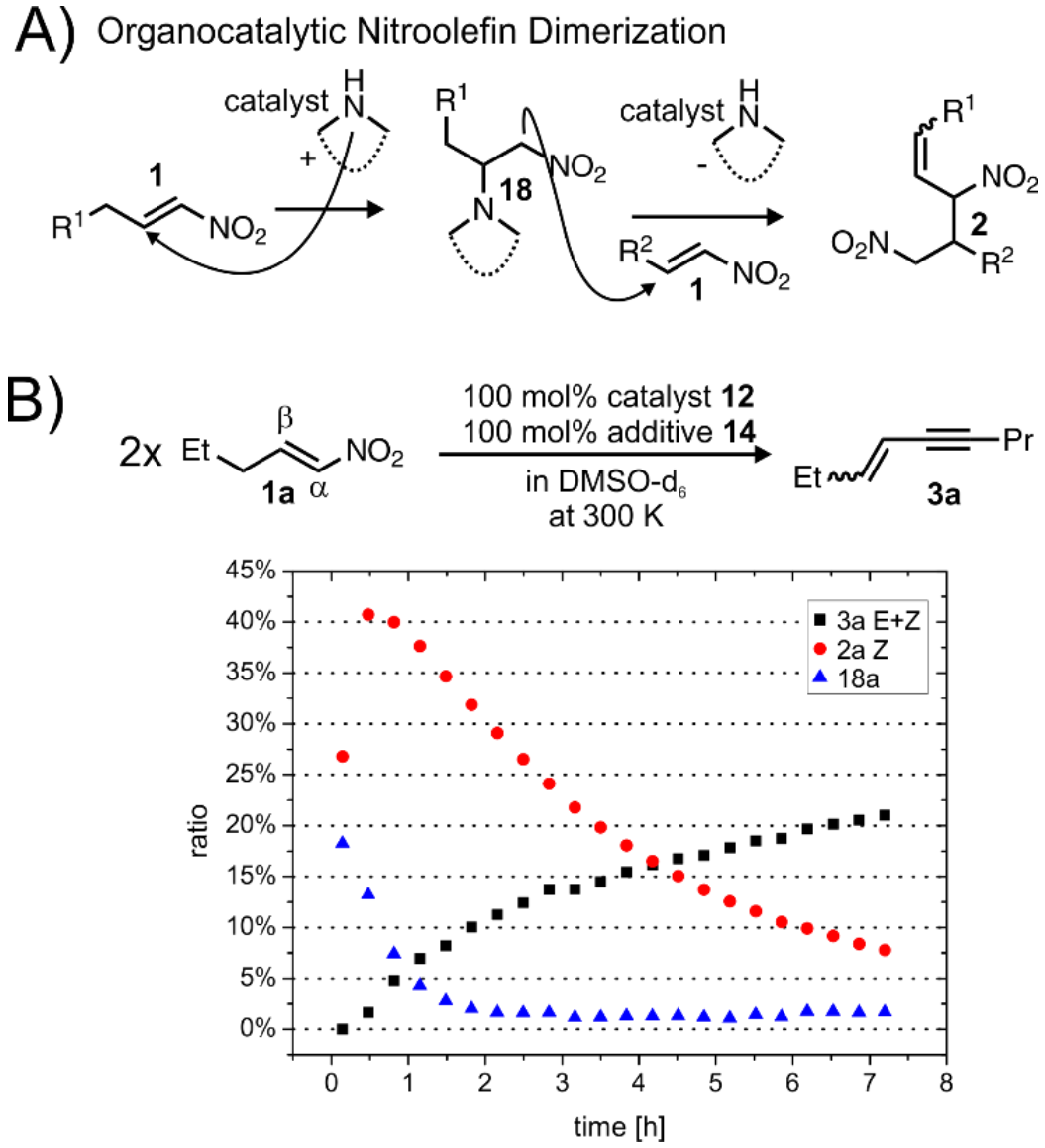

Fig. 71: Proposed mechanism of nitroalkene **1** dimerization to **2** is presented. B) Enyne **3a** formation conditions are presented starting from nitropentene **1a** (50 mM). The corresponding ^{1}H reaction monitoring below shows build-up and consumption of the intermediates nitroalkene-catalyst adduct **18a** and *Z* isomer of nitroalkene-dimer **2a**.

Starting from nitroalkenes **1** no further reaction intermediates could be detected. Furthermore, with L-proline **10** as catalyst the reaction was found to stop at the nitroalkene-dimer **2**. Therefore, the second part of the reaction was studied separately using the nitroalkene-dimer **2a** as starting material. With base and additive **14** mainly enyne **3a** is formed (see Fig. 72B, bottom profile; DBU and benzoic acid was added as the $DBUH^+PhCOO^-$ salt). Without additive the product distribution depends on the strength of the base. With increasing basicity the main product switches from enyne **3a** to nitronate **5a** (product distribution for *TEA*: 73% **3a** (67% *E*-isom.) / 27% **5a** (69% *Z*-isom.); *DPP*: 57% **3a** (58% *E*-isom.) / 43% **5a** (74% *Z*-isom.); *DBU* 24% **3a**

(51% *Z*-isomer) / 76% **5a** (84% *E*-isomer)) and the reaction rate increases drastically (the reaction was finished after 73 h with TEA, 15 h with DPP and 8 h with DBU). Under all experimental conditions used at least traces of the bicyclic intermediate **6a** were detected. Without additive and with stronger bases higher amounts of intermediate **6a** were detected, in case of DBU even a quantitative transformation at the beginning of the reaction was monitored (see Fig. 72B, top reaction profile). These data indicate a base dependent formation of the bicyclic intermediate **6** from nitroalkene-dimer **2** (see Figure 3A).

A possible mechanistic pathway starts with the deprotonation of the α-proton of the secondary nitro group. Next, either cycloaddition by intramolecular attack of the carbanion of **19** at the N=O oxygen occurs (see Fig. 72A, pathway a) and **21** is formed directly. Or the stabilized carbanion in **19** attacks the N=O nitrogen forming an unstable 4-membered intermediate **20** (see Fig. 72A, pathway b). Ring strain is than released by a rearrangement reaction and again **21** is formed. Subsequent attack of the oxyanion of **21** on the quaternary carbon atom and nitrite elimination leads to the bicyclic intermediate **6**.

The proton and carbon spin systems of the quite unusual intermediate **6a** (see chapter 5.3.2 for ^{1}H and ^{13}C chemical shifts) were identified by standard 2D NMR experiments (^{1}H-^{1}H COSY, ^{1}H-^{1}H NOESY, ^{1}H-^{13}C HSQC, ^{1}H-^{13}C HMBC). The positions of the heteroatoms were located using *in situ* ^{13}C-^{15}N coupling constant analysis on ^{15}N labeled **6a^{15}N**, applying **2a^{15}N** as starting material. For **6a^{15}N** exclusively one ^{13}C-^{15}N coupling constant was detected (6.3 Hz for *E*-isomer /6.4 Hz for *Z*-isomer) between the CH_2 carbon atom and the nitrogen atom (see orange bond of **6** in Fig. 72A). A comparison with the various detectable ^{13}C-^{15}N coupling constants in **2a^{15}N** (*Z*) ($^{1}J_{CN}$=6.5, 8.4 Hz; $^{2}J_{CN}$=~1.1 Hz; $^{3}J_{CN}$=~0.9-2.3 Hz) and **5a^{15}N** ($^{1}J_{CN}$=25.1 Hz/26.1 Hz (*Z*/*E*); $^{2}J_{CN}$=3.2 Hz (*E* and *Z*); $^{3}J_{CN}$=4.7-1.2 Hz (*E* and *Z*) for details see chapter 5.3.3) revealed this coupling in **6a^{15}N** to be a $^{1}J_{CN}$ coupling over a CN single bond. In contrast, neither ^{2}J couplings nor strong ^{1}J couplings (> 20 Hz) indicative for C=N^{+} double bonds were detected in **6a^{15}N**. Therefore, other heterocyclic structures providing the identical proton spin systems but an alternative arrangement of the heteronuclei could be excluded (for details refer to chapter 5.3.3). The quantitative formation of **6a** using DBU as base without additive and the subsequent formation of both, enyne **3a** and nitronate **5a** as products (see Fig. 72B, top profile), reveal a common mechanistic pathway of both reactions until the central intermediate **6**.

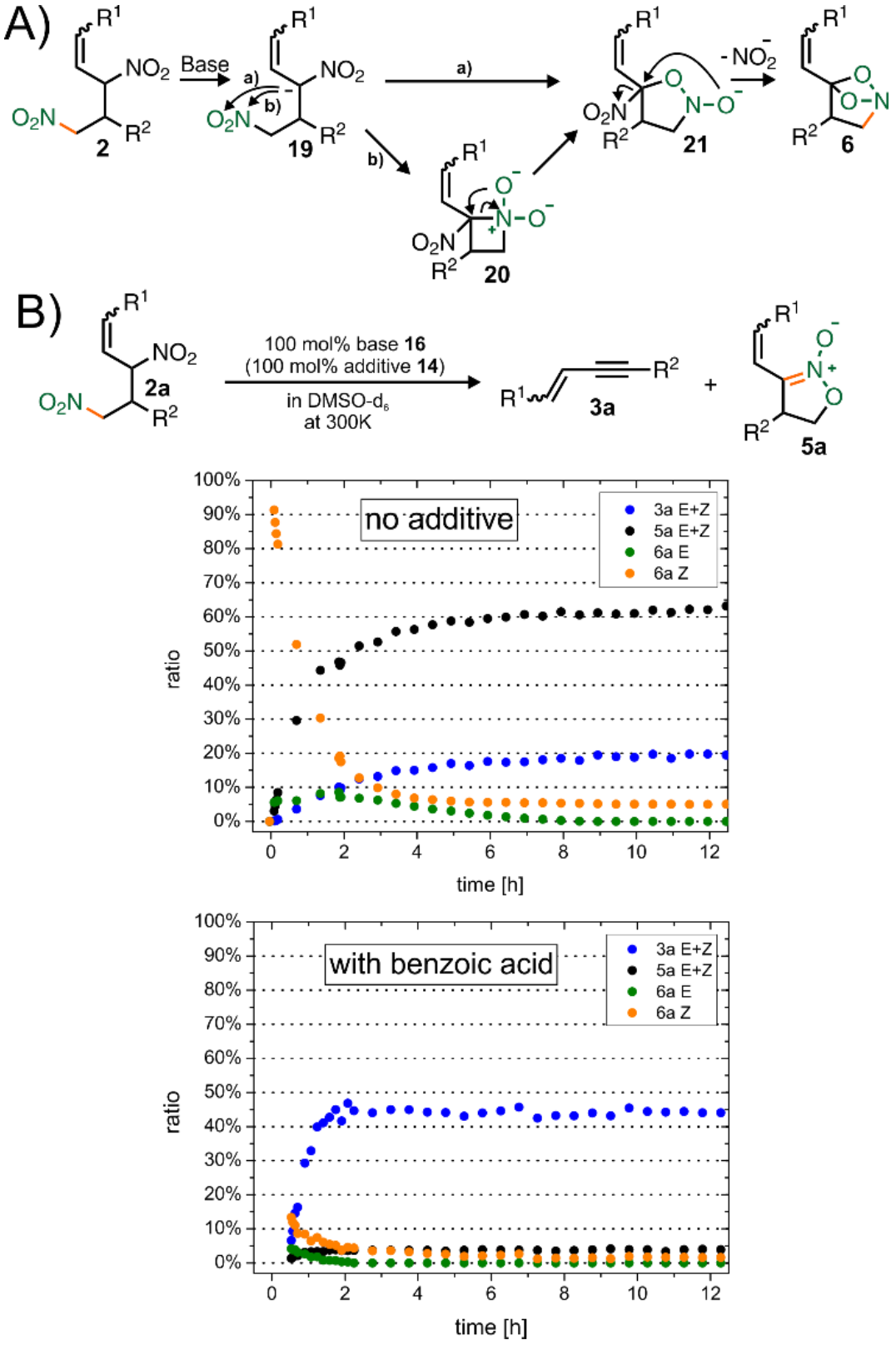

Fig. 72: A) Mechanistic proposal for the formation of the bicyclic central intermediate **6** from nitroalkene-dimers **2**. B) Reaction conditions and ^{1}H reaction monitoring for the formation of enyne **3a** and cyclic nitronate **5a** formation from nitroalkene dimer **2a** (R^1=Et, R^2=Pr) without (top) and with (bottom) the additive benzoic acid **14** as additive (the $DBUH^+PhCOO^-$ salt was applied). Final *E*/*Z* ratios with (without) benzoic acid are 1.0 (2.2) for enyne **3a** and 4.7 (2.9) for cyclic nitronate **5a**. In A) and B) the remaining nitro groups are marked in green and $^1J_{CN}$ bonds used for coupling constant analysis (see text) are marked in orange.

The reaction mechanism from the central intermediate **6** to the product enyne **3** seems to be a multi-step process (see Scheme 3A). Experimentally, evolution of $^{13}CO_2$ was detected by ^{13}C NMR applying labelled nitropentene **1a-^{13}C** and catalyst/base **12** with or without the addition of benzoic acid **14** (for details see chapter 5.3.5). *In situ* detection of $^{15}N_2$ by ^{15}N NMR was possible when labelled dimer **2a-^{15}N** was used as starting material, **12** as base and additive **14** (for details see chapter 5.3.7). Additionally, starting from the dimer **2a** and using base **12**, exclusively under acidic conditions (with additive **14**) water generation was monitored by ^{1}H NMR (for details see chapter 5.3.6).

On the basis of these experimental results, we propose a reaction mechanism (see Scheme 3A) from intermediate **6** to enyne **3** consisting of three steps, *i.e.* E1 elimination and ring opening, allylic oxidation and a retro-1,3-dipolar cycloaddition reaction. The most obvious elimination of nitromethane can be excluded, because its characteristic signals do not accumulate during the reaction and the traces sometimes detected originate from impurities of the starting materials, *i.e.* nitroalkenes. We assume that the reaction from **6** to **3** starts with an E1 elimination and ring opening reaction (see Scheme 3A). This proposal is backed by substitution pattern variation experiments on residue R^2 of the nitroalkene-dimer **2** with differently substituted phenyl rings. An electron poor *ortho* nitro substituted phenyl ring stabilizes the initially generated carbanion by the E1 mechanism and leads to higher reaction rates and yields of **3** than an electron rich *ortho* methoxy substituted phenyl ring (for details see chapter 5.3.4).

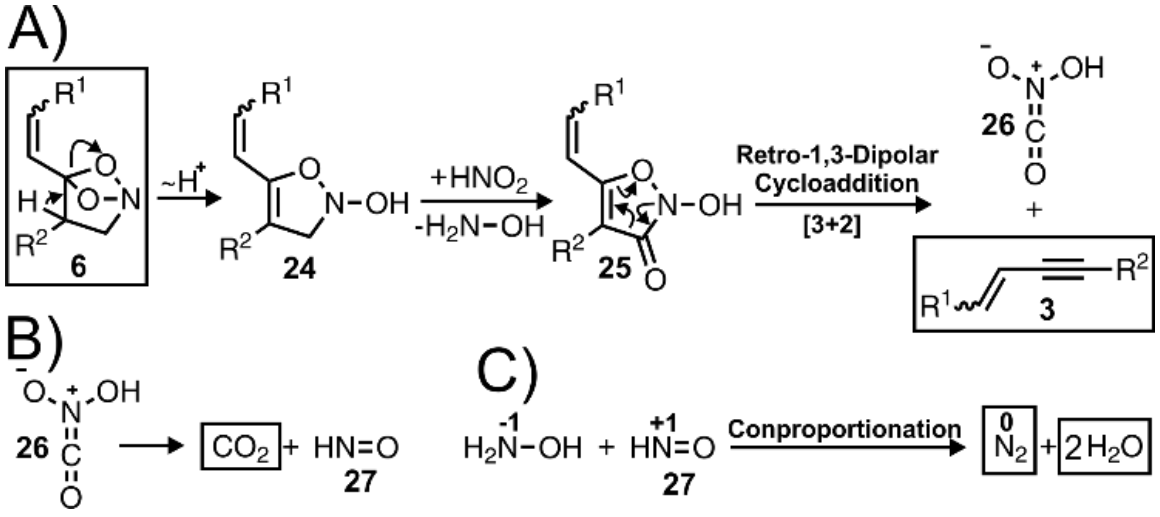

Scheme 3: Mechanistic proposals for A) the formation of enyne **3** from intermediate 6, B) the decomposition of side product **26** to carbon dioxide and oxanone **27** and C) the conproportionation of hydroxylamine and oxanone **27** to molecular dinitrogen and water. Products and intermediates which were detected by NMR are boxed.

The second reaction step is an allylic oxidation of the CH_2 group of **24** either by HNO_2 (generated from the reaction of dimer **2** to intermediate **6**, see Fig. 72A) or by HNO_3 (generated from decomposition of HNO_2) forming **25** and hydroxylamine. Subsequently, a retro-1,3-dipolar cycloaddition reaction of **25** yields product enyne **3** and **26**, a presumably very instable compound which could be described as an "oxidized nitrone". Normal nitrones **29** are well known for forward 1,3-dipolar cycloadditions with terminal alkynes in presence of copper iodide for the synthesis of β-lactams **31** (see Scheme 4A).[46] The mechanism[47] of this reaction involves a 5-membered ring **30** as cycloaddition product which shows a strong structural similarity with the retro-1,3-dipolar cycloaddition starting point **25**. We propose the decomposition of the instable side product "oxidized nitrone" **26** to carbon dioxide (as detected experimentally) and oxanone **27** (see Scheme 3B). Again, there is a similarity to normal nitrones **29**. Synthesis of nitrones **29** can be accomplished by a condensation reaction of carbonyl compounds (mostly aldehydes **32**) and N-alkylated hydroxylamines **33** (see Scheme 4B).[43,48] Furthermore, we propose a conproportionation reaction of oxanone **27** and hydroxylamine to the experimentally detected side products molecular dinitrogen and water under acidic conditions (see Scheme 3C).

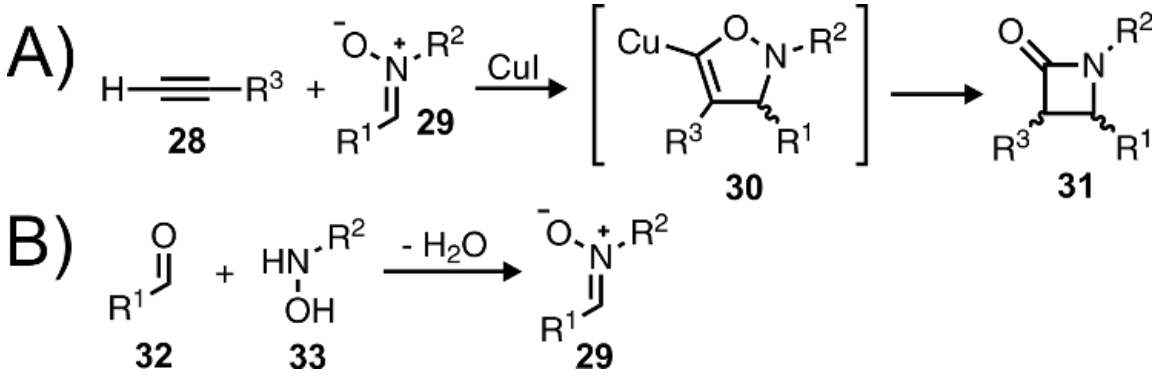

Scheme 4: The literature known A) 1,3-dipolar cycloaddition reaction of nitrones **29** and terminal alkynes **28** to β-lactams **31** (Kinugasa reaction) and B) synthesis of nitrones **29** from carbonyl compounds **32** and N-alkylated hydroxylamines **33** are shown.

Formation of the second product cyclic nitronate **5** from the bicyclic intermediate **6** presumably proceeds *via* a cascade of rearrangement steps including two strongly ring strained bicyclic intermediates (see Scheme 5).[g] The reaction is initialized by an attack of the nitrogen lone pair of **6** at the quaternary carbon center followed by a C-O bond cleavage to form intermediate **22**. Next the oxygen anion attacks the neighboring CH_2 carbon and the C-N bond breaks to form **23.** This process could be driven by ring strain reduction (4-membered to 5-membered ring). Last, opening of the

[g] An alternative mechanism would start with N-nitration of the quaternary carbon atom of **6** by nitrite, similar to a proposed pathway for the conversion of secondary nitro derivatives to oximes and ketones.[71] However, here, addition of acid would promote the reactivity. Since benzoic acid is instead suppressing the formation of nitronate, such a mechanism is excluded.

3-membered ring of **23** by C-O bond breakage and C=N double bond formation yields product **5**. Addition of benzoic acid **14** suppresses the formation of cyclic nitronate **5** (see Fig. 72B, bottom profile) but the reason is not clear so far. Surprisingly, the suppression is not due to the pure acidity of the additive, because application of *p*-nitrophenol **15** (**14** and **15** have the same acidity in DMSO) does not show this effect (for details refer to chapter 5.3.9).

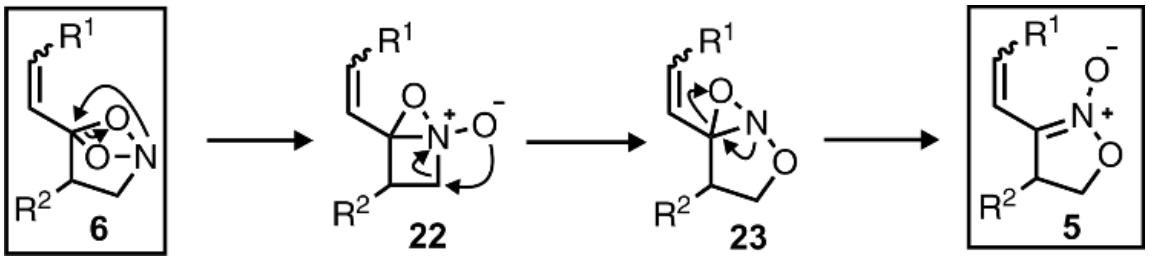

Scheme 5: Mechanistic proposal for the formation of nitronate **5** from intermediate **6**. Products and intermediates which were detected by NMR are boxed.

Conclusion

In summary, we present a mechanistical study on a new reaction of nitroalkenes. Catalyzed by a secondary amine, nitroalkene-dimers are formed, followed by a base induced cyclization to a bicyclic intermediate and subsequent competing reactions to conjugated enynes and cyclic nitronates. The central mechanistic step of enyne formation is a retro-1,3-dipolar cycloaddition reaction. Product distribution depends on the base strength and addition of benzoic acid. Stronger bases favor cyclic nitronates whereas addition of benzoic acid suppresses their formation and leads to selective formation of enynes. Key intermediate species – *e.g.* nitroalkene-catalyst adduct, nitroalkene dimer, the bicyclic intermediate – as well as unprecedented side products *e.g.* molecular dinitrogen, carbon dioxide and water - were detected by *in situ* NMR. This mechanistic study is meant to enable the development of a novel metal free reaction pathway to enynes in organic synthesis. We are planning to report synthetic studies on this enyne and nitronate formation in the near future.

5.3 Supporting Information

5.3.1 Low Temperature Measurements

In order to slow down the reaction rate and possibly enable the detection of further short lived intermediates and/or to improve the outcome of the reaction in terms of the yield, low temperature measurements were envisaged. Because of the high melting point of DMSO (292 K), these measurements were conducted in DMF which stays liquid down to 212 K. Fig. 73 (left-hand side) shows NMR reaction kinetics of **1a** (40 mM), DPP **12** (50 mol%) and benzoic acid **14** (50 mol%) in DMF-d_7 at 270 K. As expected the reaction rate is strongly decelerated compared to the reaction at 300 K in DMSO-d_6. The build-up and decrease of two intermediates in the enyne formation reaction, *e.g.* the catalyst-nitroalkene adduct **18a** and the dimer **2a** (total) (Z, both diastereoisomers) was monitored. **18a** reaches a maximum concentration after about 0.5 days, the dimer **2a** after about 1.75 days. Surprisingly, the maximum concentration of **18a** and the maximum slope of **2a** (total) do not occur simultaneously. This should be the case if the former is the direct precursor of the latter in the reaction mechanism. In fact the maximum slope of **2a** (total) already occurs earlier in the reaction profile which indicates that in DMF there must be an alternative active reaction pathway from the nitroalkene **1** to the nitroalkene-dimer **2**. In contrast, the maximum slope of the enyne build-up **3a** does occur simultaneously with the maximum concentration of the dimer **2a** (total) and therefore confirms **2** as precursor of **3** in DMF.

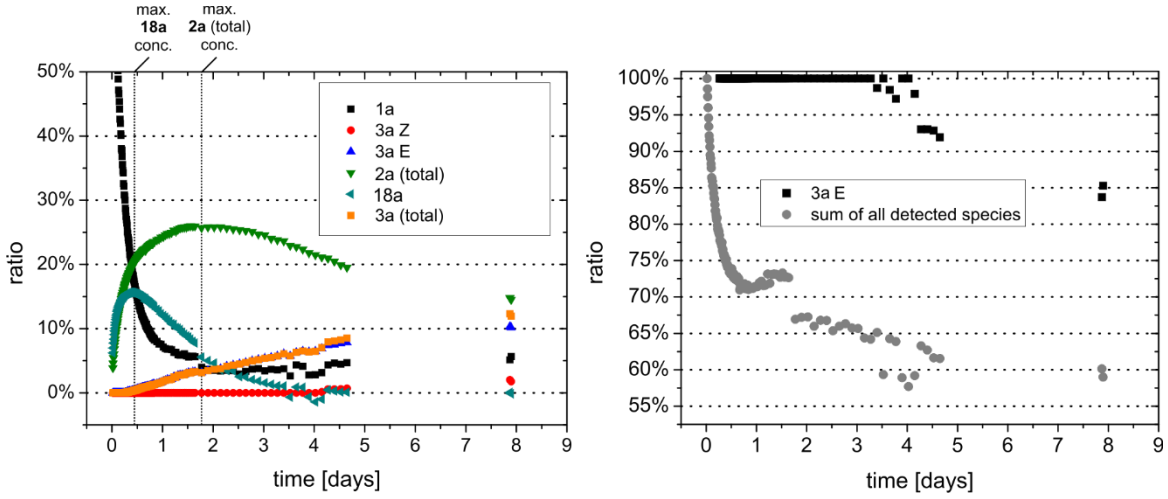

Fig. 73: Left shows NMR reaction kinetics of **1a** (40 mM), DPP **12** (50 mol%) and benzoic acid **14** (50 mol%) in DMF-d_7 @ 270 K. Right shows the E/Z ratio (in % E) of **3a** and the sum of all detected species. (The sum was set to 100% in the first spectrum)

After an initialization phase, the total enyne amount **3a** (total) shows a linear increase up to about 5 days reaction time and reaches about 12.5% (25% yield) after 8 days (34% yield after 15 days, data not shown). Interestingly, until about 3 days the

E-ratio of **3a** is 100% (see Fig. 73, right-hand side). Afterwards, the ratio starts to decrease and reaches about 85% after 8 days. This means that the enyne formation in DMF is stereoselective for the *E*-isomer and the *Z*-isomer is formed *via* a downstream isomerization process. Also noticeable is the loss of signal intensity for the sum of all detected species derived from **1a** (see Fig. 73, right-hand side) most severe in the beginning of the reaction (about 70% after 0.5 days reaching 60% after 8 days). This effect also occurs in DMSO at 300 K and is most probably connected with an active polymerization process, consuming either/and nitroalkene **1a**, dimer **2a,** or enyne **3a**.

Although the reaction rate was drastically decelerated by monitoring enyne **3a** formation from nitropentene **1a** at low temperatures (270 K), no additional short lived reaction intermediates could be detected and the yield of the reaction was not improved.

5.3.2 Miscellaneous ^{1}H and ^{13}C Chemical Shift Assignments in DMSO-d_6

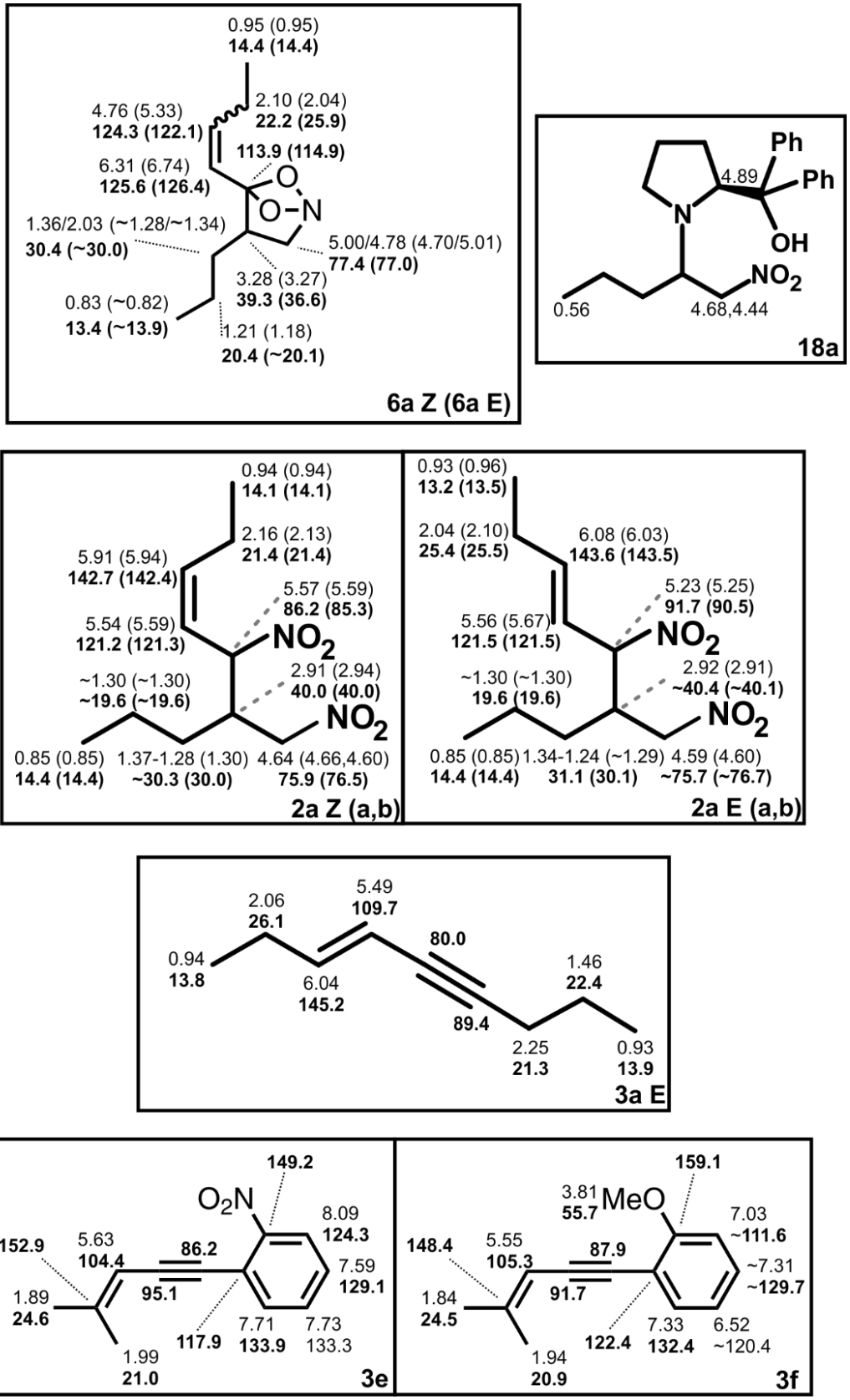

Fig. 74: ^{1}H (normal font) and ^{13}C (bold) chemical shift assignments are shown of miscellaneous molecules detected *in situ* in DMSO-d_6 @ 300 K at 600 MHz referenced to TMS.

5.3.3 Identification of the Central Intermediate 6 - $^{13}C^{15}N$ Coupling Constant Analysis

The species we identified as the central intermediate **6a** in the enyne **3a** and cyclic nitronate **5a** formation was detected applying a reaction mixture of 80 mM nitroalkene-dimer **2a** (for synthesis procedures see chapter 5.3.11) and 100mol% of either DBU **16**, triethylamine (TEA) **17** or diphenylprolinol (DPP) **12** in DMSO-d_6 at room temperature. For the samples with TEA and DPP only traces of **6a** were detected at the very beginning of the reaction. In contrast, in the DBU sample **6a** was instantly formed nearly quantitatively as a mixture of 6% *E*-isomer and 94% *Z*-isomer and reached about 25% (sum of isomers) after a reaction time of two hours (see Fig. 72B in the manuscript, bottom profile). After about 8 hours **6a** was completely consumed and with a yield of about 42% **5a** was formed. Also the corresponding enyne **3a** could be detected, but only with a final ratio of about 19%. Nevertheless this indicates that **6** is a central intermediate in the enyne **3** formation reaction as well as in the formation of cyclic nitronates **5** from nitroalkene-dimers **2**.

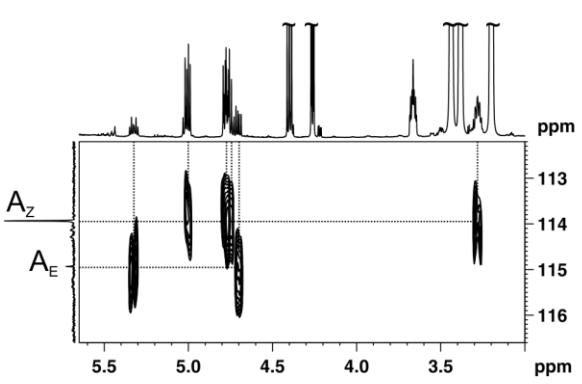

δ (^{13}C)	J_{CN}^{exp} [Hz]	$^{X}J_{CN}$(I)	$^{X}J_{CN}$(II)	$^{X}J_{CN}$(III)
113.9 (A_Z)	---	2	1	1
77.4 (B_Z)	6.3	1	2	1
39.3 (C_Z)	---*	2	2	2
125.6 (D_Z)	---	3	2	2
124.3 (E_Z)	---**	4	3	3

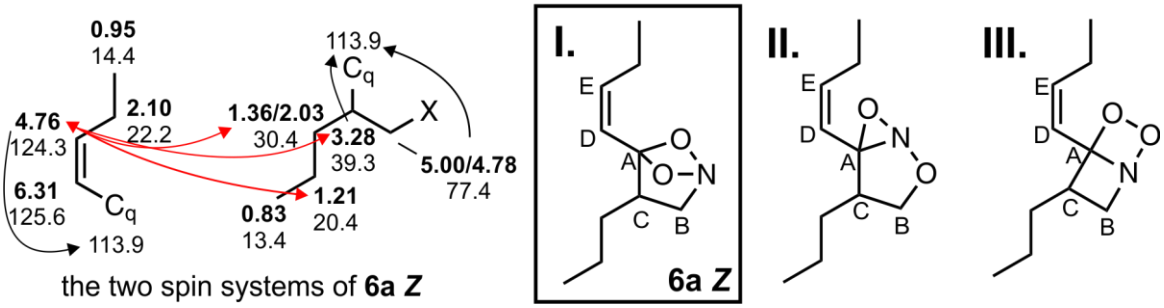

Fig. 75: Bottom left shows the two separated spin systems of **6a** *Z* including its ^{1}H (bold) and ^{13}C (normal) chemical shifts (in ppm) and the proof of their connectivity *via* the common quaternary carbon atom (C_q) through ^{1}H-^{1}H NOE contacts (red arrows) and ^{1}H-^{13}C HMBC crosspeaks (black arrows). A slice of the ^{1}H-^{13}C HMBC spectrum showing the corresponding cross peaks for **6a Z** as well as for **6a E** is depicted in the top left. Bottom right shows the three candidate structures (constitutional isomers) for **6a Z**. Top right shows experimental determined ^{13}C-^{15}N scalar coupling constants (J_{CN}^{exp}) for carbon atoms A to E of the corresponding ^{15}N labeled compound **6a** $\mathbf{Z}_{^{15}N}$. In addition the number of bonds (X) of the theoretical scalar coupling in the candidate structures is listed. * (signal overlap) / ** (a very broad ^{13}C signal) prevent reliable coupling constant extraction.

The high concentration of **6a** in the DBU sample enabled the application of 2D ^{1}H-^{1}H COSY, ^{1}H-^{13}C HSQC, ^{1}H-^{1}H NOESY and ^{1}H-^{13}C HMBC NMR experiments and the thereof generated ^{1}H and ^{13}C chemical shifts, coupling patterns and connectivities of spin systems, together with NOE data lead to three different candidates for the identity of the intermediate species (see Fig. 75 **I**-**III**). A slice of a HMBC spectrum which shows the connectivity of both separated spin systems of **6a Z** (also for **6a E**) over the quaternary carbon atom A_Z (A_E) is also shown in Fig. 75. In the first spin system, the proton resonance at 4.76 ppm shows an allylic $^{3}J_{HC}$ coupling to A_Z whereas in the second spin system three proton resonances (at 3.28 ppm, 5.00 ppm and 4.78 ppm) show J couplings to the same carbon atom which positively proofs spin system connectivity. This is further confirmed by NOE contacts of the proton at 4.76 ppm of the first spin system with protons at 1.36 ppm, 3.28 ppm and 1.21 ppm of the second spin system (see Fig. 75, bottom left-hand side, red arrows). In order to distinguish between the three candidate structures **I**-**III**, additionally, experimental ^{13}C-^{15}N coupling constants were necessary. Therefore, **2a Z**$_{15N}$**,** the double ^{15}N-labeled analogue of **2a** was synthesized starting with ^{15}N-labeled nitroalkene **1a**$_{15N}$ and applied in the reaction with DBU in DMSO-d_6. ^{13}C-^{15}N coupling constants were extracted from 1D proton decoupled ^{13}C spectra (for spectra see chapter 5.3.12). A summary of the extracted coupling constant and the number of bonds (X) of the theoretical scalar coupling in the candidate structures **I-III** for **6a Z**/**6a Z**$_{15N}$ is shown in Fig. 75, top right-hand side. Depending on the compound, typically the magnitude of $^{1}J_{CN}$ coupling constants is lying in the range of 2 – 36 Hz.[49] Medium range $^{2}J_{CN}$ and $^{3}J_{CN}$ coupling constants are smaller (1 – 11 Hz and 0.7 – 6 Hz) and especially in saturated systems sometimes are undetectable.[49] Examples for ^{13}C-^{15}N couplings over more than 3 bonds are very rare, these coupling constants typically are very low (0.3 – 3.9 Hz) and can only be extracted from unsaturated compounds.[49] In the actual experiment only the ^{13}C signal at 77.4 ppm (B) shows a distinct coupling (6.3 Hz) to a ^{15}N atom which would correspond to a ^{1}J coupling in molecules **I** and **III** and a ^{2}J coupling in molecule **II** (for spectra see chapter 5.3.12). Most importantly, for carbon A, no coupling constant could be extracted. This excludes molecules **II** and **III**, because in both structures A is directly connected to a nitrogen atom and should therefore show a strong ^{1}J coupling. (For comparison $^{1}J_{CN}$ coupling constants extracted from ^{15}N labeled **2a** (6.5-7 Hz) and **5a** (25.1-26.1 Hz) in CD_2Cl_2 are presented in chapter 5.3.12) Only in molecule **I** the coupling would be a ^{2}J coupling which may not be detectable (see above and data for **2a** and **5a** in chapter 5.3.12). Among the three candidate structures only molecule **I** remains plausible. Since the intermediate was not isolated, no exact mass is available and we cannot exclude that the molecular formula is different. However, especially the presence of a second nitrogen atom in molecule **6** is considered unlikely because, it would be most likely be attached to carbon A

(derived from its precursor the nitroalkene-dimer **2**) and carbon A therefore had to show a strong ^{1}J coupling, which is not the case. Since only one strong ^{13}C-^{15}N nitrogen coupling is observed at all, in general, a second nitrogen atom directly attached to a carbon atom can definitely be excluded. Intermediate **6a Z** is therefore assigned to molecule **I**, 4-(but-1-en-1-yl)-3-propyl-5,6-dioxa-1-azabicyclo[2.1.1]hexane. The configuration of the double bond was derived from the proton coupling constants of D and E attached protons (**6a Z**: $^{3}J_{DE}$ = 12 Hz; **6a E**: $^{3}J_{DE}$ = 16 Hz). For the chemical shift assignment of **6a** please refer to chapter 5.3.2.

5.3.4 Influence of Electronic Structure of the Nitroalkene-Dimer 2

In order to investigate the influence of the electronic structure of the starting material nitroalkene-dimer **2** on its reactivity in the enyne **3** and nitronate **5** formation reactions, the two sterically very similar but electronically different nitroalkene-dimers ,1-(5-methyl-1,3-dinitrohex-4-en-2-yl)-2-nitrobenzene **2e** and 1-methoxy-2-(5-methyl-1,3-dinitrohex-4-en-2-yl)benzene **2f** were synthesized (for procedures refer to chapter 5.3.11). The compounds only differ in the ortho-substituent of the phenyl moiety which is an electron deficient nitro group for **2e** and an electron rich methoxy group for **2f** (see Fig. 76, top left-hand side).

The proposed reaction mechanisms in the manuscript from the nitroalkene-dimers **2** to enynes **3** or cyclic nitronates **5** contain two deprotonation steps, at position 3 (nitroalkene-dimer **2e**/**2f** → central intermediate **6e**/**6f**; see Fig. 76, top left-hand side) and at position 2 *(*bicyclic intermediate **6e**/**6f** → enyne **3e**/**3f**; see Fig. 76, top right-hand side) of the longest linear carbon chain which result in electron rich carbanions, respectively. Only the carbanion located at position 2 can participate in the conjugated π-system of the phenyl moiety of the starting material and therefore it is assumed that the different ortho substituents have the strongest effect on the reaction step **6e**/**6f** → **3e**/**3f**. The electron deficient nitro substituent (-M effect) of **6e** should stabilize the carbanion (see Fig. 76, middle, left-hand side) and therefore accelerate the enyne **3e** formation. In contrast, the electron rich methoxy substituent (+M effect) of **6f** should destabilize the carbanion species and consequently reduce the corresponding reaction rate towards **3f**. If this assumptions can be confirmed, this would hint at a deprotonation step at position 2 being rate determining in the formation of enynes **3** from nitroalkene-dimers **2** and would therefore support the new reaction mechanism for this reaction proposed in the manuscript.

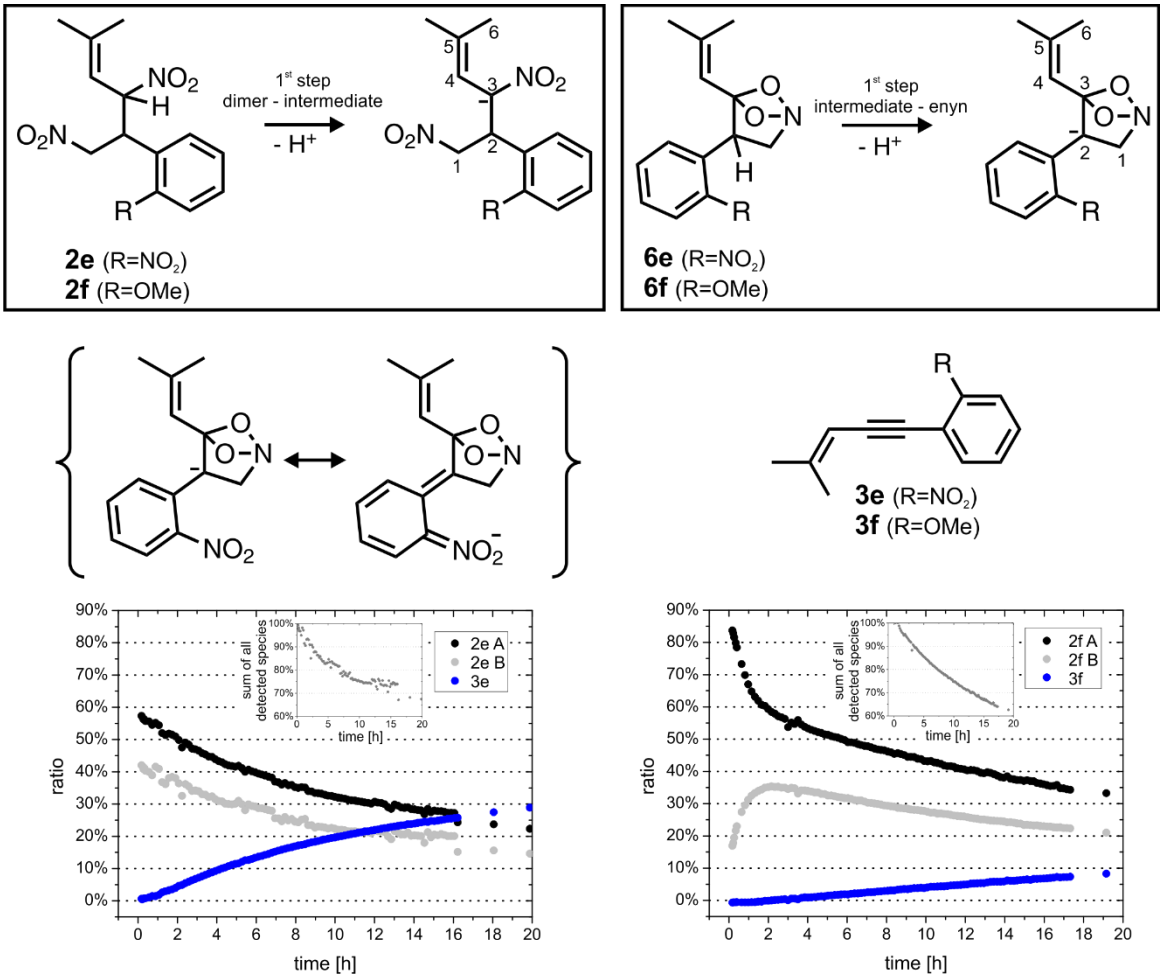

Fig. 76: Top shows the two initial deprotonation steps from the proposed mechanisms from nitroalkene-dimers **2e/2f** to the bicyclic intermediates **6e/6f** and the first reaction step from **6e/6f** to enynes **3e/3f**. Middle shows the mesomeric stabilization of the **6e** derived carbanion. No such stabilizing structure can be drawn for the carbanion derived from **6f**. Bottom shows the two ^{1}H reaction kinetics of **2e** (left) / **2f** (right) (40 mM), benzoic acid **14** (20 mM) and DPP **12** (20 mM) in DMSO-d_6 @ 300 K. The small plots show the progress of the sum of detected species during these reactions.

Both nitroalkene-dimers **2e** (nitro substituted) and **2f** (methoxy substituted) were applied in ^{1}H NMR *in situ* reaction monitoring in DMSO-d_6 at 300K, together with 50 mol% of DPP as organic base and 50 mol% benzoic acid, respectively. The results (Fig. 76, bottom) show that in both cases the nitroalkene-dimers **2e**/**2f** are consumed and enyne formation **3e**/**3f** occurs (for ^{1}H and ^{13}C chemical shift assignment refer to chapter 5.3.2). No cyclic nitronate **5e**/**5f** and no other reaction products were identified. The loss in sum of the detected species (see plots in plots), is most probably due to an active polymerization process, and is similar in both cases (30%-40%).

In fact, as assumed, the rate of enyne **3e**/**3f** formation is considerably higher for the nitro substituted starting material **2e** than for the methoxy substituted one **2f**. Nitro substituted enyne **3e** reached an *in situ* yield of about 30% after 20 hours, whereas in the same time methoxy substituted **3f** only reaches about 10%. As stated above,

this difference in rates supports the new proposed mechanism from nitroalkene-dimers **2** to enynes **3** over the bicyclic intermediates **6**. Also noticeable is the monitored active isomerization process of the two diastereoisomers of the methoxy substituted nitroalkene-dimer **2f** (see Fig. 76, bottom, right-hand side). Isomer **2f A** was consumed throughout the reaction time of 20 hours. In contrast, in the beginning of the reaction, **2f B** built up from about 15% to 35 % after two hours and in the following started to decrease, reaching an equilibrium with its isomer **2f A** in the end of the monitoring period.

As isomerization of the diastereomers of nitroalkene-dimers **2** must occur via C-C bond breakage, it is most probable that nitroalkene **1** dimerization is a reversible process (see Fig. 77), which means that always small amounts of the corresponding nitroalkenes are present during these reactions. This could explain the omnipresent polymerization process which was monitored in most of the herein presented enyne **3** and nitronate **5** formations starting from nitroalkene-dimers **2**, because the tendency for polymerization of nitroalkenes is well known.[2,8]

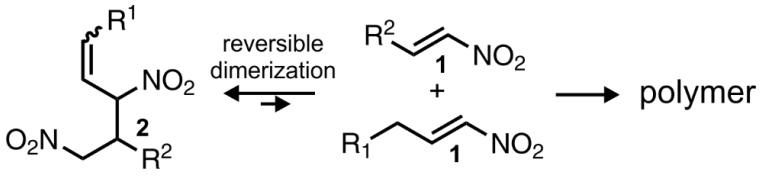

Fig. 77: Reversibility of nitroalkene **1** dimerization to dimer **2** would mean that low amounts of **1** are always present if **2** is applied in enyne **3** or nitronate **5** formation reactions and could explain the, in the current work, in that context most of the time monitored decrease of sum of detected species by the literature known polymerization of **1**. If **2** is a homo-dimer, the two involved nitroalkenes are identical *e.g.* for linear nitroalkenes length(R^1)=length(R^2)+1. If **2** is a hetero-dimer the two nitroalkenes are different.

5.3.5 Carbon Dioxide Formation

Comparing intermediate **2** (nitroalkene-dimer) with the product **3** (enyne), it is obvious that in the reaction process one carbon atom gets cleaved. The most obvious fate of this carbon would be an elimination of $[CH_2NO_2]^-$. However, accumulation of nitromethane in parallel to product formation has never been observed and the previously reported[50] amount of nitromethane present actually is a contamination of the starting material. In addition, enyne **3a** formation is always accompanied by ascending gas bubbles from the reaction mixture. In order to elucidate the fate of the lost carbon atom, starting material $\mathbf{1a}_{13C}$ was synthesized ^{13}C-labeled on the α-carbon atom, according to a literature procedure.[51] *In situ* ^{13}C NMR monitoring of the enyne formation reaction of $\mathbf{1a}_{13C}$ catalyzed by DPP **12** in DMSO-d_6 (see Fig. 78) showed that in parallel to the formation of the expected product $\mathbf{3a}_{13C}$ carbon dioxide is forming with a ^{13}C chemical shift of 124.2 ppm (literature chemical shift in DMSO-d_6: 124.2 ppm)[52]. Similar results were obtained using additionally benzoic acid (50 mol%) as additive.

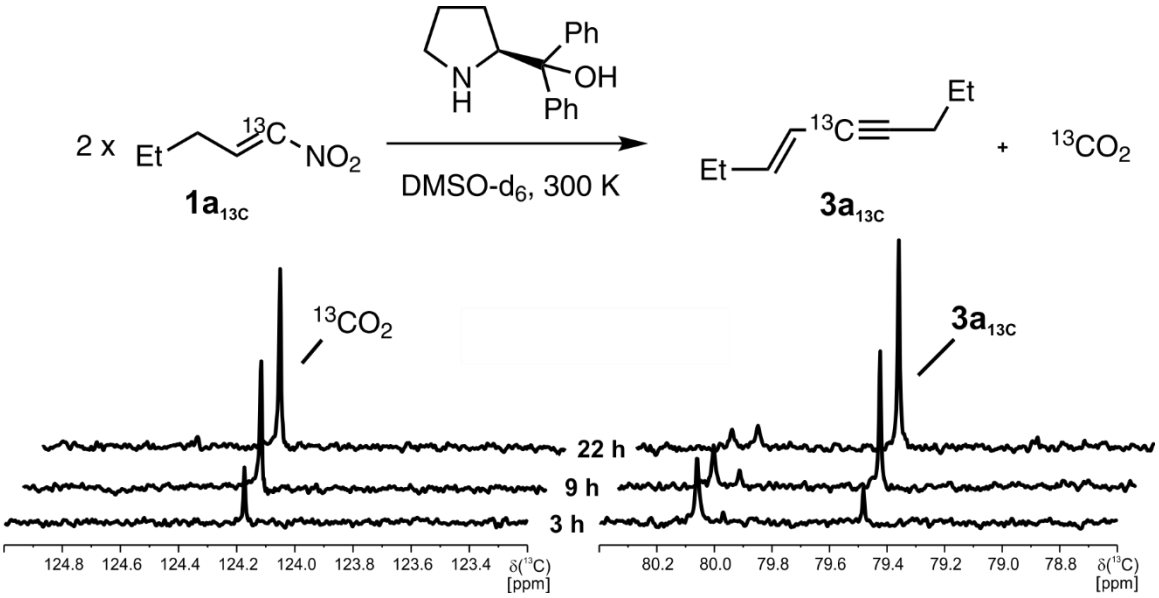

Fig. 78: Reaction conditions and ^{13}C NMR monitoring of the formation of ^{13}C labeled product **3a**$_{13C}$ and carbon dioxide is shown starting from **1a**$_{13C}$. Sample: **1a**$_{13C}$ (40 mM), DPP **12** (20 mM) in DMSO-d$_6$ @ 300 K.

The identity of the abstraction product as carbon dioxide was additionally confirmed by the classical detection reaction of carbon dioxide with barium hydroxide. Therefore the reaction depicted in Fig. 78 was performed with non-labeled **1a** on a larger scale in non-deuterated DMSO under inert conditions (argon atmosphere). The evolving gas was passed through a saturated barium hydroxide solution and the formation of a white precipitate (barium carbonate) was observed.

These results show that starting from dimer **2** the enyne **3** formation mechanism contains a carbon dioxide abstraction step.

5.3.6 Generation of Water Under Acidic Conditions

Comparing stacked plots of the ^{1}H water region for the samples **2a** + DPP **12** with and without addition of benzoic acid **14** are shown in Fig. 79. Without addition of **14**, the water amount does not significantly change during 13 h reaction time. In contrast, addition of benzoic acid **14** leads to a strong increase in ^{1}H water signal intensity together with a distinct signal broadening. This indicates, that only under acidic conditions (addition of benzoic acid) water is released.

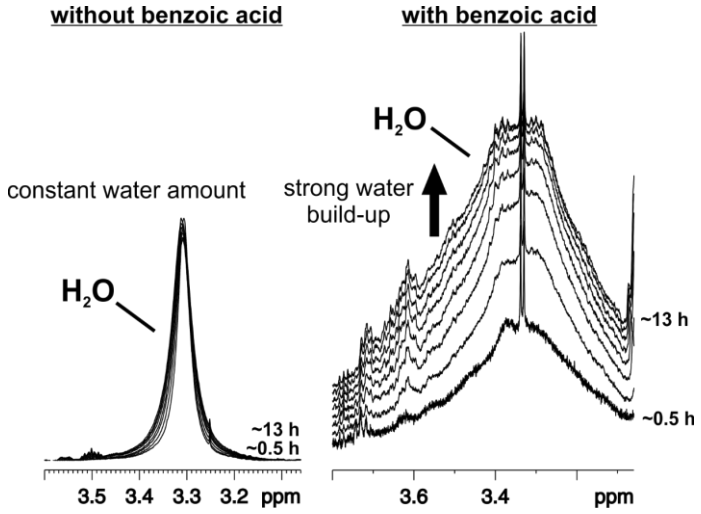

Fig. 79: Stacked plots are presented of the ^{1}H water signals of the samples DPP **12** (20 mM) and nitroalkene-dimer **2a** (40 mM, 92% Z-isomer, 8% E-isomer, d.r.(Z) = 2.03:1.00, d.r.(E) = 1.38:1.00) in DMSO-d_6 @ 300 K without (left) and with (right) benzoic acid **14** (20 mM) as additive. With **14** a strong water signal build-up was monitored.

5.3.7 Formation and Detection of Nitrogen Species (*e.g.* N_2) – ^{15}N NMR

The key part in the reaction mechanism of enyne **3** formation from nitroalkenes **1** is the reaction from the nitroalkene-dimer **2** to the product **3**. Both, the secondary and the primary nitro group in molecule **2** are cleaved in this process. Possible fates of this nitro group are *e.g.* nitromethane (or $[CH_2NO_2]^-$) and nitrous acid (HNO_2). In terms of NMR discrimination and verification of both molecules and/or other nitrogen species, in principal the NMR active nitrogen isotope ^{15}N, especially its chemical shift can be used. Since, ^{15}N natural abundance is very low (about 0.4%) ^{15}N enriched compounds have to be used in order to get acceptable signal to noise ratios with a reasonable number of scans. Therefore, ^{15}N labeled nitroalkene **1a**$_{15N}$ was synthesized following a literature procedure[51,h] and applied in the enyne formation reaction catalyzed by DPP **12** and benzoic acid **14** as additive in DMSO-d_6 at 300 K. ^{15}N NMR *in situ* reaction monitoring (Fig. 80, bottom left-hand side) revealed the formation of many ^{15}N species during the reaction, especially in the chemical shift region of 300 to 600 ppm which includes the typical chemical shift range of nitro compounds (350 to 400 ppm)[49]. In parallel ^{1}H reaction monitoring (Fig. 80, bottom right-hand side) was applied in order to enable the comparison of both ^{15}N and ^{1}H kinetic profiles. Fig. 80 (top) shows slices of ^{15}N spectra, measured after about 20 min reaction time. The signals of the nitro groups of the starting material **1a**$_{15N}$ (375.2 ppm) and the nitroalkene-dimer intermediate **2a Z (A, B)** (394.1 ppm, 385.8 ppm) could be identified and both species show the expected performance in the plotted ^{15}N reaction kinetics (Fig. 80, bottom left-hand side). In addition, five ^{15}N singlets at 395.0 ppm, 389.5 ppm,

[h] Synthesis of **1a**$_{15N}$ was performed analog to synthesis of **1a**$_{13C}$. Therefore chapter 5.3.11 only contains the synthesis procedure of the latter.

387.3 ppm, 310.8 ppm and 617.7 ppm were detected. The three signals at 395 ppm, 389.5 ppm and 387.3 ppm lie in the chemical shift range of nitro compounds, occur only in the very beginning of the ^{15}N reaction monitoring and disappear completely after a reaction time of 2 hours. Since, in a similar time frame in the ^{1}H reaction monitoring (Fig. 80, bottom right-hand side), the catalyst-nitroalkene adduct **18a** disappears, two of these three signals correspond most likely to the nitro groups of the two possible diastereoisomers of this species. The third signal probably is also a nitro group but its precise identity remains unclear so far.

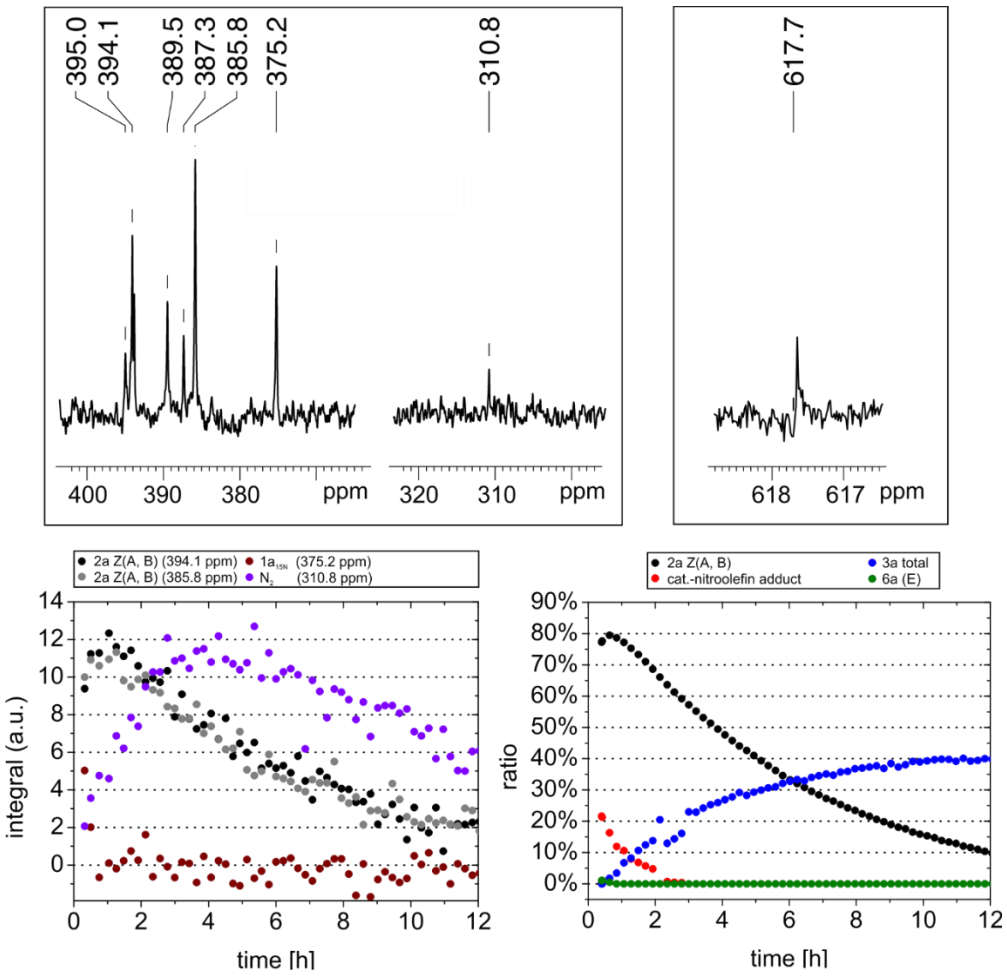

Fig. 80: Top left shows a 1D ^{15}N spectrum and top right shows a 1D ^{15}N inverse gated decoupled spectrum both after about 20 min reaction time. ^{15}N and ^{1}H kinetic data is presented in the bottom left and bottom right respectively. The *in situ* reaction mixture of the presented data was: ^{15}N labeled nitropentene **1a**$_{15N}$ (80 mM), DPP **12** (20 mM), benzoic acid **14** (20 mM) in DMSO-d_6 at room temperature.

More relevant are the signals at 310.8 ppm and 617.7 ppm (see Fig. 80), because they are not in the chemical shift region of nitro groups. The ^{15}N reaction monitoring of the signal at 310.8 ppm reveals at first glance intermediate characteristics, building up at the beginning of the reaction, reaching its maximum concentration after about 4 hours reaction time and subsequently degrading. The maximal build-up coincides with the maximal concentration of the nitroalkene-dimer intermediate **2a Z (A, B)**

which indicates that **2a** is the precursor of this species. Its chemical shift of 310.8 ppm matches different literature known organic compounds[49] *e.g.* imines (305-380 ppm), pyridines or pyridine like nitrogen atoms (250-520 ppm) and diazo compounds (255-445 ppm) as well as bimolecular nitrogen N_2 (310.1 ppm)[53]. Since only one intermediate ^{15}N signal was detected and pyridine or pyridine like nitrogen atoms as well as diazocompounds must show two different ^{15}N signals, these compounds are excluded. Imines or oximes show characteristic proton chemical shifts (6.9-8.4 ppm)[54] which were never detected and can therefore also be excluded. Initially, dissolved bimolecular nitrogen was also considered unlikely, because it is not obvious why and how it should act as an intermediate and not as a product. However, there is the possibility that the generated carbon dioxide (see chapter 5.3.5) is displacing dissolved N_2 from the solution. The detected intermediate is not the intermediate **6a** which occurs in between the nitroalkene-dimer **2a** and enyne **3a**, because in the proton spectra only traces of **6a** were detected at the very beginning of the reaction (Fig. 80, bottom right-hand side). The most probable candidate for the ^{15}N signal at 310.8 ppm therefore is molecular nitrogen (N_2) as proposed in the manuscript.

The occurring ^{15}N signal at 617.7 ppm (see Fig. 80, top right-hand side) does roughly match a literature value of sodium nitrite (608 ppm in water)[55]. No kinetics have been measured for this signal and consequently it remains unclear if the signal builds up during the enyne formation reaction. However, the mechanism proposed in the manuscript can explain the accumulation of that compound (see manuscript).

5.3.8 Application of a Substoichiometric Amount of Base 12 (DPP)

Results of the reaction monitoring of **2a** (40 mM) with DPP **12** (20 mM) as base are depicted in Fig. 81. In this case only 50 mol% of base were applied in order to check if a stoichiometric amount of base is needed to quantitatively deprotonate **2a** or if also a catalytic amount is sufficient. Indeed, in the additive free case, the reaction stops at about 50% nitroalkene-dimer **2a** (data not shown) indicating that for initializing the reaction *via* deprotonation of **2a** without additives a stoichiometric amount of base is necessary.

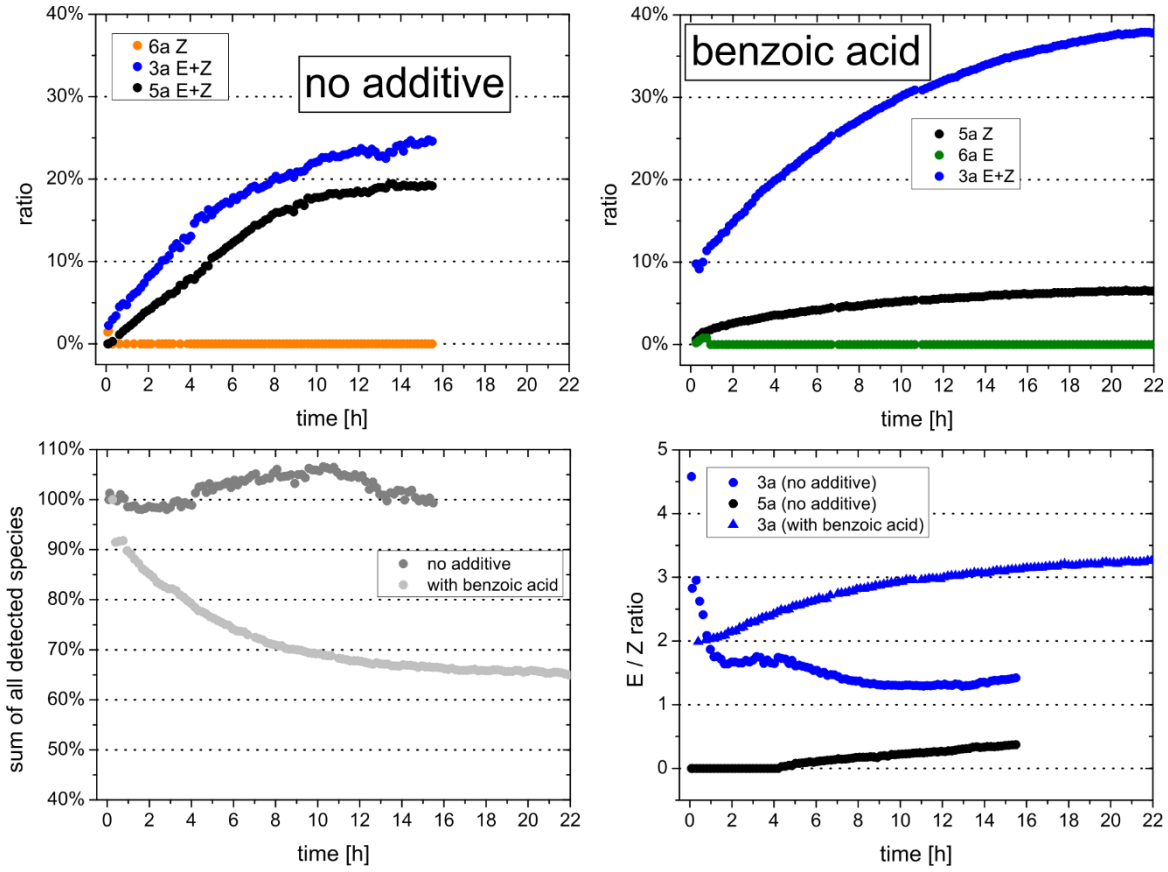

Fig. 81: Reaction kinetics are presented of DPP **12** (20 mM) and nitroalkene-dimer **2a** (40 mM, 92% Z-isomer, 8% E-isomer, d.r.(Z) = 2.03:1.00, d.r.(E) = 1.38:1.00) in DMSO-d_6 @ 300 K. Top left shows data without additive addition whereas top right shows data with the addition of benzoic acid (20 mM). In the bottom left, the sum of all detected species is presented. Bottom right shows the *E*/*Z* ratios of enyne **3a** (blue) and cyclic nitronate **5a** (black) with (triangles) and without (circles) benzoic acid **14**.

As shown in Fig. 81 (top left-hand side) this reaction conditions led to the formation of nearly equal amounts of enyne **3a** and cyclic nitronate **5a** of 25% and 19%, respectively, after a reaction time of about 16 hours. In the first 20 minutes of the reaction also the intermediate **6a Z** was detected in very low amounts (<2%). *E*/*Z* ratio of enyne **3a** started at about 4.6 decreased fast (reaching about 1.7 after 1.5 hours) and slowly decreased further reaching an end value of about 1.4 after 15 hours. This development of the *E*/*Z* ratio over time is contrary to the situation with DBU **16** as base, where the ratio slowly increased during the reaction (data not shown). In contrast, the end point of the *E*/*Z* ratios was similar for both reaction conditions (about 1.0 in the DBU case). This indicates, that the thermodynamic equilibrium is located at an *E*/*Z* ratio near 1.0 but the initial kinetic preference in the formation of **3a Z** or **3a E** is strongly depending on the structure of the applied base. Very large bases like DBU **16** favor the formation of the *Z* isomer whereas medium size bases like DPP **12** favor the formation of the *E* isomer. In the end an active isomerization process leads to the thermodynamic equilibrium situation. The *E*/*Z* ratio of cyclic

nitronate **5a** started very low (nearly 100% *Z*), stayed constant for about 4 hours and was than constantly increasing up to a value of 0.2 after 15 hours.

Interestingly, applying DPP **12** (50 mol%) as base, addition of benzoic acid **14** (50 mol%) did not accelerate the reaction as it is the case for the base DBU **16** (see Fig. 72, manuscript). The reaction was monitored for 22 hours when it was still proceeding slowly. Also consumption of the starting material **2a** (data not shown) did not stop but was almost quantitative in the end of the reaction. As the main reaction product enyne **3a** was detected (final *in situ* yield 38%). Only in the very beginning of the reaction the intermediate species **6a E** was detected at very low amounts (<1%). The *E*/*Z* ratio of product **3a** is slowly increasing during the reaction from 2.0 at the beginning to 3.3 after 22 hours, showing similar characteristics than in the reaction with DBU **16** and benzoic acid **14** as additive with a slightly higher end value.

Noteworthy, the sum of detected species (see Fig. 81, bottom left-hand side) during the reaction of **2a** with 50 mol% of DPP **12** as base is constant. It seems, that the polymerization process which otherwise is consuming a large amount of starting material is not active at lower base concentrations (normally 100 mol% base was applied). It has to be investigated further if this is only the case for the base **12** or if it is a common feature for all Brønsted base induced reactions of **2a**. If the latter is the case, the outcome of the actual described cyclic nitronate formation reaction may be improved dramatically in terms of yields by adding the base slowly while the reaction is proceeding. In contrast, the reaction with DPP **12** and benzoic acid **14** did show a decrease of the sum of all detected species of about 35% during the reaction (see Fig. 81, bottom left-hand side). Apparently, the additive **14** promotes the undesired polymerization process.

5.3.9 Additive Variation

In order to elucidate the influence of the additive on the enyne 3a formation reaction starting from **1a**, 4-nitrophenol **15** (pk_{aH}=10.8 in DMSO)[56] was tested, which has a comparable acidity as the standard additive benzoic acid **14** (pk_{aH}=11.1 in DMSO)[57]. In Fig. 82 the reaction profiles of the enyne **3a** formation with **15** as additive (top profiles) and for comparison reasons also the profiles with **14** as additive (bottom profiles) are depicted.

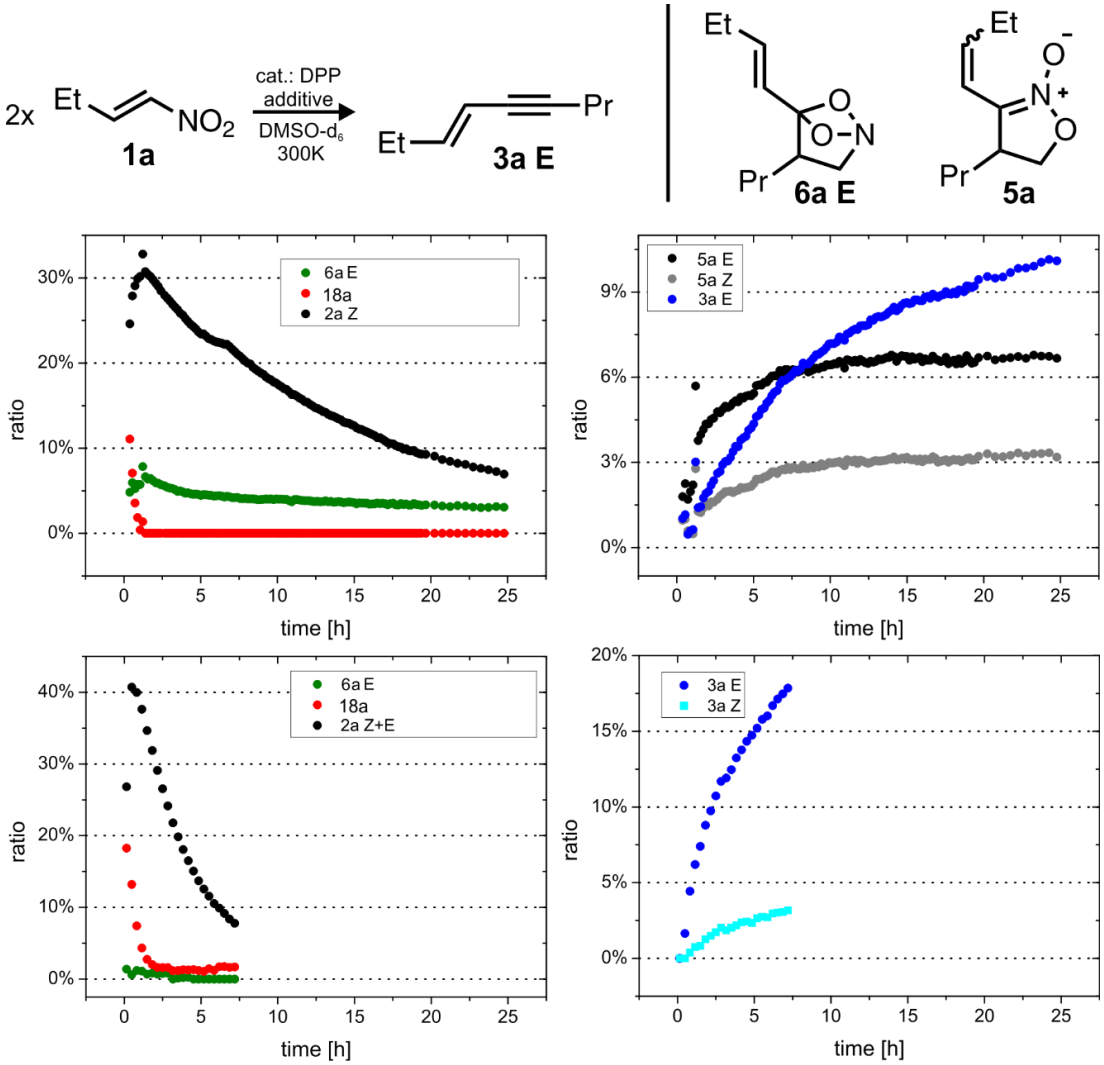

Fig. 82: Reaction scheme (top left) and reaction profiles (bottom) of the enyne **3a** formation from nitropentene are shown, catalyzed by DPP **12** with addition of additive. Also structures (top right) of the detected intermediate species **6a E** and side product **5a** are presented. Top profiles: 50 mol% **12**, 50 mol% p-nitrophenol **15** as additive, bottom profiles: 100mol% **12**, 100mol% benzoic acid **14** as additive).

Although the catalyst and additive concentrations are not identical (50 mol% **14**, 100 mol% **15**) which cannot be excluded as the main reason for the different reaction profiles, the following distinctions are notable. First the reaction with **15** is slow. The dimer ratio **2a** reaches 10% after about 19 hours (in comparison to about 7 hours for the sample with benzoic acid **14**). Second, 50 mol% of **15** is not suppressing side product **5a** formation and therefore the overall yield of **3a** reaches only about 10% (compared to 20% for sample with **14**). Interestingly, only **3a E** (except traces of the *Z* -somer) is formed when **15** is applied as additive and the ratio of the intermediate species **6a E**, peaking at about 8% is considerably higher than in the benzoic acid **14** sample (about 1 %). Most probably that difference is not due to the lower additive concentration of the applied additive but stems from the structural differences of benzoic acid **14** and *p*-nitrophenol **15** (*i.e.* aromaticity or acidic functional group).

5.3.10 Literature Known Formation of Cyclic Nitronates from Aliphatic α,γ-nitro-X compounds

The principle reactivity of aliphatic α,γ-dinitro compounds (such as **2a**) with bases towards 5-membered cyclic nitronates (such as **5a**) is already literature known and was first reported by Kohler and Barrett in 1924.[42] A variety of examples starting from α,γ-dinitro compounds exist[58–60], but in most of the reactions the starting materials only contain one nitro group whereas the second one is replaced by different leaving groups (*e.g.* Cl[61–63], Br[64–66], I[63]). The accepted S_{N2} meachnism[43] for these reactions (see Fig. 83) proceeds *via* deprotonation of the proton in α-position to the nitro group forming a carbanion. Next, a negatively charged oxygen of the mesomeric oxy-anion is performing a nucleophilic substitution of the leaving group yielding the five-membered cyclic nitronate product.

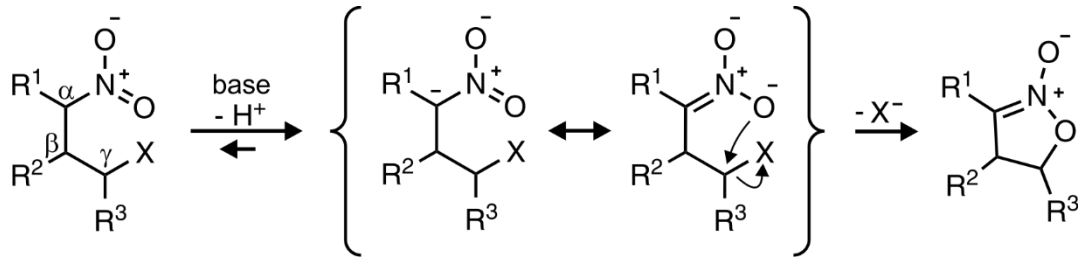

Fig. 83: Literature known S_{N2} mechanism[43] for the formation of 5-membered cyclic nitronates from aliphatic α,γ-nitro-X compounds. X is a leaving group.

At least for the cyclic nitronate formation reaction, starting from dinitro compounds **2** in DMSO, this accepted reaction mechanism seems to be too simple. As stated above, in the actual work we detected a central intermediate **6a** in between the nitroalkene-dimer **2a** and **5a** which is not consistent with this literature known mechanism (see Fig. 83). We therefore proposed new mechanisms for both, the formation of enynes **3** as well as the formation of five-membered cyclic nitronates **5** (see manuscript).

5.3.11 Synthesis Procedures

13C labeled (E)-nitropentene (1a$_{13C}$)

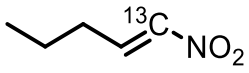

1a$_{13C}$ was synthesized following a literature procedure.[51] In a round bottom flask 1.16 g (1 equiv; 16.1 mmol) butanal (freshly distilled) and 1.00 g (1 equiv; 16.1 mmol) ^{13}C labeled nitromethane were dissolved in 4 mL methanol at a temperature below 0°C (ice, sodium chloride mixture). After drop by drop addition of a solution of 0.68 g (1.05 equiv; 16.9 mmol) sodium hydroxide in 0.8 mL water, a white precipitate was forming. The reaction mixture was kept below 0°C and stirred for 1 hour. Water was added until the precipitate was completely dissolved (about 12 mL). After addition of 17.7 mL (1.1 equiv; 17.7 mmol) of 1M HCl the reaction mixture was stirred for 15 minutes, extracted three times with dichloromethane, and dried over $MgSO_4$. The solvent was evaporated and 2.38 g of a yellowish liquid was yielded. After flash column chromatography (solvent: 100% DCM) 0.53 g (yield: 28%) of pure product **1a**$_{13C}$ was isolated (R_f=0.87, 0.81; 100% DCM, stain: $KMnO_4$).

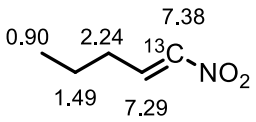

1a$_{13C}$: ^{1}H NMR (600 MHz, DMSO-d_6) δ [ppm] 7.38 (ddt, J = 97.5 Hz, 13.2 Hz, 1.4Hz, 1H), 7.29 (m, 1H), 2.24 (dtd, *J* = 14.5 Hz, 7.2 Hz, 1.4 Hz, 2H), 1.49 (tq, *J* = 14.6 Hz, 7.3 Hz, 2H), 0.90 (t. J = 7.4Hz, 3H).

5-nitro-6-(nitromethyl)non-3-ene (2a (A,B)) – Procedure 1.

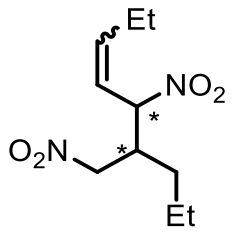

The stereoisomeric mixture (E and Z isomers, two diastereomers respectively) of **2a** was synthesized as following. In a round bottom flask 0.29 g (0.5 equiv; 2.5 mmol) L-proline and 0.31 g (0.5 equiv; 2.5 mmol) benzoic acid were dissolved in 50 mL DMSO at room temperature. 0.58 g (1.0 equiv; 5.0 mmol) nitropentene (weighted in a syringe) was added and the reaction mixture was stirred for 24 hours. During that time the color of the solution changed from yellow to orange. After the reaction was quenched by addition of 50 mL distilled water the reaction mixture was extracted four times with 50 mL diethyl ether each. The combined organic phases were washed four times with 50 mL distilled water and dried over magnesium sulfate. After evaporation the solvent, 0.89 g of the raw product, a mixture of a brownish oil and solid was isolated. Flash column chromatography (petrol ether (PE) : ethyl acetate (EA) = 19:1) yielded 0.24 g (42%) of a yellowish oil (R_f=0.35, 0.41; PE:EA=19:1, stain: $KMnO_4$, 92% Z-isomer, 8% E-isomer, d.r. (Z) = 2.03:1.00, d.r. (E) = 1.38:1.00).

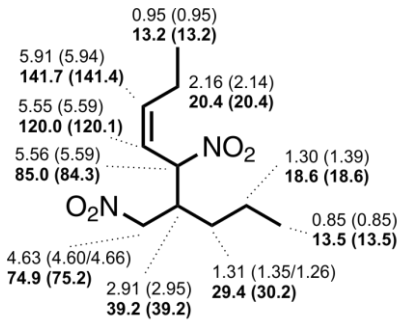

2a *Z* A (B): ^{1}H NMR (600 MHz, DMSO-d_6) δ [ppm] 5.91 (5.94) (m, 1H), 5.56 (5.59) (m, 1H), 5.55 (5.59) (m, 1H), 4.63 (4.60/4.66) (m, 2H), 2.91 (2.95) (m, 1H), 2.16 (2.14) (m, 2H), 1.31 (1.35/1.26) (m, 2H), 1.30 (1.39) (m, 2H), 0.95 (0.95) (t, J = 7.6 Hz (7.6 Hz), 3H), 0.85 (0.85) (t, J = 7.1 Hz (7.1 Hz), 3H)

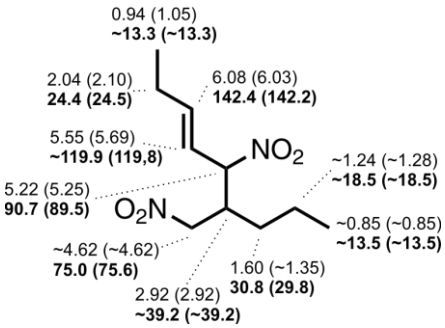

2a *E* A (B): ^{1}H NMR (600 MHz, DMSO-d_6) δ [ppm] 6.08 (6.03) (dt (dt), J = 15.3 Hz (15.3 Hz), 6.2 Hz (6.2 Hz) 1H), 5.55 (5.69) (m (ddt) (J = 15.3 Hz, 9.7 Hz, 1.5 Hz), 1H), 5.22 (5.25) (dd, J = 9.3 Hz, 8.6 Hz (9.3 Hz, 6.9 Hz), 1H), ~4.62 (~4.62) (m, 2H), 2.92 (2.92) (m, 1H), 2.04 (2.10) (m, 2H), 1.60 (~1.35) (m, 2H), ~1.24 (~1.28) (m, 2H), 0.94 (1.05) (t, J = 7.6 Hz (7.4 Hz, 3H), 0.85 (0.85) (t, J = 7.1 Hz, 3H)

5-nitro-6-(nitromethyl)non-3-ene (2a Z, (A,B)) – Procedure 2.

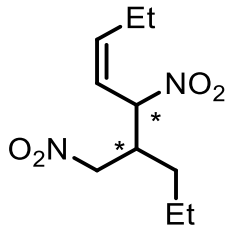

The stereoisomeric mixture of 2a Z(two diastereoisomers) was synthesized as follows. 1.34 g of **1a** (11.6 mmol, 1.0 equiv) and 1.34 g of L-proline (11.6 mmol, 1.0 equiv) were dissolved in 116 mL DMSO. The reaction mixture was stirred over-night. After product purification by column chromatography (PE : diethyl ether = 100:0, 95:5, 90:10, 80:20, 70:30) product isomers **2a Z (A)** and **2a Z (B)** were isolated (overall yield 78%).

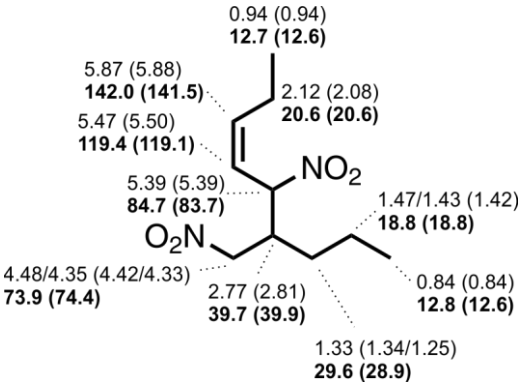

2a *Z* A (B): ^{1}H NMR (400 MHz, CD_2Cl_2) δ [ppm] 5.96 (5.97) (dt (dt), J = 10.4 Hz, 10.6 Hz, 1H), 5.55 (5.58) (ddt (ddt), J = 10.4 Hz, 10.4 Hz, 1.7 Hz (10.6 Hz, 10.6 Hz, 1.6 Hz) 1H), 5.47 (5.47) (dd (dd), J = 10.2 Hz, 8.0 Hz (9.9 Hz, 7.2 Hz), 1H), 4.46/4.43 (4.50/4.42) (dd/dd (dd/dd) J = 13.8 Hz, 5.6 Hz/13.8 Hz 5.4 Hz (13.6 Hz, 5.9 Hz/13.6 Hz, 5.9 Hz), 2H), 2.86 (2.90) (m, 1H), 2.20 (2.16) (m, 2H), 1.47/1.43 (1.42) (m, 2H), 1.40 (1.46/1.32) (m, 2H), 1.03 (1.03) (t, J = 7.4 Hz (7.5 Hz), 3H), 0.91 (0.92) (t, J = 7.2 Hz (7.2 Hz), 3H)

1-methoxy-2-(5-methyl-1,3-dinitrohex-4-en-2-yl)benzene (2f A, B).

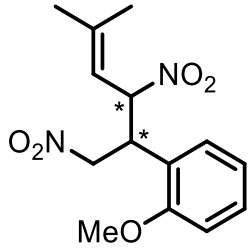

The diastereomeric mixture of **2f** was synthesized as following. 0.02 g L-proline (0.8 equiv, 0.2 mmol) and 0.03 g benzoic acid (0.8 equiv, 0.2 mmol) were dissolved in 7 mL DMSO at room temperature. Subsequently, 0.05 g (1.0 equiv, 0.3 mmol) of 1-methoxy-2-(2-nitrovinyl)benzene and 0.03 g 3-methyl-1-nitrobut-1-ene (1.0 equiv, 0.3 mmol) were added.. The solution was stirred for 24 hours under atmospheric conditions. After the reaction was quenched by adding 10 mL brine the reaction mixture was extracted 4 times with 10 mL diethyl ether each. The combined organic layers were washed 4 times with 10 mL distilled water each and dried over magnesium sulfate. After evaporation of the solvent the raw product was purified by flash column chromatography (PE:EA = 9:1) yielding 0.02 g (24%) of an orange oil which crystalized overnight (R_f=0.24; PE : EA=8:1, stain: $KMnO_4$, d.r. = 4.95:1.00).

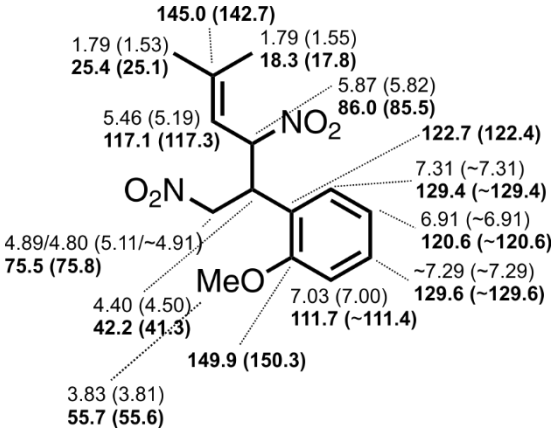

2f A (B): ^{1}H NMR (400 MHz, DMSO-d_6) δ [ppm] 7.31 (~7.31) (dd, J = 7.5 Hz 1.7 Hz), 1H), 7.29 (~7.29) (ddd, J = 7.9 Hz, 7.9 Hz, 1.6 Hz, 1H), 7.03 (7.00) (dd (dd), J = 8.3 Hz, 0.7 Hz (8.2 Hz, 0.7 Hz), 1H), 6.91 (~6.91) (ddd, J = 7.4 Hz, 7.4 Hz, 1.0 Hz, 1H), 5.87 (5.82) (dd (dd), J = 10.2 Hz, 10.2 Hz (9.9 Hz, 9.9 Hz), 1H), 5.46 (5.19) (dqq (dqq), J = 9.9 Hz, 1.4 Hz, 1.4 Hz (9.9 Hz, 1.4 Hz, 1.4 Hz), 1H), 4.89/4.80 (5.11/~4.91) (dd/dd (dd), J = 13.4 Hz, 8.8 Hz/13.4 Hz, 5.6 Hz (13.3 Hz, 10.1 Hz), 2H), 4.40 (4.50) (ddd (ddd), J = 10.2 Hz, 8.8 Hz, 5.7 Hz (9.9 Hz, 9.9 Hz, 4.7 Hz), 1H), 3.83 (3.81) (s (s), 3H) 1.79 (1.55) (d (d), J = 1.4 Hz (1.4 Hz), 3H), 1.79 (1.53) (d (d), J = 1.4Hz (1.3 Hz), 3H)

3-(but-1-en-1-yl)-4-propyl-4,5-dihydroisoxazole 2-oxide (5a).

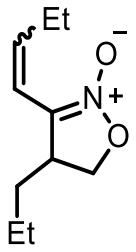

5a was synthesized *via* the following procedure. To a solution of 0.13 g **2a** (0.7 mmol, 1 equiv) in DMSO 0.10 g TBD (0.7 mmol, 1 equiv) was added and the reaction mixture was stirred over night at 50°C. The product was purified by column chromatography (pentane:diethyl ether = 1:1) and pure product **5a** was isolated (65-84%).

The following NMR data of **5a** stems from *in situ* NMR experiments of a mixture of **2a** (80mM) and potassium carbonate (80mM) in DMSO-d_6

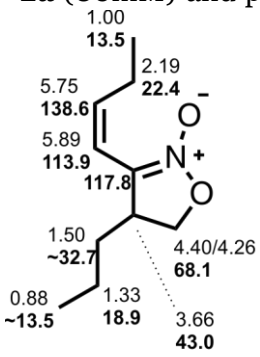

5a *Z*: ^{1}H NMR (600 MHz, DMSO-d_6) δ [ppm] 5.89 (1H), 5.75 (dt, J = 11.9 Hz, 7.7 Hz, 1H), 4.40/4.26 (dd/dd, J = 8.0 Hz, 8.0 Hz / 7.7 Hz, 3.1 Hz, 2H), 3.66 (m, 1H), 2.19 (m, 2H), 1.50 (m, 2H), 1.33 (m, 2H), 1.00 (3H), 0.88 (3H)

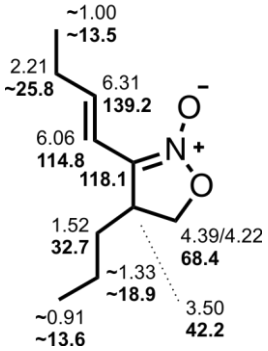

5a *E*: ^{1}H NMR (600 MHz, DMSO-d_6) δ [ppm] 6.31 (dt, J = 16.0 Hz, 6.7 Hz, 1H), 6.06 (dt, J = 16.0 Hz, 1.4 Hz, 1H), 4.39/4.22 (dd/dd, J = 8.2 Hz, 8.2 Hz / 7.8 Hz, 3.3 Hz, 2H), 3.50 (m, 1H), 2.21 (m, 2H), 1.52 (m, 2H), ~1.33 (m, 2H), ~1.00 (3H), ~0.91 (3H)

^{13}C labeled (E)-nitrooctene (1b).

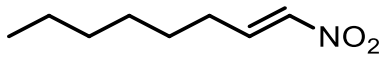

1b was synthesized following a literature procedure.[51] In a round bottom flask 8.41 g (1 equiv; 73.7 mmol) heptanal (freshly distilled) and 4.50 g (1 equiv; 73.7 mmol) nitromethane were dissolved in 20 mL methanol at a temperature below 0°C (ice, sodium chloride mixture). After drop by drop addition of a solution of 3.54 g (1.2 equiv; 88.4 mmol) sodium hydroxide in 4 mL water, a white precipitate was forming. The reaction mixture was kept below 0°C and stirred for 1 hour. Water was added until the precipitate was completely dissolved (about 50 mL). After addition of 9.15 mL (1.5 equiv; 110.5 mmol) of 12.08 M HCl the reaction mixture was stirred for 15 minutes, extracted three times with dichloromethane, and dried over $MgSO_4$. The solvent was evaporated and 13.5 g of a yellowish liquid was yielded. After flash column chromatography (solvent: PE:EA=19:1) 0.79 g (yield: 3%) of pure product **1b** was isolated (R_f=0.56; PE:EA=19:1, stain: $KMnO_4$).

1b: ^{1}H NMR (400 MHz, $CDCl_3$-d_6) δ [ppm] 7.27 (dt, J = 13.4Hz, 7.3Hz, 1H), 6.98 (dt, J = 13.4 Hz, 1.3 Hz, 1H), 2.27 (dtd, *J* = 7.3 Hz, 7.3, Hz 1.3 Hz, 2H), 1.52 (m, 6H), 0.89 (t. J = 7.24Hz, 3H).

5.3.12 Additional Analytical Data

In Situ Power Gated Proton Decoupled ^{13}C Spectrum of $6a_{15N}$.

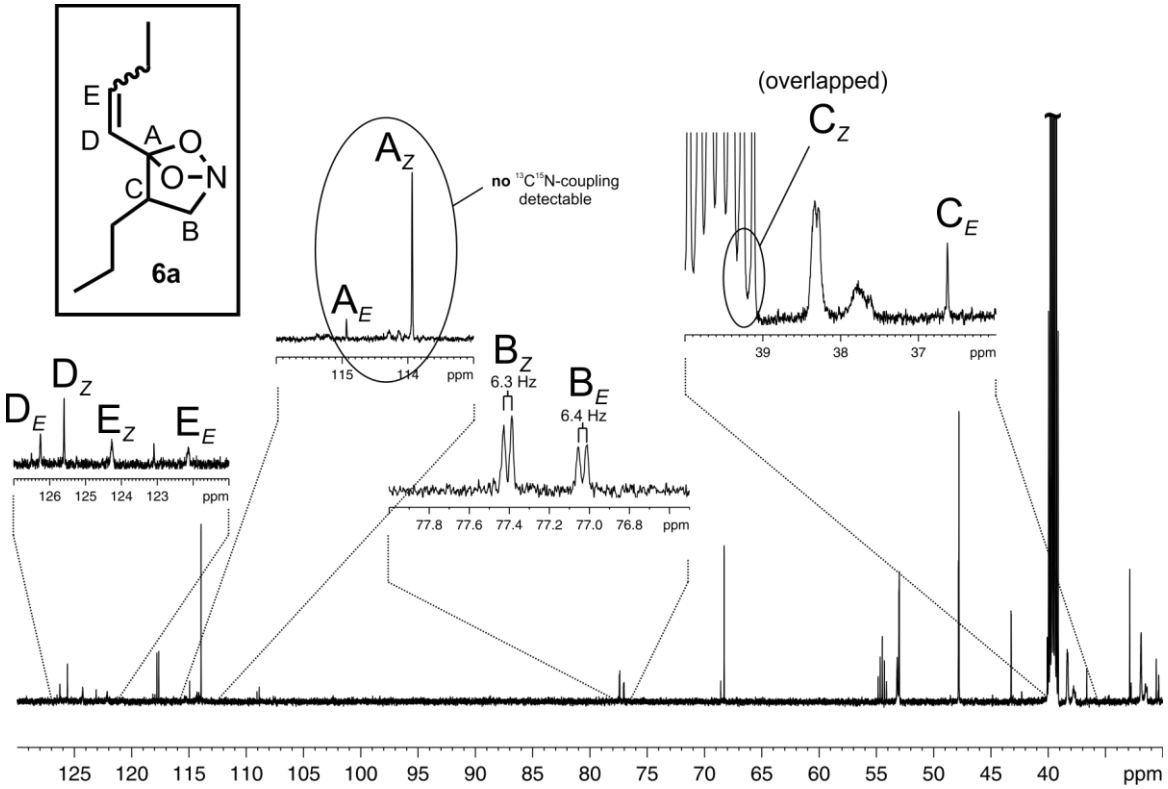

Fig. 84: Power gated decoupled spectrum of a mixture of **2a**$_{15N}$ (~250 mM) and DBU (~250 mM) in DMSO-d_6 @ 300 K at a proton resonance frequency of 600 MHz. Highlighted are the most relevant chemical shift areas for the intermediate species **6a**$_{15N}$ together with extracted ^{13}C-^{15}N coupling constants.

^{1}H in situ Spectra of Central Intermediate Species 6a Z/6a E.

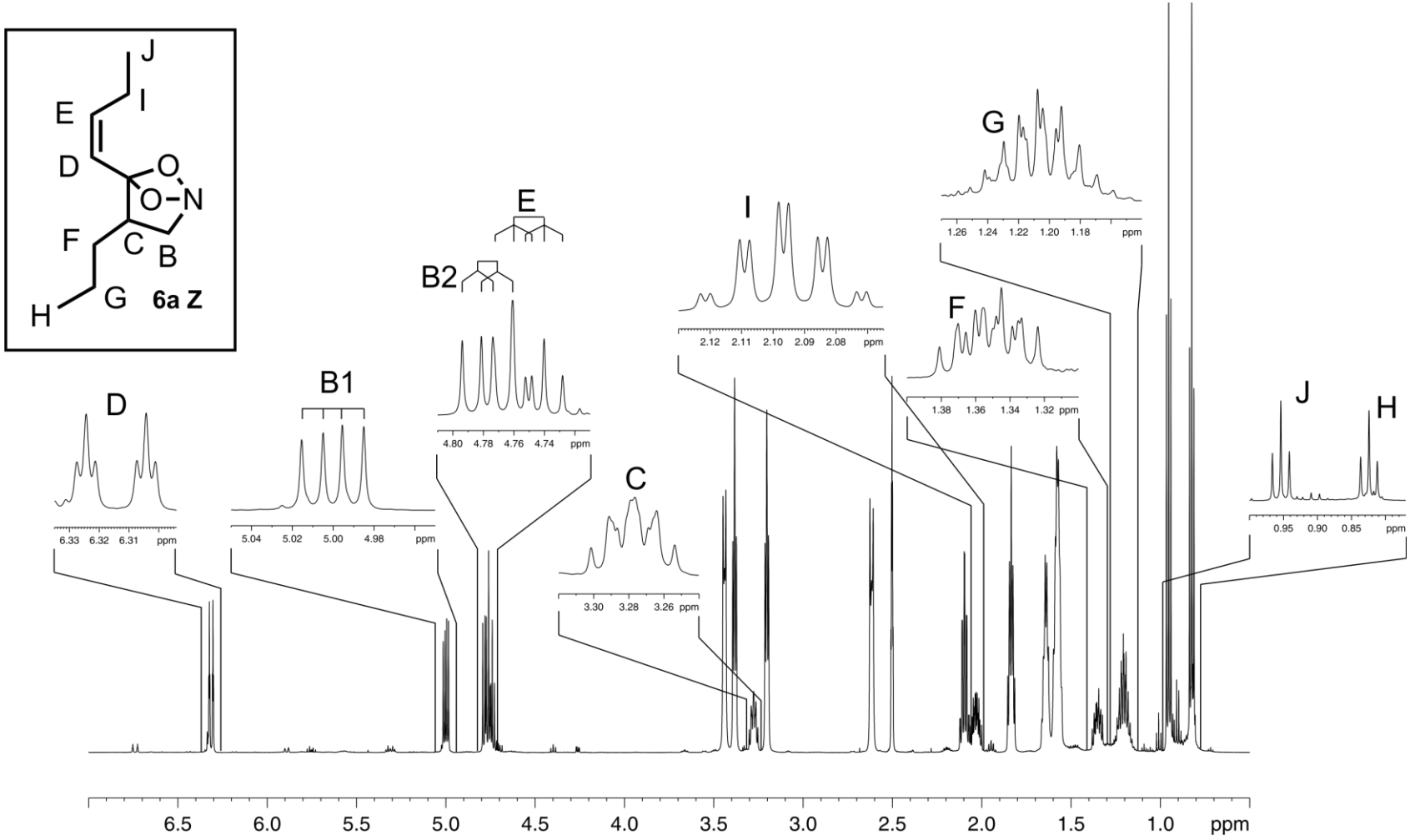

Fig. 85: Slice of ^{1}H spectrum of a mixture of **2a** (80 mM) and DBU (80 mM) after 5 min reaction time in DMSO-d_6 @ 300 K at a proton resonance frequency of 600 MHz. All ^{1}H resonances of the formed intermediate isomer **6a Z** are magnified.

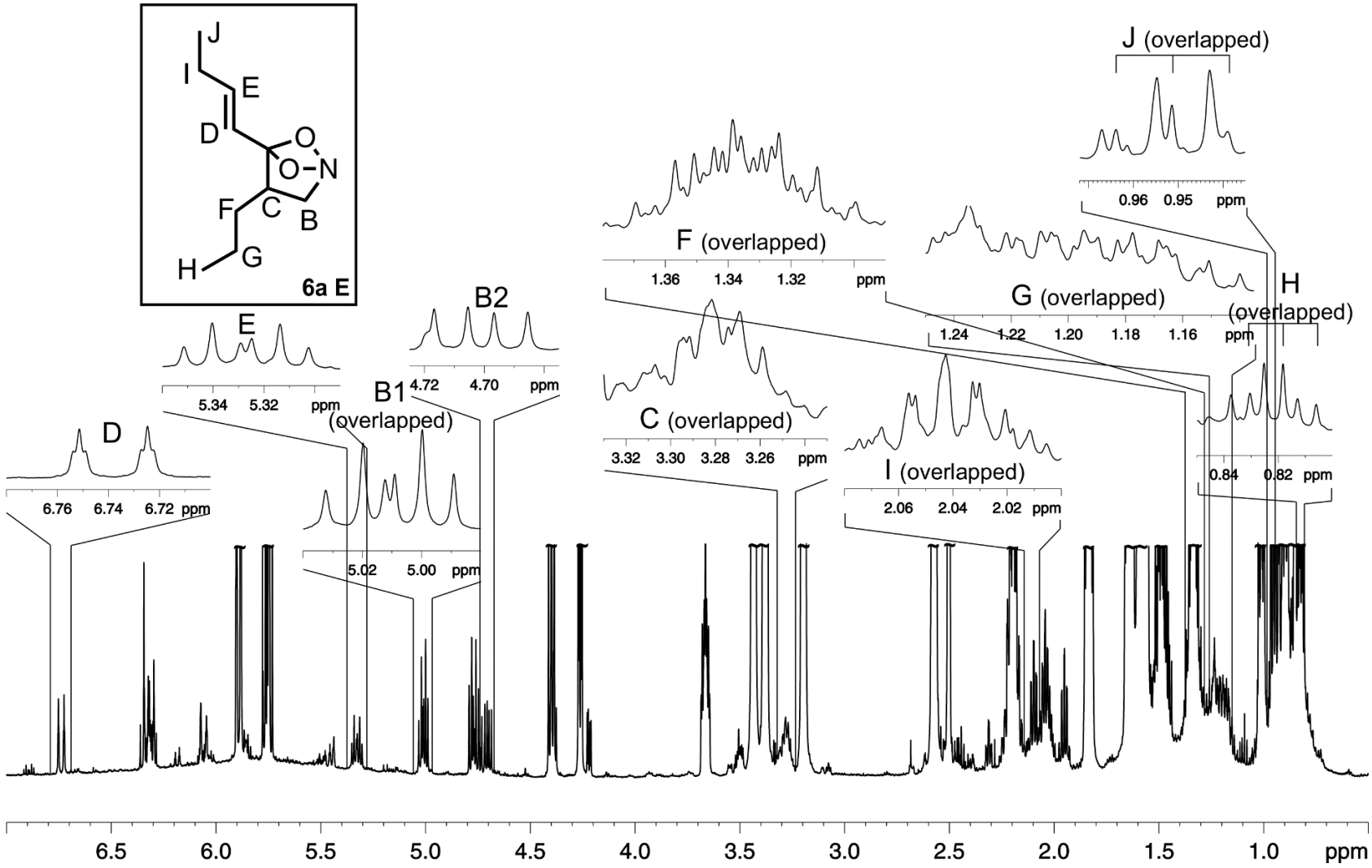

Fig. 86: Slice of ^{1}H spectrum of a mixture of **2a** (80 mM) and DBU (80 mM) after 1 h 51 min reaction time in DMSO-d_6 @ 300 K at a proton resonance frequency of 600 MHz. All ^{1}H resonances of the formed intermediate isomer **6a Z** are magnified. Resonances marked with (overlapped) are strongly overlapped by other signals.

^{13}C-^{15}N Coupling Constants of 2a Z_{15N} in CD_2Cl_2.

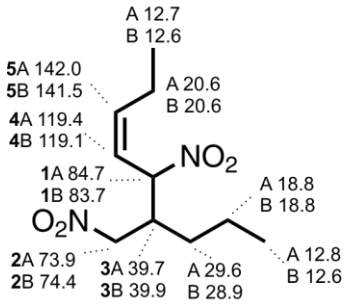

No.^{13}C (range)	J_{CN}^{exp}(A) [Hz]	J_{CN}^{exp}(B) [Hz]
1 ($^1J/^3J$)	7.0 / ~0.9	6.5 / ~0.9
2 ($^1J/^3J$)	8.4 / 1.4	8.3
3 ($^2J/^2J$)	---	---
4 ($^2J/^4J$)	~1.1	< 1.0
5 ($^3J_{al}/^5J$)	2.3	1.9

Fig. 87: Structure and corresponding ^{13}C chemical shifts of **2a Z_{15N}** (two diastereomers A and B) as well as table with experimental ^{13}C-^{15}N coupling constants for according carbons No. 1-5 extracted from a proton gated decoupled ^{13}C spectrum. Presented data was measured in CD_2Cl_2 @ 300 K at a proton resonance frequency of 600 MHz.

As expected $^1J_{CN}$ couplings of **2a Z_{15N}** (see Fig. 87) are the strongest detectable (coupling constants of 8.3 Hz / 8.4 Hz / 7.0 Hz /6.5 Hz). $^2J_{CN}$ coupling constants are very low (1.1 Hz / <1.0 Hz) or are not detectable (No. 3). $^3J_{CN}$ coupling constants (1.4 Hz) lie in the same region than ^2J coupling constants, slightly higher for allylic positions (2.3 Hz / 1.9 Hz) and sometimes not detectable (No. 2 A).

Chemical Shifts and ^{13}C-^{15}N Coupling Constants of 5a Z_{15N} in CD_2Cl_2.

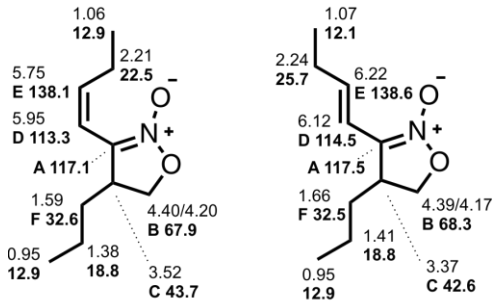

No.^{13}C (range)	J_{CN}^{exp}(Z) [Hz]	J_{CN}^{exp}(E) [Hz]
A (^1J)	25.1	26.1
B (^3J)	---	---
C (^2J)	3.2	3.2
D (^2J)	---	---
E ($^3J_{al}$)	4.7	4.7
F (^3J)	1.4	1.2

Fig. 88: Structure and corresponding ^1H and ^{13}C chemical shifts of **5a Z_{15N}** (*E* and *Z* isomer) as well as table with experimental ^{13}C-^{15}N coupling constants for carbons A-F extracted from a proton gated decoupled ^{13}C spectrum. Presented data was measured in CD_2Cl_2 @ 300K at a proton resonance frequency of 600 MHz.

Most noticeable here is the strong $^1J_{CN}$ coupling between the nitro-ester carbon and nitrogen atom (A) with a coupling constant of 25.1 Hz (Z) and 26.1 Hz (E). The second highest coupling constant (E) is a $^3J_{CN}$ allylic coupling (4.7 Hz). The remaining $^3J_{CN}$ couplings are either smaller (1.4 Hz/1.2 Hz for F) or not detectable (B). The same holds true for $^2J_{CN}$ couplings (3.2 Hz for C, not detectable for D).

5.4 Additional Findings

5.4.1 Direct Enyne Formation from Nitroalkenes – Reaction Condition Variations

Initially, the best NMR results for enyne **3a** formation from nitroalkene **1a** were obtained with a 1:1 mixture and 100 mol% of the catalyst DPP **12** and the additive benzoic acid **14** (50 mM each) in DMSO-d_6 at room temperature. Since it seemed very likely that higher yields can be achieved through reaction optimization, we decided to vary solvent, catalyst as well as the applied additive. Surprisingly, the initial NMR yields of about 35 % for the direct enyne **3a** formation from nitroalkene **1a** could not be increased significantly.

Solvent Screening. Fully deuterated DMSO, DMF, methanol, benzene, dioxane, nitromethane, acetone, dichloromethane, and acetonitrile were chosen as NMR solvents for the optimization of the enyne formation reaction. We applied nitropentene **1a** (80 mM), as well as 25 mol% of the original catalyst DPP **12** and the additive benzoic acid **14**. After a reaction time of 15–20 min ^{1}H spectra showed that enyne formation only takes place in the highly polar, aprotic solvents DMSO and DMF (ε_r of approximately 37[67]). In the unpolar aprotic solvents benzene, dioxane and dichloromethane and in the less polar aprotic solvents nitromethane, acetonitrile and acetone no reactivity was monitored at all, whereas in the polar protic solvent methanol only unproductive reactions took place. The *in situ* yield of **3a** for the reaction in DMF reached about 29% (14.5% ratio) after a reaction time of 19.5 hours and full conversion of the starting material (See Fig. 89, bottom). Therefore, we revealed that a simple change of solvent from DMSO to DMF does not improve the original yield of 35%.

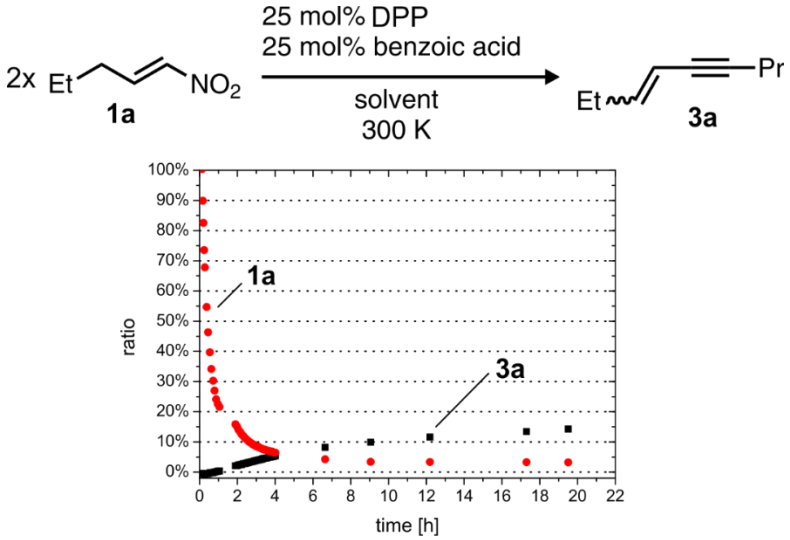

Fig. 89: Top shows Reaction conditions for the solvent screening of the reaction of **1a** to **3a** (*E* and *Z*). Bottom shows ^{1}H *in situ* NMR reaction kinetics of the formation of **3a** in DMF-d_7 @ 300 K (the sum was set to 100% for the first spectrum).

Catalyst Variation – NMR Screening. [i] In order to elucidate the influence of the aromatic substitution pattern of the catalyst **12** on the enyne formation from nitroalkenes **1** the CF_3 substituted diphenylprolinol was applied (see Fig. 90).

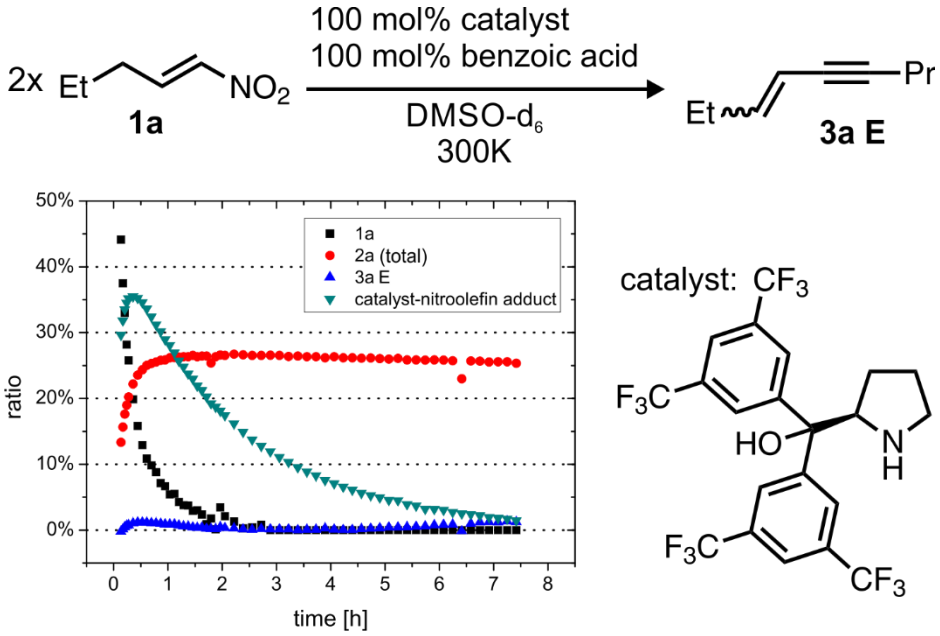

Fig. 90: Reaction conditions and reaction profile for the enyne formation are presented. In the reaction profile the sum of detected species derived from **1a** in the first spectrum was set to 100%.

The reaction profile in Fig. 90 shows, that both intermediates (catalyst-nitroalkene adduct **18a** and **2a** (total) (*E* and *Z*, both diastereomers each) can also be detected using the *meta*-trifluoromethyl substituted catalyst. In contrast to reaction with the unsubstituted catalyst **12**, the yield of enyne **3a** (about 2% after 7 hours) is drastically decreased (from 35% with **12**) and the amount of dimer **2a** (total) stays nearly constant from 3 hours to 7 hours reaction time. This can be explained by the proposed base induced mechanism (see manuscript) starting from the dimer **2a**. The basicity of the tertiary alcohol and maybe even that of the secondary amine is reduced by the introduction of *m*-CF_3 groups on the phenyl substituents (-I effect). Therefore, the basicity is not high enough to initialize the enyne **3a** formation from dimer **2a** which is consequently accumulating in solution.

Again, a loss of signal intensity regarding the sum of all detected species derived from **1a** was detected (70% after 7 hours, data not shown). Once again, we ascribe this to an active polymerization process.

Catalyst Variation – GC Screening. In order to test many catalysts for their performance in the direct enyne formation from nitroalkenes, in a shorter time than possible by NMR, a GC-FID procedure has been developed.

[i] The NMR catalyst variation was conducted together with Andreas Seegerer during a lab course.

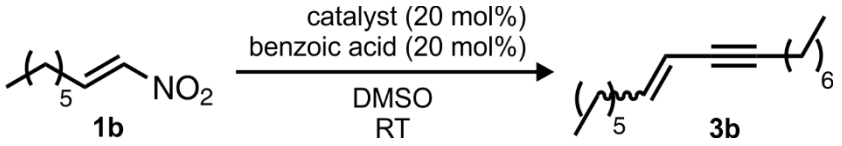

Fig. 91: Reaction conditions applied in the GC-FID screening of the catalyzed direct enyne **3b** formation from nitroalkene **1b**. Concentrations: **1b** (62.5 mM), catalyst (12.5 mM) benzoic acid (12.5 mM). Reaction time: 24-48 h. GC standard compound: pentadecan.

Since, the retention time of non-3-en-5-yne **3a** was in the region of the retention time of the solvent DMSO, nitroocten **1b** (for synthesis procedure refer to chapter 5.3.11), a nitroalkene with a longer alkyl chain, was used which yields pentadec-6-en-8-yne **3b** in the enyne formation reaction (see Fig. 91).

Table 26: Results of the GC-FID screening of potential catalysts for the direct enyne **3b** formation from **1b**. Standard conditions: **1b** (63 mM), catalyst (20 mol%), benzoic acid **14** (20mol%), in DMSO @ room temperature, open system, reaction time 21 to 48 hours. Total conversion was not determined. *no benzoic acid **reaction @ 343 K ***inert conditions. For calibration lines, retention times and raw GC data, see below.

No.	Catalyst	Reaction Time [h]	*E* / *Z* Ratio	Yield
1	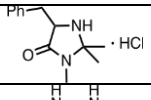	24	1.0	2%
2	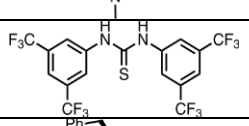	24	9.1	2%
3	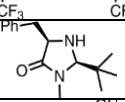	24	6.3	3%
4	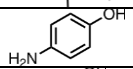	24	4.5	3%
5		24	6.6	4%
6		24	7.0	4%
7	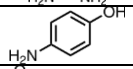	24	6.3	5%
8	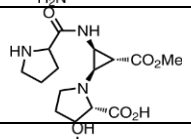	24	8.0	5%
9		24	4.3	6%
10	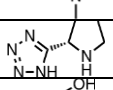	24	7.7	7%
11		24	1.6	7%
12	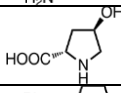	36	5.6	9%
13*	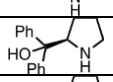	21	4.3	11%
13**	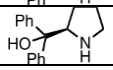	21	2.7	15%

No.	Catalyst	Reaction Time [h]	*E* / *Z* Ratio	Yield
14	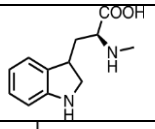	24	5.1	16%
15	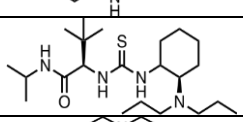	24	5.7	16%
16		24	2.2	21%
17	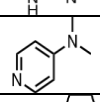	24	4.4	21%
13***	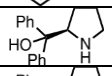	24	5.8	26%
18	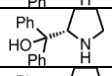	48	3.8	30%
13	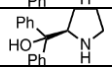	48	3.93	33%

In Table 26 the results of the GC-FID screening are summarized sorted by the determined enyne **3b** yield. Benzoic acid **14** (20 mol%) together with potential organocatalysts (20 mol%) like MacMillan Imidazolidinones (no. 1 and 3), the Ley catalyst (no. 10), a hydroxyl-substituted L-proline (no. 12), urea (no. 6), thioureas (no. 2 and 15), as well as the initially applied DPP **12** (no. 13, 18; both stereoisomers) were applied. Since the functional groups in **12** are a secondary amine as well as a primary alcohol, also simple compounds, containing alcohol groups (no. 5) or amine groups (no. 8, 14, 16, 17) or both (no. 7, 9, 11, 12) were tested. All catalysts which show a significant yield (> 10%, no. 13 - 18) contain at least one secondary or tertiary amine. On the other hand, a secondary amine alone is not sufficient for a significant catalytic activity because molecules no. 1, 3, 8, 10 and 12 are not very effective (all <10%). The best catalyst still is **12** (~30%, no. 13, 18; both stereoisomers) which contains a secondary amine as well as a tertiary alcohol. Molecule no. 12 containing a secondary amine and a carboxylic acid shows a significantly lower yield of 9%. The common property of all catalysts with moderate to high activity is a secondary or tertiary amine and a decent basic[j] character (*e.g.* contain at least one tertiary amine or alcohol). This result fits the mechanistic proposal (see manuscript) – *i.e.* the reaction from nitroalkene-dimer **2** to enyne **3** is base induced.

The enyne **3b** *E*/*Z* ratio for the catalysts that show yields over 10% varies under standard conditions from 2.2 (no. 16 a non-chiral bicyclic tertiary amine, 21% yield) to 5.7 (no. 15 a tertiary amine/amide thiourea-derivative, 16% yield). Noticeable is

[j] Molecule no. 14 (16%) is an exception. It contains two secondary amines but also a carboxylic group and therefore has only a low basicity compared to the other active compounds.

the increase of **3b** *E*/*Z* ratio from 3.9 to 5.8 generated by DPP **12**, achievable through the application of an inert atmosphere during the reaction (no. 13***).

An elevated temperature does not improve yield and selectivity (13**, DPP @ 343 K) and as expected from studies starting from the nitroalkene-dimer **2a,** omitting the addition of benzoic acid **14** (no. 13*,11%) leads to a strong decrease in the yield of enyne **3b**.

Thus, under inert conditions, the initially used catalyst DPP **12** is not only the most effective tested catalyst for the direct enyne formation from nitroalkenes in terms of total yield of enyne **3b**, but also in terms of stereoselectivity.

GC-Screening – Technical Details. The GC-FID system 7820A was used for the catalyst screening with the column HP 5 19091J 413 (30 mm x 0.32 mm x 0.25 µm), both from Agilent. For calibration, a stock solution of 33.33 mg of analytical pure **3b** (74.7% *E*, 25.3% *Z*) in 10 mL DMSO was prepared. Three calibration samples were prepared, with 1.496 mL (1.84 x 10^{-5} mol *E*-isomer, 6.21 x 10^{-6} mol *Z*-isomer), 0.6 mL (7.37 x 10^{-6} mol *E*-isomer, 2.49 x 10^{-6} mol *Z*-isomer) and 0.2 mL (2.46 x 10^{-6} mol *E*-isomer, 8.30 10^{-7} mol *Z*-isomer) of stock solution, 3.9 µL pentadecan each and DMSO (to a total volume of 1.5 mL). After GC-FID measurements of each sample, calibration lines for **3b *E*** and **3b *Z*** were generated (see Fig. 92). The retention times were 6.51 min for **3b Z**, 6.90 min for **3b E** and 6.42 min for the standard substance pentadecan. The equations derived from the calibration lines are as follows.

$$\boldsymbol{I} = \left(1.34x10^{8}\,\frac{1}{mol} \pm 5x10^{6}\,\frac{1}{mol}\right) x\,\boldsymbol{n} - (92 \pm 63) \qquad \text{for } \mathbf{3b\ E}$$

$$\boldsymbol{I} = \left(1.30x10^{8}\,\frac{1}{mol} \pm 3x10^{6}\,\frac{1}{mol}\right) x\,\boldsymbol{n} - (7 \pm 11) \qquad \text{for } \mathbf{3b\ Z}$$

(I: normed integral (a.u.); n: amount of substance [mol])

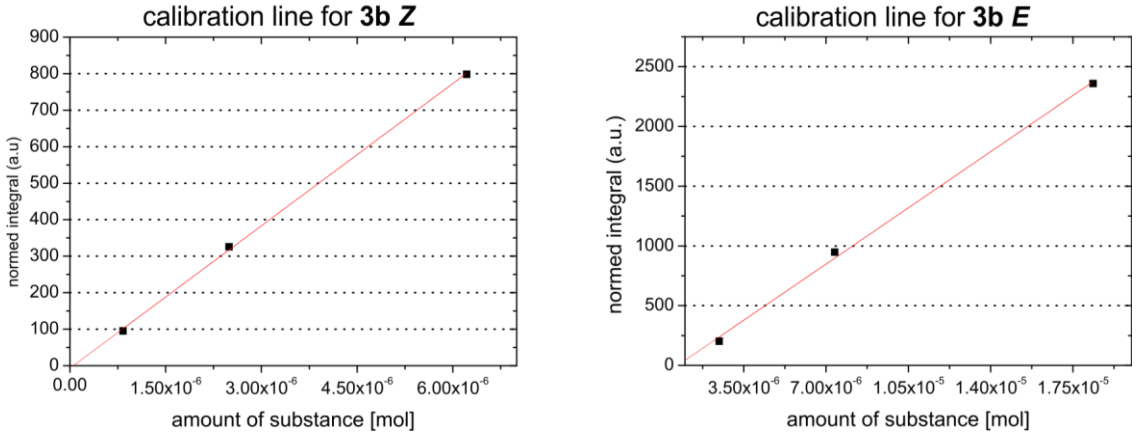

Fig. 92: Reaction scheme and calibration lines of the GC screening for the enyne **3b** formation from nitroalkene **1b**. R^2 values of the calibration lines are 0.99667 (**3b *E***) and 0.99908 (**3b *Z***). Concentrations are **1b** (62.5 mM), catalyst (12.5 mM) benzoic acid (12.5 mM). Reaction time was 21-48 h. GC standard compound was pentadecan.

The reaction conditions of the catalyst screening were as follows. Catalyst (0.2 equiv, 0.1 mmol, 12.5 mM) and 12.2 mg benzoic acid **14** (0.2 equiv, 0.1 mmol, 12.5 mM) were dissolved in 8 mL DMSO and 78.6 mg **1b** (1.0 equiv, 0.5 mmol, 62.5 mmol) was added. After the reaction time has elapsed, 1.46 mL of the reaction mixture was transferred in a GC vial, 3.9 µL pentadecan was added and a GC-FID measurement was performed. In the following, the raw results of the GC-Screening are shown in Table 27.

Table 27: Raw data of the GC-FID screening of different catalysts for the enyne **3b** formation reaction from nitroalkene **1b**. Catalyst structures and calculated yields are depicted in the manuscript.

Catalyst No.	Raw Integral (**3b** *E*)	Normed Integral (**3b** *E*)	Raw Integral (**3b** *Z*)	Normed Integral (**3b** *Z*)	Integral (Pentadec.)
1	39.2	21.9	7.4	4.1	1788.7
2	35.5	17.8	10.0	5.0	1991.5
3	104.8	61.1	29.0	16.9	1714.6
4	115.0	64.0	48.5	27.0	1797.2
5	273.8	129.7	54.3	25.7	2111.4
6	152.5	104.4	30.1	20.6	1460.6
7	175.3	145.9	35.6	29.6	1201.3
8	220.8	165.0	32.7	24.4	1337.8
9	242.9	204.7	71.2	60.0	1186.5
10	432.0	259.8	62.0	37.3	1663.0
11	284.2	158.5	252.6	140.9	1792.5
12	499.0	379.1	122.1	92.8	1316.2
13*	651.7	457.1	166.2	116.6	1425.7
13**	665.9	569.9	273.3	233.9	1168.5
14	1193.1	740.7	244.0	151.5	1610.7
15	1076.1	719.5	195.3	130.6	1495.7
16	1252.3	801.0	600.2	383.9	1563.5
17	962.1	961.8	225.0	224.9	1000.3
13***	1831.6	1249.4	318.8	217.5	1466.0
18	2723.0	1360.9	726.9	363.3	2000.9
13	1955.0	1489.4	502.6	382.9	1312.6

5.4.2 Direct Enyne Formation from Nitroalkenes – Potential Participation of Solvent Molecules

Variation of reaction conditions showed that the enyne **3** formation from nitroalkenes **1** is strongly solvent dependent (see chapter 5.4.1). Only in the polar aprotic solvents DMSO and DMF the desired enyne formation was detected. Therefore, the possibility that solvent molecules are directly involved in the reaction was considered likely. Through variation of the ratio of fully deuterated DMSO (99.9% d_6 / 0.1% d_5) to non-deuterated DMSO and acquisition of proton and deuterium spectra, such a direct involvement of solvent molecules was investigated.

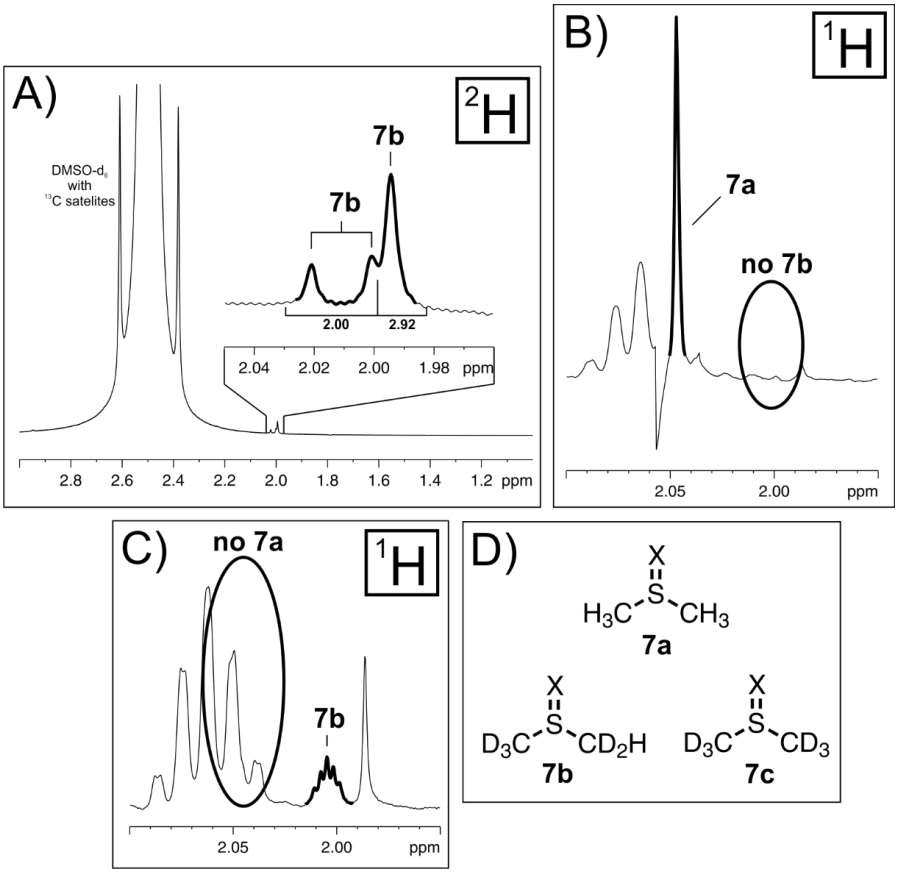

Fig. 93: A) shows a section of ^{2}H spectrum with signals of detected DMSO-derivatives formed during the reaction of nitropentene **1a**, DPP **12** (50 mol%) and benzoic acid **14** (50 mol%) in DMSO-d_6 (plus one droplet of DMSO) @ room temperature. B) shows a section of ^{1}H spectrum (acquired with solvent presaturation) with signals of detected DMSO-derivatives formed during the reaction of **1a**, **12** (50 mol%) and **14** (50 mol%) in a mixture of DMSO-d_6 and DMSO (1:1) @ room temperature. C) shows a section of ^{1}H spectrum with signals of detected DMSO-derivatives formed during the reaction of **1a**, **12** (100 mol%) and **14** (100 mol%) in 100% DMSO-d_6 @room temperature. D) shows proposed structures of the detected DMSO-derivatives where X is a unknown substituent.

Deuterium spectra of a mixture of the nitroalkene **1a**, catalyst/base DPP **12** and the additive benzoic acid **14** showed, in addition to the expected solvent signal (DMSO @ 2.5 ppm), the occurrence of two new signals, *i.e.* a doublet at 2.01 ppm (coupling constant: 1.8 Hz) as well as a singlet at 2.00 ppm with the relative integrals of 2.00 to 2.92. These integrals are approximately 0.02% of the solvent integral, which is

one order of magnitude lower than the specified single protonated DMSO-d_5 ratio of the applied solvent (0.1%). The coupling constant of the doublet is very similar to the $^2J_{HD}$ coupling constant of DMSO-d_5 (1.9 Hz).[68] Together with the relative integrals it would fit to a substituted DMSO-d_5 derivative **7b** as shown in Fig. 93D (X is an unknown substituent). The corresponding proton spectra showed two signals in the same chemical shift region of the deuterium signals of **7b**. Depending on the applied amount of undeuterated DMSO, one quintet at 2.00 ppm (1.8 Hz) (see Fig. 93C) and one singlet at 2.04 ppm (see Fig. 93B) were detected. Using DMSO-d_6 (DMSO-d_5 ratio of 0.1%) as solvent only the quintet is showing up which would fit to the proton of **7b**. The singlet occurs upon addition of 50 vol% undeuterated DMSO and would fit to **7a** the corresponding derivative of non-deuterated DMSO (see Fig. 93D).

Since the chemical shift of the deuterium signals of **7b** and **7a** (see Fig. 93A) is about 0.5 ppm lower than that of DMSO-d_5, the shielding effect of the substituent X has to be stronger than that of the sulfoxide oxygen. The substituent X apparently is not breaking the symmetry with respect to a line of the molecule **7a** (the two CH_3 groups are chemically identical), because it shows only one singlet (instead of two). Otherwise the identity of substituent X remains unclear.

No deuterium signal which would fit to the fully deuterated species **7c** (see Fig. 93D) was detected which is very surprising at first glance because the corresponding fully deuterated DMSO-d_6 is present in a very large excess compared to the DMSO-d_5 molecule (0.1%). This could be explained if the mechanism leading to **7a** and **7b** contains both, a deprotonation-/dedeuteration step of DMSO as well as a reprotonation step. Since the water amount in these samples is pretty high and water molecules are very acidic in comparison to DMSO molecules, the probability that reprotonation instead of redeuteration occurs is very high. Therefore the product molecule **7** would almost always contain at least one proton which would explain that the amount of fully deuterated derivative **7c** is below the NMR detection limit. Also the vanishing of **7b** upon the usage of a one to one mixture of deuterated and non-deuterated DMSO can be explained assuming such a protonation/deprotonation type of mechanism. The probability for deprotonation of the solvent molecule DMSO leading to **7a** is by orders of magnitude higher than the deprotonation of the single protonated residue of DMSO-d_5 in the deuterated solvent leading to **7b**. In addition the formation of a doubly protonated species **7** is unlikely because the isotope effect makes α-deprotonation about three to seven times more likely than α-dedeuteration.[69]

5.4.3 Direct Enyne Formation from Nitroalkenes – Variation of the Nitroalkene Structure

In order to further shed light into the enyne **3** formation mechanism, the two differently branched nitroalkenes 2-nitrohex-2-ene **1c** and 2-methyl-1-nitrobut-1-ene **1d** were tested for their reaction performance (catalyst: DPP **12**, additive: benzoic acid **14** in DMSO-d_6) monitored by *in situ* NMR. These substrates were chosen, because their structure prevents two possible reaction steps in an alternative mechanism after formation of the nitroalkene-dimer **2** (see Fig. 94). Starting from nitroalkene **1c**, after dimerization to **2c**, 1,2-elimimation of nitrous acid is possible and would lead to 5-methyl-6-(1-nitroethyl)nona-3,5-diene **8c** (see Fig. 94, top) with the nitro group not being part of the conjugated π-system. Since now, compared to linear nitroalkenes, a methyl substituent replaces the proton in position 4, subsequent deprotonation at this position, is blocked. There is the theoretical possibility of nitroethane elimination *via* deprotonation of the CH_2 group in position 4'. But the result of such an unlikely elimination step would be an allene instead of an enyne. By identification of either the nitrous acid elimination product **8c** or the corresponding allene formed *via* nitroethane elimination starting from the α-branched nitroalkene **1c**, an alternative mechanistic proposal can be validated.

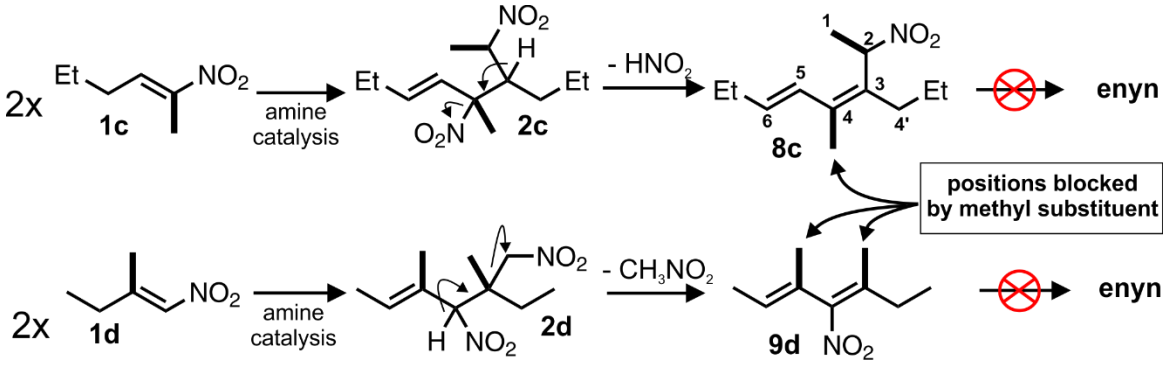

Fig. 94: Reaction path of the branched nitroalkene **1c** and **1d** in the enyne formation reaction according to an alternative reaction mechanism. In both cases enyne formation should not be possible. The introduced methyl groups that block elimination of nitrous acid or nitromethane are marked with arrows.

Starting from nitroalkene **1d**, after secondary amine catalyzed dimerization to **2d**, deprotonation at the carbon with the secondary nitro group attached is possible and could initiate a nitromethane elimination leading to 3,5-dimethyl-4-nitrohepta-2,4-diene **9d** (see Fig. 94, bottom) with the nitro group being attached to a sp^2 carbon, which is part of the conjugated dien π-system. From here on 1,2-elimination of the remaining nitro group as nitrous acid is not possible, because both β-positions (relative to the nitro group) are blocked by the introduced methyl substituents. Identification of **9d** as a product would validate an active nitro methane elimination.

1c was synthesized previously in our working group and after purification its reactivity with DPP **12** and benzoic acid **14** in DMSO-d_6 was monitored (see. Fig. 95). **1c** was rapidly consumed and remained stable at a ratio of about 20% after 5 hours. In this reaction mixture, neither the dimer intermediate **2c** nor the expected products **8c** or allene derivative could be identified. Instead the main product was identified as (*E*)-2-nitrohex-3-ene **10** building up fastest in the beginning of the reaction, simultaneously with the strongest decline of **1c**. The reaction mechanism that leads to **10** is assumed to start with a reversible nucleophilic attack of the secondary nitrogen of the catalyst **12** to the β-position of the nitroalkene **1c**, forming a catalyst-adduct (see Fig. 95). Apparently, 1,2-elimination initialized by deprotonation of the CH_2 proton in position 4, leading to the less crowded double bond in **10** is favored (Hofmann product). This reaction step is irreversible, because the resulting double bond is no longer activated for a nucleophilic attack *via* conjugation with the nitro group. The active base that initializes the elimination process has to be considerably sterically demanding, otherwise the higher substituted and more stable Zaitsev product **1c** would be formed. Most probably, the active base in this case is again the secondary amine DPP **12**.

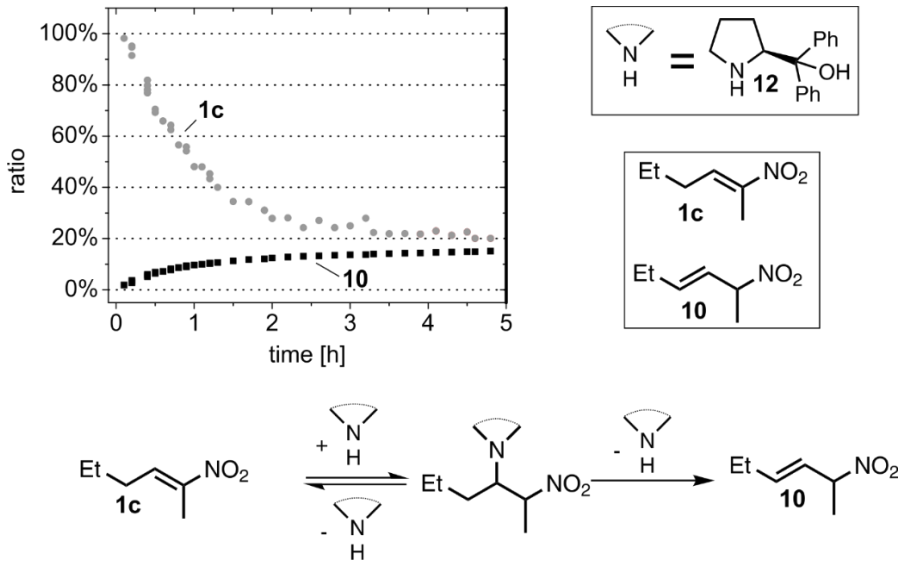

Fig. 95: ^{1}H NMR reaction monitoring of a mixture of **1c** (100 mM), **12** (38 mM) and **14** (50 mM) in DMSO-d_6 @ 298 K shows the consumption of **1c** and the formation of **10** as the main product. The secondary amine DPP **12** is abbreviated as shown in the top right corner.

No other reaction products could be identified. The disproportionate loss of starting material compared to the amount of product formed is assigned to an active polymerization process of **1c**. Since, not even the dimerization to **2c** takes places, this shows that α-branched nitroalkenes like **1c** cannot be applied in the enyne formation reaction.

A mixture of *E*/*Z* isomers of **1d** was synthesized according to a literature procedure and its reactivity with DPP **12** and benzoic acid **14** in DMSO-d_6 was monitored by *in situ* by NMR (see Fig. 96, top).[k] The isomeric mixture of starting material is consumed fast and an *E*/*Z* mixture of 2-methyl-1-nitrobut-2-ene **11** is formed. The mechanism of this reaction is assumed to start with a nucleophilic addition (see Fig. 96, bottom) of the secondary amine functionality of the catalyst **12** on the β-position of **1d** to form a catalyst-nitroalkene adduct. From here on, three different E2 eliminations are occurring parallel, first *via* deprotonation of a α-CH_2 proton back to the stabilized nitroalkene **1d**, second and third, *via* deprotonation of a γ-CH_2 proton to the product **11 E** and **11 Z**. After the starting material vanished completely (after about 3 hours) **11 Z** is still building-up slowly while **11 E** starts to degrade. Therefore, either isomer **11 Z** is thermodynamically more stable than isomer **11 E**, or, more likely, the formation of **11 E** is reversible whereas the formation of **11 Z** is irreversible (see Fig. 96, bottom).

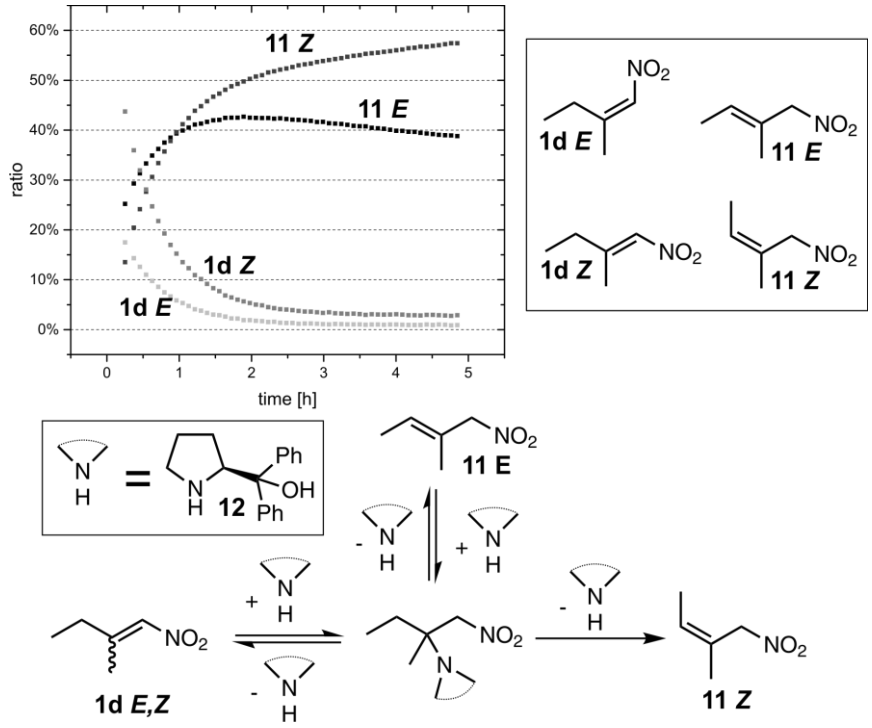

Fig. 96: ^{1}H NMR reaction monitoring of a mixture of **1d** (mixture of *E* and *Z* isomer) (in sum ≈50 mM), DPP **12** (≈50 mM) and benzoic acid **14** (≈50 mM) in DMSO-d_6 @ 300 K shows the consumption of **1d** and the formation of **11** (mixture of *Z* and *E*) as the main product. A possible reaction mechanism is depicted.

Again, the desired reactivity *i.e.* the nitroalkene-dimerization of **1d** and subsequent reaction steps were not detected. Therefore again, these results show that also β-branched nitroalkenes are not applicable in the enamine formation reaction, because they show a complete different reactivity.

[k] Synthesis and NMR investigations on **1d** were performed together with M. Sc. Andreas Seegerer during a lab course.

It is noted here, that in contrast to the α-branched nitroalkene **1c**, β-branched **1d** is not consumed by a polymerization process. Presumably, alkyl substituents in β-position of nitroalkenes hamper their polymerization tendency.

5.4.4 Enyne Formation from Nitroalkene-Dimers – NMR Base Screening

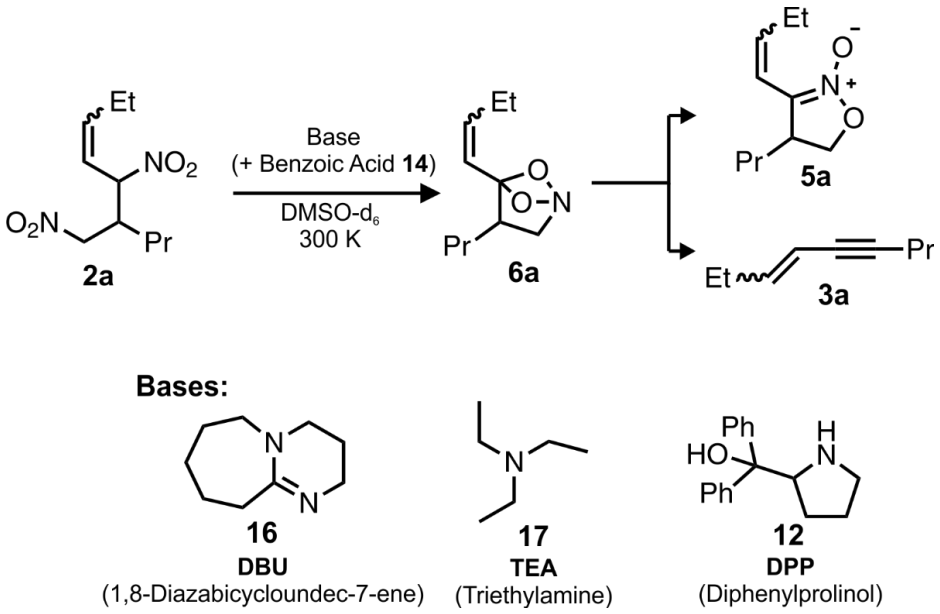

Fig. 97: Reaction scheme and applied bases in the NMR reaction monitoring screening of the bases DBU **16**, TEA **17** and DPP **12** for the enyne **3a** and cyclic nitronate **5a** formation from nitroalkene-dimer **2a**.

In order to elucidate the influence of different bases on the formation reaction of enyne **3** and cyclic nitronate **5** from nitroalkene-dimer **2**, *in situ* ^{1}H NMR reaction monitoring of reaction mixtures of **2a** and base as well as of **2a**, base and benzoic acid **14** in DMSO-d_6 at 300 K were conducted (see Fig. 97). Three neutral bases *i.e.* DBU **16** (pk_{aH}=24.3), DPP **12** (pk_{aH}(pyrrolidine)=19.6)[1], and TEA **17** (pk_{aH}=18.8) with decreasing literature pk_{aH}-values[70] in acetonitrile were chosen. **16** (without additive) is the only base in this row, which led to the selective formation of cyclic nitronate **5a** and showed the highest yield (40%). Since **16** is the strongest base in the row, this indicates that for the selective formation of **5a** a high basicity is crucial. All bases in combination with the additive benzoic acid **14** showed a selective formation of enyne **3a** (**3a** *vs.* **5a**), but the level of *E*/*Z* selectivity and the *in situ* yields of **3a** varied. **17** plus **14** provided the highest *E*/*Z* selectivity (4.0) whereas **16** plus **14** showed the highest yield (45%). Therefore, selective enyne formation is not dependent on the application of an especially strong base. In the following, a detailed discussion of the results of ^{1}H NMR reaction monitoring applying **16**, **17** and **12** with and without **14** as additive is presented.

[1] The pk_{aH} value of DPP in acetonitrile was not known. Instead, the pk_{aH} of pyrrolidine was applied because its structures is closely related (both are 5-membered cyclic secondary amines) and the missing tertiary alcohol functionality in pyrrolidine was assumed not to increase significantly the basicity of the compound.

DBU. Results of the reaction monitoring with DBU **16** (100 mol%) as base are depicted in Fig. 98. Without addition of benzoic acid **14**, at the very beginning of the reaction after about 10 minutes, nitroalkene-dimer **2a** was already quantitatively transformed to the central intermediate **6a** which then reacted selectively to the product cyclic nitronate **5a** (61% after 8 hours). Enyne **3a** was the side product here, which amounted to 20% in the same time. The *E*/*Z* ration of **5a** (see Fig. 98, bottom right-hand side) continuously decreased from about 35 at the beginning to 5 at the end of the reaction, whereas the *E*/*Z* ratio of the side product **3a** started very low (0.2), and reached equilibrium (1.0) in the end.

With additive **14** (100 mol%), the reaction rate is accelerated (see Fig. 98, top right-hand side). Because of the faster reaction rate, the amount of intermediate **6a** was already low (about 20%) in the first spectrum after about 10 minutes. The main product is now enyne **3a** with an *in situ* yield of about 45% after 2 hours and cyclic nitronate **5a** is the side product (about 4%). Applying **14** as additive is not only raising the yield of **3a** but also switches the *E*/*Z* selectivity in favor of *Z* reaching a value > 2.0 at the end of the reaction (see Fig. 98, bottom right-hand side). Interestingly, the *E*/*Z* ratio of the side product cyclic nitronate **5a** started lower than in the additive free case (2.2) and was not significantly changing throughout the reaction.

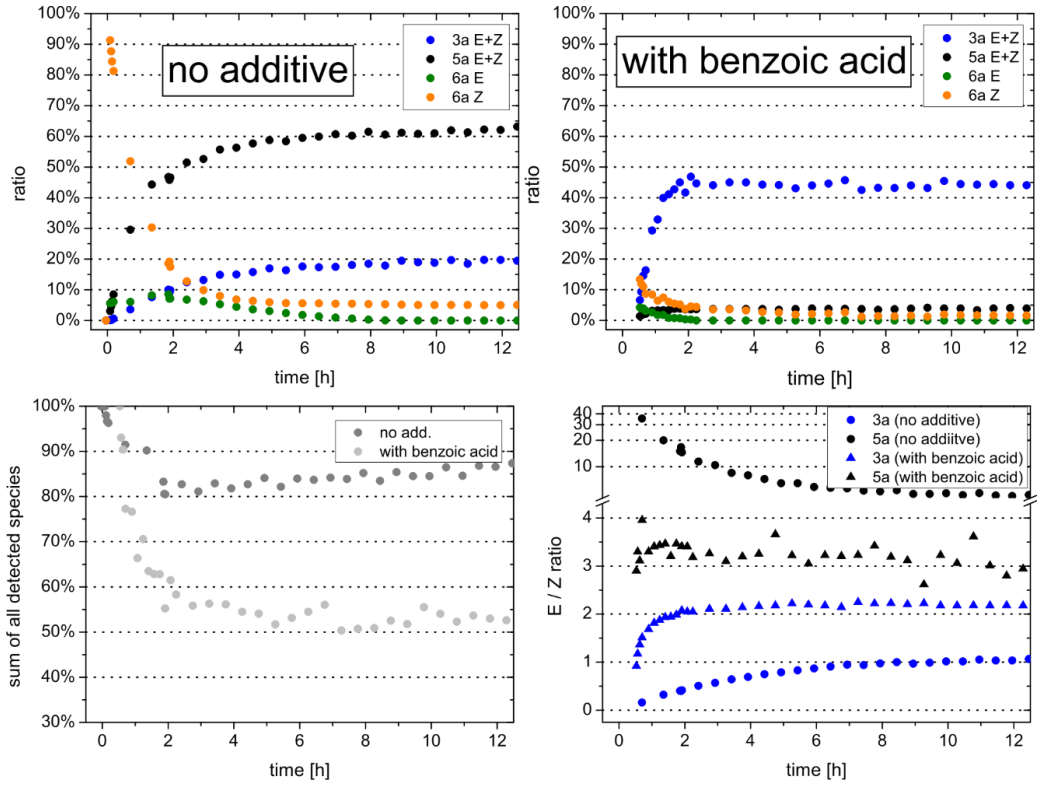

Fig. 98: Reaction kinetics are presented of **16** (80 mM) and **2a** (80 mM, 92% *Z*-isomer, 8% *E*-isomer, d.r.(*Z*) = 2.03:1.00, d.r.(*E*) = 1.38:1.00) in DMSO-d_6 @ 300 K. Top left shows data without addition of additive **14** whereas top right shows data with the addition of **14** (80 mM). In the bottom left the sum of all detected species is presented. Bottom right shows the *E*/*Z* ratios of enyne **3a** (blue) and cyclic nitronate **5a** (black) with (triangles) and without (circles) addition of **14**.

The sum of all detected species (see Fig. 98, bottom left-hand side) was decreasing considerably faster with additive **14** (loss of about 45%) than without (loss of about 18%). No other reaction products were detected which could compensate this loss in the sum of signal intensities. Remarkably, with **16** as base, independent of the addition of **14**, the sum of detected species reached the minimum value after a reaction time of about 3 hours when the reaction with additive **14** was already finished but the reaction without additive was still running. In this ongoing reaction, apparently neither **3a** nor **5a** formation was accompanied by polymerization. This indicates, that the polymerization process which is responsible for the loss of material is not directly connected to neither enyne **3a** nor nitronate **5a** formation but happens independent of these reactivities.

DPP. Results with DPP as base were already described in chapter 5.3.8.

TEA. Results of the reaction monitoring of **2a** with TEA **17** (50 mol%) as base without additive are depicted in Fig. 99, top left-hand side. The reaction was very slow, compared to the reactions with **16** and **12**, lasting about 3 days. At the same time the final *in situ* yield of enyne **3a** was exceptionally high (55%) whereas the amount of formed cyclic nitronate **5a** was low (about 20%). This represents the highest yield of enyne **3a** formation from nitroalkene-dimer **2a** so far, and also considerably exceeds the best results (yield of 35%) obtained during the reaction condition variations (see 5.4.1) of the direct **3a** formation from nitropentene **1a**. One reason for this high yield is the low loss of material (about 25%), deduced from the decrease of sum of all detected species (see Fig. 99, bottom left-hand side). This loss of material which is probably due to a polymerization process was lower than in the samples with **16** as base but slightly higher compared to the samples with **12**. Since, only 50 mol% **12** but 100 mol% of **16** and **17** were applied, this advantage of **12** may be only due to that concentration difference.

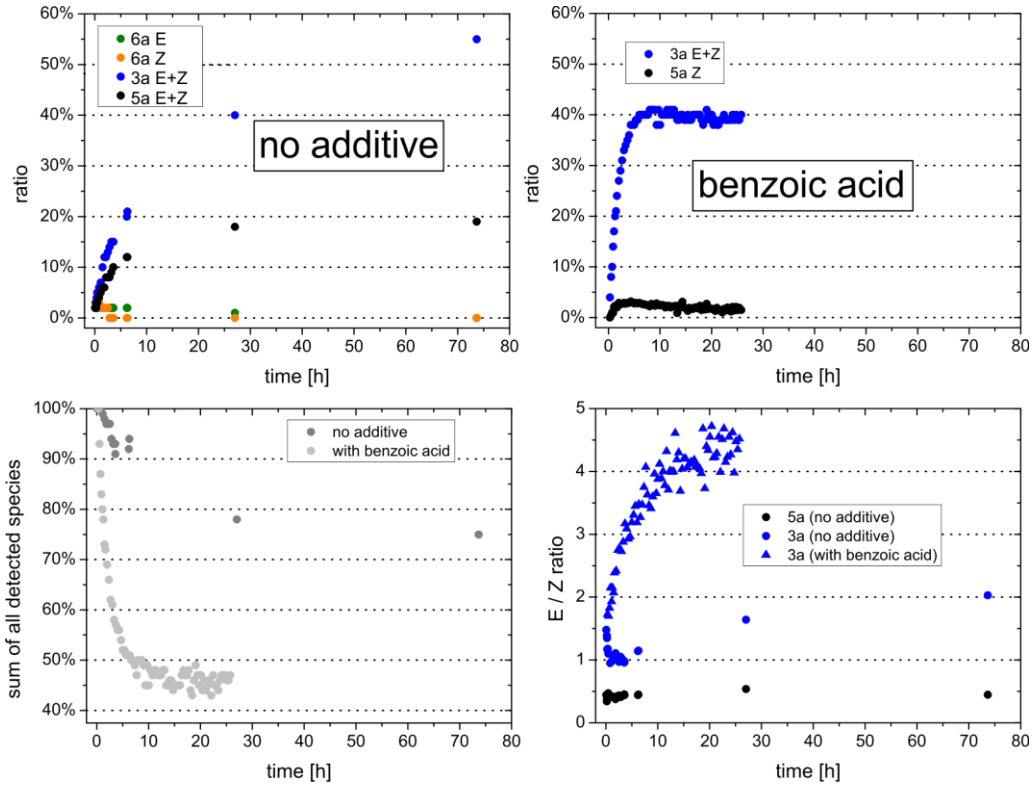

Fig. 99: Reaction kinetics are presented of **17** (80 mM) and **2a** (80 mM, 92% *Z*-isomer, 8% *E*-isomer, d.r.(*Z*) = 2.03:1.00, d.r.(*E*) = 1.38:1.00) in DMSO-d_6 @ 300 K. Top left shows data without additive addition whereas top right shows data with the addition of **14** (80 mM). In the bottom left the sum of all detected species is presented. Bottom right shows the *E* / *Z* ratios of enyne **3a** (blue) and cyclic nitronate **5a** (black) with (triangles) and without (circles) addition of **14**.

Both stereoisomers of the intermediate species **6a** were detected at the beginning of the reaction in low amounts. Similar to the sample with **16** as base and in contrary to the sample with **12**, the *E*/*Z* ratio of enyne **3a** was increasing during the reaction, started at about 1.0 and reached 2.0 after 3 days. Comparing all three additive free reactions (**17**, **12** and **16**), this represents the highest final *E*/*Z* value of **3a**. Like in the sample with **12** as base, the final *E*/*Z* ratio of the side product **5a** was about 0.5 which does not change significantly throughout the reaction. It is surprising that even though **14** was not added the *in situ* yield of **3a** is very high.

Addition of **14** to the sample dramatically changed the outcome of the reaction. The reaction rate was strongly accelerated and **3a** was formed almost exclusively while only traces of **5a** were observed (see Fig. 99, top right-hand side). However, the *in situ* yield of **3a** (40%) was considerably reduced by the additive, once again probably due to an active polymerization process which is exceptionally strong under these conditions and consumed more than 50% of the starting material (see sum of all detected species in Fig. 99, bottom left-hand side). Intermediate **6a** was not detected, most probably due to its short lifetime under these conditions. The *E*/*Z* ratio of **3a** started at an equal distribution (1.0) and was than rising until a value of about 4.0.

These reaction conditions are therefore very selective not only for the formation of **3a** (**3a** *vs.* **5a**) but also in terms of the *E*/*Z* ratio. Should it be possible to suppress the unproductive polymerization process somehow (*e.g.* through very slow addition of the base during the reaction), the reaction of nitroalkene-dimer **2a** with 100 mol% **17** as base and 100 mol% additive **14** has the potential to produce enyne **3a** in almost quantitative yields with good *E*-selectivity.

5.5 References

(1) Aitken, L.; Arezki, N.; Dell'Isola, A.; Cobb, Alexander, J. A. *Synthesis* **2013**, *45*, 2627.

(2) Seebach, D.; Beck, A. K.; Badine, D. M.; Limbach, M.; Eschenmoser, A.; Treasurywala, A. M.; Hobi, R.; Prikoszovich, W.; Linder, B. *Helv. Chim. Acta* **2007**, *90*, 425.

(3) Wiesner, M.; Revell, J. D.; Wennemers, H. *Angew. Chem. Int. Ed.* **2008**, *47*, 1871.

(4) Betancort, J. M.; Barbas, C. F. *Org. Lett.* **2001**, *3*, 3737.

(5) Bächle, F.; Duschmalé, J.; Ebner, C.; Pfaltz, A.; Wennemers, H. *Angew. Chem. Int. Ed.* **2013**, *52*, 12619.

(6) Seebach, D.; Sun, X.; Ebert, M. O.; Schweizer, W. B.; Purkayastha, N.; Beck, A. K.; Duschmalé, J.; Wennemers, H.; Mukaiyama, T.; Benohoud, M.; Hayashi, Y.; Reiher, M. *Helv. Chim. Acta* **2013**, *96*, 799.

(7) Duschmalé, J.; Wiest, J.; Wiesner, M.; Wennemers, H. *Chem. Sci.* **2013**, *4*, 1312.

(8) Ballini, R.; Bosica, G.; Fiorini, D.; Palmieri, A.; Petrini, M. *Chem. Rev.* **2005**, *105*, 933.

(9) Ono, N.; Hamamoto, I.; Kamimura, A.; Kaji, A.; Tamura, R. *Synthesis* **1987**, *1987*, 258.

(10) Alcántara, M.-P. D.; Escribano, F. C.; Gómez-Sánchez, A.; Diánez, M. J.; Estrada, M. D.; López-Castro, A.; Pérez-Garrido, S. *Synthesis* **1996**, *1996*, 64.

(11) Lu, S.-F.; Du, D.-M.; Xu, J.; Zhang, S.-W. *J. Am. Chem. Soc.* **2006**, *128*, 7418.

(12) Wang, J.; Li, H.; Zu, L.; Jiang, W.; Wang, W. *Adv. Synth. Catal.* **2006**, *348*, 2047.

(13) Ooi, T.; Takada, S.; Doda, K.; Maruoka, K. *Angew. Chem. Int. Ed.* **2006**, *45*, 7606.

(14) Dong, X.-Q.; Teng, H.-L.; Wang, C.-J. *Org. Lett.* **2009**, *11*, 1265.

(15) Rabalakos, C.; Wulff, W. D. *J. Am. Chem. Soc.* **2008**, *130*, 13524.

(16) Barbier, V.; Couty, F.; David, O. R. P. *Eur. J. Org. Chem.* **2015**, *2015*, 3679.

(17) Dadwal, M.; Mohan, R.; Panda, D.; Mobin, S. M.; Namboothiri, I. N. N. *Chem. Commun.* **2006**, 338.

(18) Shanbhag, P.; Nareddy, P. R.; Dadwal, M.; Mobin, S. M.; Namboothiri, I. N. N. *Org. Biomol. Chem.* **2010**, *8*, 4867.

(19) Anderson, J. C.; Blake, A. J.; Mills, M.; Ratcliffe, P. D. *Org. Lett.* **2008**, *10*, 4141.

(20) Konishi, M.; Ohkuma, H.; Matsumoto, K.; Tsuno, T.; Kamei, H.; Miyaki, T.; Oki, T.; Kawaguchi, H.; Vanduyne, G. D.; Clardy, J. *J. Antibiot.* **1989**, *42*, 1449.

(21) Rudisill, D. E.; Castonguay, L. A.; Stille, J. K. *Tetrahedron Lett.* **1988**, *29*, 1509.

(22) Stutz, A.; Petranyi, G. *J. Med. Chem.* **1984**, *27*, 1539.

(23) Huang, W.-S.; Metcalf, C. a.; Sundaramoorthi, R.; Wang, Y.; Zou, D.; Thomas, R. M.; Zhu, X.; Cai, L.; Wen, D.; Liu, S.; Romero, J.; Qi, J.; Chen, I.; Banda, G.; Lentini, S. P.; Das, S.; Xu, Q.; Keats, J.; Wang, F.; Wardwell, S.; Ning, Y.; Snodgrass, J. T.; Broudy, M. I.; Russian, K.; Zhou, T.; Commodore, L.; Narasimhan, N. I.; Mohemmad, Q. K.; Iuliucci, J.; Rivera, V. M.; Dalgarno, D. C.; Sawyer, T. K.; Clackson, T.; Shakespeare, W. C. *J. Med. Chem.* **2010**, *53*, 4701.

(24) Masaoka, T.; Hasegawa, Y.; Ueda, T.; Takubo, T.; Shibata, H. *Eur. J. Cancer* **1976**, *12*, 143.

(25) Hatanaka, Y.; Hiyama, T. *J. Org. Chem.* **1988**, *53*, 918.

(26) Hatanaka, Y.; Matsui, K.; Hiyama, T. *Tetrahedron Lett.* **1989**, *30*, 2403.

(27) Andreini, B. P.; Carpita, A.; Rossi, R.; Scamuzzi, B. *Tetrahedron* **1989**, *45*, 5621.

(28) Shao, L. X.; Shi, M. *J. Org. Chem.* **2005**, *70*, 8635.

(29) Saha, D.; Chatterjee, T.; Mukherjee, M.; Ranu, B. C. *J. Org. Chem.* **2012**, *77*, 9379.

(30) Miyaura, N.; Yamada, K.; Suzuki, A. *Tetrahedron Lett.* **1979**, *20*, 3437.

(31) Li, P. F.; Wang, H. L.; Qu, J. *J. Org. Chem.* **2014**, *79*, 3955.

(32) Jiang, H.; Elsner, P.; Jensen, K. L.; Falcicchio, A.; Marcos, V.; Jørgensen, K. A. *Angew. Chem. Int. Ed.* **2009**, *48*, 6844.

(33) Shi, Z.; Tan, B.; Leong, W. W. Y.; Zeng, X.; Lu, M.; Zhong, G. *Org. Lett.* **2010**, *12*, 5402.

(34) Zhong, C.; Gautam, L. N. S.; Petersen, J. L.; Akhmedov, N. G.; Shi, X. *Chem. Eur. J.* **2010**, *16*, 8605.

(35) Kano, T.; Yamamoto, A.; Song, S.; Maruoka, K. *Chem. Commun.* **2011**, *47*, 4358.

(36) Guo, Z.-W.; Xie, J.-W.; Chen, C.; Zhu, W.-D. *Org. Biomol. Chem.* **2012**, *10*, 8471.

(37) Trost, B. M.; Li, L.; Guile, S. D. *J. Am. Chem. Soc.* **1992**, *114*, 8745.

(38) Trost, B. M.; Chupak, L. S.; Lübbers, T. *J. Am. Chem. Soc.* **1998**, *120*, 1732.

(39) Karthikeyan, K.; Veenus Seelan, T.; Lalitha, K. G.; Perumal, P. T. *Bioorg. Med. Chem. Lett.* **2009**, *19*, 3370.

(40) Maurya, R.; Gupta, P.; Ahmad, G.; Yadav, D. K.; Chand, K.; Singh, A. B.; Tamrakar, A. K.; Srivastava, A. K. *Med. Chem. Res.* **2008**, *17*, 123.

(41) Pirrung, M. C.; Tumey, L. N.; Raetz, C. R. H.; Jackman, J. E.; Snehalatha, K.; McClerren, A. L.; Fierke, C. A.; Gantt, S. L.; Rusche, K. M. *J. Med. Chem.* **2002**, *45*, 4359.

(42) Kohler, E. P.; Barrett, G. R. *J. Am. Chem. Soc.* **1924**, *46*, 2105.

(43) *Nitrile Oxides, Nitrones, and Nitronates in Organic Synthesis: Novel Strategies in Synthesis*, 2nd ed.; Feuer, H., Ed.; John Wiley & Sons, Inc., New Jersey, 2008.

(44) Hesse, G.; Hatz, R.; König, H. *Justus Liebigs Ann. Chem.* **1967**, *709*, 79.

(45) Ballini, R.; Barboni, L.; Bosica, G.; Fiorini, D.; Mignini, E.; Palmieri, A. *Tetrahedron* **2004**, *60*, 4995.

(46) Kinugasa, M.; Hashimoto, S. *J. Chem. Soc., Chem. Commun.* **1972**, 466.

(47) Miura, M.; Okuro, K.; Nomura, M. *J. Org. Chem.* **1995**, *60*, 4999.

(48) Torssell, K.; Zeuthen, O. *Acta Chem. Scand.* **1978**, *B32*, 118.

(49) *Nitrogen-15 Nuclear Magnetic Resonance Spectroscopy*; John Wiley & Sons, Inc., New York, 1979.

(50) Schmid, M. B. Ph.D. Thesis, University of Regensburg, Regensburg-Germany, January 2011.

(51) Trost, B. M.; Müller, C. *J. Am. Chem. Soc.* **2008**, *130*, 2438.

(52) Fulmer, G. R.; Miller, A. J. M.; Sherden, N. H.; Gottlieb, H. E.; Nudelman, A.; Stoltz, B. M.; Bercaw, J. E.; Goldberg, K. I. *Organometallics* **2010**, *29*, 2176.

(53) Bradley, C. H.; Hawkes, G. E.; Randall, E. W.; Roberts, J. D. *J. Am. Chem. Soc.* **1975**, *97*, 1958.

(54) *Spektroskopische Daten zur Strukturaufklärung organischer Verbindungen*, 3rd ed.; Springer, Heidelberg, 2000.

(55) Lambert, J. B.; Binsch, G.; Roberts, J. D. *Proc. Natl. Acad. Sci. U. S. A.* **1964**, *51*, 735.

(56) Bordwell, G. *Acc. Chem. Res* **1988**, *21*, 456.

(57) Olmstead, W. N.; Margolin, Z.; Bordwell, F. G. *J. Org. Chem.* **1980**, *45*, 3295.

(58) Krasnaya, Z. A.; Stytsenko, T. S.; Prokof'ev, E. P.; Yakovlev, I. P.; Kucherov, V. F. *Bull. Acad. Sci. USSR Div. Chem. Sci.* **1974**, *23*, 809.

(59) Zen, S.; Kaji, E. *Chem. Pharm. Bull.* **1974**, *22*, 477.

(60) Chatterjee, A.; Jha, S. C.; Joshi, N. N. *Tetrahedron Lett.* **2002**, *43*, 5287.

(61) Conrad, F.; Shechter, H. *J. Am. Chem. Soc.* **1954**, 2716.

(62) Chlenov, I. E.; Tartakovskii, V. A.; Khudak, V. I.; Novikov, S. S. *Bull. Acad. Sci. USSR Div. Chem. Sci.* **1969**, *18*, 2113.

(63) Kanemasa, S.; Yoshimiya, T.; Wada, E. *Tetrahedron Lett.* **1998**, *39*, 8869.

(64) Kohler, E. P.; Barrett, G. R. *J. Am. Chem. Soc.* **1926**, *48*, 1770.

(65) Galli, C.; Marotta, E.; Righi, P.; Rosini, G. *J. Org. Chem.* **1995**, *60*, 6624.

(66) Marotta, E.; Baravelli, M.; Maini, L.; Righi, P.; Rosini, G. *J. Org. Chem.* **1998**, *63*, 8235.

(67) Essex, J. W.; Jorgensen, W. L. *J. Phys. Chem.* **1995**, *99*, 17956.

(68) *The Merck Index, an Encyclopedia of Chemicals, Drugs, and Biolocicals*, 14th ed.; O'Neil, M. J., Heckelman, P. E., Koch, C. B., Roman, K. J., Eds.; Merck & Co., Inc., New Jersey, 2006.

(69) *The Proton in Chemistry*, 2nd ed.; Cornell University Press, Ithaca, 1973.

(70) Kaljurand, I.; Kütt, A.; Sooväli, L.; Rodima, T.; Mäemets, V.; Leito, I.; Koppel, I. a. *J. Org. Chem.* **2005**, *70*, 1019.

(71) Gissot, A.; N'Gouela, S.; Matt, C.; Mioskowski, C. *J. Org. Chem.* **2004**, *69*, 8997.

6 Summary and Outlook

A strong focus of this work was the detection and investigation of intermediates in organocatalytic and organic reactions in order to clarify the underlying reaction mechanisms. Knowing an intermediate structure is often the key for understanding a chemical reaction, because by comparison with starting materials and products they can reveal, which bonds are broken and which bonds are newly formed in that process. But this is by far not the only reason intermediates are so useful for mechanistic investigations. In the case, more than one intermediate species can be detected simultaneously by liquid NMR, in principal, the dynamic of the ongoing reaction can be exploited by EXSY Spectroscopy. These NMR experiments are sensible for chemical exchange processes and allow for the revelation of the inter-connectivities of starting materials, intermediates and products in the reaction mechanism. From EXSY build-up curves *i.e.* data plots of rows of EXSY spectra with increasing mixing times, even rate constants can be determined. However, if the classical 2D EXSY experiment (2D NOESY) is chosen for this purpose, often an obstacle occurs – the needed NMR measurement time. It gets too long, typically many hours for one EXSY build-up curve. This is a problem, because in order to gain meaningful results, the ratios of the investigated species are not allowed to change a lot during the measurement. Since ongoing reactions are investigated, this means that even if the reaction is slow, the experimental time must be in the range of minutes, not hours. So, although in principal a powerful method, for practical reasons the classical 2D EXSY experiment is not suitable for intermediate-intermediate rate constant analysis.

To overcome that obstacle we had the idea of combining two well-known concepts. The first concept is selective NMR Spectroscopy. By selective irradiation of a proton resonance frequency, the classic 2D NOESY experiment becomes a 1D experiment. This means, depending on the number of increments necessary for the 2D experiment, saving a factor of roughly 10 to 100 in the measurement time. The second concept is the initial rate approximation (IRA). Normally the whole EXSY build-up has to be determined. With the help of IRA, only the initial linear part has to be taken into account which saves another factor of about 2 to 4 in the measurement time.

That combination of concepts (selective NMR and IRA) was the key which enabled the investigation of the enamine formation pathway in the proline catalyzed self-condensation reaction of aldehydes in DMSO by the NMR determination of intermediate-intermediate rate constants (chapter 2). In combination with high quality theoretical calculations, we discovered most strikingly, that the direct precursor of the enamine intermediate in that reaction is the iminium ion, not the oxazolidinone as previous

studies suggested. On the other hand, the results also show that the reaction mechanism can be very dependent on the reaction conditions and can change if the conditions are changed. Basic additives for example were shown to switch the initial deprotonation step from internal to external and water addition presumably favors a water assisted enamine formation pathway. While these are only little variations of the same mechanism, switching the solvent from DMSO to acetonitrile and adding a strong nucleophile changes the picture completely. In parallel to this work, the working group of Prof. Vetticatt could show by a kinetic isotope effect study that under such α-amination reaction conditions the enamine is not formed from the iminium ion but most probably, in deed from the oxazolidinone species. Both studies together show that the common picture from reactions and their reaction mechanisms being intrinsically tied to each other is not true everywhere.

Mechanistic investigations can also lead to the discovery of completely new reactions. Chapter 5 presents the continuation of a study started by Dr. Markus Schmid where the original mechanistic investigation of secondary amine catalyzed Michael additions of nitroalkenes to aldehydes revealed that nitroalkenes can be dimerized and subsequently form enynes under those reaction conditions. This mechanistic NMR study now shows that at the same time cyclic nitronates are formed and that both enyne and nitronate formation occur simultaneously *via* a common, bicyclic intermediate. The reaction was split by finding conditions where the nitroalkene-dimer can be isolated. From the dimer on, the reactions are both base induced and as the applied bases get stronger, the balance is shifted towards the nitronate product. A not yet clarified effect of the addition of benzoic acid was observed, that suppresses nitronate formation and enables the selective formation of enyne. Overall the resolved mechanistic picture should enable a targeted synthetic optimization of those reactions which may in the end even be possible in a stereoselective manner.

In a NMR stability study of the popular diphenylprolinol trimethylsilyl ether organocatalyst (chapter 3) we showed that in principal, the catalyst has a high stability in solution at room temperature. However, combining solvents with a high dielectric constant and hydrogen bond acceptor properties (DMSO or DMF) with weak acids like benzoic acid, the TMS protecting group is cleaved in a very short time. This may be of great importance for reaction planning, because the protected and deprotected catalyst possibly have opposite stereoinduction modes and the deprotected diphenylprolinol shows lower catalytic activity.

Finally, in chapter 4, a combined NMR and computational study is presented were the relevance of *cis*-peptide conformations is elucidated on the example of a short glycine pseudo-dipeptide in DMSO. Since, in many computational studies *cis*-conformations have been omitted, it is very striking, that both possible *cis*-conformers

could be detected experimentally. Thermodynamic analysis confirmed that the population is indeed very low (12 kJ mol^{-1} endergonic at 300 K). However, determination of the *cis*-conformer formation rate constants, again by a combination of 1D selective EXSY spectroscopy and the IRA approach, revealed that they are easily accessible kinetically and get formed with rate constants of roughly 0.02 s^{-1} from the main all-*trans* isomer. Therefore, in order to account for their, at least kinetically, high relevance in solution, they should not be ignored in future computational investigations.

The author hopes that the presented results of this thesis in the field of NMR spectroscopic investigations of reaction intermediates, reaction mechanisms, catalysts and peptides could show that solution NMR is a very powerful spectroscopic method for those purposes. Until today, it allows for exciting discoveries especially in the chemistry of small organic molecules, or in other words – yes, small molecules *are* still hot.